6-27-2019 1:00 PM

Identification of Human Postnatal Progenitor Cells with Multifaceted Regenerative Functions

Tyler T. Cooper
The University of Western Ontario

Supervisor
Hess, David A.
Robarts Research Institute

Graduate Program in Physiology and Pharmacology
A thesis submitted in partial fulfillment of the requirements for the degree in Doctor of Philosophy
© Tyler T. Cooper 2019

Abstract

Regenerative medicine is a multidisciplinary effort to regenerate or replace a deficiency of functional cells/tissues, such as deteriorated vasculature in cardiovascular pathologies or depleted β-cell mass in diabetes. The transplantation of pro-regenerative progenitor cell populations has demonstrated therapeutic benefits in pre-clinical models, although translation to clinical efficacy is limited by the paradoxical balance between cell expansion *ex vivo* and loss of regenerative functions *in vivo*. Herein, this thesis encompasses two distinct approaches to circumvent translational deficiencies; 1) prevention of hematopoietic progenitor cell differentiation during *ex vivo* expansion and 2) utilizing the secretome of pancreas-derived multipotent stromal cell as a biotherapeutic agent. Across the first two studies, I investigated whether the inhibition of retinoic acid (RA)-signaling would limit HPC differentiation and retain pro-vascular and islet regenerative functions *in vivo*. These studies identified a bias of HPC towards megakaryopoiesis with prolonged culture; however, also demonstrated that the reversible inhibition of RA-signaling enhances the expansion of HPC progeny that retain a primitive phenotype and multifaceted pro-regenerative functions *in vivo*. Albeit, cell transplantation is limited by transplanted cell survival and subsequent secretion of pro-regenerative stimuli. Accordingly, we have demonstrated the transplantation of conditioned media generated by therapeutic cells by-passes these limitations while stimulating endogenous mechanisms of tissue regeneration. To this end, I isolated a heterogenous Panc-MSC population during culture of human islets *in vitro*. Using label-free mass spectrometry and flow cytometry analyses, I provide the first in-depth characterization of human Panc-MSC in comparison to BM-MSC. Specifically, I demonstrated the proteome of Panc-MSC restricts adipogenesis and RA-signaling; albeit, is competent to pro-neural stimuli and primed for robust expansion *ex vivo*. Next, I determined that Panc-MSC secrete pro-angiogenic and islet regenerative stimuli which are harbored within extracellular vesicles. Collectively, this body of work provides novel insights towards multifaceted therapeutic cell populations and lays a foundation to explore the cell-free biotherapeutics for applications of regenerative medicine.

Summary

This body of work undertakes a broad experimental approach to identify "stem cell" populations cells from human post-natal or adult tissues, such as umbilical cord blood, bone marrow, or pancreas. Specifically, I sought to identify cells which may be used as a biological agent to activate endogenous (self-) regeneration to treat diabetes and life-threating complications of blood vessels. In diabetes, a loss or dysfunction of insulin-producing β-cells leads to elevated blood sugars that damage blood vessels in organs throughout the body. In the first half of this thesis, I developed a method to increase the number of blood lineage-specific stem cell populations that can regenerate beta-cells and blood vessels in mouse models. Albeit, I present early evidence that cells of the megakaryocyte (platelet-producing)-lineage may have therapeutic potential. The second half of this thesis characterized a mesenchymal progenitor population from human pancreas tissue using high-sensitive equipment to detect over >7000 proteins in an effort to establish a "proteomic fingerprint" of therapeutic cell populations. Accordingly, I proceeded to show that cell transplantation can be avoided, and media conditioned by mesenchymal progenitors can be concentrated for use as a biological cocktail to stimulate blood vessel and β-cell regeneration in mouse models. This body of work provides foundational evidence to further explore the use of post-natal and adult stem/progenitor cell populations as a therapeutic tool to treat diabetes and/or vascular complications.

Keywords

Co-Authorship Statement

All studies presented in this thesis were completed by Tyler T. Cooper in the laboratory of Dr. David Hess with experimental contributions from the co-authors listed below. Dr. David Hess contributed to design, analysis, interpretation, and manuscript preparation for all experiments.

Chapter 2:

Dr. Stephen Sherman provided support with *in vivo* experimentation. Dr. Miljan Kuljanin helped with the cell lysate preparation and analysis by mass spectrometry. Gillian Bell assisted with *in vivo* experimentation. Dr. Gilles Lajoie provided mass spectrometry expertise.

Cooper, T.T., Sherman, S.E., Kuljanin, M., Bell, G.I., Lajoie, G.A. and Hess, D.A., 2018. Inhibition of Aldehyde Dehydrogenase-Activity Expands Multipotent Myeloid Progenitor Cells with Vascular Regenerative Function. Stem Cells, 36(5), pp.723-736.

Chapter 3:

Gillian Bell assisted with *in vivo* experimentation and histological analyses.

Cooper, T.T., Bell, G.I. and Hess, D.A., 2018. Inhibition of retinoic acid production expands a megakaryocyte-enriched subpopulation with islet regenerative function. Stem cells and development, 27(20), pp.1449-1461.

Chapter 4:

Dr. Jun Ma helped with the cell lysate preparation and analysis by mass spectrometry. Shauna Jose helped with assessing growth dynamics multipotency, and phenotypic profile of Panc-MSC. Dr. Giles Lajoie provided mass spectrometry expertise. Manuscript for submission.

Cooper TT, Ma J, Jose SE, Lajoie GA, Hess DA. The Proteome of Human Pancreas-derived Multipotent Stromal Cells Restricts Adipogenesis, Drives Cell Division and Defines a Unique Surface Marker Profile.

Chapter 5:

Dr. Stephen Sherman provided support with *in vivo* experimentation. Dr. Miljan Kuljanin and Dr. Jun Ma helped with the cell lysate/CM preparation and analysis by mass spectrometry. Danielle McRae assisted with atomic force analysis. Shauna Jose helped with the collection and processing of CM. François Lagugné-Labarthet provided atomic force microscopy expertise. Dr. Gilles Lajoie provided mass spectrometry expertise. Manuscript for submission:

Cooper TT, Sherman SE, Kuljanin M, Ma J, McRae DM, Jose, SE, Lagugné-Labarthet F, Lajoie GA, Hess DA. Human Pancreatic Multipotent Stromal Cells Secrete Pro-angiogenic Stimuli.

Chapter 6:

Gillian Bell assisted with *in vivo* experimentation and histological analyses.

Acknowledgments

I must humbly acknowledge my supervisor Dr. David Hess. Thank you for giving me the opportunity to learn, develop and refine myself as a student, a scientist, and as a human being in a dynamically challenging, albeit very supportive environment. Specifically, you provided me my first research position as an overly-eager and ambitious 4th -year thesis student, subsequently taking me on as I refined my graduate school optimism to a realm of matured scientific realism and execution. The autonomy I received under your supervision was instrumental to my evolution as scientist and has only increased my passion to perform more research in order to advance the field of regenerative medicine. Most importantly, I must thank you for your genuine patience as I juggled graduate school with raising a young family. My dream would not be possible without you.

I would like to equally thank the members of my advisory committee: Dr. Cheryle Seguin, Dr. Dean Betts, and Dr. Lauren Flynn for you moral, technical, and philosophical advice.

I would like to thank OGS for providing funding to subsidize my studies and ultimately allow me to make the next steps in my career.

At this point I would like to collectively thank all members of the Hess and Lajoie Laboratory who have I have collaborated with throughout my studies. Gillian Bell, David Putman, Ayesh Senenviratne, Stephen Sherman, Miljan Kuljanin, Ruth Elgamal, Jun Ma, Shauna Jose. I would also like to thank Dr. Giles Lajoie for his expertise.

I would like to thank Dr. Ayesh Seneviratne for the training he provided me as a 4th year thesis student. You went beyond what was required from you and helped me to focus my goals as a student and scientist. You are truly an inspiring person and I am extremely happy I can call you a friend and colleague. I wish you much success through your career.

Dr. Stephen Sherman, I am at a loss of words to tell you what it meant to obtain a friend like you throughout my studies. I was fortunate that we began our studies together and were able help facilitate each other's scientific development in many aspects. It is mind-blowing to look back at this point and realize what we have experienced and what we have accomplished. From the "dark days" of bootstrap experiments to where we are today. I am happy that I have obtained a life-long collaborator early in my career and a friend for the rest of my life. May the dark forces of Shrek guide you through your scientific journeys.

To my beautiful wife, Hannah, it is finally over. Within this stack of paper, is the 5+ years of our relationship that you been by my side and have helped me to achieve my goals. If you are reading this, it means this thesis is serving as more than a coffee coaster. All jokes aside, I cannot repay you for what you have sacrificed to make this work. You have held my head, when I was low on myself and wanted to give up. You have helped me to become more patient, disciplined and fearless. Ultimately, this work would not have been possible without you by my side. Over the last 7 years we have bought a house, raised 2 kids, and accumulated 3 dogs. Our life has been chaotic, but I would not trade it for the world. I look forward to the next chapter in our life together. I love you.

To my children, Jaden and Olivia (and any that may come after this thesis), I am proud to be your dad and love you all to the moon. Jaden, you are almost 7 at the time I am writing and defending this thesis. I wish you could remember our treks through the snow and crammed bus rides into campus; however, our journeys together have only begun. I have watched you grow into a very creative, compassionate and intelligent boy. I hope you never lose those characteristics as you become a man and change the world (because you will!). Olivia, you are $1^{1/2}$ at the time I am writing this thesis. Our years together are early, yet you have already made an impact on my whole world.

To my Mom, Jennifer Varga, I love you with all my heart and thank you for the moral and financial support you have continuously provided me throughout my undergraduate and graduate studies. I am not sure how many sons can proudly say their mom works harder than they do on any given day. You have taught me the value of hard work and the

meaning of sacrifice. To Gene and Margaret Varga, thank you for the moral and financial support throughout my graduate and undergraduate studies. To the rest of the "Varga/Crots" side, I love you all and thank you all for the moral support you have provided along the way.

To my Dad, Sherwood Cooper Jr., I love you and appreciate everything you have taught me. I would almost need a second thesis to recall the adventures we have had together and the experiences we have gathered. You have always encouraged me to be creative, appreciate the beauty of science, and push my mind beyond its limits. I am not sure how I would have got through all my studies without you. To the rest of the Cooper clan, I love you all and thank you for the moral support you have provided me along the way.

I would like to thank other family members, including Machelle and Matthew Milton, for supporting my family as we triumphed through this chapter of our life. Nonetheless, I would like to recognize Paul Beauregard and Bryan Crots for your impact on my life.

I would like to close by dedicating this work to my late brother, Travis Cooper.

One Love.

"In great attempts, it is even glorious to fail." – Vincent Lombardi

Table of Contents

List of Tables

List of Figures

List of Appendices

List of Abbreviations

7-AAD 7-aminoactinomycin D
ABC ATP-binding Cassette
ABI Ankle-brachial Index
ADH Alcohol Dehydrogenase
AFM Atomic Force Microscopy
ALDH Aldehyde Dehydrogenase
ALDH^{hi} High ALDH-activity
ALDH^{lo} Low ALDH-activity
ANGPT Angiopoietin
ARX Aristaless Related Homeobox
ATP Adenosine Triphosphate
AUC Area Under Curve
BM Bone Marrow
CD Cluster of Differentiation; also known as surface markers
CFU Colony Forming Unit
CK19 Cytokeratin 19
CLI Critical Limb Ischemia
CPA2 Carboxypeptidase A2
CRABP Cellular retinoic acid binding protein
CRBP Cellular retinol binding protein
CVD Cardiovascular Disease
CYP26 Cytochrome P450 Family 26
DAPI 4',6-diamidino-2-phenylindole
DEAB Diethylaminobenzaldehyde
DIVAA^{TM} Directed *in vivo* Angiogenesis Assay^{TM}
DM Diabetes Mellitus
DNA Deoxyribose Nucleic Acid
DRAQ5 Deep Red Anthraquinone 5
EBM Endothelial Basal Media
ECM Extracellular Matrix
EdU 5-ethynyl-2-deoxyuridine
EGM Endothelial Growth Media
ESC Embryonic Stem Cell
FACS Fluorescent Activated Cell Sorting
FAL Femoral Artery Ligation
Flt-3L Fms-like Tyrosine Kinase 3 Ligand
FOXA2 Forkhead Box A2
GATA4 GATA Binding Protein
GIP Gastric Inhibitory Peptide
GLP-1 Glucagon-like Peptide 1
GLUT2 Glucose Transporter 2
GLUT4 Glucose Transporter 4
GP1B Glycoprotein Ib; CD42
GP9 Glycoprotein IX

GUSB Beta-Glucuronidase
HLA Human Leukocyte Antigen
HMVEC Human Microvascular Endothelial Cells
HPC Hematopoietic Progenitor Cell
HSC Hematopoietic Stem Cell
HSPC Hematopoietic Stem/Progenitor Cell
INSR1/2 Insulin Receptor 1/2
iPSC Induced Pluripotent Stem Cell
ISCT International Society of Cellular Therapies
ITGA2B Integrin alpha-IIb; aka CD41
LC Liquid Chromatography
LDL Low-density Lipoprotein
LDPI Laser Doppler Perfusion Imaging
LT-HSC Long Term-HSC
MAFA MAF BZIP Transcription Factor A
MCL1 BCL2 Family Apoptosis Regulator
MEP Megakaryocyte-erythrocyte Progenitor
miRNA Micro-RNA
MMP Matrix metalloproteinases
MNC Mononuclear Cells
MPL Thrombopoietin Receptor
MS Mass Spectrometry
MSC Multipotent Stromal Cell; aka Mesenchymal Stem Cell
NEUROG3 Neurogenin 3; aka Ngn3
NKX6.1 NK6 Homeobox 1
NOD Nonobese Diabetic
PAD Peripheral Artery Disease
PAGE Polyacrylamide Gel Electrophoresis
PAX4 Paired Box 4
PBS Phosphate Buffered Saline
PDGFR Platelet Derived Growth Factor Receptor
PDX1 Pancreatic and Duodenal Homeobox 1
PLAUR Plasminogen Activator, Urokinase Receptor
POSTN Periostin
PR Perfusion Ratio
PTF1 Pancreas Associated Transcription Factor 1a
qPCR Quantitative Polymerase Chain Reaction
RAR Retinoic Acid Receptor
RARE Retinoic Acid Response Element
RNA Ribose Nucleic Acid
ROS Reactive Oxygen Species
RXR Retinoid X Receptor
SCF Stem Cell Factor
SCID Severe Combined Immunodeficiency
SDS Sodium Dodecyl Sulfate
SEM Mean Standard Error

SLGT2 Sodium-glucose Co-transporter 2
SMA Smooth Muscle Actin
SOX9 SRY-box 9
STZ Streptozotocin
TPO Thrombopoietin
UCB Umbilical Cord Blood
USD Dollars (United States)
VEGF Vascular Endothelial Growth Factor
vWF Von Willebrand Factor
Wnt5A Wingless-type MMTV Integration Site Family, member 5A

Chapter 1

1   Introduction

1.1   Diabetes Mellitus

Over 2000 years ago, physicians in India provided the first 'clinical' diagnosis of "madhumeha" or "honey urine" when excessive urine excretion (polyuria) from patients attracted an unexpected infestation of insects[1,2]. Today, madhumeha is diagnosed as diabetes mellitus (DM) or 'passing through of honey' which more accurately segregates the glucose-rich polyuria of diabetes mellitus from non-related polyuria conditions (i.e. diabetes insipidus)[3]. Although DM has challenged scientists and clinicians for over 2000 years, only in the last century has clinical interventions that mitigate early death become available[4]. At the root of disease, DM is the dysregulation of blood glucose homeostasis and/or peripheral insulin sensitivity; ultimately leading to system-wide cardiometabolic imbalances that contribute to secondary pathologies.

DM can be further segregated based on etiology and central pathology, albeit both types of DM will ultimately succumb to comparable cardiovascular comorbidities[5-9]. Briefly, DM is made-up of individuals with autoimmune Type 1 and insulin-resistant Type II pathologies; although, other forms of DM, such as gestational diabetes, also exist[10-13]. Presently, DM has reached epidemic proportions (>400 million individuals globally) and has financially burdened the international healthcare system (>700 billion USD per year) without a foreseeable plateau[13]. Throughout this chapter, I will discuss the etiology, pathology and common cardiovascular comorbidities of DM. Specifically, I will focus on the limitations of therapeutic approaches aiming to provide long-term glucose control and how regenerative medicine is progressing towards novel therapies to treat diabetes and vascular comorbidities.

1.1.1 Human Pancreas Development

Organogenesis of the human pancreas occurs at anatomical region of the endoderm-derived distal foregut morphogenesis followed by subsequent budding of the FOXA2$^+$ (Forkhead Box A2)/PDX1$^+$ (Pancreatic and Duodenal Homeobox 1) dorsal and ventral pancreatic epithelium at 4-5 weeks post-conception[14,15] (Figure 1.1). Accordingly, the larger dorsal bud and common bile duct rotate and fuse to the smaller ventral bud, creating the common pancreatic duct network that drains exocrine secretions towards the duodenum around embryonic week 7. During these morphological changes, PDX1$^+$ progenitor cells within pancreatic buds undergo robust proliferation and differentiate into either duct-supported exocrine tissue or endocrine-functioning islets of Langerhans. In a brief summary, SOX9$^+$ (SRY-box 9)/PDX1$^+$ progenitors will acquire an exocrine fate through the acquisition of GATA4 (GATA Binding Protein 4) expression defining 'tip' progenitor cells committed toward acinar cell fate. In contrast, 'trunk' progenitor cells serve as a bipotent progenitor cell pool which commits to ductal or endocrine-lineage fate through sustained expression of SOX9 or transient expression of NEUROG3, respectively[15]. Exocrine tissue makes up the vast majority of the adult pancreas (>95%) and provide an essential supply of pro-isoform digestive enzymes that are subsequently activated in the duodenum of the small intestine. Endocrine tissue makes up ~1-2% of total pancreas mass despite containing a unique composition of at least 5 hormone-releasing islet cell types. In summary, exclusive expression of lineage specific transcriptional factors in NEUROG3+ endocrine-lineage progenitors, such as NKX6.1 (NK6 Homeobox 1) and MAFA (MAF BZIP Transcription Factor A) , lead to the differentiation and maturation of insulin-producing β-cells[15]. Similarly, the balance between ARX (Aristaless Related Homeobox) and PAX4 (Paired Box 4) expression regulates α-cell versus β-cell identity[16], respectively. The coordinated development of
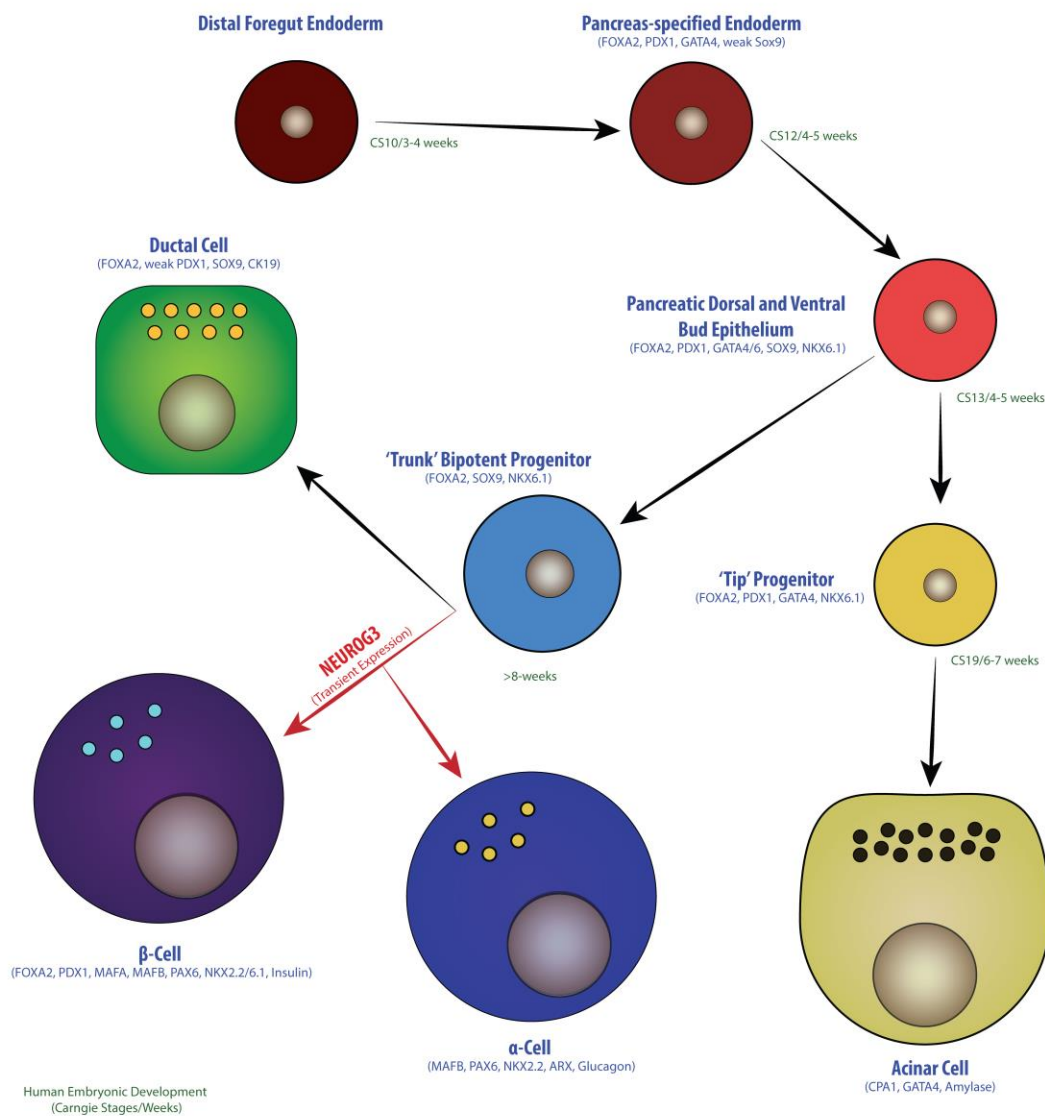
Figure 1.1 Overview of Human Pancreas Development and Lineage-specification.
Organogenesis of pancreas begins in distal foregut endoderm at 3-4 weeks post-conception. FOXA2 and PDX1 expression defines Distal Foregut Endoderm commitment to the pancreatic lineage. High GATA4 expression commits PDX1+ pancreatic bipotent progenitors towards acinar-cell fate. Sustained NKX6.1 expression commits bipotent progenitors towards ductal cell fate through sustained expression of SOX9. Alternatively, endocrine progenitors will lose SOX9 expression and transiently express NEUROG3. NEUROG3^{+} progenitors will give rise to endocrine cells, including insulin-secreting β-cells and glucagon-secreting α-cells.

these specialized cell-types bestows the pancreas as a multifunctional organ which provides central components for nutrient absorption and energy homeostasis.

Acinar cells can be histologically identified by ductal-centric organization, distinct cytoplasmic zymogen granules, and basolateral nucleus[17,18] (Figure 1.2). During development, acinar cells differentiate from PDX1 pancreatic endoderm progenitors through the activation of Notch signaling pathways and expression of GATA4, PTF1 (Pancreas Associated Transcription Factor 1a), and CPA2 (Carboxypeptidase A2)[15,17,19-21]. Pancreatic acini are composed of acinar cells centered around centroacinar cells located at the terminal end of intercalated ductal epithelium[22]. Networks of ductal epithelium converge to form intralobular ducts that transport digestive zymogens released from acinar cells. Exocrine secretions of the pancreas to lead enzymatic breakdown and absorption of carbohydrates, lipids, or proteins in the small intestine. Disruption of acinar homeostasis can lead chronic inflammation of the pancreas, also known as pancreatitis. Towards this end, acinar cells have been proposed to regenerate exocrine pancreas tissues via dynamic differentiation and plasticity[23,24]. Exocrine regeneration by acinar cell expansion has been thoroughly investigated[24,25], however convincing evidence of acinar cell reprogramming towards an endocrine fate has only been demonstrated using exogenous vectors[26].
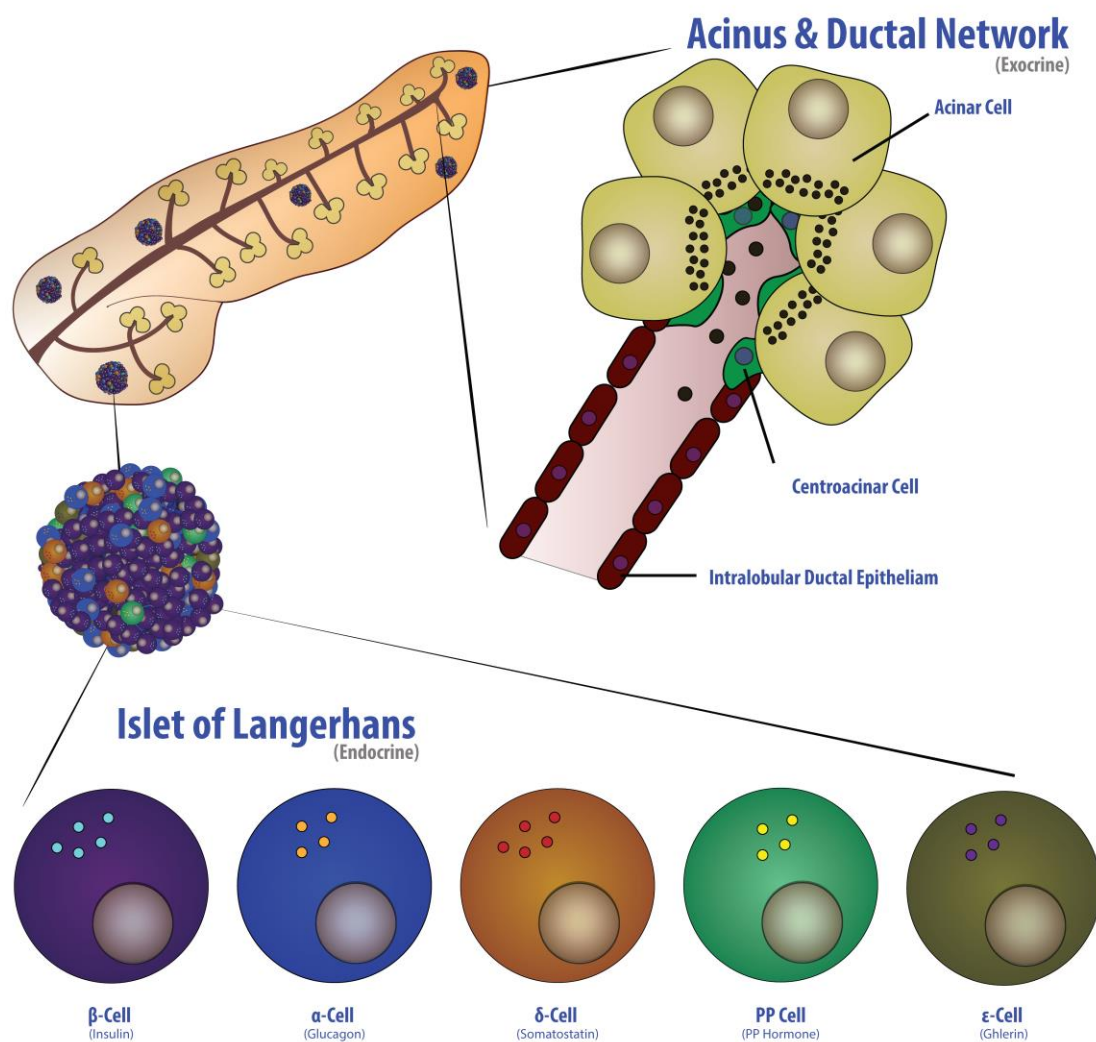
Figure 1.2 Overview of Exocrine and Endocrine Cell Populations of the Pancreas.
The pancreas contains exocrine (acinar and ductal cells) and endocrine (islet of
Langerhans) cell populations, each with unique functions.

The endocrine compartment of the pancreas is composed several cell-types marked by specialized hormone secretion[27]; including ∝-cells (glucagon), β-cells (insulin), δ-cells (somatostatin), ε-cells (ghrelin), PP-cells[14,28-30]. The ratio of cells within islets of Langerhans is estimated around 35-40% ∝-cells and 40-60% β-cells with infrequent representation by δ-cells, PP, and ε-cells. Spatial arrangement of endocrine cells within islets is distinct between rodents and humans, such that β-cells dispersed through the human pancreas and centered at the islet core in rodent models. Nonetheless, the architecture of mammalian pancreatic islets is integrated with a dense microvascular network, that serves to transport secreted hormones to peripheral tissues[31]. In the context of diabetes, reciprocal balance of ∝- and β-cell function maintains glucose homeostasis by controlling the glucose release from the liver and uptake from the circulation[32-35]. Briefly, ∝-cells release of glucagon in response hypoglycemic or energy-demanding conditions. Activation of the glucagon receptor on hepatocytes increases glycogenolysis and gluconeogenesis to elevate blood glucose levels. In contrast, insulin functions to reduce blood glucose levels by stimulating glucose uptake into peripheral tissues after ingestion of food. In the context of diabetes, the loss of functional β-cell mass and/or peripheral insulin sensitivity leads to damaging hyperglycemia[36].

1.1.2   Insulin Secretion and Glucose Homeostasis

Following the ingestion of food and absorption of carbohydrates in the small intestine, systemic blood glucose concentration can rapidly elevate nearly 2-fold in a healthy adult[32]. In order to counteract toxicity from prolonged hyperglycemia, β-cells sense hyperglycemia and rapidly restore normoglycemia (within ~60 minutes) through the hormonal actions of insulin (Figure 1.3). β-cells are equipped with bidirectional glucose transporter, GLUT2 (Glucose Transporter 2), that allows β-cells to gauge systemic glycemia levels and regulate glucose metabolism[37,38]. Homeostatic blood glucose levels are maintained by a fine-tuned balance of glucagon or insulin secretion. In periods of normoglycemia, the low affinity of GLUT2 transporter facilitates glucose uptake from circulation at concentrations that maintains membrane potential in β-cells[38]. In contrast, hyperglycemia elevates glucose uptake via GLUT2 and increases the production of cytosolic ATP, ultimately leading to insulin secretion (Figure 1.3). ATP generated by glycolytic activities of the β-cell will inhibit ATP-sensitive K^+-channel function, and in return, indirectly open voltage-gated Ca^{++} channels[38-40]. Decreased K+ efflux leads to rapid depolarization of the plasma membrane and increased cytosolic calcium concentrations mediate insulin release. The initial pool of insulin released via exocytosis by β-cells is replenished by the glucose-sensitive regulation of pro-insulin translation. During this period, glucagon secretion from α-cells
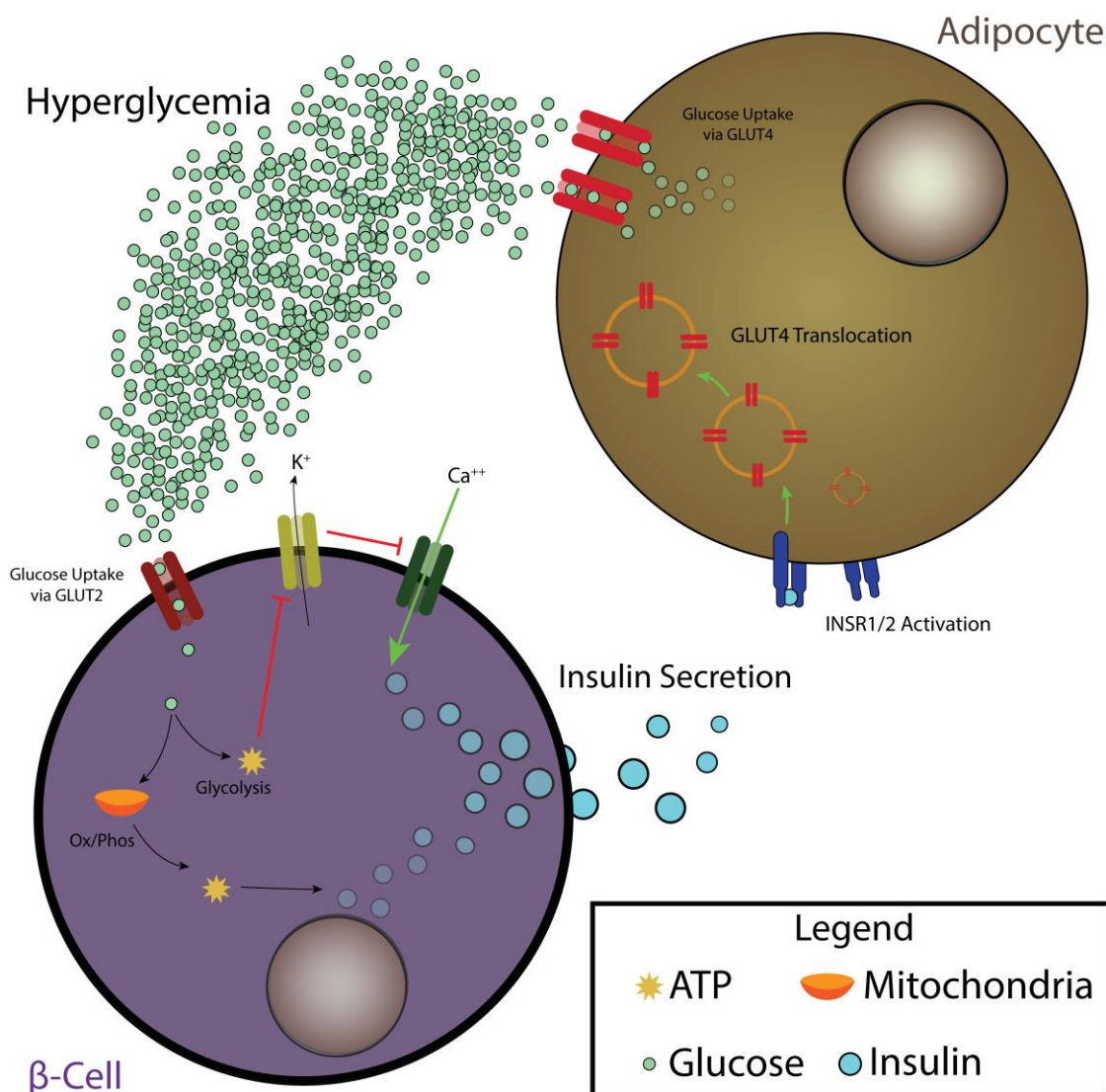
Figure 1.3 Overview of Insulin Secretion and Glut4 Translocation in Response to Hyperglycemia. Glucose uptake through GLUT2 transporters leads to increased cytosolic ATP in beta-cells. Inhibition of ATP-sensitive K^+ channels will lead to an influx of Ca^{++} and insulin vesicle release and translation. Insulin will activate INSR1/2 on peripheral cells (i.e. adipocytes) and translocation of GLUT4 to the plasma membrane will occur. Subsequently, glucose will be up taken through GLUT4 transporters to satisfy metabolic demands.

is dampened, and glucose storage is promoted within the liver by the inhibition of glucagon-regulated glycogenolysis enzymes and activation of glycogen synthase to promote glycogen formation[33]. Circulating insulin activates insulin-receptors to stimulate translocation of GLUT4 transporters to the plasma membrane of competent (i.e. liver, adipose, skeletal muscle) cells to increase the glucose clearance from systemic circulation and meet the metabolic demands of tissues[35,41,42]. In type 2 DM, insulin-dependent GLUT4-translocation is disrupted in peripheral cells.

Insulin secretion and/or function is also regulated by additional effectors which either act in a positive or negative manner. Incretins hormones including Gastric Inhibitory Polypeptide (GIP) and Glucagon-like Peptide 1 (GLP-1) are released from the intestinal mucosa shortly after oral nutrient ingestion[43,44]. Both GIP and GLP-1 potentiate insulin secretion from the pancreas, whereas the later also reduces glucagon secretion. Ghrelin-secretion from epsilon-cells also increases insulin secretion from β-cells in rodent model, although the relevance of this in humans is not completely understood[29,30]. In contrast, effectors such as glucagon, catecholamines, growth hormone, cortisol, and free fatty acids dampen the secretion or peripheral actions of insulin[32,34]. Intra-islet hormones, such as somatostatin and PP, also provide overlapping regulation of glucagon and insulin secretion[45,46]. In the context of diabetes, disruption of insulin production and/or peripheral sensitivity leads to dysregulated systemic glucose homeostasis. As a result, a wide spectrum of cardiometabolic pathologies develop leading to life-threatening complications.

1.1.3   Type 1 Diabetes

Accounting for ~10% of individuals with DM, Type 1 DM affects roughly >40 million individuals internationally and is most prominent in populations of Northern European descent[13,47]. Type 1 DM is commonly referred to as juvenile diabetes, although this terminology may be viewed as a misnomer as symptoms occasionally manifest in adults as latent autoimmune DM or 'Type 1.5'[48]. The international rates of Type 1 DM have gradually increased over time[47,49,50], which has only complicated our understanding of the etiology of Type 1 DM[47,50-55]. Although genetic mutations (i.e. HLA-DR3/4) have been identified in a proportion of individuals with Type 1 DM, other studies have suggested *in utero* or post-natal environmental insults, combined with genetic predisposition, may trigger initiation of autoimmunity in Type 1 DM[51,54,55]. Common models of Type 1 DM, include NOD mice which spontaneously develop autoimmune diabetes and reflect the human pathophysiology of inflammatory cell infiltration into islets[56]. Other genetic and chemical-induced models have also been used to further our understanding the pathophysiology of Type 1 diabetes and/or facilitate the transplantation of human islets and/or regenerative cell populations for the development of novel therapies[57,58].

The underlying pathology of Type 1 DM is targeted T-cell mediated destruction of pancreatic β-cells (Figure 1.4). Specifically, $CD4^+$ T-helper Cells and $CD8^+$ cytotoxic T-cells are responsible for the targeted destruction of β-cells following the generation of autoantibodies by activated B cells, respectively[54,59]. Although mechanisms are not completely understood, autoantigen presentation is initially mediated by B-lymphocytes and antigen-presenting cells of the innate immunity, such as macrophages and/or dendritic cells. Interestingly, α-cells, δ-cells, PP cells, and ϵ-cells of the islet are not targeted by cytolytic $CD8^+$ T-cells, thus suggesting the autoantigen is exclusive to the β-cell lineage. Recent studies have suggested early senescence of a β-cell population may be the root of autoantibody generation[60], eventually leading to the destruction of functional β-cells. The destruction of insulin-generating β-cell leads to systematic complications, such as neuropathy, nephropathy, retinopathy and gastrointestinal disorders, as a result of prolonged periods of hyperglycemia[8,61-64].
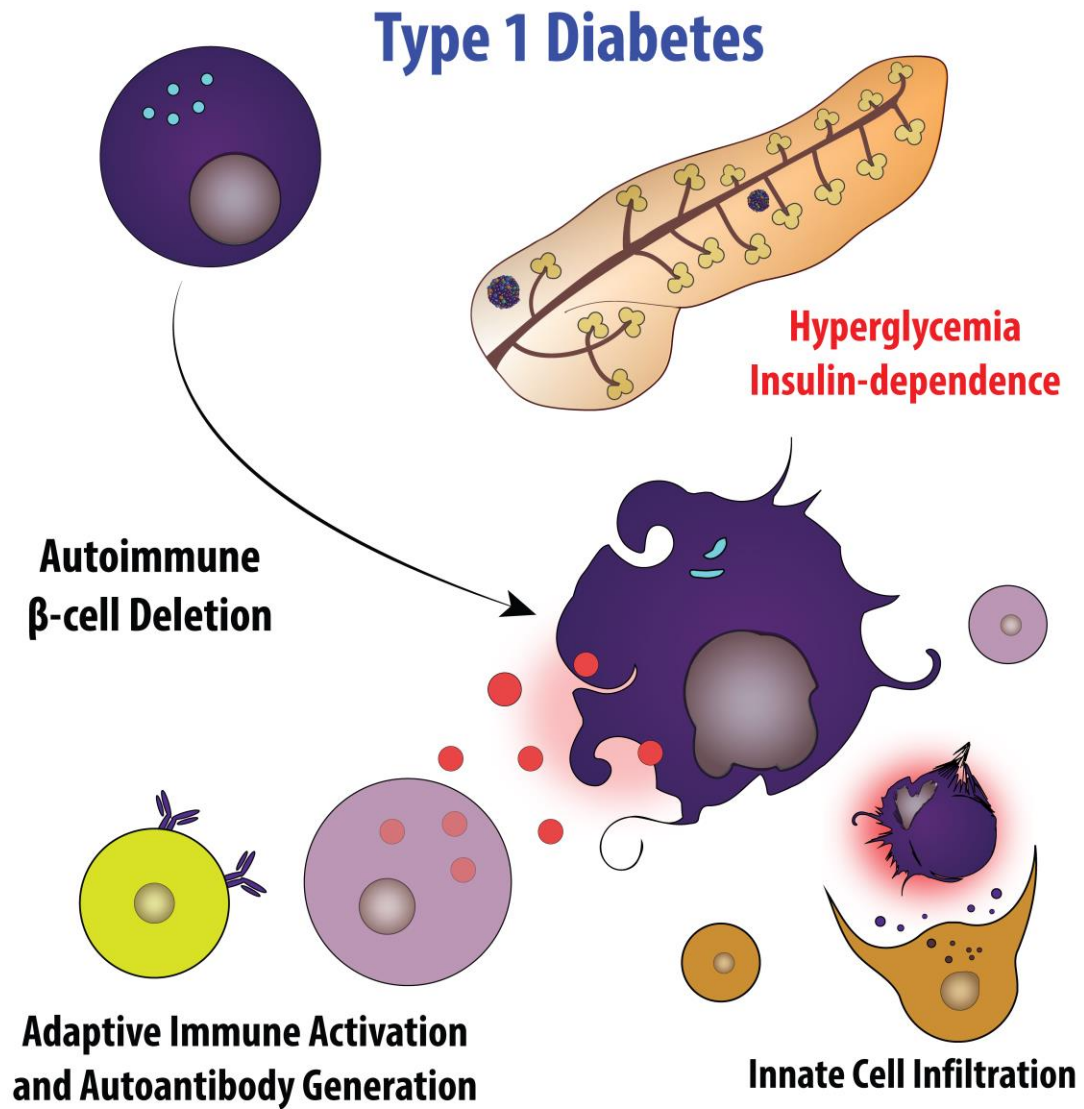
Figure 1.4 Overview of Autoimmune-induced Type 1 Diabetes and Insulin-dependent Hyperglycemia. Autoantigens, generated by antigen presenting cells of the innate and adaptive immune system, activate cytolytic T-cells. Activated T-cells will selectively induce apoptosis in β-cells, leading to a loss of insulin-producing cell mass. The loss of β-cell mass will lead to sustained hyperglycemia and insulin-dependence.

In a clinical setting, individuals with Type 1 diabetes present with a spectrum of symptoms[59]; however, the initial diagnosis typically following the rapid onset of severe hyperglycemia-induced coma. In addition to severe hyperglycemia, patients with Type 1 diabetes may present with sub-average muscle mass, chronic fatigue, polyuria, and/or secondary infections of oral and genital orifices. Ultimately, individuals diagnosed with Type-1 diabetes are insulin-dependent and require daily exogenous injection or automated pump therapies.

1.1.4   Type 2 Diabetes

The prevalence of Type 2 diabetes has increased at an alarming rate. With an estimated >30% increase of afflicted individuals in next 5 years, Type 2 diabetes continues to burden the global healthcare system due poor diet, central obesity, and sedentary lifestyles[65-71]. In 2015, Type 2 diabetes patients numbered >400-million individuals globally and despite a notable number of individuals remaining undiagnosed, Type 2 DM and related health issues caused the global healthcare system >$800 billion[13,67,70,71]. Unfortunately, in many cases this financial burden is placed on the afflicted individuals who struggle to secure and retain employment due to complications of the disease[67]. Notably, Type 2 diabetes is largely preventable through proper diet and exercise regimens, which outlines the importance of public educational programs and individual care[65,66,72-77]. Furthermore, both proactive and preventative measures must be taken to counteract the alarming rate of Type 2 diabetes presently diagnosed in children and adolescents[61]. Several genetic pre-dispositions have been proposed by genome-wide association studies and have correlated variations in genetic loci to the onset and progression of Type 2 DM in human tissues[68,71,78]. To this end, evidence from epigenetic studies following gestational insufficiency have demonstrated important non-genetic contributions towards β-cell maturation and susceptibility to disease later in life[15,79,80]. Without effective management of hyperglycemia, individuals with Type 2 DM will

eventually become insulin-dependent (Figure 1.5); although, early diagnosis could prevent this outcome.

Skeletal muscle and adipose tissues are the primary targets for circulating insulin to stimulate the rapid removal of glucose from the blood[35]. Insulin binds to insulin receptor 1/2 (INSR1/2) on the membrane of target cells, in return leading to a cascade of downstream effectors that stimulate translocation of GLUT4 transporter to the plasma membrane[42,81]. Chronic activation of INSR1/2 can lead sustained receptor internalization leading to a global decrease in the expression of GLUT4 on peripheral tissues. As a result, when β-cells increase the production and secretion of insulin, in an attempt to combat prolonged periods of hyperglycemia, peripheral tissues, such as skeletal muscle, become desensitized to chronic exposure of circulating insulin and fail to facilitate the uptake of glucose from systemic circulation. As a result of concurrent obesity, individuals with Type 2 DM are prone to elevated level of free fatty acids which additionally compromise β-cell function[82]. This paradoxical dysfunction of glucose homeostasis eventually leads to β-cell exhaustion, free-radical generation, and β-cell death[83,84]. Ultimately, the capacity of the pancreas in Type 2 diabetics to produce enough endogenous insulin is compromised, thus individuals with late-stage Type 2 DM will require exogenous insulin therapy similar to individuals with Type 1 DM[70,71,83].
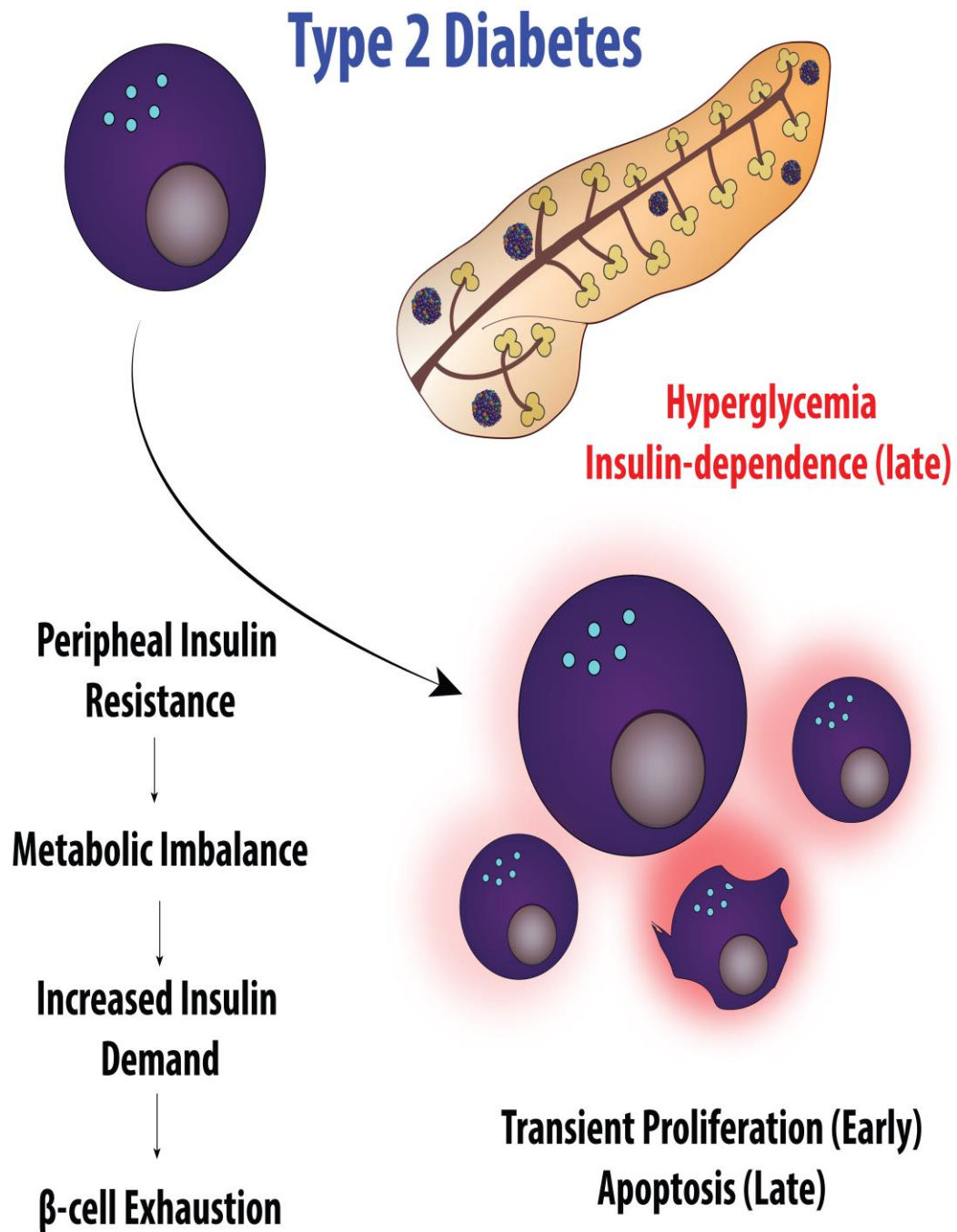
Figure 1.5 Overview of Insulin-resistant Type 2 Diabetes and Insulin-dependent hyperglycemia. Sustained periods of elevated glucose levels and cardiometabolic imbalances lead to peripheral insulin desensitization. As a result, insulin demand will increase and eventually lead to beta-cell exhaustion and apoptosis. In late stages of Type 2 diabetes, the loss of beta-cell mass leads to insulin-dependence.

1.1.5   Clinical Strategies to Combat Diabetes

Insulin-dependence in Type 1 and Type 2 DM is a result diminished β-cell mass where insulin secretion is no longer sufficient to maintain glucose homeostasis. Interestingly, rodent models that received >90% excision of the pancreas did not become insulin-dependent despite a considerable loss of β-cell mass[25,85]. In contrast, a 40-50% resection of the pancreas in human patients has led to insulin-dependence following surgery[86]. These differences reflect genetic and physiological differences between species, such as architectural organization and distribution of islets of Langerhans[87-92]. Nonetheless, current therapies must supplement the loss of insulin-secreting β-cells by providing sufficient exogenous insulin to counteract chronic hyperglycemia[93,94]. However, exogenous insulin therapy can lead to fluctuations in blood glucose that lead to diabetic complications, which reduces the life expectancy of individuals with DM by ~15 years despite current clinical intervention. Briefly, I will highlight the current clinical strategies and limitations encountered during the treatment of Type 1 or Type 2 DM.

1.1.5.1   Clinical Therapies for Type 1 Diabetes

From a pioneering studies performed in Canada, the discovery of insulin by Fredrick Banting, Charles Best, and John McLeod has prolonged the survival of Type 1 DM patients[95,96]. Insulin, a 29 a.a. peptide, was first discovered through intravenous administration of pancreatic extracts which temporary alleviated hyperglycemia in diabetic dogs. The first human patient to demonstrate clinical improvements was injected with purified insulin from bovine pancreas[97]. Today, insulin is primarily synthesized and purified from bacteria or yeast[98,99]; although this has not limited the considerable financial burden placed on insulin-dependent patients[67,100,101]. Moreover, there exists several types of insulin that differ based on their pharmacological onset and duration of therapeutic effect. Endogenous insulin is packages as a hexameric molecule within cytoplasmic vesicles and cleaved into monomers upon secretion. Exogenous insulin has exploited these properties to engineering insulin subunits which only exist as monomers

to longer-lasting insulin subunits. Despite these advancements, insulin therapy fails to recapitulate the fine-tuned physiological response observed in healthy subjects, thus replacement of functional β-cell mass is sought to achieve sustained reversal of insulin-dependence in individuals with Type 1 DM.

The Edmonton protocol provided pioneering evidence that replacement of functional β-cell mass could reverse severe Type 1 DM[102,103]. Specifically, Shapiro and colleagues demonstrated the infusion of human islets from 2-3 donor pancreas into the portal vein of the liver could alleviate insulin-dependence for up to 1-year in patients with Type 1 DM[104]. This procedure is still performed today yet is severely limited by the lack of donor pancreases and continued autoimmunity and islet rejection despite a parallel immunosuppressive regimen which leaves patients vulnerable to secondary infections[105]. These studies set the foundation for current regenerative medicine approaches which aim to either replace or regenerate endogenous β-cell mass. Current evidence suggests the orchestration of endocrine cell regeneration may entail a combination of endocrine-cell replication, transdifferentiation, and/or islet neogenesis[22,23,58,106-110]. Therefore, effective therapies entail a broad activation pro-regenerative signaling pathways, possibly in multiple cell targets. Albeit, the true effectiveness of either replacement or regeneration strategies will also depend upon the dampening of autoimmunity[111]. Accordingly, several strategies are currently being investigated to mitigate autoimmunity[112-114].

1.1.5.2 Clinical Therapies for Type 2 Diabetes

Individuals with Type 2 diabetes are commonly treated with pharmaceutical agents which aim to lower hyperglycemia independent of exogenous insulin administration. For example, Metformin is commonly prescribed to reduce blood glucose by dampening gluconeogenic activity of the liver and increasing peripheral insulin sensitivity[115]. In contrast, other pharmaceuticals, such as Sulfonylureas, act to lower blood glucose by enhancing the secretion of insulin from β-cells[116]. Recently, pharmaceutical inhibitors of SLGT2 (sodium-glucose co-transporter 2) aim to reduce glucose reuptake in the proximal tubule of the kidney[117]. For example, Empagliflozin administration reduced

hyperglycemia and Hemoglobin A1c by promoting the excretion of glucose through urination. Nonetheless, early diagnosis of Type 2 diabetes may permit reversal the disease through dietary and lifestyle changes[65,73,75,76,93,118,119]. As previously noted, public education is crucial to circumvent the epidemic progression of Type 2 DM. In contrast to Type 1 diabetes, undiagnosed Type 2 DM does not produce an immediate threat to survival; however, Type 2 DM occurs frequently with hyperlipidemia and leads to life-threatening cardiovascular comorbidities[5-7,9]. Therefore, individuals with Type 2 DM often require therapeutics to simultaneously combat cardiometabolic syndromes and peripheral insulin-resistance.

1.2 Cardiovascular Comorbidities of Diabetes

Individuals with DM are highly susceptible to developing secondary comorbidities, including neuropathy, nephropathy, retinopathy and gastrointestinal disorders[5-9,63,64]. Notably, prolonged periods of hyperglycemia and/or hyperlipemia leads to irreversible macrovessel and microvessel damage in 90% individuals with DM. Damage of microvasculature has be implicated in stroke, myocardial infarction, and peripheral limb ischemia[7,120]. Likewise, the disruption to microvascular networks can lead to renal[121] and neurological dysfunction[62,122], and loss of vision[123]. Collectively, loss of vascular networks reduces the delivery of oxygen and nutrients to tissues leading to system-wide cardiometabolic dysfunction. Thus, restoration of cardiovascular function using regenerative medicine approaches are relevant to the treatment of diabetic-related cardiovascular comorbidities, such as peripheral artery disease.

1.2.1 Vascular Biology and Architecture

Tissues in the human body require dynamic microvascular networks to receive vital nutrients and oxygen[124,125]. The cardiovascular system is quickly established during embryogenesis, such that embryonic tissues rely on paracrine signaling from endothelial

cells during organogenesis[126-129]. Development of vasculature is initiated during blood island formation within the early yolk sac[130]. Peripheral cells of blood islands generate angioblasts or endothelial-lineage committed stem cells[131], which migrate to the embryo to establish *de novo* vasculature structures, a process termed vasculogenesis. Subsequently, endothelial cell progenitors will undergo extensive proliferation and mediate sprouting from pre-existing vessels, i.e. angiogenesis, to establish well-defined vascular networks. Gradients of vessel-supportive cytokines, such as VEGF[132,133] or Angiopoietin family members[134-136], are primarily established by secondary cell populations [137,138], such as circulating hematopoietic cells[131,139,140] that provide stimuli which contribute to vasculature development.

The cardiovascular system is composed of a well-defined hierarchy of macro- and micro-vessel structures with distinct functions to maintain homeostasis[125]. At the center of the cardiovascular system, the heart continuously pumps oxygenated blood from the left ventricle through aorta[141] and downstream arteries (0.1-10mm diameter) and arterioles (100-300 um diameter) comprised of three distinct anatomical layers[142]. The tunica externa is outer most layer of arterial vessels and is primary composed of elastic fibers which function to support vessel stretching when encountering large volumes of blood flow. The tunica media is located between the Tunica externa and a basement membrane that separates the tunica intima. The tunica media is composed of smooth muscle cells which contribute to hemodynamic regulation throughout the body, such as regulation of arterial flow[142]. The tunica intima, found throughout all vessel types, is recognized as the continuous layer of endothelial cells that interacts with systemic circulation. Capillaries are the smallest vessels of the cardiovascular system and are the primary site of gas and nutrient exchange[143,144]. Depending on the tissue, endothelial cell permeability can become fenestrated to facilitate filtration (i.e. kidney glomeruli) or selectively impermeable, as seen in the blood brain barrier[145,146]. Subsequent networks of venules and veins return deoxygenated blood from capillaries towards pulmonary circulation for reoxygenation[147]. Similar to arteries, venules and veins contain three layers; however, differ by the relative thinness of the outer tunic layers, increased luminal diameter, and possess valves that prevent retrograde movement of blood as it is returned through the vena cava to the right atrium of the heart.

1.2.2   Endothelial Cells

Endothelial cells line the tunica intima of arterial and venous networks and act as the functional units of blood vessel to mediate communication between tissue cells and the systemic circulation. Based on the tissue type, endothelial cells receive extrinsic cues that guide their phenotype and function, relative to the needs of the tissue[145,148]. Additionally, endothelial cells provide paracrine signals that maintain vital cell populations in a variety of tissues, such as β-cells[128,149]. The symbiotic relationship between endothelial cells and adjacent cell populations has been previously demonstrated, such that the depletion of one population affects the development and survival of the other. Furthermore, revascularization during organ and tissue transplantation is crucial to the integration and function of transplanted tissues.   Endothelial cells are in constant communication the hematopoietic system during homeostasis and will release chemotactic and pro-inflammatory upon injury[150]. Additionally, endothelial cells are the primary source of nitric oxide production, a potent vasodilator that acts on adjacent smooth muscle cells when endothelial cells encounter elevated hemodynamics[151,152]. Endothelial cells are also sensitive to elevated lipid and glucose levels in the circulation and succumb to metabolic dysfunction[153]. In the context diabetes, injury-induced signals released from endothelial cells accelerate the infiltration of pro-inflammatory monocytes/macrophages, stimulate the proliferation and migration of mesenchymal cells, and activate pro-apoptotic signaling pathways neighbouring cells[5,153-158].

1.2.3   Smooth Muscle Cells and Pericytes

Within the Tunica media of large vessels, smooth muscle cells function to maintain endothelial cell homeostasis and can respond to innervating nervous tissues[142,159]. Smooth muscle cells maintain structural integrity of arterial vessels and regulate blood flow through vasomotor responses. As previously mentioned, endothelial cells release nitric oxide to stimulate vasodilation through activation of smooth muscle cells, preventing

downstream damage on fragile capillary networks. Smooth-muscle cells can be identified by the expression of α-SMA and lack markers of the endothelial lineage.

Related to smooth muscle cells, pericytes also provide structural and paracrine support with microvessel endothelial networks[143,160]. Pericytes support capillary homeostasis by maintaining a delicate balance of growth and regression and are recruited to site of angiogenesis via a PDGFRβ signaling axis[161]. Cardiometabolic disorders directly and indirectly affect pericyte and smooth muscle cell populations, generally leading to aberrant proliferation and fibrosis in response to elevated metabolic stress[159]. Pericytes can be detected by the expression of melanoma cell adhesion molecular (CD146) in the absence of hematopoietic or endothelial markers[161,162]. Crisan et al. demonstrated the selection of CD146^{+} cells from could establish multipotent stomal cell colony formation from a variety of postnatal tissues[163].

1.2.4   Atherosclerosis

Disruption of endothelial homeostasis and elevated levels of inflammation can lead to narrowing of blood vessels through the progressive formation of atherosclerotic plaques[138,152,164,165]. Specifically, prolonged periods of hyperglycemia or hyperlipidemia disturb endothelial permeability by increasing reactive oxygen species and decreasing homeostatic nitric oxide production. Subsequently inflammation initiates a cascade of monocyte infiltration, proliferation and M1 macrophage specification in response to excessive lipid deposition within the intimal layers of large vessels (Figure 1.6). Pro-inflammatory macrophages will readily scavenge excess lipids from interstitial layers of arterial vessels to generate pathogenic foam cells. Progressive accumulation of foam cells will develop into the first pathological hallmark of atherosclerosis, the fatty streak. Pro-inflammatory cytokines stimulate the proliferation and migration of smooth muscle cells towards the fatty streak. Activated smooth muscle cells will deposit fibrotic extracellular matrix that lead to the formation of a fibrous cap and *de novo* plaque formation. Extensive apoptosis of foam and smooth muscle cells will occur within the core of early plagues, accelerating the plaque growth through the deposition of lipids, lipoproteins, and

calcified deposits. Expansion of atherosclerotic plaques can lead to vessel occlusion and reduction of distal blood flow, as observed in patients with peripheral artery disease. These processes exacerbate over time until aggregation of platelet aggregation and infiltration of cytolytic leukocytes disrupts plaque integrity. Spontaneous rupturing of atherosclerotic plaques and subsequent thrombotic events can impose life-threatening events, such a myocardial infarction or stroke, by completely occluding arterial blood flow to the heart or brain[164]. Common risk factors that lead to atherosclerosis include: hypertension, hyperlipidemia, sedentary lifestyle, smoking, and diabetes.

1.2.5   Cardiovascular Disease

Cardiovascular disease (CVD) encompasses a broad range of pathophysiological conditions that primarily affect the function of the heart and/or vasculature[5-7,9]. These include a broad spectrum of ailments such as several clinical presentations of cardiac arrhythmias or myocardial infarction, heart failure, stroke, and peripheral artery disease. Collectively, CVD remains one of the leading causes of mortality in the world, accounting for ~30% of deaths [166,167]. Furthermore, CVD has placed a crippling burden on the healthcare system, total costs of $22 billion in Canada per year[168]. The manifestation of CVD is multifactorial and commonly presents in parallel with several cardiometabolic syndromes (i.e. diabetes, obesity, atherosclerosis etc.)[158,165,169]. Although genetic pre-dispositions exist, risk factors such as smoking, obesity, etc., are often avoidable[73,76,77,118,119]. Nonetheless, escalating rates of diabetes, hypertension, and obesity globally will inevitably lead to increased prevalence of CVD. It is estimated that nearly half of the population in the United States will develop CVD in the next decade[167], leading to a >2-fold increase in annual healthcare costs[170].

1.2.6   Peripheral Artery Disease and Critical Limb Ischemia

Atherosclerotic manifestation in the peripheral vasculature can lead to a partial or complete occlusion of blood flow to distal tissues (Figure 1.6), as observed in individuals with peripheral artery disease (PAD). 1 in 5 individuals with DM will eventually develop some form of PAD as a result of diabetes-induced dysfunction of the microvasculature[13,120,171-173]. It is estimated 800,000 individuals in Canada and >8 million individuals in the United States are afflicted with PAD[120,174]; and many patients with PAD do not present in the clinic until symptoms are severe. Peripheral artery disease can be diagnosed with a combination of physical exam, ankle-brachial index (ABI) measurements, ultrasound, blood tests, and/or angiography[172]. In many cases, non-healing wounds or ulcers in diabetic patients lead to diagnosis of PAD, at which point PAD has progressed beyond reversible stages (i.e. intermittent claudication) and intervention may be required. Critical limb ischemia (CLI) is the most severe form of PAD. Individuals with CLI present with resting pain, non-healing ulcers, secondary infections and tissue necrosis due to the severe ischemia in tissues distal to occluded vasculature. An estimated 1 in 3 patients diagnosed with CLI will require limb amputation; and >60% of patients will succumb to cardiovascular-related deaths within 5 years[175]. Current therapeutic strategies for PAD and CLI aim to target symptoms, slow disease progression, and/or prevent secondary adverse cardiovascular events[176].
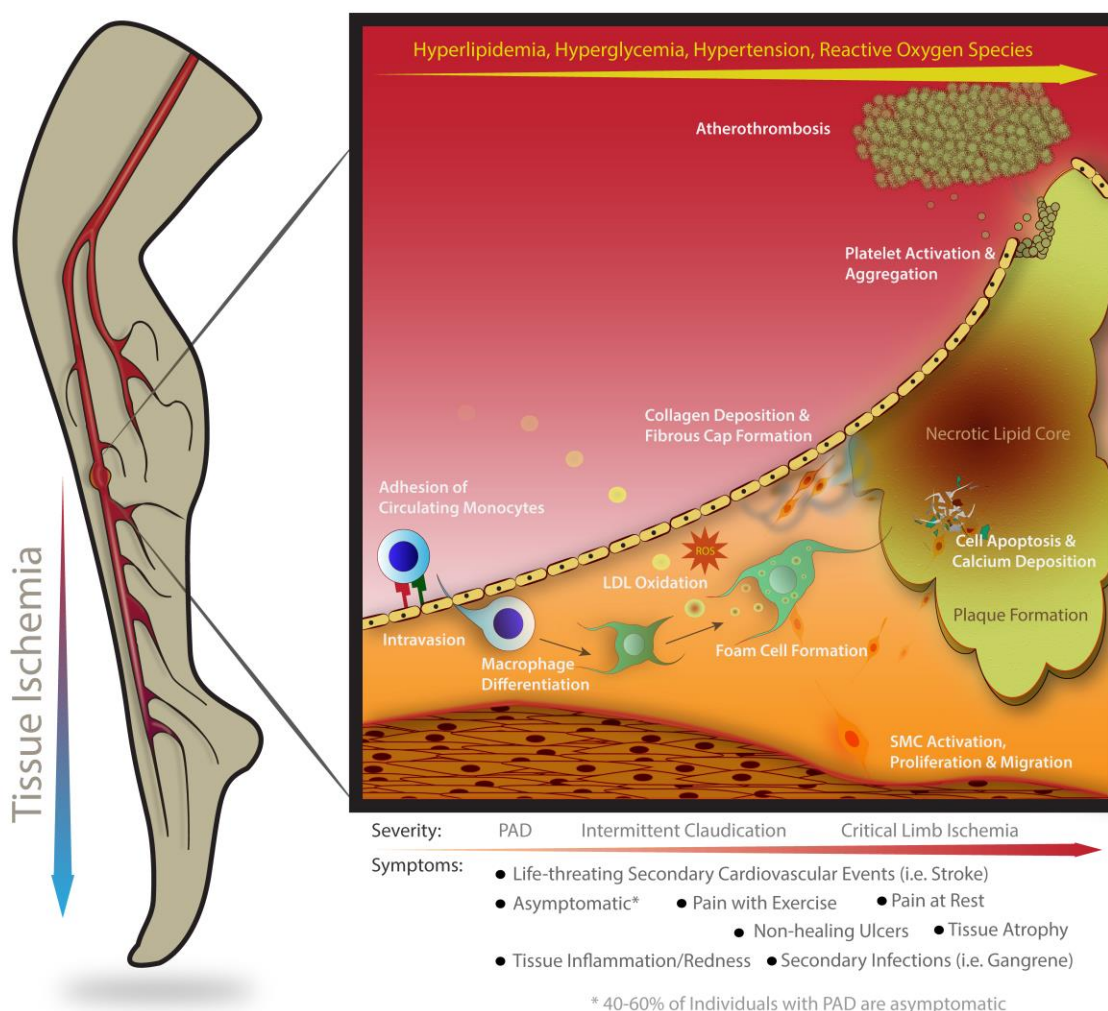
Figure 1.6 Overview of Atherosclerosis and Peripheral Artery Disease.
Cardiometabolic imbalances will disrupt endothelial health and permeability, leading to subintimal lipid accumulation and monocyte infiltration. Infiltrating monocytes will rapidly proliferate and differentiate into lipid-scavenging macrophages. Lipid accumulation within macrophages leads to foam cells formation and apoptosis within the atherosclerotic plaques. Plaque formation is also mediated by smooth muscle cell activation, proliferation, and the deposition of collagen and fibrous cap formation. As atherosclerosis progresses, endothelium is compromised, and platelet aggregation will occur. Late stages, plaque integrity is comprised and atherothrombosis formation occurs.

1.2.7   Strategies to Combat Vascular Disease

Currently, patient care for the primary treatment of PAD has two main goals; 1) management of symptoms to increase quality of life, and 2) mitigate the progression of atherosclerosis to prevent heart attack and stroke via pharmaceuticals and/or life-style changes[177]. Depending on the underlying health of an individual, pharmaceuticals primarily aim to reduce hyperlipidemia, hyperglycemia, hypertension, or the risk of platelet aggregation and clot formation[65,93]. To mitigate limb amputation for CLI, surgical interventions may be performed to increase the luminal diameter of a restricted artery (i.e. balloon-catheter angioplasty) or bypass occluded vasculature using autologous or synthetic grafts which re-establish blood flow from proximal to distal vasculature[176,178,179]. Unfortunately, a significant proportion of individuals with severe PAD are unsuitable surgical candidates due to diffuse microvascular blockage and underlying comorbidities. Alternative therapies that re-establish blood flow via the restoration of endothelial homeostasis and function have demonstrated preclinical potential. The field of regenerative medicine is actively investigating pharmaceutical, and gene or cell-based therapies to stimulate revascularization and restore tissue homeostasis[180,181].

1.3   Regenerative Medicine: A Historical Perspective

For centuries, scientists and physicians have proposed that the human body possessed considerable capacity to heal itself through tissue regeneration. For example, Greek mythology describes the story of Prometheus. As a punishment for stealing fire from the gods, Prometheus is chained to a rock where his liver is removed daily by an eagle of Zeus, only to have his liver grow back by the next day. The Greek physician Hippocrates was quoted as saying "Let food be thy medicine and medicine be thy food". In the context of Type 2 diabetes and cardiovascular comorbidities, Hippocrates' view would address a critical need to circumvent these pathologies through individual nutrition and lifestyle habits. Hippocrates' philosophy could also translate to the foundation of current

approaches which aim to discover therapeutic strategies that enhance regeneration and re-establish tissue homeostasis by activation of endogenous signaling networks. Within the following section, I will provide a foundational overview on the field regenerative medicine; specifically focusing on the applications of post-natal regenerative cell sources to develop biotherapeutics for DM and/or comorbid CVD pathologies.

1.3.1   Regenerative Medicine

Regenerative medicine encompasses a broad spectrum of therapeutic approaches and multidisciplinary efforts to restore physiological tissue function in the face of disease[182]. For example, regenerative medicine approaches to treat vascular complications of diabetes encompass efforts including: pro-angiogenic gene therapies[183], pro-vascular stem/progenitor cell transplantation[184], pharmaceutical or biological activation of pro-angiogenic pathways[185], biological and synthetic scaffold transplantation[186] and related efforts of tissue engineering[187]. At the core of regenerative medicine, is the aim to reverse deficiencies in tissue mass, cell function, and/or homeostatic signaling networks which underlie the pathophysiology of a disease. Stem cells hold undetermined potential to replace or regenerate damaged tissues; albeit, further research is critical to realize this potential. Accordingly, many labs are investigating the use of stem cells to treat chronic ailments, such as Type 1 DM and CLI.

1.3.2   Stem Cell Biology

First discovered by Canadian scientists, James Till and Ernest McCulloch[188], stem cells are defined by their capacity to undergo symmetric division without differentiation (self-renewal) while also demonstrating the capacity to differentiate into cells of multiple lineages (potency)[189]. Self-renewal is necessary for the long-term survival of stem cell pools throughout the lifetime of an individual so that expendable and functionally mature cells can be continuously replaced when damage or senescence occurs. The hierarchy of

cell potency apexes with totipotency (the ability to generate cells of the embryo and extraembryonic tissue) represented at fertilization and subsequent generation of a zygote. As embryogenesis proceeds and the morphogenesis of the blastocysts occurs, and cells of the inner cell mass (i.e. embryonic stem cells) are pluripotent (Figure 1.7). Pluripotency is the capacity of a cell to differentiate to all 3 germ layers of the embryo proper; i.e., ectoderm, mesoderm, endoderm. Embryonic stem cells are the only native tissue that
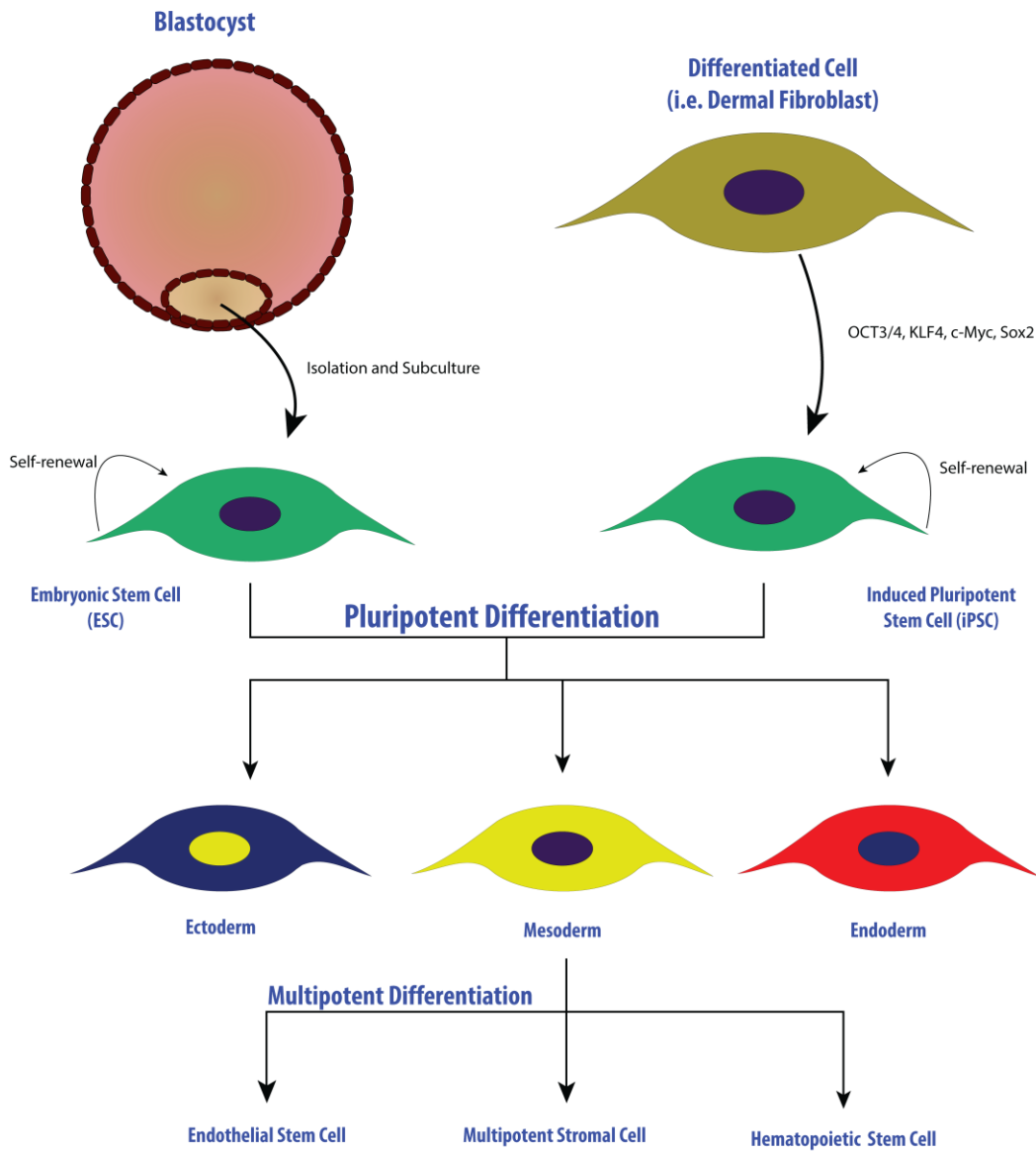
Figure 1.7 Working Model of Pluripotency and Multipotency in Stem Cells

demonstrate pluripotency in the human body, as adult stem cells exhibit multipotency generating multiple cell types within a specific germ layer. Notably, these barriers in potency have been shattered by Yamanaka's generation of induced-pluripotent stem cells from differentiated cells that may represent a potential source of patient specific-stem cells[190].

The turnover of cell in the human body requires compartmentalized differentiation of lineage-specific stem and progenitor cells that demonstrate multipotency, or the capacity to differentiate into multiple lineages of a single germ-layer[191,192]. For example, mesoderm-derived hematopoietic stem cells give rise to multipotent progenitor cells that are committed to differentiation of myeloid or lymphoid lineages of the hematopoietic system; moreover, these cells do not readily differentiate into related lineages such as endothelial or multipotent stromal cells. These stem and progenitor cells of the mesodermal lineage have been targeted in pre-clinical and clinical studies to treat diabetes and related cardiovascular complications[57,193-197]. The phenotypic identity of stem cell populations can be differentiated according to surface marker expression, such as CD34 expression on hematopoietic stem cells[198,199]. However, cell surface marker expression is dynamic and changes in response to injury or culture *in vitro*.

 Molecular functions unique to stem and progenitor that provide protection from cytotoxic insults can be used alone or in combination with surface markers to identify long-lived stem cell populations in a variety of fetal, postnatal, and adult cancerous tissues[200]. As an example, aldehyde dehydrogenase activity has been used as a conserved self-protective enzymatic function that protects against oxidative damage within multiple stem and progenitor cells lineages in tissues including blood[201], pancreas[202], brain, and colon[203]. In general, as cells differentiate toward functional maturity, ALDH-activity is reduced. Despite these protective mechanisms, accumulating evidence has demonstrated a microenvironment of chronic metabolic disease such as type 2 diabetes can lead to the depletion of stem and progenitor numbers, in addition to perturbation of regenerative function[74]. In the context of regenerative medicine, tissue specific stem and progenitor cells possess the potential to replace damaged or dysfunctional cells (i.e. β-cells or microvessels) through directed differentiation *ex vivo*[204] or through the activation of

dormant tissue-resident-progenitor cells via paracrine signaling mechanisms *in situ*[205]. To exemplify the latter, umbilical cord blood (UCB)-derived hematopoietic progenitor cells (HPC) with high aldehyde dehydrogenase activity demonstrate a multifaceted secretome that can stimulate β-cell and endothelial cell proliferation *in vivo* following cell transplantation without long-term engraftment or differentiation into damaged cell phenotypes[58,206].

1.3.3   Aldehyde Dehydrogenase and Retinoic Acid Signaling Pathway

Aldehyde dehydrogenase (ALDH) plays an essential role in embryogenesis and provides post-natal stem and progenitor cell populations long-term protection from cytotoxic insults[207]. The aldehyde dehydrogenase enzyme family contains 19 isoforms, with localization to cytosolic or mitochondrial compartments. Previously studies have demonstrated that ALDH2 is the main isoform expressed during early embryogenesis, whereas ALDH1 and ALDH3 isoforms are primarily expressed throughout post-natal tissues. In addition to providing cytosolic protection to reactive aldehyde species, ALDH is a rate-limiting step in the metabolism of retinol to retinoic acid (Figure 1.8).

Retinol (Vitamin A) is a cholesterol derivative taken up from circulation through Retinoic Acid 6/STRA6 expression at the plasma membrane of competent cells. Cytosolic retinol is metabolized by alcohol dehydrogenase family members (i.e. ADH10/11) to generate retinaldehyde (retinal). ALDH1A1 or ALDH1A3 oxidizes retinaldehyde to produce the lipophilic morphogen retinoic acid (RA). Following production, RA can be rapidly translocated from the cytosol to the nucleus by cellular retinoic acid-binding protein 2 (CRBP2) and presented to RA-receptor complexes to regulate transcriptional and epigenetic events. RA receptors exist as heterodimers consisting of one retinoic acid receptor (RARα, RARβ, RARγ) in conjunction with a retinoid X receptor isoform (RXRα, RXRβ, RXRγ)[208]. The binding of RA to the RAR alters the conformation of the complex from a transcriptional repressor to a transcriptional activator of numerous targets containing retinoic acid receptor elements (RAREs). Furthermore, induction by RA-signaling pathways regulates the transcription of several important genes that code for

proteins involved in RA-signaling including CRBP1/2 (cellular retinol binding protein), CRABP1/2 (cellular retinoic acid binding protein), and CYP26 (Cytochrome P450 family).
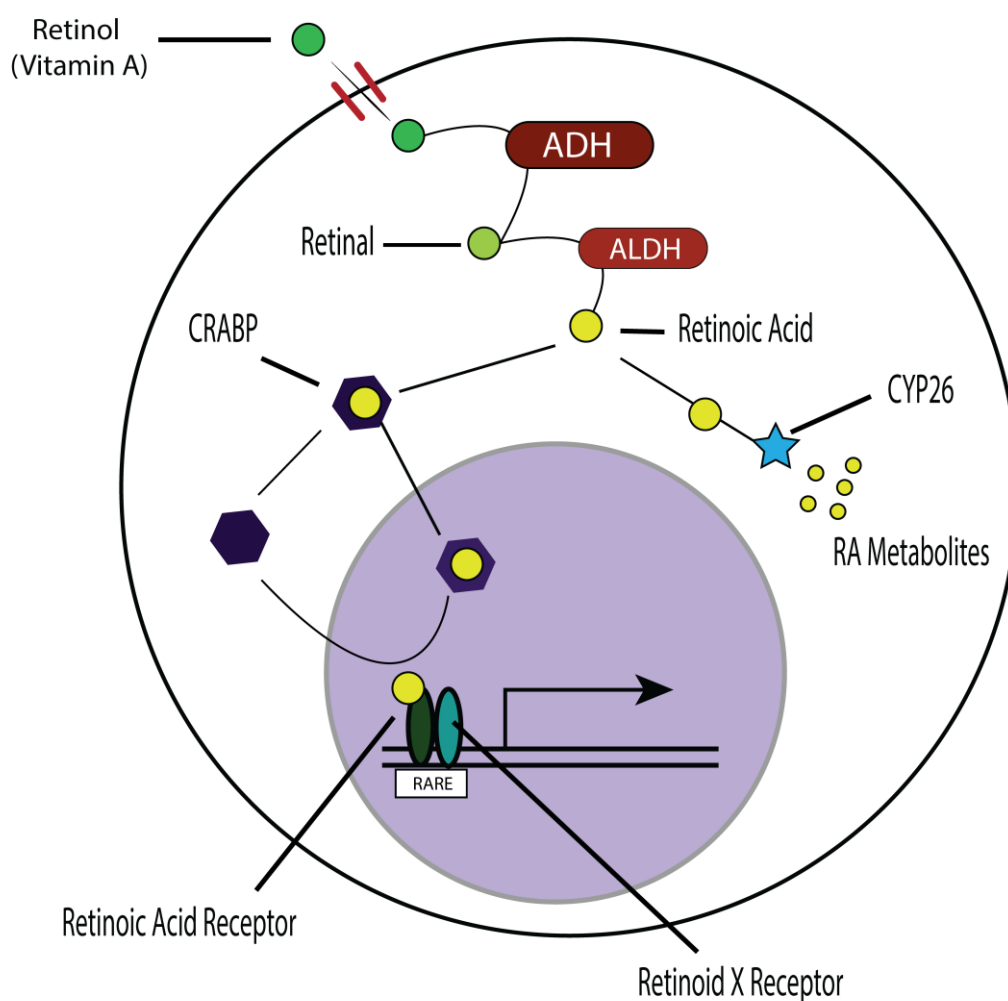
Figure 1.8 Working Model of Canonical Retinoic Acid Signaling Pathway. Retinol is imported through STRA6 (Stimulated by Retinoic Acid Receptor 6) and metabolize by ADH (Alcohol Dehydrogenase) to Retinal. Retinal is further metabolized by ALDH (Aldehyde Dehydrogenase) into RA (Retinoic Acid). RA is bound by CRABP (Cytosolic Retinoic Acid Binding Protein) which will translocate to the nucleus and present RA to RAR/RXR (Retinoic Acid Receptor/Retinoid X Receptor) heterodimer complexes bound to RARE (Retinoic Acid Response Element) which will regulate the transcription of downstream targets.

RA signaling was has been shown to function together with several other mitogens for the proper development and segmentation of the hindbrain, forebrain, upper limb buds, and foregut[207]. Previous studies have demonstrated that RA forms an opposing concentration gradient with CYP26 expression to set developmental boundaries during tissue patterning and organogenesis. RA gradients also play a crucial role during foregut development, more specifically, the proper development of the insulin-producing pancreas. Interestingly, xenopus models have demonstrated retinoic acid signaling to induce the endocrine-specification of ventral and dorsal buds[209]. Collectively, there exists a paradoxical and complex balance between the maintenance of high ALDH-activity in primitive stem cell populations while preventing differentiation through RA-signaling pathways.

1.3.4   Hematopoietic Stem and Progenitor Cells

Cells of the hematopoietic system serve multifunctional roles to maintain homeostasis in the body, overseeing processes such as immunity, tissue remodeling, wound response and delivery of oxygen. Therefore, maintenance of hematopoietic stem and progenitor cells is crucial and requires an intricate balance between self-renewal and differentiation[210]. Hematopoietic stem cells are originally derived from the blood islands of the yolk sac, before repopulating the aorta-gonad mesonephros regions of the developing embryo[131,210]. Subsequently, hematopoiesis takes place in the fetal liver before establishing permanent residence within the bone-marrow microenvironment[211]. Hematopoietic stem cells reside within the endosteal niche of the bone marrow that allows communication via endothelial and mesenchymal stromal cell populations. Accordingly, hematopoietic stem cells will receive signals that influence progenitor cell production and commitment towards myeloid or lymphoid lineages.
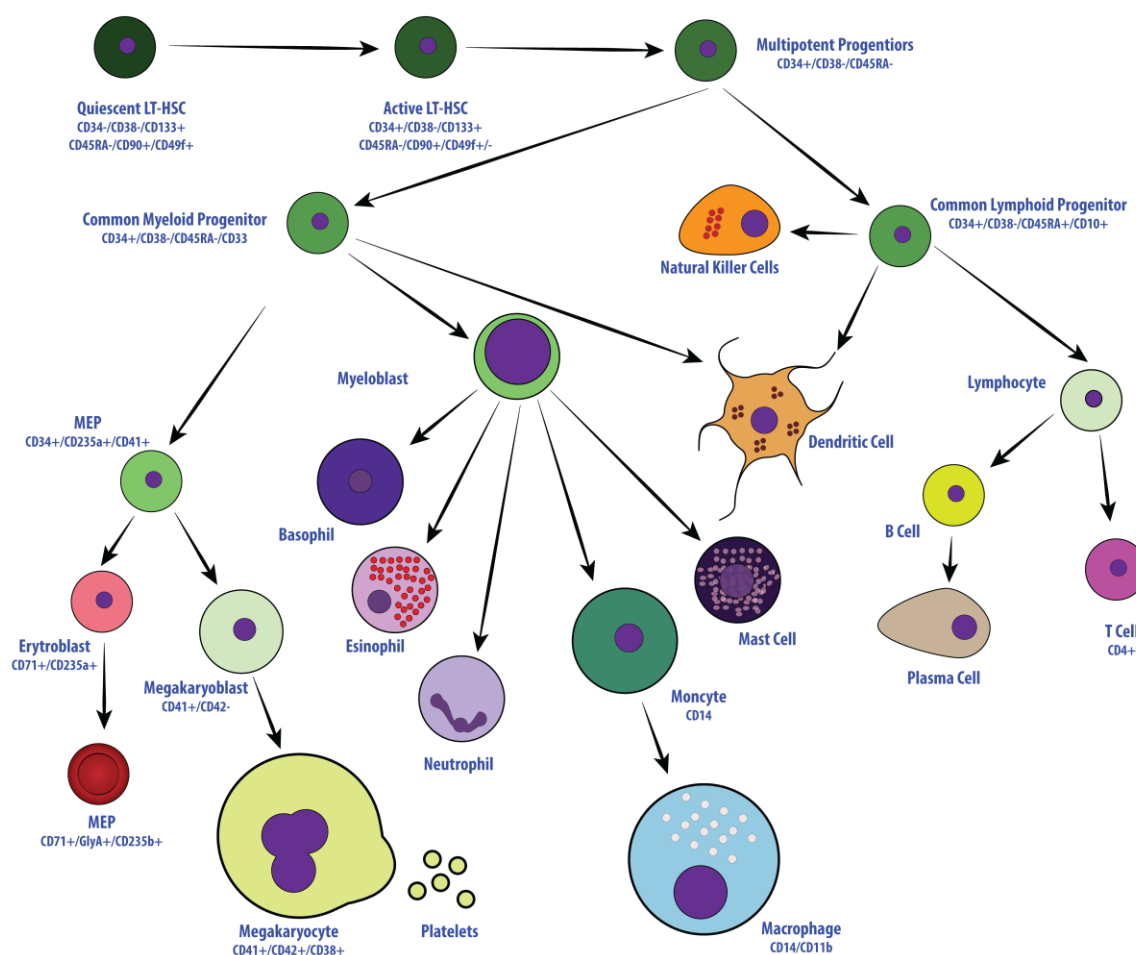
Figure 1.9 Overview of Hierarchy of Hematopoiesis with a specific focus on megakaryopoiesis**.** Working model of human hematopoiesis/megakaryopoiesis beginning with quiescent LT-HSC (Long-term Hematopoietic Stem Cell) and transiting to common myeloid progenitor cells. Unipotent MEP (Megakaryo-erythocyte progenitors) will give rise to CD41^{+} megakaryoblasts Megakaryopoiesis will continue with the emergence of CD41^{+}/CD42^{+} megakaryocytes capable of platelet generation.

Several phenotypic markers have been used to purify hematopoietic stem cells from fetal and adult tissues, such as CD34 and CD133[198,199]. Similarly, functional characteristics such a high ALDH-activity also identifies hematopoietic cells with primitive phenotypic and progenitor cell functions. The collective efforts of the Dick laboratory have primarily advanced our understanding of human hematopoiesis, including demonstrate single-cell HSC transplants can repopulate irradiated murine bone marrow[198]. Extending from this knowledge, members of the Bonnet laboratory have demonstrated that the apex of adult hematopoiesis may be a cell which lacks CD34 and co-expresses a phenotypic profile including $CD90^+/CD49f^+/CD45RA^-/CD38^-$[199] (Figure 1.9). Nonetheless, FACS purification based on CD34 expression and/or high ALDH-activity enriches for primitive hematopoietic cells capable of long-term hematopoietic reconstitution in immunodeficient mice (i.e. NOD/SCID)[212]. As hematopoietic stem and progenitor cells differentiate towards maturity the loss of CD34 expression occurs, combined with the acquisition of mature hematopoietic cell markers such as CD38[213]. Common myeloid progenitor cells will extensively proliferate and give rise to a bipotent progenitor that generates cells of the erythroid and megakaryocytic lineages, or a unipotent progenitor that generates neutrophils and monocytes. Conversely, select cell types may be derived from myeloid and/or lymphoid lineages (i.e. Dendritic cells)[214-216], rendering the phenotypic identification of intermediate stages of differentiation challenging. Towards this end, ALDH-activity is uniformly dampened as differentiation occurs across multiple hematopoietic lineages[201], suggesting sustained stem cells functions may be more indicative of primitive identity compared to the transient nature of cell surface marker expression[212,217].

Hematopoietic stem/progenitor cells (HSPC) have been used in a diverse range of clinical studies, including bone marrow transplantation for blood disorders[218] and revascularization strategies for CLI[193,194]. HSPC are readily isolated from a post-natal tissue, such as bone marrow, peripheral blood, and umbilical cord blood[219]. Unfortunately, therapeutic HSPC are rare, thus *ex vivo* expansion may be required for clinical translation for many potential applications. The expansion of HSPC has been met with multiple challenges such as tissue source, primitive cell selection, and culture conditions. Expansion of HSPC is challenged by the rapid induction of differentiation

due to intrinsic signaling networks, such as RA-signaling pathways. Previous studies have demonstrated the pharmacological inhibition or activation of select signaling pathways can enhance the expansion of therapeutic HSPC[220,221]. Furthermore, the Zandstra lab has demonstrated the dynamic regulation of microenvironmental signaling networks can lead to robust expansion of HSPC populations experimentally model *in silico*[222-225]. Finally, HSPC can be used in alternative therapies for their multifaceted therapeutic functions such as the stimulation of islet regeneration[57,58] or blood vessel formation[206,226]. Collectively, HSPC harbour multifunctional therapeutic potential that is limited by differentiation and loss of regenerative functions during expansion *ex vivo*. Further research is required to identity targetable signaling pathways which may retain or expand therapeutic HSPC.

1.3.5   Mesenchymal/Multipotent Stromal Cells

Since initial clinical use in 1995, multipotent stromal cells (MSC) has been the focus of over 200 clinical trials world-wide[227-229]. MSC, as known as mesenchymal stem cells, possess unique characteristics and can be enriched from several tissues according to the guidelines established by the International Society of Cellular Therapies (ISCT)[230]. According to these guidelines, MSC must demonstrate 1) plastic adherence 2) mesodermal multipotency (into adipose, bone, cartilage lineages), and 3) exhibit a distinct surface marker profile (Figure 1.10), which distinguishes it from related mesodermal cell contaminants (i.e. hematopoietic and endothelial). Specifically, MSC must express surface marker CD90 (Thy-1), CD73 (Ecto-5'-nucleotidase), and CD105 (Endoglin) after plastic adherent culture; meanwhile, lack the expression of CD45, CD31, CD14, HLA-DR, CD19, CD79a and CD34. MSC demonstrate a fibroblast-like morphology when cultured *ex vivo*, which has brought controversy to whether the fibroblasts and MSC are interchangeable[231-233]. Despite several groups reporting that select fibroblast lines can satisfy the ISCT guidelines[232-234], other studies have reported transcriptional and/or functional differences that may distinguish MSC from committed fibroblasts[231,235,236]. For example, MSC are highly proangiogenic and contribute to tissue

regeneration and immunomodulation via paracrine signaling networks. Therefore, the capacity for MSC to initiate tissue regeneration may be a defining characteristic to segregate MSC from fibroblasts[235], especially considering the well-established role of fibroblast activation during aging and many forms of pathogenesis[237,238].

MSC can be obtained from a variety of adult and fetal tissues, each with a unique phenotype and functional characteristics attributed to the tissue of origin[239,240]. For example, MSC classically isolated from BM express higher levels of pericyte marker CD146 and alkaline phosphatase compared to placental-derived MSC[241]; which reflects differences in osteogenic potential. Nonetheless, MSC should be considered highly heterogeneous and possess distinct subsets with unique surface marker expression (CD271, CD56, CD146), enzymatic expression (ALDH) and functional characteristics *in vitro* or *in vivo*[242,243]. For example, it has been reported that two distinct populations of BM MSC may exist[244,245]. A CD271$^+$/CD146$^+$ population that regulates the endosteal niche and hematopoiesis, while a 271$^+$/CD146$^-$ population that serves as a progenitor pool to generate osteoblasts of the skeletal bone. We have recently reported that the selection of high ALDH-activity *ex vivo* enriches for a BM-MSC with enhanced pro-angiogenic secretome[243]. Collectively, MSC are an attractive cell type with a safe therapeutic history and multifaceted regenerative functions, that may be further modulated by the selection of tissue-specific MSC and/or MSC subsets within heterogeneous expansion cultures.

Multipotent Stromal Cell (MSC)

Phenotype (*in vitro*)

CD73+   CD105+   CD90+
CD146+/-   CD31-   CD45-

Secretion of
Proregenerative Stimuli

Plastic Adhesion

Pro-angiogenic
Functions

Mesodermal Multipotency

Osteocyte (Bone)   Chrondrocyte (Cartilage)   Adipocyte (Fat)
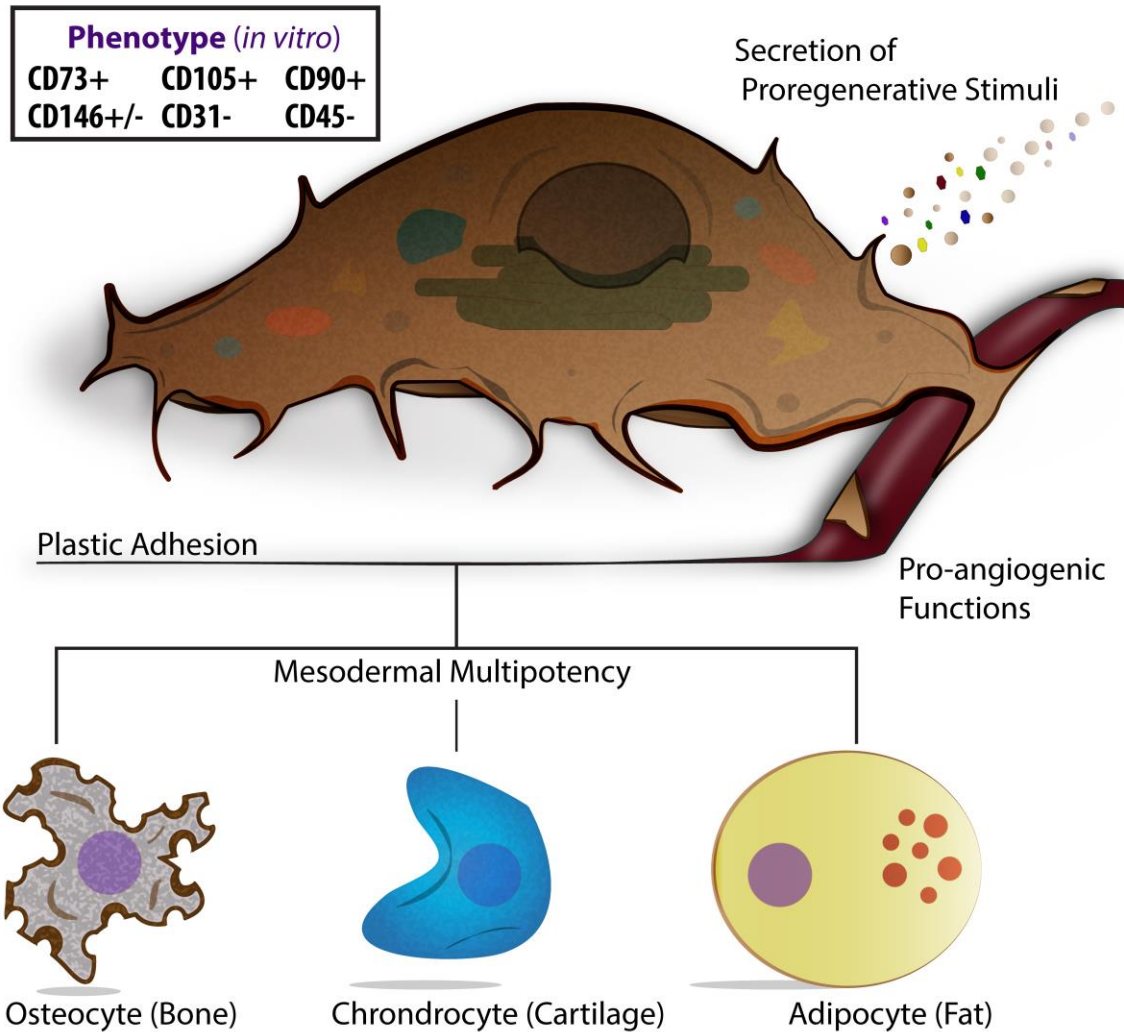
Figure 1.10 Working model of MSC phenotype, multipotency, and pro-regenerative secretome.

1.3.6   Cellular Therapies for Diabetes

The clinical demonstration that diabetes could be reversed via the restoration of functional β-cell mass[103,105], prompted researchers to discover novel methods to either replace or regenerate lost β-cell *in situ*. Currently, the leading approach to restore functional β-cell mass is through the transplantation of an exogenous β-cell source[246-248]. Whole pancreas transplantation has reversed diabetes in human patients, however the scarcity of donor pancreas tissue and a necessity for HLA-matching and/or immunosuppression has limited this approach[249]. Likewise, islet transplantation can reverse diabetes for prolonged periods, however, this approach is met with the same limitations as pancreas transplantation. The potential use of pluripotent stem cell (ESC or iPSC) technologies has promoted many laboratories to focus their efforts on *ex vivo* generation of an unlimited number of β-cells for transplantation[246]. Notably, Kieffer and colleagues have demonstrated that transplantation of ESC-derived PDX1$^+$ pancreatic progenitors was sufficient to reverse diabetes in rodent models (Ref). Transplanted PDX1$^+$ cells differentiated *in vivo* to generate a mixture of endocrine cell phenotypes, with significant representation by insulin-secreting β-like cells[204,250]. However, careful characterization of cell function revealed insulin secretion from PDX1$^+$ progenitors were ~10% of native β-cells, which highlights further work is needed to guide β-cell maturation either *ex vivo* or *in vivo*. In addition, the suppression of the autoimmune destruction of the transplanted β-like cells is necessary to sustain euglycemia. In pioneering efforts, bioengineering approaches have been tested to encapsulate transplanted PDX1$^+$ cells in a device that is permeable to the release of insulin while preventing immune cell infiltration[248].

In 2010, the Joslin "Medalist" study demonstrated residual β-cell mass and functional insulin secretion within individuals who have lived with Type 1 DM for >50 years[251]. Moreover, histological analysis of post-mortem patients has identified the presence of proliferating β-cells coinciding with β-cell apoptosis. Collectively, this study provided two foundational concepts; 1) residual β-cell mass is present in individuals with long-standing Type 1 DM and 2) β-cell proliferation can occur in the face of ongoing autoimmunity. Considering the destruction of β-cell mass is heterogeneous across the

pancreas and select regions may promote immune cells invasion, these results suggest that the stimulation of endogenous β-cell regeneration *in situ* may be feasible approach in T1 DM patients if autoimmunity can be controlled[107]. Towards this goal, our lab has pioneered studies demonstrating the transplantation of blood-derived progenitor cell populations can stimulate the regeneration of endogenous islets in murine models of DM[57,58,195,196,205]. Specifically, human HSPC and MSC populations derived from human UCB and/or BM can reduce hyperglycemia in NOD/SCID mice subjected to streptozotocin-induced β-cell ablation. The Prochymal trial was the first to attempt to alleviate early-onset Type 1 DM through the infusion of allogeneic BM-derived MSC harvested from a healthy donor[252]. Despite promising preclinical results, therapeutic efficacy observed in this study was transient and modest. Recently, we have demonstrated the secretome of expanded human MSC can act as an injectable biotherapeutic to potently stimulate islet regeneration[205], potentially circumventing the limitations encountered by direct cell transplantation, discussed below.

1.3.7   Cellular Therapies for Vascular Disease

The therapeutic goal for treating ischemic damage induced by vascular disease is to promote angiogenesis to revascularize and restore cardiometabolic homeostasis[253]. Initial trials for treating critical limb ischemia with progenitor cell transplantation, have primarily entailed the infusion of mononuclear cells derived from autologous sources[254,255]. Collectively, the efficacy of this approaches has been variable, showing improvements in ankle brachial index measurements and improved quality of life scores (Rutherford index), yet amputation rates were not improved in patients with severe CLI. Therefore, refined the cell selection, expansion, or transplantation of therapeutic cell populations is currently under intense investigation. Accordingly, Perin et al. recently concluded a clinical trial which explored the transplantation of autologous BM-cells purified for high ALDH-activity in patients with both critical limb ischemia and intermittent claudication[193,194]. The results of these studies did not show improved clinical efficacy over the transplantation of unpurified mononuclear cells. It is becoming evident

that the microenvironment of cardiometabolic disorders (i.e. diabetes, obesity, etc.) and cardiovascular disease can deplete progenitor cell numbers and diminish regenerative functions of pro-angiogenic cell types[256-259]. Thus, autologous progenitor cell transplantation carries severe limitations in the clinical setting.

Pre-clinical studies have demonstrated the therapeutic potential of progenitor cell transplantation for treating vascular disease, yet the translational rate to clinical efficacy has been notably underwhelming. In addition to the limitations linked to progenitor cell biology, current murine models of CVD and PAD do not accurately reflect pathophysiological observations observed in human studies[260]. Despite mice sharing ~95% of the protein-coding genome, there exists a measurable distinction between the regulatory or non-protein coding regions of the genome. These regions generate nucleic acid effectors that provide post-transcriptional/translational regulation of homeostatic and inflammatory pathways (i.e. micro-RNAs). As a result, cardiometabolic disorders and pathophysiology of vascular disease are not completely recapitulated in current murine models[261,262]. Specifically, transgenic models lack pathological hallmarks of human CVD such as lesion development, atherosclerotic plaque complexity, localization to coronary arteries, intimal thickening, and thrombotic plaque rupturing observed in human patients. Recently, vascular organoids have been generated from both adult[263-265] and pluripotent stem cell sources[266] that organize into a hierarchical arrangement and can be induced to exhibit characteristics of human pathology. The Penninger lab recently demonstrated organoids derived from human iPSC produced a physiologically-relevant arrangement of mesenchymal, endothelial, and hematopoietic cell that could self-assemble, and these vessels could mimic diabetic vasculopathy *in vitro* and *in vivo*[266]. From a speculative point-of-view, the use of vascular organoids to refine our understanding of vessel assembly will lead to development of novel therapies to treat vascular complications of diabetes[169].

1.3.8 Limitations of Cell Transplantation and the Development of Cell-free Biotherapeutics

Limitations of progenitor cell transplantation to treat diabetes and vascular disease primarily center around progenitor cell source and extensive expansion required for clinical application in humans. We have recently demonstrated additional 3-days of *ex vivo* culture significantly diminished primitive progenitor cell marker expression and provascular functions of UCB-derived HPC transplanted into in a murine model of hindlimb ischemia[226]. Our previous studies indicate that the regenerative function of transplanted progenitor cells may vary on an individual basis, such as donor health, body composition, co-morbidities and/or age[267,268]. Accumulating evidence has demonstrated the chronic diseases such as diabetes can disrupt progenitor cell homeostasis leading to the generation of a pro-inflammatory and pro-fibrotic secretome in mesenchymal cell populations[269-273]. The engraftment of transplanted progenitor cell populations is often transient[274], thus prolonging engraftment of transplanted cells may enhance therapeutic outcomes *in vivo*. Although, it is difficult to track the biodistribution of transplanted cells in human patients[275], recent advancements of biomedical imaging is allowing for high-resolution mapping of transplanted cell populations[276]. Collectively, current cell transplantation strategies are in need of approaches to enhance the expansion of therapeutic cell populations *ex vivo* or prolong engraftment *in vivo* without the loss of regenerative functions.

We have recently demonstrated that the secretome of BM-MSC can be concentrated to an injectable volume and used to stimulate human islet cell proliferation *in vitro*[277] and murine islet neogenesis *in vivo*[205]. Combining the benefits of protein and cell-based approaches are now warranted to: 1) identify therapeutic effectors and their recipient cell populations, 2) to determine if therapeutic secretome are progenitor cell-specific, and 3) investigate the generation of 'designer cells' to tailor the secretome of progenitor cell populations toward a treatable disease.

1.3.9   Extracellular Vesicles

The secretome of MSC contains regenerative stimuli secreted in the form of both protein and nucleic acids (miRNA and mRNA), which can contribute to pro-regenerative and pathological responses *in vivo*[278-282]. These regenerative cargoes can be packaged into extracellular vesicles (EVs) that signal in an autocrine and paracrine fashion to initiate tissue regeneration. EVs are lipid bi-layered vesicles which facilitate intercellular communication by protecting and transporting a unique set of cargo distinct from traditional cytokine secretion. Specifically, EVs contain protein, nucleic acids, and bioactive lipids each with a unique role in cellular communication (Figure 1.11). EVs can be subclassified based on their size and cellular-origin into exosomes and microparticles. Moreover, EVs are distinct from cell remnants, such as apoptotic bodies. Exosomes (30nm-100nm) are the smaller of the two EV sub-classifications and are derived from the endosomal pathway. Multivesicular bodies of the endosomal pathways are either shuttled to the lysosome for degradation or are repackage with unique cargo and released as exosomes via exocytosis[283]. In contrast, microparticles are larger in size (from 100nm-1μm) and are generated by blebbing of the cytoplasm and pinching of the cell membrane, leading to the direct release of microparticles to the environment surrounding the cell[284]. The generation of exosomes and microparticles is a highly regulated, although the mechanism of this organization remains obscure. Nonetheless, EVs contain cargo which can activate signaling pathways to significantly alter the physiology of recipient cells[285]. With these properties in mind, the contribution of EVs towards the MSC-generated secretome needs to be further investigated to develop novel regenerative therapies.

Extracelluar Vesicles (EVs) for Regenerative Medicine

Extracellular Vesicles (EVs)
Exosomes (30nm-100nm)
Micoparticles (100nm-1000nm)
Apoptotic Bodies (>1000nm)

Detection of EVs
Nanoscale Flow Cytomtery
Atomic Force Microscopy
Confocal Microscopy (Celluar Uptake)
Flow Cytomtery (Celluar Uptake)
Mass Spectomtery
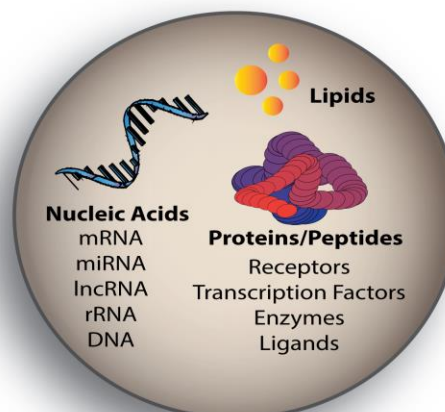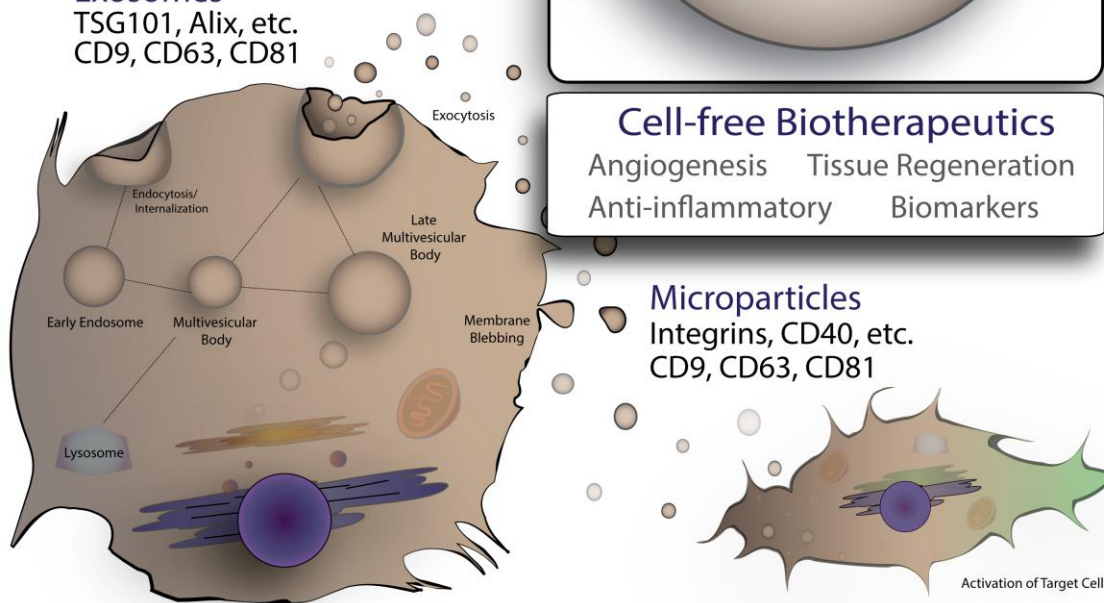
Figure 1.11 Overview of Extracellular Vesicle Secretion, Detection, and Applications of Regenerative Medicine

1.3.10   Designer Cells and the Future of Regenerative Medicine

Recent advancement in genetic engineering strategies, such as CRISPR[286-288], and in-depth molecular analyses (i.e. Mass Spectrometry, Single-cell RNAseq) hold the potential to be used as vital tools of regenerative medicine. More specifically, global transcriptional and translational analyses provide us with a better understanding of the molecular characteristics within 1) therapeutic donor cell populations, 2) targeted endogenous cell populations for tissue regeneration, 3) dysfunctional/depleted cell populations during disease. In return, this insight will permit the directed activation of pro-regenerative pathways within therapeutic donor and target cell populations, in an attempt to combat disease. As an example of this concept, we have recently demonstrated that canonical Wnt-signaling within MSC is dampened as regenerative functions are lost during *ex vivo* culture[277]. Accordingly, the activation of Wnt-signaling during cell propagation enhanced the therapeutic efficacy of the BM-MSC secretome following intrapancreatic delivery of this 'designer' biotherapeutic. Other examples of current designer cell strategies to advance the field of regenerative medicine, include the generation of β-cells from pluripotent stem cell sources[246], modelling of human diabetes and/or cardiovascular disease within cultured organoid systems[266], and T cell[289] or NK cell[290] engineering to target tumor cells. On the horizon of regenerative medicine is the advancement of biological scaffold design[186,291], 3D tissue engineering[292], and *in silico* experimentation with machine learning[293]. Therefore, this is an exciting time for regenerative medicine approaches yet there currently exists a need to characterize the molecular properties of regenerative cell populations with multifaceted therapeutic potential.

1.4 Thesis Overview and Hypotheses

Patients with diabetes are burdened with an increased risk of developing life-threating cardiovascular comorbidities. Regenerative medicine and cellular therapies possess the potential to develop curative therapies for diabetes and/or cardiovascular complications. Unfortunately, the depletion and dysfunction of therapeutic cell populations occurs as a result of chronic disease, limiting the clinical efficacy of autologous cell transplantation. Allogenic sources, such as UCB, offer an alternative source of therapeutic progenitor cells that are untouched by chronic inflammation and oxidative stress; but require extensive expansion *ex vivo* to generate clinically relevant cell numbers without the loss of regenerative functions. Similarly, MSC represents another therapeutic cell population which requires extensive expansion for clinical applications. In addition, the secretome of MSC may be used as cell-free biotherapeutic[278-282], although further research is necessary to refine this approach. During the course of my thesis, I focused on addressed two major challenges faced by direct cell transplantation; 1) the limitations of progenitor cell expansion *ex vivo*, and 2) directed delivery of pro-regenerative stimuli to damaged tissues. First, I demonstrated that the inhibition of RA-signaling could enhance the expansion of UCB-derived HSPC with multifaceted therapeutic potential. Second, I demonstrated that MSC derived from human pancreatic tissue generate extracellular vesicles with both vascular and islet regenerative stimuli. Throughout these studies, I utilized mass spectrometry and multiparametric flow cytometry to identify novel proteomic characteristics of both HPC and MSC subsets. Additionally, I performed xenotransplantation studies to investigate tissue regeneration induced by human cells after femoral artery ligation-induced hindlimb ischemia or streptozotocin-induced β-cell ablation.

1.4.1   Chapter 2: Objective & Hypothesis

1. To characterize proteomic changes during the expansion of UCB ALDH^{hi} cells using label-free mass spectrometry and multiparametric flow cytometry.

2. To assess whether inhibition of ALDH-activity will enhance the expansion of UCB ALDH^{hi} cells while retaining primitive surface marker and hematopoietic functions *in vitro*.

3. To determine whether inhibition of ALDH-activity will expand hematopoietic progeny that stimulate vascular regeneration in a murine model of hindlimb ischemia.

In chapter 2, *I hypothesized that reversible inhibition of ALDH-activity, using diethylaminobenzaldehyde (DEAB), will enhance expansion of UCB-derived hematopoietic progenitor cells while retaining primitive surface marker phenotype and pro-angiogenic functions in vivo.*

1.4.2   Chapter 3: Objective & Hypothesis

1. To investigate the enrichment of the megakaryocyte-lineage during expansion of UCB ALDH^{hi} cells.

2. To determine whether FACS purification of ALDH^{hi} cells, after *ex vivo* expansion under DEAB-treated conditions, reselects for cells with pro-angiogenic functions *in vitro*.

3. To determine whether FACS purification of ALDH^{hi} cells, under DEAB-treated conditions, reselects for cells retaining islet regenerative functions.

In chapter 3, *I hypothesized that reversible inhibition of ALDH-activity, via diethylaminobenzaldehyde (DEAB), will enhance the expansion of UCB-derived hematopoietic progenitor cells retaining a primitive surface marker phenotype and islet regenerative functions in vivo.*

1.4.3   Chapter 4: Objective & Hypothesis

1. To determine fibroblast-like cells derived from human islet cultures demonstrate MSC-like phenotype and multipotent functions *in vitro*.

2. To conduct proteomic comparison of Panc-MSC to BM-MSC using mass spectrometry

3. To determine the competency of Panc-MSC to respond to pro-neural or pro-adipogenic stimuli

In chapter 4, *I hypothesized that fibroblast-like cells established from human islets will demonstrate phenotypic and functional characteristics of MSC with tissue-specific functional characteristics.*

1.4.4   Chapter 5: Objective & Hypothesis

1. To characterize the protein content within extracellular vesicle versus the soluble fraction generated by Panc-MSC

2. To determine whether pro-vascular stimuli within extracellular vesicles generated by Panc-MSC can improve revascularization after injection into ischemic hindlimbs.

In chapter 5, *I hypothesized that extracellular vesicles generated by Panc-MSC would contain pro-vascular stimuli capable that accelerate the recovery of hindlimb blood perfusion and revascularization in a murine model of hindlimb ischemia.*

1.4.5   Chapter 6: Objective & Hypothesis

3. To characterize the protein content within extracellular vesicle versus the soluble fraction generated by Panc-MSC

4.   To determine whether islet regenerative stimuli within extracellular vesicles generated by Panc-MSC can improve hyperglycemia after injection into pancreas of streptozotocin-treated NOD/SCID mice.

In chapter 6, *I hypothesized that the secretome of Panc-MSC contains islet-regenerative stimuli that can reduce hyperglycemia in NOD/SCID subjected to STZ-induced β-cell ablation.*

1.5 References

1 Trowell, H. C. Ants distinguish diabetes mellitus from diabetes insipidus. *British medical journal (Clinical research ed.)* **285**, 217 (1982).

2 MacCracken, J., Hoel, D. & Jovanovic, L. From ants to analogues: Puzzles and promises in diabetes management. *Postgraduate medicine* **101**, 138-150 (1997).

3 Robertson, G. L. Diabetes insipidus. *Endocrinology and metabolism clinics of North America* **24**, 549-572 (1995).

4 Bliss, M. *The discovery of insulin*. (University of Chicago Press, 2013).

5 Stern, M. P. Diabetes and cardiovascular disease: the "common soil" hypothesis. *Diabetes* **44**, 369-374 (1995).

6 Kannel, W. B. & McGee, D. L. Diabetes and cardiovascular disease: the Framingham study. *Jama* **241**, 2035-2038 (1979).

7 Sowers, J. R., Epstein, M. & Frohlich, E. D. Diabetes, hypertension, and cardiovascular disease: an update. *Hypertension* **37**, 1053-1059 (2001).

8 Control, D., Interventions, C. T. E. o. D. & Group, C. S. R. Intensive diabetes treatment and cardiovascular disease in patients with type 1 diabetes. *New England Journal of Medicine* **353**, 2643-2653 (2005).

9 Gæde, P. *et al.* Multifactorial intervention and cardiovascular disease in patients with type 2 diabetes. *New England Journal of Medicine* **348**, 383-393 (2003).

10 Group, N. D. D. Classification and diagnosis of diabetes mellitus and other categories of glucose intolerance. *Diabetes* **28**, 1039-1057 (1979).

11 Association, A. D. Diagnosis and classification of diabetes mellitus. *Diabetes care* **33**, S62-S69 (2010).

12 Association, A. D. Gestational diabetes mellitus. *Diabetes care* **27**, s88-s90 (2004).

13 Atlas, I. D. 1-145 (Brussels, Belgium 2018).

14 Jennings, R. E. *et al.* Development of the human pancreas from foregut to endocrine commitment. *Diabetes* **62**, 3514-3522 (2013).

15 Jennings, R. E., Berry, A. A., Strutt, J. P., Gerrard, D. T. & Hanley, N. A. Human pancreas development. *Development* **142**, 3126-3137 (2015).

16 Collombat, P. *et al.* Opposing actions of Arx and Pax4 in endocrine pancreas development. *Genes & development* **17**, 2591-2603 (2003).

17 Lebenthal, E. & Lee, P. Development of functional response in human exocrine pancreas. *Pediatrics* **66**, 556-560 (1980).

18 Vacca, J. B., Henke, W. J. & Knight, W. A. The exocrine pancreas in diabetes mellitus. *Annals of internal medicine* **61**, 242-247 (1964).

19 Inada, A. *et al.* Carbonic anhydrase II-positive pancreatic cells are progenitors for both endocrine and exocrine pancreas after birth. *Proceedings of the National Academy of Sciences* **105**, 19915-19919 (2008).

20 Furuyama, K. *et al.* Continuous cell supply from a Sox9-expressing progenitor zone in adult liver, exocrine pancreas and intestine. *Nature genetics* **43**, 34 (2011).

21 Wells, J. M. *et al.* Wnt/β-catenin signaling is required for development of the exocrine pancreas. *BMC developmental biology* **7**, 4 (2007).

22 Beer, R. L., Parsons, M. J. & Rovira, M. Centroacinar cells: at the center of pancreas regeneration. *Developmental biology* **413**, 8-15 (2016).

23 Zhou, Q. & Melton, D. A. Pancreas regeneration. *Nature* **557**, 351 (2018).

24 Murtaugh, L. C. & Keefe, M. D. Regeneration and repair of the exocrine pancreas. *Annual review of physiology* **77**, 229-249 (2015).

25 Lehv, M. & Fitzgerald, P. Pancreatic acinar cell regeneration. IV. Regeneration after resection. *The American journal of pathology* **53**, 513 (1968).

26   Zhou, Q., Brown, J., Kanarek, A., Rajagopal, J. & Melton, D. A. In vivo reprogramming of adult pancreatic exocrine cells to β-cells. *nature* **455**, 627 (2008).

27   Muraro, M. J. *et al.* A single-cell transcriptome atlas of the human pancreas. *Cell systems* **3**, 385-394. e383 (2016).

28   Bouwens, L., Lu, W. & De Krijger, R. Proliferation and differentiation in the human fetal endocrine pancreas. *Diabetologia* **40**, 398-404 (1997).

29   Andralojc, K. *et al.* Ghrelin-producing epsilon cells in the developing and adult human pancreas. *Diabetologia* **52**, 486-493 (2009).

30   Tschöp, M., Smiley, D. L. & Heiman, M. L. Ghrelin induces adiposity in rodents. *Nature* **407**, 908 (2000).

31   Richards, O. C., Raines, S. M. & Attie, A. D. The role of blood vessels, endothelial cells, and vascular pericytes in insulin secretion and peripheral insulin action. *Endocrine reviews* **31**, 343-363 (2010).

32   Röder, P. V., Wu, B., Liu, Y. & Han, W. Pancreatic regulation of glucose homeostasis. *Experimental & molecular medicine* **48**, e219 (2016).

33   Quesada, I., Tudurí, E., Ripoll, C. & Nadal, A. Physiology of the pancreatic α-cell and glucagon secretion: role in glucose homeostasis and diabetes. *Journal of Endocrinology* **199**, 5-19 (2008).

34   Drucker, D. J. The role of gut hormones in glucose homeostasis. *The Journal of clinical investigation* **117**, 24-32 (2007).

35   Meyer, C., Dostou, J. M., Welle, S. L. & Gerich, J. E. Role of human liver, kidney, and skeletal muscle in postprandial glucose homeostasis. *American Journal of Physiology-Endocrinology And Metabolism* **282**, E419-E427 (2002).

36   Collaboration, E. R. F. Diabetes mellitus, fasting glucose, and risk of cause-specific death. *New England Journal of Medicine* **364**, 829-841 (2011).

37   Johnston, N. R. *et al.* B cell hubs dictate pancreatic islet responses to glucose. *Cell metabolism* **24**, 389-401 (2016).

38   Thorens, B. GLUT2, glucose sensing and glucose homeostasis. *Diabetologia* **58**, 221-232 (2015).

39   Li, J., Shuai, H., Gylfe, E. & Tengholm, A. Oscillations of sub-membrane ATP in glucose-stimulated β cells depend on negative feedback from Ca 2+. *Diabetologia* **56**, 1577-1586 (2013).

40   Meissner, H. & Schmelz, H. Membrane potential of β-cells in pancreatic islets. *Pflügers Archiv* **351**, 195-206 (1974).

41   Abel, E. D. *et al.* Adipose-selective targeting of the GLUT4 gene impairs insulin action in muscle and liver. *Nature* **409**, 729 (2001).

42   Leto, D. & Saltiel, A. R. Regulation of glucose transport by insulin: traffic control of GLUT4. *Nature reviews Molecular cell biology* **13**, 383 (2012).

43   Baggio, L. L. & Drucker, D. J. Biology of incretins: GLP-1 and GIP. *Gastroenterology* **132**, 2131-2157 (2007).

44   Vilsbøll, T. & Holst, J. J. Incretins, insulin secretion and type 2 diabetes mellitus. *Diabetologia* **47**, 357-366 (2004).

45   Ekblad, E. & Sundler, F. Distribution of pancreatic polypeptide and peptide YY. *Peptides* **23**, 251-261 (2002).

46   Strowski, M., Parmar, R., Blake, A. & Schaeffer, J. Somatostatin inhibits insulin and glucagon secretion via two receptor subtypes: an *in vitro* study of pancreatic islets from somatostatin receptor 2 knockout mice. *Endocrinology* **141**, 111-117 (2000).

47   Daneman, D. Type 1 diabetes. *The Lancet* **367**, 847-858 (2006).

48   Palmer, J. P. & Hirsch, I. B.   (Am Diabetes Assoc, 2003).

49   Patterson, C. *et al.* Trends in childhood type 1 diabetes incidence in Europe during 1989–2008: evidence of non-uniformity over time in rates of increase. *Diabetologia* **55**, 2142-2147 (2012).

50   Eisenbarth, G. S. Type I diabetes mellitus. *New England journal of medicine* **314**, 1360-1368 (1986).

51   Virtanen, S. M. Dietary factors in the development of type 1 diabetes. *Pediatric diabetes* **17**, 49-55 (2016).

52   Stankov, K., Benc, D. & Draskovic, D. Genetic and epigenetic factors in etiology of diabetes mellitus type 1. *Pediatrics* **132**, 1112-1122 (2013).

53   Patel, K. A. *et al.* Type 1 diabetes genetic risk score: a novel tool to discriminate monogenic and type 1 diabetes. *Diabetes* **65**, 2094-2099 (2016).

54   Van Belle, T. L., Coppieters, K. T. & Von Herrath, M. G. Type 1 diabetes: etiology, immunology, and therapeutic strategies. *Physiological reviews* **91**, 79-118 (2011).

55   Hyöty, H. Viruses in type 1 diabetes. *Pediatric diabetes* **17**, 56-64 (2016).

56   Rees, D. & Alcolado, J. Animal models of diabetes mellitus. *Diabetic medicine* **22**, 359-370 (2005).

57   Seneviratne, A. K. *et al.* Expanded hematopoietic progenitor cells reselected for high aldehyde dehydrogenase activity demonstrate islet regenerative functions. *Stem Cells* **34**, 873-887 (2016).

58   Bell, G., Putman, D., Hughes-Large, J. & Hess, D. Intrapancreatic delivery of human umbilical cord blood aldehyde dehydrogenase-producing cells promotes islet regeneration. *Diabetologia* **55**, 1755-1760 (2012).

59   DiMeglio, L. A., Evans-Molina, C. & Oram, R. A. Type 1 diabetes. *The Lancet* **391**, 2449-2462 (2018).

60   Thompson, P. J. *et al.* Targeted Elimination of Senescent B Cells Prevents Type 1 Diabetes. *Cell metabolism* (2019).

61   Eppens, M. C. *et al.* Prevalence of diabetes complications in adolescents with type 2 compared with type 1 diabetes. *Diabetes care* **29**, 1300-1306 (2006).

62   Boulton, A. J. *et al.* Diabetic neuropathies: a statement by the American Diabetes Association. *Diabetes care* **28**, 956-962 (2005).

63   González-Clemente, J. *et al.* Diabetic neuropathy is associated with activation of the TNF-α system in subjects with type 1 diabetes mellitus. *Clinical endocrinology* **63**, 525-529 (2005).

64   Shakil, A., Church, R. J. & Rao, S. S. Gastrointestinal complications of diabetes. *American family physician* **77** (2008).

65   Association, A. D. 7. Obesity management for the treatment of type 2 diabetes. *Diabetes care* **40**, S57-S63 (2017).

66   Hu, F. B. *et al.* Diet, lifestyle, and the risk of type 2 diabetes mellitus in women. *New England journal of medicine* **345**, 790-797 (2001).

67   Seuring, T., Archangelidi, O. & Suhrcke, M. The economic costs of type 2 diabetes: a global systematic review. *Pharmacoeconomics* **33**, 811-831 (2015).

68   DeFronzo, R. A. Pathogenesis of type 2 diabetes mellitus. *Medical Clinics* **88**, 787-835 (2004).

69   Zhu, Y. & Zhang, C. Prevalence of gestational diabetes and risk of progression to type 2 diabetes: a global perspective. *Current diabetes reports* **16**, 7 (2016).

70   Chatterjee, S., Khunti, K. & Davies, M. J. Type 2 diabetes. *The Lancet* **389**, 2239-2251 (2017).

71   Jaacks, L. M., Siegel, K. R., Gujral, U. P. & Narayan, K. V. Type 2 diabetes: a 21st century epidemic. *Best Practice & Research Clinical Endocrinology & Metabolism* **30**, 331-343 (2016).

72   van der Berg, J. D. *et al.* Associations of total amount and patterns of sedentary behaviour with type 2 diabetes and the metabolic syndrome: The Maastricht Study. *Diabetologia* **59**, 709-718 (2016).

73   Powers, M. A. *et al.* Diabetes self-management education and support in type 2 diabetes: a joint position statement of the American Diabetes Association, the American Association of Diabetes Educators, and the Academy of Nutrition and Dietetics. *The Diabetes Educator* **43**, 40-53 (2017).

74   Hartstra, A. V., Bouter, K. E., Bäckhed, F. & Nieuwdorp, M. Insights into the role of the microbiome in obesity and type 2 diabetes. *Diabetes care* **38**, 159-165 (2015).

75   Tuomilehto, J. *et al.* Prevention of type 2 diabetes mellitus by changes in lifestyle among subjects with impaired glucose tolerance. *New England Journal of Medicine* **344**, 1343-1350 (2001).

76   Coppola, A., Sasso, L., Bagnasco, A., Giustina, A. & Gazzaruso, C. The role of patient education in the prevention and management of type 2 diabetes: an overview. *Endocrine* **53**, 18-27 (2016).

77   Henson, J., Dunstan, D. W., Davies, M. J. & Yates, T. Sedentary behaviour as a new behavioural target in the prevention and treatment of type 2 diabetes. *Diabetes/metabolism research and reviews* **32**, 213-220 (2016).

78   Besseling, J., Kastelein, J. J., Defesche, J. C., Hutten, B. A. & Hovingh, G. K. Association between familial hypercholesterolemia and prevalence of type 2 diabetes mellitus. *Jama* **313**, 1029-1036 (2015).

79   Li, Y. *et al.* Exposure to the Chinese famine in early life and the risk of hyperglycemia and type 2 diabetes in adulthood. *Diabetes* **59**, 2400-2406 (2010).

80   de Rooij, S. R., Painter, R. C., Holleman, F., Bossuyt, P. M. & Roseboom, T. J. The metabolic syndrome in adults prenatally exposed to the Dutch famine. *The American journal of clinical nutrition* **86**, 1219-1224 (2007).

81   Pessin, J. E. & Saltiel, A. R. Signaling pathways in insulin action: molecular targets of insulin resistance. *The Journal of clinical investigation* **106**, 165-169 (2000).

82   Bollheimer, L. C., Skelly, R. H., Chester, M. W., McGarry, J. D. & Rhodes, C. J. Chronic exposure to free fatty acid reduces pancreatic β cell insulin content by increasing basal insulin secretion that is not compensated for by a corresponding increase in proinsulin biosynthesis translation. *The Journal of clinical investigation* **101**, 1094-1101 (1998).

83   Cerasi, E., Kaiser, N. & Leibowitz, G. Type 2 diabetes and β cell apoptosis. *Diabetes & metabolism* **26**, 13-16 (2000).

84   Cerf, M. E. B cell dysfunction and insulin resistance. *Frontiers in endocrinology* **4**, 37 (2013).

85   Bonner-Weir, S., Trent, D. & Weir, G. Partial pancreatectomy in the rat and subsequent defect in glucose-induced insulin release. *The Journal of clinical investigation* **71**, 1544-1553 (1983).

86   Kumar, A. F., Gruessner, R. W. & Seaquist, E. R. Risk of glucose intolerance and diabetes in hemipancreatectomized donors selected for normal preoperative glucose metabolism. *Diabetes Care* **31**, 1639-1643 (2008).

87   Kim, A. *et al.* Islet architecture: a comparative study. *Islets* **1**, 129-136 (2009).

88   e Drigo, R. A. *et al.* New insights into the architecture of the islet of Langerhans: a focused cross-species assessment. *Diabetologia* **58**, 2218-2228 (2015).

89   Steiner, D. J., Kim, A., Miller, K. & Hara, M. Pancreatic islet plasticity: interspecies comparison of islet architecture and composition. *Islets* **2**, 135-145 (2010).

90   Sato, T., Herman, L. & Fitzgerald, P. J. The comparative ultrastructure of the pancreatic islet of Langerhans. *General and Comparative Endocrinology* **7**, 132-157 (1966).

91   In't Veld, P. & Smeets, S. Microscopic anatomy of the human islet of Langerhans. *Islets of Langerhans, 2. ed.*, 1-18 (2013).

92   Bosco, D. *et al.* Unique arrangement of α-and β-cells in human islets of Langerhans. *Diabetes* **59**, 1202-1210 (2010).

93   Association, A. D. 7. Approaches to glycemic treatment. *Diabetes care* **39**, S52-S59 (2016).

94   Mirouze, J., Selam, J., Pham, T. & Cavadore, D. Evaluation of exogenous insulin homoeostasis by the artificial pancreas in insulin-dependent diabetes. *Diabetologia* **13**, 273-278 (1977).

95   Banting, F. G. & Best, C. H. The internal secretion of the pancreas. *Indian Journal of Medical Research* **125**, L251 (2007).

96   Banting, F. G., Best, C. H., Collip, J. B., Campbell, W. R. & Fletcher, A. A. Pancreatic extracts in the treatment of diabetes mellitus. *Canadian Medical Association Journal* **12**, 141 (1922).

97   King, K. M. & Rubin, G. A history of diabetes: from antiquity to discovering insulin. *British journal of nursing* **12**, 1091-1095 (2003).

98   Johnson, I. S. Human insulin from recombinant DNA technology. *Science* **219**, 632-637 (1983).

99   Walsh, G. Therapeutic insulins and their large-scale manufacture. *Applied microbiology and biotechnology* **67**, 151-159 (2005).

100   Cummins, E. *et al.* in *NIHR Health Technology Assessment programme: Executive Summaries*   (NIHR Journals Library, 2010).

101   Association, A. D. Economic costs of diabetes in the US in 2017. *Diabetes care* **41**, 917-928 (2018).

102   Shapiro, A. J. *et al.* Islet transplantation in seven patients with type 1 diabetes mellitus using a glucocorticoid-free immunosuppressive regimen. *New England Journal of Medicine* **343**, 230-238 (2000).

103   Ryan, E. A. *et al.* Clinical outcomes and insulin secretion after islet transplantation with the Edmonton protocol. *Diabetes* **50**, 710-719 (2001).

104   Shapiro, A. J. *et al.* International trial of the Edmonton protocol for islet transplantation. *New England Journal of Medicine* **355**, 1318-1330 (2006).

105   Brennan, D. C. *et al.* Long-term follow-up of the Edmonton protocol of islet transplantation in the United States. *American Journal of Transplantation* **16**, 509-517 (2016).

106   Joglekar, M., Parekh, V. & Hardikar, A. Islet-specific microRNAs in pancreas development, regeneration and diabetes. (2011).

107   Aguayo-Mazzucato, C. & Bonner-Weir, S. Pancreatic β cell regeneration as a possible therapy for diabetes. *Cell metabolism* **27**, 57-67 (2018).

108   QADIR, F. *et al.*   (Am Diabetes Assoc, 2018).

109   Ben-Othman, N. *et al.* Long-term GABA administration induces α cell-mediated β-like cell neogenesis. *Cell* **168**, 73-85. e11 (2017).

110   Druelle, N. *et al.* Ectopic expression of Pax4 in pancreatic δ cells results in β-like cell neogenesis. *J Cell Biol* **216**, 4299-4311 (2017).

111   Notkins, A. L. & Lernmark, Å. Autoimmune type 1 diabetes: resolved and unresolved issues. *The Journal of clinical investigation* **108**, 1247-1252 (2001).

112   Hu, C.-y. *et al.* Treatment with CD20-specific antibody prevents and reverses autoimmune diabetes in mice. *The Journal of clinical investigation* **117**, 3857-3867 (2007).

113   Zhao, Y. Stem cell educator therapy and induction of immune balance. *Current diabetes reports* **12**, 517-523 (2012).

114   Zhao, Y. *et al.* Targeting insulin resistance in type 2 diabetes via immune modulation of cord blood-derived multipotent stem cells (CB-SCs) in stem cell educator therapy: phase I/II clinical trial. *BMC medicine* **11**, 160 (2013).

115   Setter, S. M., Iltz, J. L., Thams, J. & Campbell, R. K. Metformin hydrochloride in the treatment of type 2 diabetes mellitus: a clinical review with a focus on dual therapy. *Clinical therapeutics* **25**, 2991-3026 (2003).

116   Yu, O., Azoulay, L., Yin, H., Filion, K. B. & Suissa, S. Sulfonylureas as initial treatment for type 2 diabetes and the risk of severe hypoglycemia. *The American journal of medicine* **131**, 317. e311-317. e322 (2018).

117   Zinman, B. *et al.* Empagliflozin, cardiovascular outcomes, and mortality in type 2 diabetes. *New England Journal of Medicine* **373**, 2117-2128 (2015).

118   Association, A. D. 4. Foundations of care: education, nutrition, physical activity, smoking cessation, psychosocial care, and immunization. *Diabetes care* **38**, S20-S30 (2015).

119   Eisenberg, D. M. & Burgess, J. D. Nutrition education in an era of global obesity and diabetes: thinking outside the box. *Academic Medicine* **90**, 854-860 (2015).

120   Wang, C. C. L. *et al.* Cardiovascular and Limb Outcomes in Patients With Diabetes and Peripheral Artery Disease: The EUCLID Trial. *Journal of the American College of Cardiology* **72**, 3274-3284 (2018).

121   Pan, H.-z. *et al.* The oxidative stress status in diabetes mellitus and diabetic nephropathy. *Acta diabetologica* **47**, 71-76 (2010).

122   Peng, L., Liu, W., Zhai, F., He, L. & Wang, H. Microvessel permeability correlates with diabetic peripheral neuropathy in early stage of streptozotocin-induced diabetes rats. *Journal of Diabetes and its Complications* **29**, 865-871 (2015).

123   Bosma, E. K., van Noorden, C. J., Klaassen, I. & Schlingemann, R. O. in *Diabetic Nephropathy*   305-321 (Springer, 2019).

124   Adams, R. H. Molecular control of arterial–venous blood vessel identity. *Journal of anatomy* **202**, 105-112 (2003).

125   Heinke, J., Patterson, C. & Moser, M. Life is a pattern: vascular assembly within the embryo. *Frontiers in bioscience (Elite edition)* **4**, 2269 (2012).

126   Risau, W. & Flamme, I. Vasculogenesis. *Annual review of cell and developmental biology* **11**, 73-91 (1995).

127   Gonzalez-Crussi, F. Vasculogenesis in the chick embryo. An ultrastructural study. *American Journal of Anatomy* **130**, 441-459 (1971).

128   Matsumoto, K., Yoshitomi, H., Rossant, J. & Zaret, K. S. Liver organogenesis promoted by endothelial cells prior to vascular function. *Science* **294**, 559-563 (2001).

129   Auerbach, R. & Auerbach, W. Profound effects on vascular development caused by perturbations during organogenesis. *The American journal of pathology* **151**, 1183 (1997).

130   Shalaby, F. *et al.* Failure of blood-island formation and vasculogenesis in Flk-1-deficient mice. *Nature* **376**, 62 (1995).

131   Choi, K., Kennedy, M., Kazarov, A., Papadimitriou, J. C. & Keller, G. A common precursor for hematopoietic and endothelial cells. *Development* **125**, 725-732 (1998).

132   Peters, K. G., De Vries, C. & Williams, L. T. Vascular endothelial growth factor receptor expression during embryogenesis and tissue repair suggests a role in endothelial differentiation and blood vessel growth. *Proceedings of the National Academy of Sciences* **90**, 8915-8919 (1993).

133   Coultas, L., Chawengsaksophak, K. & Rossant, J. Endothelial cells and VEGF in vascular development. *Nature* **438**, 937 (2005).

134   Thurston, G. *et al.* Angiopoietin-1 protects the adult vasculature against plasma leakage. *Nature medicine* **6**, 460 (2000).

135   Suri, C. *et al.* Increased vascularization in mice overexpressing angiopoietin-1. *Science* **282**, 468-471 (1998).

136   Suri, C. *et al.* Requisite role of angiopoietin-1, a ligand for the TIE2 receptor, during embryonic angiogenesis. *Cell* **87**, 1171-1180 (1996).

137   Yamamoto, K. *et al.* Proliferation, differentiation, and tube formation by endothelial progenitor cells in response to shear stress. *Journal of Applied Physiology* **95**, 2081-2088 (2003).

138   Lehoux, S. & Jones, E. A. Shear stress, arterial identity and atherosclerosis. *Thrombosis and haemostasis* **115**, 467-473 (2016).

139   Crosby, J. R. *et al.* Endothelial cells of hematopoietic origin make a significant contribution to adult blood vessel formation. *Circulation research* **87**, 728-730 (2000).

140   Frenette, P. S., Subbarao, S., Mazo, I. B., Von Andrian, U. H. & Wagner, D. D. Endothelial selectins and vascular cell adhesion molecule-1 promote hematopoietic progenitor homing to bone marrow. *Proceedings of the National Academy of Sciences* **95**, 14423-14428 (1998).

141   Rhodin, J.   (American Physiological Society, Bethesda, 1980).

142   Mulvany, M. & Aalkjær, C. Structure and function of small arteries. *Physiological reviews* **70**, 921-961 (1990).

143   Tilton, R. G., Kilo, C. & Williamson, J. R. Pericyte-endothelial relationships in cardiac and skeletal muscle capillaries. *Microvascular research* **18**, 325-335 (1979).

144   Han, S. S. & Avery, J. K. The ultrastructure of capillaries and arterioles of the hamster dental pulp. *The Anatomical Record* **145**, 549-571 (1963).

145   Kumar, S., West, D. C. & Ager, A. Heterogeneity in endothelial cells from large vessels and microvessels. *Differentiation* **36**, 57-70 (1987).

146   Griep, L. *et al.* BBB on chip: microfluidic platform to mechanically and biochemically modulate blood-brain barrier function. *Biomedical microdevices* **15**, 145-150 (2013).

147   Caggiati, A., Phillips, M., Lametschwandtner, A. & Allegra, C. Valves in small veins and venules. *European Journal of Vascular and Endovascular Surgery* **32**, 447-452 (2006).

148   Cleaver, O. & Melton, D. A. Endothelial signaling during development. *Nature medicine* **9**, 661 (2003).

149   Ballian, N. & Brunicardi, F. C. Islet vasculature as a regulator of endocrine pancreas function. *World journal of surgery* **31**, 705-714 (2007).

150   Ruggeri, Z. Von Willebrand factor, platelets and endothelial cell interactions. *Journal of Thrombosis and Haemostasis* **1**, 1335-1342 (2003).

151   Palmer, R. M., Ferrige, A. & Moncada, S. Nitric oxide release accounts for the biological activity of endothelium-derived relaxing factor. *Nature* **327**, 524 (1987).

152   Förstermann, U., Xia, N. & Li, H. Roles of vascular oxidative stress and nitric oxide in the pathogenesis of atherosclerosis. *Circulation research* **120**, 713-735 (2017).

153   Hink, U. *et al.* Mechanisms underlying endothelial dysfunction in diabetes mellitus. *Circulation research* **88**, e14-e22 (2001).

154   Association, A. D. 9. Microvascular complications and foot care. *Diabetes care* **39**, S72-S80 (2016).

155   Association, A. D. 10. Microvascular complications and foot care: standards of medical care in diabetes—2018. *Diabetes Care* **41**, S105-S118 (2018).

156   Hinkel, R. *et al.* Diabetes mellitus–induced microvascular destabilization in the myocardium. *Journal of the American College of Cardiology* **69**, 131-143 (2017).

157   Pyšná, A. *et al.* Endothelial progenitor cells biology in diabetes mellitus and peripheral arterial disease and their therapeutic potential. *Stem Cell Reviews and Reports*, 1-9 (2018).

158   Signorelli, S. S. & Katsiki, N. Oxidative stress and inflammation: Their role in the pathogenesis of peripheral artery disease with or without type 2 diabetes mellitus. *Current vascular pharmacology* **16**, 547-554 (2018).

159   Bennett, M. R., Sinha, S. & Owens, G. K. Vascular smooth muscle cells in atherosclerosis. *Circulation research* **118**, 692-702 (2016).

160   Nehls, V., Denzer, K. & Drenckhahn, D. Pericyte involvement in capillary sprouting during angiogenesis in situ. *Cell and tissue research* **270**, 469-474 (1992).

161   Chen, J. *et al.* CD146 is essential for PDGFRβ-induced pericyte recruitment. *Protein & cell* **9**, 743-747 (2018).

162   da Bandeira, D. S., Casamitjana, J. & Crisan, M. Pericytes, integral components of adult hematopoietic stem cell niches. *Pharmacology & therapeutics* **171**, 104-113 (2017).

163   Crisan, M. *et al.* A perivascular origin for mesenchymal stem cells in multiple human organs. *Cell stem cell* **3**, 301-313 (2008).

164   Beckman, J. A., Creager, M. A. & Libby, P. Diabetes and atherosclerosis: epidemiology, pathophysiology, and management. *Jama* **287**, 2570-2581 (2002).

165   Libby, P., Ridker, P. M. & Maseri, A. Inflammation and atherosclerosis. *Circulation* **105**, 1135-1143 (2002).

166   Wilkins, E. *et al.* European cardiovascular disease statistics 2017. (2017).

167   Mozaffarian, D. *et al.* Heart disease and stroke statistics-2016 update a report from the American Heart Association. *Circulation* **133**, e38-e48 (2016).

168   Smolderen, K. G. *et al.* One-year costs associated with cardiovascular disease in Canada: insights from the REduction of Atherothrombosis for Continued Health (REACH) registry. *Canadian Journal of Cardiology* **26**, e297-e305 (2010).

169   Cooper, T. T., Hess, D. A. & Verma, S. Vascular Organoids: Are We Entering a New Area of Cardiometabolic Research? *Cell metabolism* **29**, 792-794 (2019).

170   Dunbar, S. B. *et al.* Projected costs of informal caregiving for cardiovascular disease: 2015 to 2035: a policy statement from the American Heart Association. *Circulation* **137**, e558-e577 (2018).

171   Association, A. D. Peripheral arterial disease in people with diabetes. *Diabetes care* **26**, 3333-3341 (2003).

172   Morley, R. L., Sharma, A., Horsch, A. D. & Hinchliffe, R. J. Peripheral artery disease. *bmj* **360**, j5842 (2018).

173   Thiruvoipati, T., Kielhorn, C. E. & Armstrong, E. J. Peripheral artery disease in patients with diabetes: Epidemiology, mechanisms, and outcomes. *World journal of diabetes* **6**, 961 (2015).

174   Makowsky, M. *et al.* Prevalence and treatment patterns of lower extremity peripheral arterial disease among patients at risk in ambulatory health settings. *Canadian Journal of Cardiology* **27**, 389. e311-389. e318 (2011).

175   Davies, M. G. Criticial limb ischemia: epidemiology. *Methodist DeBakey cardiovascular journal* **8**, 10 (2012).

176   Varu, V. N., Hogg, M. E. & Kibbe, M. R. Critical limb ischemia. *Journal of vascular surgery* **51**, 230-241 (2010).

177   Hiatt, W. R. Medical treatment of peripheral arterial disease and claudication. *New England Journal of Medicine* **344**, 1608-1621 (2001).

178   Aboyans, V. *et al.* 2017 ESC Guidelines on the Diagnosis and Treatment of Peripheral Arterial Diseases, in collaboration with the European Society for Vascular Surgery (ESVS) Document covering atherosclerotic disease of extracranial carotid and vertebral, mesenteric, renal, upper and lower extremity arteries Endorsed by: the European Stroke Organization (ESO) The Task Force for the Diagnosis and Treatment of Peripheral Arterial Diseases of the European Society of Cardiology (ESC) and of the European Society for Vascular Surgery (ESVS). *European heart journal* **39**, 763-816 (2017).

179   Hertzer, N. R. *et al.* Coronary artery disease in peripheral vascular patients. A classification of 1000 coronary angiograms and results of surgical management. *Annals of surgery* **199**, 223 (1984).

180   Gupta, N. K., Armstrong, E. J. & Parikh, S. A. The current state of stem cell therapy for peripheral artery disease. *Current cardiology reports* **16**, 447 (2014).

181   Isner, J. M. *et al.* Arterial gene therapy for therapeutic angiogenesis in patients with peripheral artery disease. *Circulation* **91**, 2687-2692 (1995).

182   Kemp, P. History of regenerative medicine: looking backwards to move forwards. (2006).

183   Koransky, M. L., Robbins, R. C. & Blau, H. M. VEGF gene delivery for treatment of ischemic cardiovascular disease. *Trends in cardiovascular medicine* **12**, 108-114 (2002).

184   Cooper, T. T. *et al.* Inhibition of Aldehyde Dehydrogenase-Activity Expands Multipotent Myeloid Progenitor Cells with Vascular Regenerative Function. *Stem Cells* **36**, 723-736 (2018).

185   Sutton, J. T., Haworth, K. J., Pyne-Geithman, G. & Holland, C. K. Ultrasound-mediated drug delivery for cardiovascular disease. *Expert opinion on drug delivery* **10**, 573-592 (2013).

186   Young, S. A. *et al.* Mechanically resilient injectable scaffolds for intramuscular stem cell delivery and cytokine release. *Biomaterials* **159**, 146-160 (2018).

187   Berthiaume, F., Maguire, T. J. & Yarmush, M. L. Tissue engineering and regenerative medicine: history, progress, and challenges. *Annual review of chemical and biomolecular engineering* **2**, 403-430 (2011).

188   Till, J. E. & McCulloch, E. A. A direct measurement of the radiation sensitivity of normal mouse bone marrow cells. *Radiation research* **14**, 213-222 (1961).

189   Reya, T., Morrison, S. J., Clarke, M. F. & Weissman, I. L. Stem cells, cancer, and cancer stem cells. *nature* **414**, 105 (2001).

190   Takahashi, K. *et al.* Induction of pluripotent stem cells from adult human fibroblasts by defined factors. *cell* **131**, 861-872 (2007).

191   Conboy, I. M. & Rando, T. A. Aging, stem cells and tissue regeneration: lessons from muscle. *Cell cycle* **4**, 407-410 (2005).

192   Childs, B. G., Durik, M., Baker, D. J. & Van Deursen, J. M. Cellular senescence in aging and age-related disease: from mechanisms to therapy. *Nature medicine* **21**, 1424 (2015).

193   Perin, E. C. *et al.* Evaluation of cell therapy on exercise performance and limb perfusion in peripheral artery disease: the CCTRN PACE trial (patients with intermittent claudication injected with ALDH bright cells). *Circulation* **135**, 1417-1428 (2017).

194   Perin, E. C. *et al.* Rationale and design for PACE: patients with intermittent claudication injected with ALDH bright cells. *American heart journal* **168**, 667-673. e662 (2014).

195   Hess, D. *et al.* Bone marrow–derived stem cells initiate pancreatic regeneration. *Nature biotechnology* **21**, 763 (2003).

196   Bell, G. I. *et al.* Combinatorial human progenitor cell transplantation optimizes islet regeneration through secretion of paracrine factors. *Stem cells and development* **21**, 1863-1876 (2012).

197   Chhabra, P. & Brayman, K. L. Stem cell therapy to cure type 1 diabetes: from hype to hope. *Stem cells translational medicine* **2**, 328-336 (2013).

198   Notta, F. *et al.* Isolation of single human hematopoietic stem cells capable of long-term multilineage engraftment. *Science* **333**, 218-221 (2011).

199   Anjos-Afonso, F. *et al.* CD34− cells at the apex of the human hematopoietic stem cell hierarchy have distinctive cellular and molecular signatures. *Cell stem cell* **13**, 161-174 (2013).

200   Ma, I. & Allan, A. L. The role of human aldehyde dehydrogenase in normal and cancer stem cells. *Stem cell reviews and reports* **7**, 292-306 (2011).

201   Chanda, B., Ditadi, A., Iscove, N. N. & Keller, G. Retinoic acid signaling is essential for embryonic hematopoietic stem cell development. *Cell* **155**, 215-227 (2013).

202   Liu, Y. *et al.* Proliferating pancreatic β-cells upregulate ALDH. *Histochemistry and cell biology* **142**, 685-691 (2014).

203   Huang, E. H. *et al.* Aldehyde dehydrogenase 1 is a marker for normal and malignant human colonic stem cells (SC) and tracks SC overpopulation during colon tumorigenesis. *Cancer research* **69**, 3382-3389 (2009).

204   Kieffer, T. J., Woltjen, K., Osafune, K., Yabe, D. & Inagaki, N. B-cell replacement strategies for diabetes. *Journal of diabetes investigation* **9**, 457-463 (2018).

205   Kuljanin, M. *et al.* Human multipotent stromal cell secreted effectors accelerate islet regeneration. *Stem cells* **37**, 516-528 (2019).

206   Putman, D. M., Liu, K. Y., Broughton, H. C., Bell, G. I. & Hess, D. A. Umbilical cord blood-derived aldehyde dehydrogenase-expressing progenitor cells promote recovery from acute ischemic injury. *Stem cells* **30**, 2248-2260 (2012).

207   Rhinn, M. & Dollé, P. Retinoic acid signalling during development. *Development* **139**, 843-858 (2012).

208   Mark, M., Ghyselinck, N. B. & Chambon, P. Function of retinoid nuclear receptors: lessons from genetic and pharmacological dissections of the retinoic acid signaling pathway during mouse embryogenesis. *Annu. Rev. Pharmacol. Toxicol.* **46**, 451-480 (2006).

209   Chen, Y. *et al.* Retinoic acid signaling is essential for pancreas development and promotes endocrine at the expense of exocrine cell differentiation in Xenopus. *Developmental biology* **271**, 144-160 (2004).

210   Orkin, S. H. & Zon, L. I. Hematopoiesis: an evolving paradigm for stem cell biology. *Cell* **132**, 631-644 (2008).

211   Moore, K. A. & Lemischka, I. R. Stem cells and their niches. *Science* **311**, 1880-1885 (2006).

212   Eaves, C. J. Hematopoietic stem cells: concepts, definitions, and the new reality. *Blood* **125**, 2605-2613 (2015).

213   Munshi, C. B., Graeff, R. & Lee, H. C. Evidence for a causal role of CD38 expression in granulocytic differentiation of human HL-60 cells. *Journal of Biological Chemistry* **277**, 49453-49458 (2002).

214   Steinman, R. M. & Inaba, K. Myeloid dendritic cells. *Journal of leukocyte biology* **66**, 205-208 (1999).

215   Guilliams, M. *et al.* Dendritic cells, monocytes and macrophages: a unified nomenclature based on ontogeny. *Nature Reviews Immunology* **14**, 571 (2014).

216   Geissmann, F. *et al.* Development of monocytes, macrophages, and dendritic cells. *Science* **327**, 656-661 (2010).

217   Beerman, I. *et al.* Functionally distinct hematopoietic stem cells modulate hematopoietic lineage potential during aging by a mechanism of clonal expansion. *Proceedings of the National Academy of Sciences* **107**, 5465-5470 (2010).

218   Atkinson, K. *et al. Clinical bone marrow and blood stem cell transplantation.* (Cambridge University Press, 2004).

219   Huss, R. Isolation of primary and immortalized CD34− hematopoietic and mesenchymal stem cells from various sources. *Stem cells* **18**, 1-9 (2000).

220   Sauvageau, G., Iscove, N. N. & Humphries, R. K. In vitro and *in vivo* expansion of hematopoietic stem cells. *Oncogene* **23**, 7223 (2004).

221   Chute, J. P. *et al.* Inhibition of aldehyde dehydrogenase and retinoid signaling induces the expansion of human hematopoietic stem cells. *Proceedings of the National Academy of Sciences* **103**, 11707-11712 (2006).

222   Madlambayan, G. J. *et al.* Dynamic changes in cellular and microenvironmental composition can be controlled to elicit *in vitro* human hematopoietic stem cell expansion. *Experimental hematology* **33**, 1229-1239 (2005).

223   Kirouac, D. C. & Zandstra, P. W. Understanding cellular networks to improve hematopoietic stem cell expansion cultures. *Current Opinion in Biotechnology* **17**, 538-547 (2006).

224   Csaszar, E. *et al.* Rapid expansion of human hematopoietic stem cells by automated control of inhibitory feedback signaling. *Cell stem cell* **10**, 218-229 (2012).

225   Csaszar, E., Chen, K., Caldwell, J., Chan, W. & Zandstra, P. W. Real-time monitoring and control of soluble signaling factors enables enhanced progenitor cell outputs from human cord blood stem cell cultures. *Biotechnology and bioengineering* **111**, 1258-1264 (2014).

226   Putman, D. M. *et al.* Expansion of umbilical cord blood aldehyde dehydrogenase expressing cells generates myeloid progenitor cells that stimulate limb revascularization. *Stem cells translational medicine* **6**, 1607-1619 (2017).

227   Squillaro, T., Peluso, G. & Galderisi, U. Clinical trials with mesenchymal stem cells: an update. *Cell transplantation* **25**, 829-848 (2016).

228   Giordano, A., Galderisi, U. & Marino, I. R. From the laboratory bench to the patient's bedside: an update on clinical trials with mesenchymal stem cells. *Journal of cellular physiology* **211**, 27-35 (2007).

229   Barry, F. P. & Murphy, J. M. Mesenchymal stem cells: clinical applications and biological characterization. *The international journal of biochemistry & cell biology* **36**, 568-584 (2004).

230   Dominici, M. *et al.* Minimal criteria for defining multipotent mesenchymal stromal cells. The International Society for Cellular Therapy position statement. *Cytotherapy* **8**, 315-317 (2006).

231   Ishii, M. *et al.* Molecular markers distinguish bone marrow mesenchymal stem cells from fibroblasts. *Biochemical and biophysical research communications* **332**, 297-303 (2005).

232   Haniffa, M. A., Collin, M. P., Buckley, C. D. & Dazzi, F. Mesenchymal stem cells: the fibroblasts' new clothes? *haematologica* **94**, 258-263 (2009).

233   Cappellesso-Fleury, S. *et al.* Human fibroblasts share immunosuppressive properties with bone marrow mesenchymal stem cells. *Journal of clinical immunology* **30**, 607-619 (2010).

234   Yates, C. C. *et al.* Multipotent stromal cells/mesenchymal stem cells and fibroblasts combine to minimize skin hypertrophic scarring. *Stem cell research & therapy* **8**, 193 (2017).

235   Blasi, A. *et al.* Dermal fibroblasts display similar phenotypic and differentiation capacity to fat-derived mesenchymal stem cells, but differ in anti-inflammatory and angiogenic potential. *Vascular cell* **3**, 5 (2011).

236   Shumakov, V., Onishchenko, N., Rasulov, M., Krasheninnikov, M. & Zaidenov, V. Mesenchymal bone marrow stem cells more effectively stimulate regeneration of deep burn wounds than embryonic fibroblasts. *Bulletin of experimental biology and medicine* **136**, 192-195 (2003).

237   Diaz-Flores, L. *et al.* CD34+ stromal cells/fibroblasts/fibrocytes/telocytes as a tissue reserve and a principal source of mesenchymal cells. Location, morphology, function and role in pathology. *Histology and histopathology* **29**, 831-870 (2014).

238   Trial, J., Entman, M. L. & Cieslik, K. A. Mesenchymal stem cell-derived inflammatory fibroblasts mediate interstitial fibrosis in the aging heart. *Journal of molecular and cellular cardiology* **91**, 28-34 (2016).

239   Bühring, H. J. *et al.* Phenotypic characterization of distinct human bone marrow–derived MSC subsets. *Annals of the New York Academy of Sciences* **1176**, 124-134 (2009).

240   Hass, R., Kasper, C., Böhm, S. & Jacobs, R. Different populations and sources of human mesenchymal stem cells (MSC): a comparison of adult and neonatal tissue-derived MSC. *Cell Communication and Signaling* **9**, 12 (2011).

241   Pilz, G. A. *et al.* Human term placenta-derived mesenchymal stromal cells are less prone to osteogenic differentiation than bone marrow-derived mesenchymal stromal cells. *Stem cells and development* **20**, 635-646 (2010).

242   Crisan, M. *et al.* Perivascular multipotent progenitor cells in human organs. *Annals of the New York Academy of Sciences* **1176**, 118-123 (2009).

243   Sherman, S. E. *et al.* High aldehyde dehydrogenase activity identifies a subset of human mesenchymal stromal cells with vascular regenerative potential. *Stem Cells* **35**, 1542-1553 (2017).

244   Álvarez-Viejo, M., Menéndez-Menéndez, Y. & Otero-Hernández, J. CD271 as a marker to identify mesenchymal stem cells from diverse sources before culture. *World journal of stem cells* **7**, 470 (2015).

245   Tormin, A. *et al.*   (Am Soc Hematology, 2009).

246   D'amour, K. A., Bang, A. & Baetge, E. E.   (Google Patents, 2012).

247   Pullen, L. C. Stem Cell–Derived Pancreatic Progenitor Cells Have Now Been Transplanted into Patients: Report from IPITA 2018. *American Journal of Transplantation* **18**, 1581-1582 (2018).

248   Agulnick, A. D. *et al.* Insulin-producing endocrine cells differentiated *in vitro* from human embryonic stem cells function in macroencapsulation devices *in vivo*. *Stem cells translational medicine* **4**, 1214-1222 (2015).

249   White, S. A., Shaw, J. A. & Sutherland, D. E. Pancreas transplantation. *The Lancet* **373**, 1808-1817 (2009).

250   Ellis, C., Ramzy, A. & Kieffer, T. J. Regenerative medicine and cell-based approaches to restore pancreatic function. *Nature Reviews Gastroenterology & Hepatology* **14**, 612 (2017).

251   Keenan, H. A. *et al.* Residual insulin production and pancreatic β-cell turnover after 50 years of diabetes: Joslin Medalist Study. *Diabetes* **59**, 2846-2853 (2010).

252   Patel, A. N. & Genovese, J. Potential clinical applications of adult human mesenchymal stem cell (Prochymal®) therapy. *Stem Cells and Cloning: Advances and Applications* **4**, 61 (2011).

253   Farkouh, M. E. *et al.* Strategies for multivessel revascularization in patients with diabetes. *New England journal of medicine* **367**, 2375-2384 (2012).

254   Raval, Z. & Losordo, D. W. Cell therapy of peripheral arterial disease: from experimental findings to clinical trials. *Circulation research* **112**, 1288-1302 (2013).

255   Qadura, M., Terenzi, D. C., Verma, S., Al-Omran, M. & Hess, D. A. Concise review: cell therapy for critical limb ischemia: an integrated review of preclinical and clinical studies. *Stem Cells* **36**, 161-171 (2018).

256   Gremmels, H. *et al.* Exhaustion of the bone marrow progenitor cell reserve is associated with major events in severe limb ischemia. *Angiogenesis*, 1-10 (2019).

257   Terenzi, D. C. *et al.* Vascular Regenerative Cell Exhaustion in Diabetes: Translational Opportunities to Mitigate Cardiometabolic Risk. *Trends in Molecular Medicine* (2019).

258   Pietras, E. M. Inflammation: a key regulator of hematopoietic stem cell fate in health and disease. *Blood* **130**, 1693-1698 (2017).

259   Xing, J. *et al.* Hypoxia induces senescence of bone marrow mesenchymal stem cells via altered gut microbiota. *Nature communications* **9**, 2020 (2018).

260   von Scheidt, M. *et al.* Applications and limitations of mouse models for understanding human atherosclerosis. *Cell metabolism* **25**, 248-261 (2017).

261   McNeill, E., Channon, K. & Greaves, D. Inflammatory cell recruitment in cardiovascular disease: murine models and potential clinical applications. *Clinical science* **118**, 641-655 (2010).

262   Zaragoza, C. *et al.* Animal models of cardiovascular diseases. *BioMed Research International* **2011** (2011).

263   Evensen, L. *et al.* Mural cell associated VEGF is required for organotypic vessel formation. *PloS one* **4**, e5798 (2009).

264   Manikowski, D. *et al.* Human adipose tissue-derived stromal cells in combination with exogenous stimuli facilitate three-dimensional network formation of human endothelial cells derived from various sources. *Vascular pharmacology* **106**, 28-36 (2018).

265   Andrée, B. *et al.* Formation of three-dimensional tubular endothelial cell networks under defined serum-free cell culture conditions in human collagen hydrogels. *Scientific reports* **9**, 5437 (2019).

266   Wimmer, R. A. *et al.* Human blood vessel organoids as a model of diabetic vasculopathy. *Nature* (2019).

267   Kuljanin, M. *et al.* Quantitative Proteomics Evaluation of Human Multipotent Stromal Cell for β Cell Regeneration. *Cell reports* **25**, 2524-2536. e2524 (2018).

268   Bell, G. I. *et al.* Transplanted human bone marrow progenitor subtypes stimulate endogenous islet regeneration and revascularization. *Stem cells and development* **21**, 97-109 (2011).

269   Yao, B. *et al.* Age-associated changes in regenerative capabilities of mesenchymal stem cell: impact on chronic wounds repair. *International wound journal* **13**, 1252-1259 (2016).

270   Klinkhammer, B. M. *et al.* Mesenchymal stem cells from rats with chronic kidney disease exhibit premature senescence and loss of regenerative potential. *PloS one* **9**, e92115 (2014).

271   Jansen, B. J. *et al.* Functional differences between mesenchymal stem cell populations are reflected by their transcriptome. *Stem cells and development* **19**, 481-490 (2010).

272   Kornicka, K., Houston, J. & Marycz, K. Dysfunction of mesenchymal stem cells isolated from metabolic syndrome and type 2 diabetic patients as result of oxidative stress and autophagy may limit their potential therapeutic use. *Stem Cell Reviews and Reports* **14**, 337-345 (2018).

273   van de Vyver, M. Intrinsic mesenchymal stem cell dysfunction in diabetes mellitus: implications for autologous cell therapy. *Stem cells and development* **26**, 1042-1053 (2017).

274   Sherman, S. E. The Purification of Human Adult Progenitor Cell Types to Promote Angiogenesis. (2019).

275   Bulte, J. W. & Daldrup-Link, H. E. Clinical tracking of cell transfer and cell transplantation: Trials and tribulations. *Radiology* **289**, 604-615 (2018).

276   Rosenholm, J. M. *et al.* Prolonged Dye Release from Mesoporous Silica-Based Imaging Probes Facilitates Long-Term Optical Tracking of Cell Populations In Vivo. *Small* **12**, 1578-1592 (2016).

277   Kuljanin, M., Bell, G. I., Sherman, S. E., Lajoie, G. A. & Hess, D. A. Proteomic characterisation reveals active Wnt-signalling by human multipotent stromal cells as a key regulator of β cell survival and proliferation. *Diabetologia* **60**, 1987-1998 (2017).

278   Bollini, S., Gentili, C., Tasso, R. & Cancedda, R. The regenerative role of the fetal and adult stem cell secretome. *Journal of Clinical Medicine* **2**, 302-327 (2013).

279   Bruno, S., Deregibus, M. C. & Camussi, G. The secretome of mesenchymal stromal cells: role of extracellular vesicles in immunomodulation. *Immunology letters* **168**, 154-158 (2015).

280   Kim, H. O., Choi, S.-M. & Kim, H.-S. Mesenchymal stem cell-derived secretome and microvesicles as a cell-free therapeutics for neurodegenerative disorders. *Tissue Engineering and Regenerative Medicine* **10**, 93-101 (2013).

281   Konala, V. B. R. *et al.* The current landscape of the mesenchymal stromal cell secretome: a new paradigm for cell-free regeneration. *Cytotherapy* **18**, 13-24 (2016).

282   Tran, C. & Damaser, M. S. Stem cells as drug delivery methods: application of stem cell secretome for regeneration. *Advanced drug delivery reviews* **82**, 1-11 (2015).

283   Jeppesen, D. K. *et al.* Reassessment of exosome composition. *Cell* **177**, 428-445. e418 (2019).

284   VanWijk, M. J., VanBavel, E., Sturk, A. & Nieuwland, R. Microparticles in cardiovascular diseases. *Cardiovascular research* **59**, 277-287 (2003).

285   Mulcahy, L. A., Pink, R. C. & Carter, D. R. F. Routes and mechanisms of extracellular vesicle uptake. *Journal of extracellular vesicles* **3**, 24641 (2014).

286   Cong, L. *et al.* Multiplex genome engineering using CRISPR/Cas systems. *Science* **339**, 819-823 (2013).

287   Hsu, P. D., Lander, E. S. & Zhang, F. Development and applications of CRISPR-Cas9 for genome engineering. *Cell* **157**, 1262-1278 (2014).

288   Ran, F. A. *et al.* Genome engineering using the CRISPR-Cas9 system. *Nature protocols* **8**, 2281 (2013).

289   Newick, K., O'Brien, S., Moon, E. & Albelda, S. M. CAR T cell therapy for solid tumors. *Annual review of medicine* **68**, 139-152 (2017).

290   Chen, X. *et al.* A combinational therapy of EGFR-CAR NK cells and oncolytic herpes simplex virus 1 for breast cancer brain metastases. *Oncotarget* **7**, 27764 (2016).

291   Londono, R. & Badylak, S. F. Biologic scaffolds for regenerative medicine: mechanisms of *in vivo* remodeling. *Annals of biomedical engineering* **43**, 577-592 (2015).

292   Zhu, W. *et al.* 3D printing of functional biomaterials for tissue engineering. *Current opinion in biotechnology* **40**, 103-112 (2016).

293   Fan, K. *et al.* A machine learning assisted, label-free, non-invasive approach for somatic reprogramming in induced pluripotent stem cell colony formation detection and prediction. *Scientific reports* **7**, 13496 (2017).

294   Putman, D. M. *et al.* Expansion of Umbilical Cord Blood Aldehyde Dehydrogenase Expressing Cells Generates Myeloid Progenitor Cells that Stimulate Limb Revascularization. *Stem cells translational medicine* (2017).

295   Caplan, A. I. & Correa, D. The MSC: an injury drugstore. *Cell stem cell* **9**, 11-15 (2011).

296   Caplan, A. I. MSCs: the sentinel and safe-guards of injury. *Journal of cellular physiology* **231**, 1413-1416 (2016).

297   Leibacher, J. & Henschler, R. Biodistribution, migration and homing of systemically applied mesenchymal stem/stromal cells. *Stem Cell Research & Therapy* **7**, 7 (2016).

298   Kumar, S. & Ponnazhagan, S. Bone homing of mesenchymal stem cells by ectopic α4 integrin expression. *The FASEB Journal* **21**, 3917-3927 (2007).

299   Nitzsche, F. *et al.* Concise review: MSC adhesion cascade—insights into homing and transendothelial migration. *Stem Cells* **35**, 1446-1460 (2017).

300   Rombouts, W. & Ploemacher, R. Primary murine MSC show highly efficient homing to the bone marrow but lose homing ability following culture. *Leukemia* **17**, 160 (2003).

301   Martino, M. M. *et al.* Inhibition of IL-1R1/MyD88 signalling promotes mesenchymal stem cell-driven tissue regeneration. *Nature communications* **7**, 11051 (2016).

302   Fiore, D. *et al.* Pharmacological blockage of fibro/adipogenic progenitor expansion and suppression of regenerative fibrogenesis is associated with impaired skeletal muscle regeneration. *Stem cell research* **17**, 161-169 (2016).

303   Hoffmann, J. *et al.* Angiogenic effects despite limited cell survival of bone marrow-derived mesenchymal stem cells under ischemia. *The Thoracic and cardiovascular surgeon* **58**, 136-142 (2010).

304   Soundararajan, M. & Kannan, S. Fibroblasts and mesenchymal stem cells: Two sides of the same coin? *Journal of Cellular Physiology* (2018).

305   Kaufman, L. *et al.* in *Plasmonics in Biology and Medicine XVI.* 108940B (International Society for Optics and Photonics).

306   Bian, S. *et al.* Extracellular vesicles derived from human bone marrow mesenchymal stem cells promote angiogenesis in a rat myocardial infarction model. *Journal of molecular medicine* **92**, 387-397 (2014).

307   Andaloussi, S. E., Mäger, I., Breakefield, X. O. & Wood, M. J. Extracellular vesicles: biology and emerging therapeutic opportunities. *Nature reviews Drug discovery* **12**, 347 (2013).

308   Phinney, D. G. *et al.* Mesenchymal stem cells use extracellular vesicles to outsource mitophagy and shuttle microRNAs. *Nature communications* **6**, 8472 (2015).

309   Raposo, G. & Stoorvogel, W. Extracellular vesicles: exosomes, microvesicles, and friends. *J Cell Biol* **200**, 373-383 (2013).

Chapter 2

2 Inhibition of Aldehyde Dehydrogenase-Activity Expands Multipotent Myeloid Progenitor Cells with Vascular Regenerative Function[i]

i A version of this chapter has been published: Cooper, T.T., Sherman, S.E., Kuljanin, M., Bell, G.I., Lajoie, G.A. and Hess, D.A., 2018. Inhibition of Aldehyde Dehydrogenase-Activity Expands Multipotent Myeloid Progenitor Cells with Vascular Regenerative Function. Stem Cells, 36(5), pp.723-736.

2.1 Introduction

Systemic atherosclerosis results in impaired blood vessel architecture and function[1], leading to peripheral arterial disease (PAD) characterized by obstructed blood flow within the peripheral vasculature, limiting delivery of oxygen and nutrients to afflicted tissues[2]. Clinical presentation of PAD ranges from asymptomatic ischemia to exercise-induced intermittent claudication, which may progress toward critical limb ischemia (CLI), the most severe manifestation of PAD. Patients with CLI suffer from pain at rest, non-healing tissue ulceration, and life-threatening infections. Current pharmaceutical therapies target risk factors to reduce cardiovascular events, whereas endovascular or surgical bypass interventions aim to recover perfusion to afflicted tissues. Unfortunately, these therapies provide only short-term benefit and are not offered to individuals with diffuse CLI[3-6]. As a result, 25%–30% of CLI patients require limb amputation within the first year of diagnosis[7], and>60% of CLI patients will succumb to death within 5 years[8]. There is a need to develop effective therapies for the 8–12 million North Americans and >200 million individuals worldwide afflicted with advancing PAD[7,8]. Tissue revascularization via "therapeutic angiogenesis" has been proposed as a potential target for combating severe PAD. Robust angiogenesis can occur in skeletal muscle following ischemic injury; however, this requires activation of several cell types to orchestrate vascular remodeling or to activate flow within collateral vessels[9,10]. Pro-angiogenic cytokine/chemokine secretion by hematopoietic progenitor cells (HPCs) direct sprouting by vessel-forming endothelial progenitor cells (EPC) and encourage infiltration by vessel wrapping pericytes, respectively; two processes essential for stable neovessel formation[10]. Thus, cellular therapies to induce revascularization uses the secretory properties of transplanted blood-derived progenitor cells to generate a pro-angiogenic microenvironment and restore revascularization within ischemic tissues[11]. We have previously demonstrated the vascular regenerative potential of HPC isolated from healthy human bone mar-row (BM) and umbilical cord blood (UCB)[12,13]. Notably, purification of cells with high aldehyde dehydrogenase (ALDH)activity (ALDH[hi]), a detoxification function conserved in pro-genitor cells of multiple lineages, promoted revascularization following transplantation into mice with hind-limb ischemia, by stimulating endogenous

capillary formation at the site of injury without permanent incorporation into regenerating murine neovessels[13]. Moreover, ALDH^{hi} cells from BM or UCB are also enriched for rare non-HPCs (EPC and multipotent stromal cells), with a larger representation of myeloid HPC[12-15]. In 2011, a randomized Phase I clinical trial by Perin et al. demonstrated that intramuscular (i.m.) transplantation of autologous BM ALDH^{hi} cells significantly improved Rutherford's Category scores and ankle-brachial index measurements from baseline in patients with non-operational CLI but did not improve ischemic ulcer healing[16]. These results provided rationale for a Phase II trial (PACE trial) which aimed to stimulate revascularization in patients with intermittent claudication, thereby mitigating progression toward end-stage CLI[17]. This double-blinded multicenter study recently reported that transplantation of autologous BM-derived ALDH^{hi} cells was unable to effectively improve exercise performance or blood perfusion via collateral vessel formation after 6 months[18]. Although the preclinical data used to initiate early clinical studies were promising[13], several factors may explain why preclinical efficacy in murine models does not accurately predict clinical efficacy in humans. The preclinical experiments were performed using healthy human BM ALDH^{hi} cells trans-planted into immunodeficient mice with surgically induced limb ischemia. Femoral artery ligation (FAL) in mice has been the gold-standard preclinical model to assess therapeutic angiogenesis elicited by pharmaceuticals or cells; however, the model does possess several limitations which need to be addressed to improve clinical translation. Specifically, this model mimics an acute ischemic injury occurring in young and healthy animals and does not reflect the chronic ischemic microenvironment occurring in human patients due to the buildup of atherosclerotic plaques over an extended period of time. In addition to physiological differences between species (i.e., heart rate and plasma cholesterol), patients with PAD commonly demonstrate other influential factors, chronic inflammation, smoking, and sedentary lifestyles, which are difficult to mimic in a murine model. Furthermore, emerging preclinical evidence also indicates autologous BM mononuclear cells (MNC) harvested from patients with chronic atherosclerosis and associated comorbidities exhibit severe functional impairments[19,20]. Endothelial cells derived from healthy animals exhibited vascular regenerative functions in a diabetic model of myocardium ischemia, whereas, cells harvested from diabetic animals failed to

induce vasculogenesis[21]. Several studies have aimed to increase clinical efficacy by purification of select subpopulations (CD341) derived from autologous BM-MNC [22]; however, this approach has provided a modest benefit over transplantation of unpurified BM-MNC. Alternatively, using healthy allogenic sources may improve the efficacy of cell-based therapies, by limiting the exposure of therapeutic cells to the damaging microenvironment of chronic disease[23,24]. ALDH provides protection to long-lived stem and progenitor cell populations from cytotoxic insults[25]. Representing a conserved stem cell function and coinciding with primitive surface marker expression (CD341), ALDH^{hi}-activity rapidly diminishes as multipotent HPC differentiate toward more expendable lineage-restricted phenotypes[15]. ALDH also rep-resents the rate-limiting enzyme in the production of retinoic acid (RA), a potent driver of hematopoietic differentiation. RA activates the retinoic acid receptor (RAR) - retinoid X receptor (RXR) nuclear receptor complex that regulates mRNA transcription and epigenetic modifications[26], resulting in hematopoietic cell differentiation. For example, activation of RAR/RXR induces the expression cyclic-ribose ADP hydrolase (CD38), a membrane-bound enzyme implicated with hematopoietic cell differentiation[27]. Therefore, the *ex vivo* expansion of UCB ALDH^{hi} cells represents a paradoxical challenge to increase primitive and pro-angiogenic ALDH^{hi} cell numbers while limiting RA-induced hematopoietic differentiation. We have recently shown that UCB ALDH^{hi} cells can be efficiently expanded under serum-free conditions to generate hematopoietic progeny retaining vascular regenerative functions *in vivo*[28]. However, as culture time was increased from 6 to 9 days, expanded progeny failed to retain vascular regenerative functions. In addition, reducing RA-production by inhibition of ALDH-activity during *ex vivo* expansion augmented the number of CD34 HPC with SCID-repopulation capacity[29,30]. Therefore, we sought to determine whether inhibition of ALDH-activity, using diethylaminobenzaldehyde (DEAB) treatment, would enhance the expansion of UCB ALDH^{hi} cells without loss of vascular regenerative functions assessed after i.m. transplantation into mice with FAL-induced unilateral hind-limb ischemia

2.2   Methods

2.2.1   Isolation of Human UCB ALDH^{hi} Cells

Human UCB samples were obtained with informed consent by venipuncture of the umbilical vein following Ceasarian section at Victoria Hospital Birthing Centre, London, ON, Canada. The Human Studies Research Ethics Board (HSREB) at Western University approved all procedures. Within 24 hours of collection, UCB samples were initially depleted of mature myeloid, lymphoid and red blood cells (RosetteSep Human Cord Blood Progenitor Cell Enrichment Cocktail, Stem Cell Technologies, Vancouver, BC, Canada). Lineage-depleted (Lin-) mononuclear cells were isolated by Hypaque Ficoll centrifugation and incubated with Aldefluor regent prior to purification by FACS (FACS Aria III, BD Biosciences, Mississauga, Ontario, Canada). UCB ALDH^{hi} cells were selected based on low side scatter and high ALDH-activity with >98% purity, as previously described[12,15,28].

.

2.2.2   Expansion of UCB ALDH^{hi} Cells in Culture

UCB ALDH^{hi} cells were plated on fibronectin-coated flasks and expanded in serum-free X-vivo 15 (Lonza, Basel, Switzerland) supplemented with 10 ng/ml thrombopoietin (TPO), Fms-like tyrosine kinase 3 ligand (FLT-3L), and stem cell factor (SCF) for up to 9 days, herein referred to as Basal conditions. All growth factors were purchased from Life Technologies (Carlsbad, CA). To inhibit ALDH-activity and limit cell differentiation, 1.0×10^{-5} mol/l diethylaminobenzaldehyde (DEAB) (Stem Cell Technologies, Vancouver, Canada) was added to Basal conditions between days 3 and 6 of *ex vivo* expansion, herein referred to as DEAB-treated conditions. DEAB dose and treatment kinetics were optimized based on maximal retention of ALDH^{hi} cells at endpoint. Complete media change was performed every 3 days.

.

2.2.3 Generation of HPC-Conditioned Media and Cell Lysates for Proteomic Analyses

Expanded cells were harvested and washed with phosphate-buffered saline (PBS) to remove residual growth factors and resuspended in fresh RPMI 1640 + 10 ng/ml of SCF, TPO, and FLT-3L for 24 hours to generate conditioned media (CM) in biological triplicate. CM was centrifuged to remove cellular debris and concentrated using 3 kDa molecular weight cutoff filter units (Millipore, Bedford, MA). Concentrated CM was lyophilized overnight and resuspended in 8 mol/l urea, 5.0×10^{-2} mol/l ammonium bicarbonate, 1.0×10^{-2} mol/l dithiothreitol, and 2% SDS solution before secreted protein quantitation and fractionation. Expanded cell pellets were lysed in 8 M urea buffer, and sonicated (20×0.5 second pulses; level 1) to shear DNA. Protein concentrations were estimated using the Pierce 660 nm protein assay (ThermoFisher Scientific, Waltham, MA).

2.2.4 Chloroform/Methanol Precipitation and Protein Digestion

Cell lysates or CM were reduced in 1.0×10^{-2} mol/l dithiothreitol for 30 minutes and alkylated in 1.0×10^{-1} mol/l iodoacetamide for 30 minutes. Samples were precipitated in chloroform/methanol in 1.5 ml microfuge tubes[31]; 50 μg aliquots of each sample were topped up to 150 μl with 5.0×10^{-2} mol/l ammonium bicarbonate, 600 μl of ice-cold methanol, followed by 150 μl of chloroform; 450 μl of water was added before vortexing and centrifugation at 14,000g for 5 minutes. The upper/aqueous methanol phase was removed and 450 μl of ice-cold methanol was added before vortexing and centrifugation. Precipitated protein pellet was air dried before protein digestion. For on-pellet protein digestion, 100 μl of 5.0×10^{-2} mol/l ammonium bicarbonate (pH 8.0) trypsin/LysC (1:50 ratio, enzyme:sample) (Promega, Madison, WI) solution was added before incubation overnight at 37°C in water bath shaker. Trypsin (1:100 ratio) was added for 4 hours before acidifying with 10% formic acid (pH 3–4). Digests were centrifuged at 16,000g to remove insoluble material. Peptide concentrations were estimated using a BCA assay (ThermoFisher Scientific).

2.2.5   SCX Peptide Fractionation

Tryptic peptides recovered from chloroform/methanol precipitation of cell lysates or CM (50 μg) were fractionated using SCX StageTips[32]. Peptides were acidified using 1% Trifluoroacetic acid and loaded onto a 12-plug StageTips. Six SCX fractions were collected by eluting in 7.5×10^{-2}, 1.25×10^{-1}, 2.0×10^{-1}, 2.50×10^{-1}, and 3.0×10^{-1} mol/l ammonium acetate/20% acetonitrile/0.5% formic acid (FA) solutions followed by elution with 5% (w/v) ammonium hydroxide/80% ACN. Fractions were dried in a SpeedVac, resuspended in double distilled water and dried again to remove residual ammonium acetate. All samples were resuspended in 0.1% FA before liquid chromatography–tandem mass spectrometry (LC-MS)/MS analysis.

2.2.6   Liquid Chromatography–Tandem Mass Spectrometry

One microgram of sample was injected into a Waters nanoAcquity HPLC system (Waters, Milford, MA) coupled to an ESI Orbitrap mass spectrometer (Orbitrap Elite or QExactive, ThermoFisher Scientific). Buffer A consisted of water/0.1% FA and buffer B consisted of ACN/0.1% FA. All samples were trapped for 5 minutes at a flow rate of 10 μl/minute using 99% Buffer A, 1% Buffer B on a Symmetry BEH C18 Trapping Column, 5 μm, 180 μm × 20 mm (Waters). Peptides were separated using a Peptide BEH C18 Column, 130Å, 1.7 um, 75 um × 250 mm operating at a flow rate of 300 nl/minute at 35°C (Waters). Cell lysate samples were separated using a nonlinear gradient consisting of 5%–7.5% B over 1 minute, 7.5%–25% B over 180 minutes and 25%–60% B over 240 minutes before increasing to 98% B and washing. CM samples were separated using a nonlinear gradient consisting of 1%–7% B over 3.5 minutes, 7%–19% B over 90 minutes, and 19%–30% B over 120 minutes before increasing to 95% B and washing. Settings for data acquisition on the Orbitrap Elite and QExactive are provided in Table 2.1.

Table 2.1 Overview of parameters used for data acquisition on a Q Exactive and LTQ Orbitrap Elite.

Parameters	Q Exactive	LTQ Orbitrap Elite
Mass Range (m/z)	400-1450	400-1400
Isolation Window (m/z)	3.0	2.0
MS Resolution	35K @ 200m/z	60K @ 400m/z
MSMS Resolution	17.5K	66000 Da/s (Rapid CID)
MS Injection Time (ms)	250	200 (FTMS)
MSn Injection Time (ms)	120	150(ITMS)
AGC Target (MS)	1E6	1E6 (FTMS)
AGC Target (MSn)	2E5	1E5
Preview Scan	n/a	enabled
Threshold (counts)	50K	500
Underfill Ratio	3%	n/a
Data Dependent Aquisition	Top 15	Top 20
Dynamic Exclusion (s)	30	30
Exclusion Mass Width (m/z)	n/a	0.5(low), 1.5(high)
Exlcude Isotopes/ Monoisotopic precursor Selection	enabled	enabled
Fragmentation Type	HCD	CID
Normalized Collision Energy	23	35
Lock Mass (445.120025m/z)	best	enabled
Charge State Rejection	unassigned and +1	unassigned and +1
Default Charge State	+2	+2

.

2.2.7   Proteomic Data Analyses

Data analysis was performed using PEAKS 8.0 software (Bioinformatics Solutions Inc., Waterloo, ON, Canada). Raw data files were refined using correct precursor mass and de novo sequencing was performed using the following parameters: parent mass tolerance 20 ppm; fragment ion tolerance 0.80 Da; enzyme was set to trypsin. Data analyses were searched against the Uniprot human sequence database (20,178 entries). Quantitative data analysis was performed using MaxQuant version 1.5.2.8[33]. Protein and peptide false discovery rate were set to 0.01 (1%), while the decoy database was set to revert. All parent and fragment tolerances were set as described above. The match between runs was enabled and all other parameters left at default. Data were analyzed using label free quantitation and intensity-based absolute quantification as described previously[34]. Bioinformatic analysis was performed using Perseus version 1.5.0.8 and proteins identified by site, reverse and contaminants were removed manually. When using the match between runs feature, datasets were filtered for proteins containing a minimum of one unique peptide in at least two biological replicates. Missing values were replaced using data imputation by using a width of 0.3 and a downshift of 1.2[35].

2.2.8   Flow Cytometry

Expanded HPC were harvested following 6- or 9-day expansion and enumerated by trypan blue exclusion using hemocytometer counts. Cells were labelled with Aldefluor to assess ALDH-activity and co-stained with 7-amino-actinomycin D to determine viability. Cells also were labeled with anti-human antibodies for CD45 (pan-hematopoietic marker), CD33 (myeloid), CD14 (monocytes), CD31 (PECAM), CD41 (ITGA2), and CD42 (megakaryocyte). Cells were assessed for the retention of primitive HPC phenotypes using CD34 and differentiation of

expanded cells was determined using CD38 (cyclic ADP ribose hydrolase). Cell surface marker expression for total cells, as well as ALDH^{hi} versus ALDH^{lo} subsets was determined using an LSRII flow cytometer (BD Biosciences) at the London Regional Flow Cytometry Facility. Analyses were performed using FlowJo software v8.2.

2.2.9 Hematopoietic Colony Formation

To assess the retention of hematopoietic colony forming function following expansion, day 9 expanded HPC were harvested and seeded in semi-solid methylcellulose media (H4434, Stem Cell Technologies) at 500 cells/well in 12-well plates, in duplicate. Hematopoietic colonies were enumerated after 12-14 days *in vitro* and scored based on morphological characteristics.

2.2.10 qRT-PCR analysis of Retinoic Acid Signaling Pathway

Total mRNA was extracted from Day 9 Basal or DEAB-expanded HPC using PerfectPure RNA Purification kits (5Prime, Beverly, MA). Nanodrop^{TM} was performed to establish mRNA concentration and purifty at the London Regional Genomics Facility prior to production of 500ng of cDNA using iScript cDNA conversion kits (Bio-Rad; Hercules, CA), according to manufactures protocol. qRT-PCR was performed using the Sofast Evagreen Supermix detection system (Bio-Rad) in conjunction with a CFX384 (Bio-Rad, Hercules, CA). Validated primers for ALDH1A3 (HQP005252), CYP26A1 (HQP003919), RARA (HQP016114) and RARG (HQP016118) were purchased from Genecopoeia (Rockville, MD). Quantification of transcripts was assessed using the housekeeping gene GUSB and normalized to Day 9 HPC harvested from Basal conditions.

2.2.11 Femoral Artery Ligation and Transplantation

Unilateral hind limb ischemia was induced in anesthetised (100mg/kg ketamine/xylazine, maintain with 2% isoflurane, 0.8L/min) NOD/SCID mice via surgical ligation and excision of the femoral artery and vein (FAL), as previously described[206]. NOD/SCID mice with unilateral hind-limb ischemia (perfusion ratio <0.1, 24-hours after surgery (Day 0) were transplanted with a total of 5.0x10^5 expanded cells from Basal or DEAB-treated conditions, or non-cellular vehicle control, by intramuscular (i.m) injection (20uL) at three sites between ligation landmarks. To serve as a non-cellular vehicle control, mice received i.m.-injections of 60μl of PBS in a similar fashion to cell-transplanted mice.

2.2.12   Laser Doppler and Catwalk

Anesthetised NOD/SCID mice were warmed to 37ºC for 5 minutes and hindlimb blood perfusion was measured using Laser Doppler perfusion imaging (LDPI). Recovery of blood flow was quantified on 3, 7, 14, 21, 28, and 35 days post-transplantation by comparing the perfusion ratio (ischemic/non-ischemic) of transplanted mice. Recovery of limb usage in transplanted mice was determined by the ratio of paw print area in transplanted limb versus the contralateral control was assessed at Day 7 and 35 using the Noldus Catwalk Imaging system, as previously described[28].

2.2.13   Immunofluorescent Microscopy

Adductor muscle) from both ischemic and non-ischemic thighs were harvested, embedded in OCT, and cryosectioned (12μm) to obtain three sections per slide ≥50μm apart. Cryosections were fixed in 10% formalin (Sigma) and blocked with 5% serum. Capillary density was quantified at 7 and 35-days post-transplantation using rat anti-mouse CD31 (BD Biosciences; 1:100) detected with fluorescein-labeled rabbit anti-rat secondary antibodies (Vector; 1:200). CD31+ cells were enumerated from 4 randomly selected fields of view per section of murine thigh muscles, totaling 12 images per limb. EdU+ proliferating cells were detected using the Click-iT imaging kit (Alexafluor 594; Life Technologies), co-stained with CD31 to allow quantification of proliferating endothelial cells. Functional vessel density was also visualized using rabbit anti-mouse von Willebrand factor (1:100) detected with goat anti-rabbit fluorescein-labeled secondary antibodies (1:200). DAPI was used as counterstain to label nuclei.

2.2.14   Determination of Human Cell Engraftment into Murine Tissues

Serial cryosections (25 μm) were obtained across 150μm of ischemic adductor muscles harvested 7 days post-transplantation (n=4). Cryosections were fixed in 10% formalin and blocked mouse-on-mouse reagent (Vector Labs, Burlingame, CA, USA). Human cell engraftment was visualized by staining muscle sections with mouse anti-human HLA-A,B,C (1:100) detected with horse anti-mouse fluorescein-labelled secondary antibodies (1:200). DAPI was used as counterstain to label nuclei.

2.2.15   Statistical Analyses

A multiple sample t test was performed in Perseus comparing the cell lysates for day 9 Basal versus DEAB for proteomic analysis; and day 6 Basal versus day 9 Basal for secretome analysis. Statistical analysis for flow cytometry, quantitative polymerase chain reaction (qPCR), hematopoietic colony forming-cell analyses was performed using a student's t test within each time point. Analysis of significance was performed by one-way analysis of variance with Tukey's multiple comparisons tests for all *in vivo* experiments and enumeration of myeloid-specific colony formation. Outliers were identified using Grubb's test; $p < .05$.

2.3   Results

2.3.1   Basal Conditions Promoted Expansion of Cells with Megakaryocyte Secretory Profile

We have recently demonstrated UCB ALDH^{hi} cells expanded under Basal conditions for 6 but not 9 days, accelerated the recovery of hindlimb perfusion after transplantation[28]. This led us to investigate whether additional culture time (3 days) changed the secretory profile of expanded hematopoietic progeny, thereby limiting vascular regenerative function *in vivo*. Mass spectrometry proteomic analysis was used to determine changes in the secretome of cells harvested after culture under Basal conditions (N = 3) at day 6 or day 9. A total of 5,404 unique proteins were detected, with 3,636 proteins identified in CM generated by both day 6 and day 9 expanded cells; 325 proteins or 1443 proteins were exclusively contained within CM generated from day 6 or day 9 cells, respectively. Major cytokines associated with angiogenesis were present in CM generated from both expanded cell populations. Therefore, we focused on the relative quantity of proteins commonly secreted. Of the 3,636 common proteins secreted, 144 and 317 proteins were significantly increased in day 6 and day 9 CM, respectively. Distinct patterns of expression were identified reflecting widespread changes in protein expression as culture time was increased (Fig. 2.1A). Although day 6 and day 9 cells demonstrated polarized regenerative function *in vivo*[28], the secretion of proangiogenic proteins, such as vascular

endothelial growth factor (VEGF)-A and angiopoietin 1 (ANGPT1), was comparable between expanded cell populations. Interestingly, proteins involved in inflammation and platelet activation were enriched within CM generated from day 9 cells (Figure 2.1B). For example, platelet activation-associated proteins significantly increased in CM generated from day 9 cells included integrin α-IIb (ITGA2B, CD41), glycoprotein Ib (GP1B, CD42), glycoprotein IX (GP9), and platelet endothelial aggregation receptor 1 (Fig. 2.1C). Flow cytometry was used to validate expression of CD41 and CD42, classic markers of megakaryocyte-lineage differentiation (Fig. 2.1D). These analyses demonstrated that expansion of UCB-derived ALDH^{hi} cells under Basal conditions enriched for cells with a committed megakaryocyte (CD41+/CD42+) phenotype as culture time progressed from 6 to 9 days (25.76 $\pm$ 5.14% vs. 54.7 $\pm$ 6.50%; *, $p < .05$; Figure 2.1E). Importantly, this end-stage megakaryocyte differentiation was also associated with the loss of vascular regenerative capacity after transplantation[28].
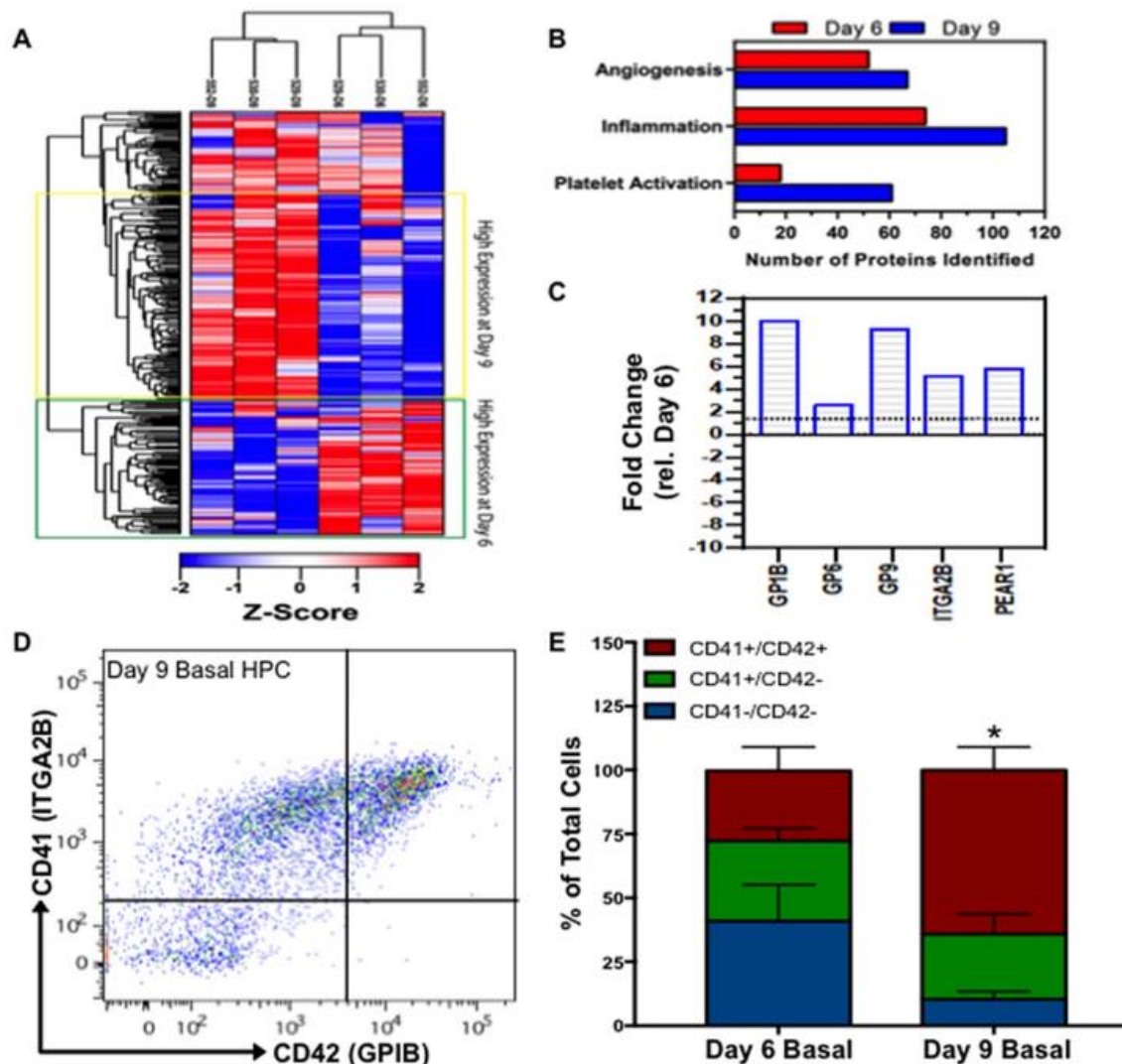
Figure 2.1 Umbilical Cord blood ALDH^{hi} cells differentiated toward a megakaryocyte phenotype when cultured under Basal conditions. Viable day 6 (N=3) or day 9 (N=3) cells expanded under basal conditions were replated in RPMI 1640+ stem cell factor, thrombopoietin, Fms-like tyrosine kinase 3 ligand for 24 hours to generate conditioned media (CM). (A) Mass Spectomtery analyses of CM revealed distinct secretome profiles. (B) Secretory profile of day 9 cells was highly enriched with proteins implicated in platelet activation. (C) Day 9 cells significantly upregulated the expression of CD41 (ITGA2B) and CD42 (GPIB), compared with day 6 cells. (D, E) Increased culture time under Basal conditons enriched for cells with a megakaryocyte phenotype (CD41+/CD42+). Data represented as mean $\pm$ SEM (*, p <.05; N=5-7). Statistical analyses were determined by paired Student's t test.

2.3.2 DEAB-Treatment Augmented ALDH^{hi} Cell Expansion

ALDH^{hi} cells represented only 2.47 $\pm$ 1.33% Lin– cells (Fig. 2.2A) correlating to <0.5% of total MNC collected. In addition, UCB ALDH^{hi} cells rapidly reduce ALDH-activity (Fig. 2.2B) during *ex vivo* expansion 28. Therefore, ALDH^{hi} cells were expanded with or without DEAB-treatment, to inhibit ALDH-activity and limit RA-induced differentiation during culture (Fig. 2.2B). Exposure of cells to DEAB-treatment at days 3–6 was selected based on the optimal preservation of ALDH^{hi} cells during 6- and 9-days expansion *ex vivo* (Figure 2.3). Temporal DEAB-treatment from days 3 to 6 increased expanded ALDH^{hi} cell frequency at day 6 (40.98 $\pm$ 8.43% vs. 13.85 $\pm$ 2.38%; **, $p < .01$) and at day 9 (31.04 $\pm$ 5.48% vs. 6.58 $\pm$ 1.03%; **, $p < .01$; Fig. 2.2C). Total cell expansion kinetics were equivalent over 9 days with or without DEAB-treatment (82.62 $\pm$ 9.51-fold vs. 79.22 $\pm$ 16.49-fold increase; Fig. 2.2D). Taken together, DEAB-treatment led to a 25.42 $\pm$ 4.35-fold increase in ALDH^{hi} cell numbers obtained after 9 days; a significant increase compared with Basal conditions (5.40 $\pm$ 1.27-fold increase; ***, $p < .001$; Fig. 2.2E). Therefore, DEAB-treatment from days 3 to 6 during a 9-day expansion protocol was selected for further assessment of primitive progenitor cell phenotype and function.
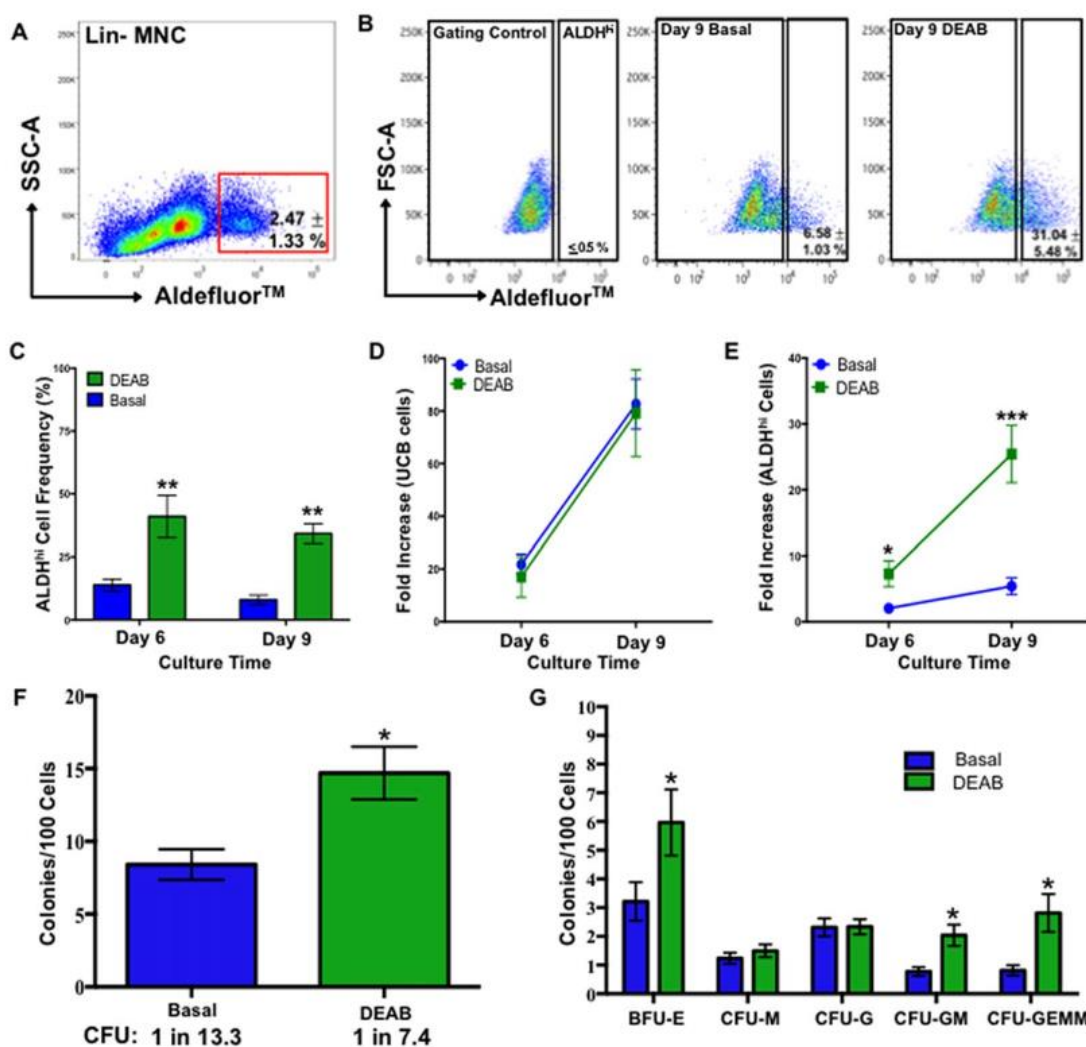
Figure 2.2 Diethylaminobenzaldehyde (DEAB)-treatment augmented the expansion of early myeloid progenitors with high ALDH-activity. (A) Umbilical cord blood ALDH^{hi} cells were isolated by fluorescence-activated cell sorting and expanded with or without DEAB-treatment between days 3 and 6. (B) Representative flow cytometry plots showing DEAB-treatment enhanced (C) the frequency of ALDH^{hi} cells retained after 9 days (N=7). (D) Total cell expansion was not affected by DEAB-treatment, whereas (E) total ALDH[hi] cell number was increased ~25-fold under DEAB-treated conditions. (F) DEAB-treatment increased hematopoietic colony forming capacity of expanded cells seeded in methylcellulose media (N=5). (G) DEAB-treatment enhanced the production of colonies with multiple myeloid phenotypes. Data represented as mean $\pm$ SEM (*, $p<.05$; **$p<.01$;***$p<.001$). Statistical analyses were determined by paired Student's t test.
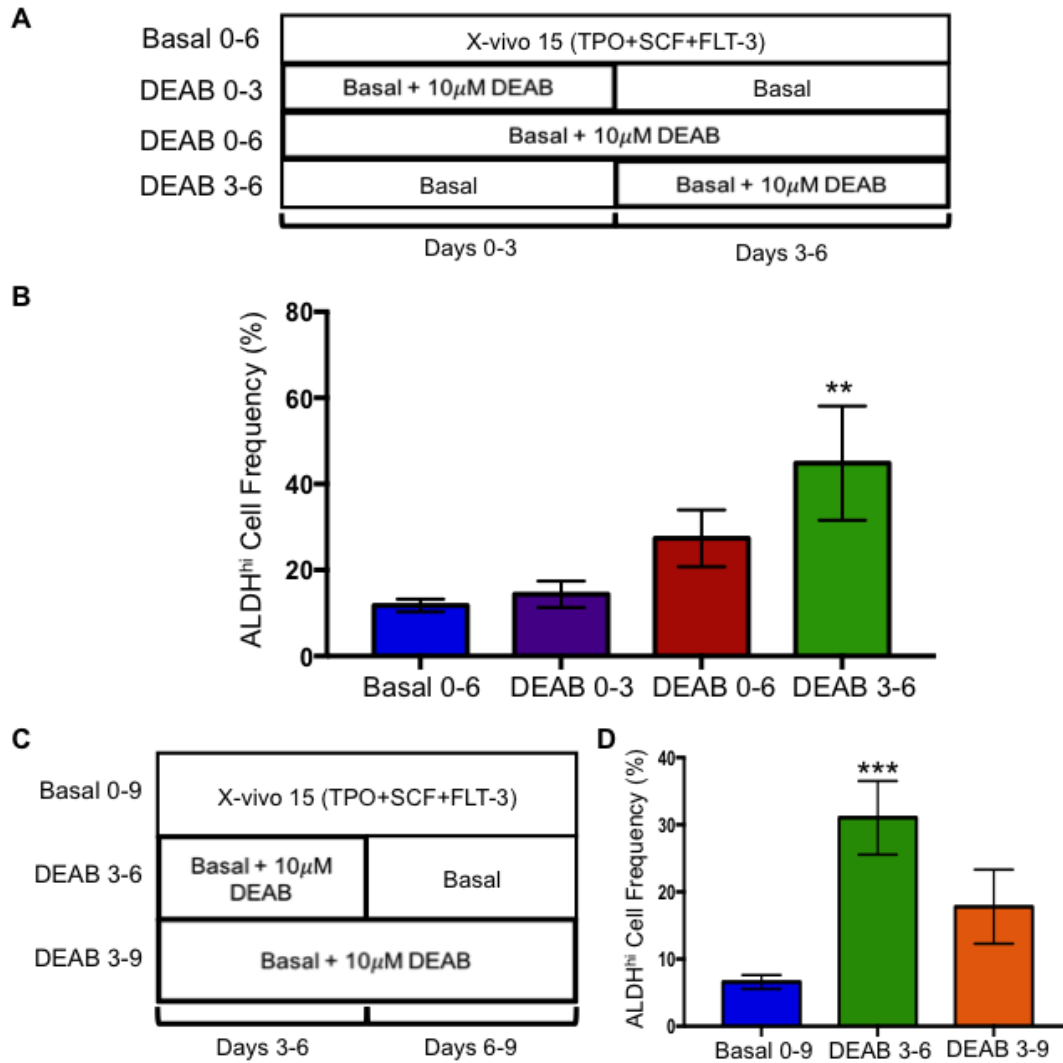
Figure 2.3 Temporal DEAB-treatment increases the retention of ALDH^{hi} cells
during *ex vivo* expansion. (A) UCB ALDHhi cells were cultured under Basal
conditions (X-vivo 15 + 10ng/mL TPO, SCF, FLT-3L) for 6 days and treated with
10uM of DEAB between days 0-3, 0-6, or 3-6. (B) DEAB-treatment occurring
between Days 3-6 increased enrichment of ALDHhi cells. (C-D) Extending on these
results, DEAB-treatment was either removed (DEAB 3-6) or extended (DEAB 3-9)
for an additional 3 days of culture. Interestingly, temporal DEAB-treatment (DEAB
3-6) increased the frequency of ALDHhi cells retained after 9 days of culutre,
compared to Basal conditions. Data represented as Mean ± SEM (**p<0.01,
***p<0.001; N=3-13). Statistical analyses were determined by ANOVA with
Tukey's multiple comparisons test.

2.3.3　RA-Signaling Was Modified following DEAB-Treatment

ALDH-activity leads to the production of RA, a potent driver of hematopoietic differentiation. To validate that DEAB-treatment modulated RA-signaling during expansion, we first performed reverse transcriptase-qPCR on transcriptional targets of the RAR/RXR complex. Activation of the RAR/RXR complex was expected to increase transcription of target genes such as CYP26A1, ALDH1A3 isoform, and RAR[25]. DEAB-treatment significantly reduced transcription of ALDH1A3, CYP26A1, and RAR subunit while transcription of RAR　was increased (Figure 2.4). Collectively, this suggested RA-signaling networks were modified following DEAB-treatment.
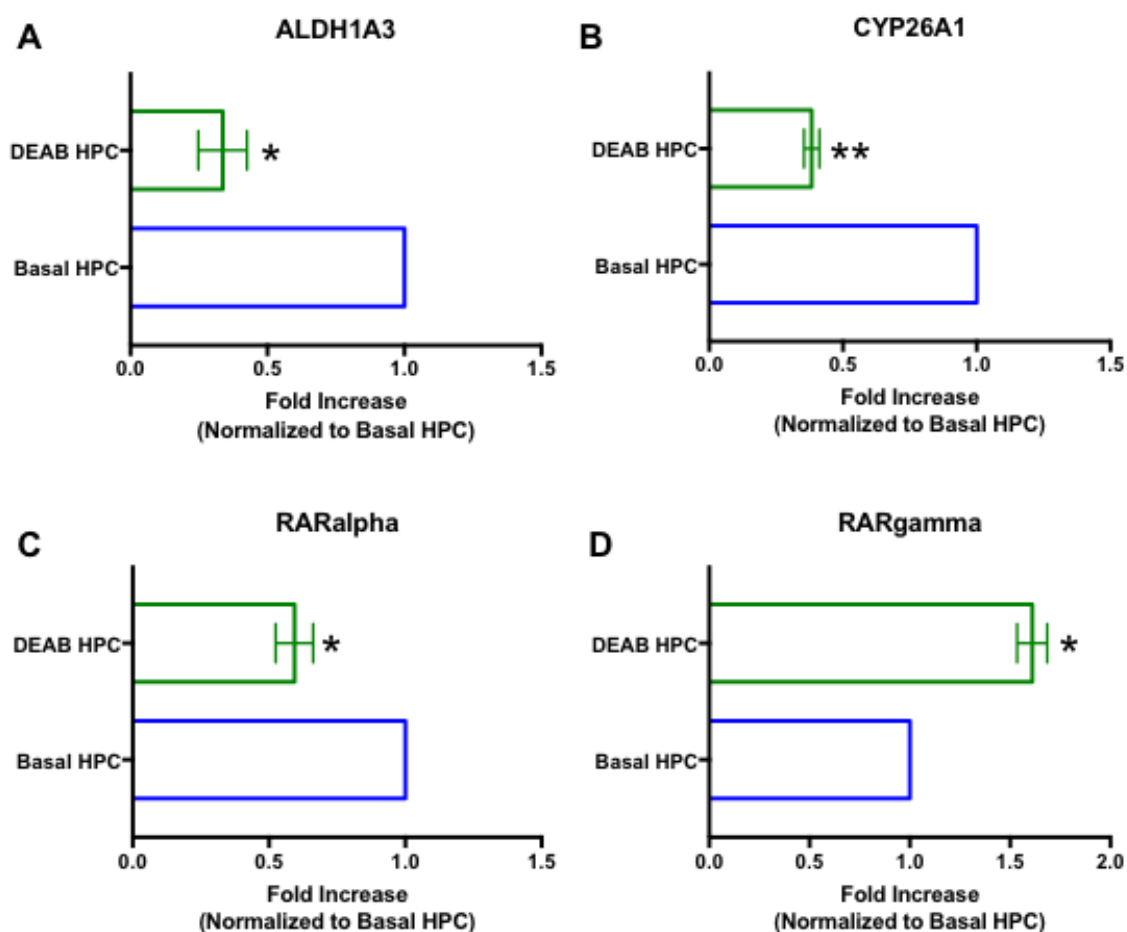
Figure 2.4 Transcriptional analysis of Day 9 cells cultured under Basal or DEAB-treated conditions. RT-qPCR was performed on cell lysates (n=3) of UCB ALDH^{hi} cells cultured under Basal or DEAB-treated conditions for 9 days. Fold changes are relative to Day 9 Basal cells. DEAB-treated conditions decreased the transcription of (A) Aldehyde Dehydrogenase 1A3, (B) Cytochrome P450 Retinoic Acid-Inactivating 1, (C) Retinoic Acid Receptor-Alpha, (D) Whereas, DEAB-treated conditions increased the transcription of (G) Retinoic Acid Receptor-Gamma. β-glucuronidase (GUSB) was used as a housekeeping gene. Data represented as Mean ± SEM. (*p<0.05, **p<0.01). Statistical analyses were determined by Student's t-test.

2.3.4 DEAB-Treatment Enriched for Cells with Multipotent Myeloid Progenitor Function

To determine whether expanded cells retained hematopoietic colony forming unit (CFU) functions *in vitro*, day 9 cultured cells were seeded in methylcellulose media and enumerated for myeloid-lineage colony formation after 14 days. DEAB-treated cells demonstrated a significantly higher frequency (*, $p < .05$) of total colony formation (1 CFU in 7.4 cells) compared with cells expanded under Basal conditions (1 CFU in 13.3 cells; Fig. 2.2F). DEAB-treatment enriched specifically for early HPC with myeloid multipotency; enumerated by colonies demonstrating multiple myeloid morphologies (Fig. 2.2G). Thus, DEAB treatment augmented the expansion of ALDH^{hi} cells that retained multipotent hematopoietic CFU capacity *in vitro*.

2.3.5 DEAB-Treatment Enriched for Cells with Primitive Surface Marker Expression

To determine whether DEAB-treatment also prevented the loss of primitive cell surface phenotype (ALDH^{hi}/CD34$^+$/CD38$^-$) during expansion, cells were analyzed using multicolor flow cytometry (Table 2.2). At day 9, expanded cells were exclusively hematopoietic determined by pan-leukocyte marker (CD45) expression (>99%), and the majority of Basal or DEAB-treated cells expressed the early myeloid cell surface marker CD33 (96.1 $\pm$ 0.85 and 94.5 $\pm$ 1.53%, Table 2.3). Monocyte-specific marker (CD14) expression was comparable between Basal and DEAB-treated conditions (2.96 $\pm$ 1.23 vs. 4.08 $\pm$ 1.64% of total cells). compared with Basal conditions, expression of the hematopoietic differentiation marker CD38 was significantly reduced following DEAB-treatment (31.06 $\pm$ 2.52 vs. 21.16 $\pm$ 2.56% of total cells; **, $p < .01$; Table 1). Futhermore, DEAB-treatment enriched for cells with primitive ALDH^{hi}/CD34+ (2.18 $\pm$ 0.42 vs. 6.20 $\pm$ 0.73% of total cells; *, $p < .05$) and ALDH^{hi}/CD34+/CD38– (2.29 $\pm$ 0.35 vs. 5.46 $\pm$ 0.59% of total cells; ***, $p < .001$) phenotypes (Table 2.2). Collectively, DEAB-treatment generated 5- and 10-fold increase in the total number of ALDH^{hi} CD34+ or ALDH^{hi} CD34+/CD38– after 9 days, respectively (Table 2.3). In contrast, Basal conditions generated a modest 1.7- and 4.1-fold increase in the number of ALDH^{hi}

CD34+ or ALDH^{hi} CD34^{+}/CD38^{-}, respectively. Basal conditions highly enriched for cells with mature hematopoietic cell (ALDH^{lo}/CD38^{+}) phenotype (24.59 $\pm$ 2.70% of total cells; ***, $p < .001$; Table 2.2). Collectively, DEAB-treatment enhanced the expansion of hematopoietic cells retaining ALDH^{hi}-activity and primitive cell surface marker expression patterns.

.

Table 2.2 DEAB-treatment enhanced the expansion of cells with a primitive surface phenotype

Expanded HPC		% of Total Cells			
Population	Phenotype	Day 6 Basal	Day 6 DEAB	Day 9 Basal	Day 9 DEAB
BULK	CD34+	20.71 ± 2.09	22.20 ± 2.51	9.49 ± 1.03	9.37 ± 1.53
	CD34+ CD38-	11.77 ± 2.14	**17.19 ± 2.09***	7.43 ± 1.05	7.57 ± 1.21
	CD38+	20.24 ± 5.77	**11.09 ± 2.36***	31.06 ± 2.52	**21.16 ± 2.56****
ALDH^{hi}	CD34+	5.7.2 ± 1.36	**11.46 ± 1.77***	2.18 ± 0.42	**6.20 ± 0.73***
	CD34+ CD38-	2.77 ± 0.70	**9.20 ± 1.36***	2.29 ± 0.35	**5.46 ± 0.59*****
	CD38+	6.22 ± 1.95	5.31 ± 0.90	2.95 ± 0.84	**8.94 ± 1.73***
ALDH^{lo}	CD34+	**10.98 ± 1.32***	6.34 ± 1.48	5.64 ± 0.80	**2.47 ± 0.76*****
	CD34+ CD38-	7.01 ± 1.17	5.56 ± 1.36	3.96 ± 0.69	**1.75 ± 0.58***
	CD38+	6.62 ± 2.60	3.78 ± 1.04	24.59 ± 1.81	**6.25 ± 2.70*****

Data expressed as Mean ± SEM; (*p<0.05, **p<0.01, ***p<0.001; N=5-9). Statistical analyses were determined by Student's t-test compared within each time point.

Table 2.3 UCB ALDH^{hi} cell expansion under Basal or DEAB-treated conditions generates myeloid-specific cell progeny.

		% of Total Cells	
Population	Phenotype	Day 9 Basal	Day 9 DEAB
Bulk	CD33+	96.1 ± 0.85	94.5 ± 1.53
	CD14+	2.96 ± 1.23	4.08 ± 1.64

Data expressed as Mean ± SEM; N=8. Statistical analyses were determined by Student's t-test.

Table 2.4 . DEAB-treatment enhanced the number of expanded cells with primitive surface phenotype

Expanded UCB ALDH^{hi} cells		Fold Increase (rel. Day 0 UCB ALDH^{hi} Cells)	
Population	Phenotype	Day 9 Basal	Day 9 DEAB
BULK	CD34+	8.13± 0.87	7.62± 1.49
	CD34+ CD38-	15.65 ± 1.98	15.01 ± 2.77
ALDH^{hi}	CD34+	1.77 ± 0.30	**5.06 ± 0.87****
	CD34+ CD38-	4.96 ± 0.80	**10.93 ± 1.79****
ALDH^{lo}	CD34+	**4.75 ± 0.64***	2.00 ± 0.58
	CD34+ CD38-	**8.08 ± 1.09****	3.46 ± 0.94

Data expressed as Mean ± SEM; (*p<0.05, **p<0.01, ***p<0.001; N=5-9). Statistical analyses were determined by Student's t-test.

2.3.6   DEAB-Treatment Reduced Megakaryocyte Lineage Maturation

Basal culture conditions led to UCB ALDH^{hi} cell differentiation toward a megakaryocyte phenotype as culture time progressed (Fig. 2.1). Therefore, we sought to determine whether DEAB-treatment delayed differentiation of expanded ALDH^{hi} cells toward the megakaryocyte lineage (Fig. 2.5A). Although we did not observe differences in the frequency of expanded cells acquiring mature megakaryocyte phenotype (CD41$^+$/CD42$^+$) at day 9 (Fig. 2.5B), DEAB-treatment significantly reduced the frequency of CD41+ cells that coexpressed CD38 (17.3 $\pm$ 2.7 vs. 26.2 $\pm$ 6.4% of CD41$^+$ cells; Fig. 2.5C; *, p < .05, and Table 2.5). Furthermore, DEAB-treatment significantly reduced the expression of CD38 on CD41$^+$/CD42$^+$ megakaryocytes, compared with Basal conditions (*, p < .05; Fig. 3D). Previous reports have also suggested that expanded CD41$^+$/CD42$^-$ hematopoietic cells retain myeloid multipotency *in vitro* and SCID-repopulating capacities *in vivo* when coexpressing a CD34$^+$/CD38$^-$ phenotype[36]. At day 9, DEAB-treatment enriched the CD41$^+$/CD42$^-$ megakaryoblast fraction with primitive CD34$^+$/CD38$^-$ phenotype (13.1 $\pm$ 2.4% vs. 8.2 $\pm$ 2.0%; *, p < .05; Table 2.5). Collectively, these results suggested that DEAB-treatment delayed the maturation of CD41$^+$/CD42$^-$ megkaryoblasts by delaying CD38 acquisition and loss of CD34 expression.

.
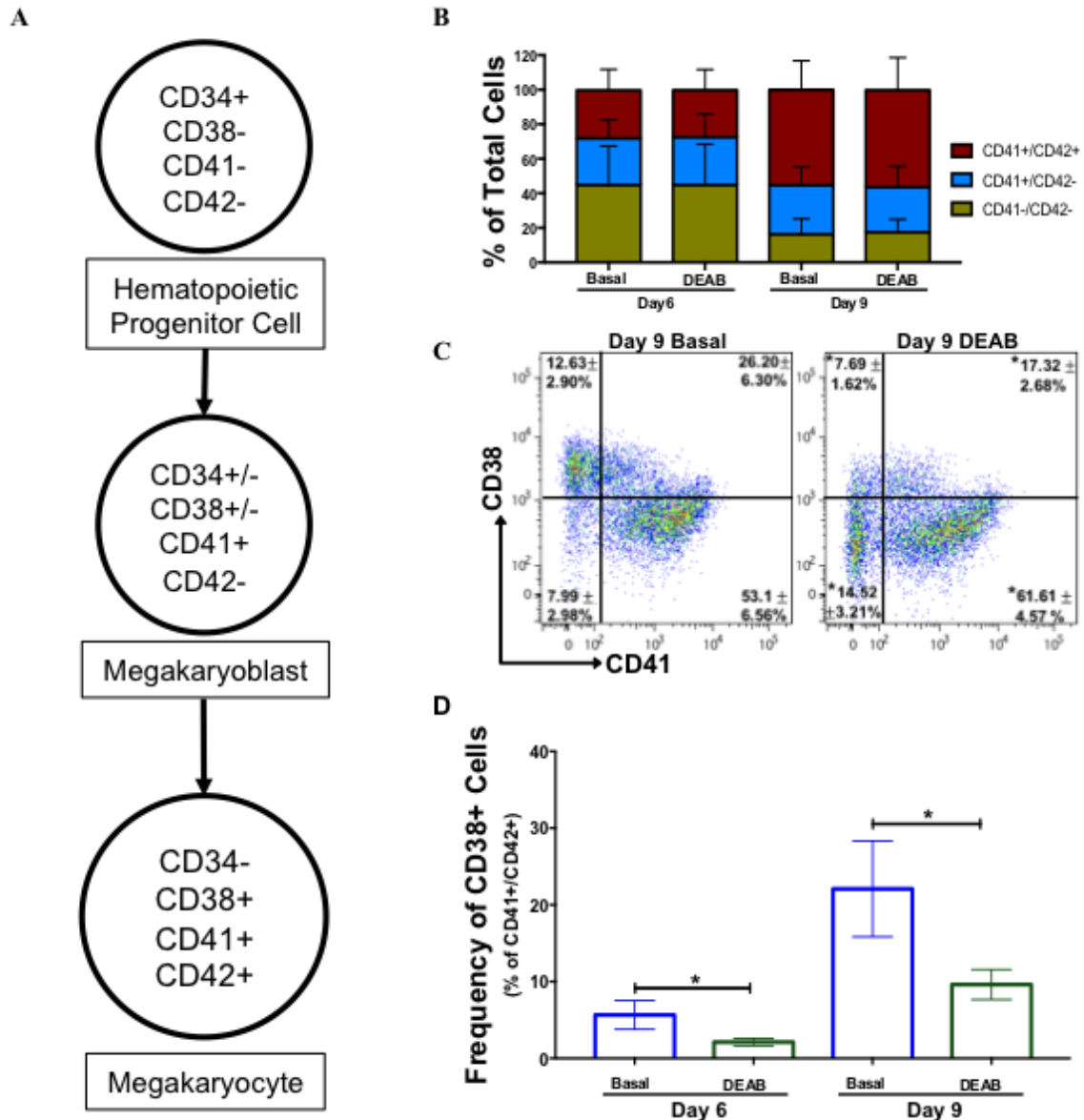
Figure 2.5 DEAB-treatment reduced differentiation towards megakaryocyte phenotype. Schematic of megakaryopoiesis and acquisition of mature megakaryocyte phenotype (CD41^{+}/CD42^{+}/CD38^{+}). (B) DEAB-treatment did not alter CD41 and CD42 expression patterns at 6 or 9 days. (C) Representative flow cytometry plots showing reduced expression of CD38 on CD41^{+/-} cells generated under DEAB-treated conditions. (D) CD38 expression was reduced on megakaryocytes (CD41^{+}/CD42^{+}) under DEAB-treated conditions. Data represented as Mean $\pm$ SEM (*p<0.05; N=5-8). Statistical analyses were performed by paired Student's t-test.

Table 2.5 DEAB-treatment retains primitive progenitor cells within CD41+/-subpopulations coinciding with reduced CD38 expression.

Population	Phenotype	% of Population			
		Day 6 Basal	Day 6 DEAB	Day 9 Basal	Day 9 DEAB
CD41-/ CD42-	CD34+	28.98 ± 5.43	31.63 ± 6.51	18.44 ± 3.27	**12.85 ± 2.14***
	CD34+ CD38-	16.91 ± 4.44	**23.96 ± 4.53****	7.83 ± 1.76	7.61 ± 1.65
	CD38+	43.75 ± 5.31	**28.45 ± 4.46***	55.31 ± 6.27	**30.11 ± 7.98***
CD41+/ CD42-	CD34+	29.91 ± 7.43	23.58 ± 7.19	22.09 ± 4.15	20.63 + 2.60
	CD34+ CD38-	18.62 ± 4.23	19.62 ± 5.91	8.24 ± 2.01	**13.14 + 2.44***
	CD38+	22.10 ± 7.15	**9.16 ± 3.14***	44.43 ± 5.23	**27.45 + 4.56***
CD41+/ CD42+	CD34+	6.29 ± 2.39	6.60 ± 3.84	5.77 ± 2.77	4.49 ± 2.01
	CD34+ CD38-	4.84 ± 2.27	6.06 ± 3.73	1.14 ± 0.50	2.27 ± 0.93
	CD38+	5.66 ± 1.87	2.12 ± 0.48	24.32 ± 8.47	9.31 ± 2.39

Data expressed as Mean ±SEM; Paired Students t-test, (*p<0.05, **p<0.01; n=5-7). Statistical analyses were determined by Student's t-test.

2.3.7 DEAB-Treated Cells Demonstrated a Pro-Survival and Pro-Angiogenic Proteome

We used highly sensitive mass spectrometry to compare global proteome changes after 9 days expansion under either Basal (N = 3) or DEAB-treated (N = 3) conditions. Expanded UCB ALDH^{hi} cells generated a heterogeneous cell population comprised of several hematopoietic cell types after 9 days[28]; therefore, detectable changes in the global proteome should reflect changes within influential signaling networks. The proteomic profiles of these expanded cell populations were remarkably similar. Of the 6,804 unique proteins detected, only 121 proteins were unique to cells harvested from DEAB-treated conditions, and 164 were unique to cells harvested from Basal conditions, (Fig. 2.6A). Proteins exclusively expressed under DEAB-treated conditions were largely associated with anti-apoptotic activity (i.e., NEMO, IKBKG; Caspase Recruitment Domain-containing protein 6, CARD6; Table 2.6). Conversely, proteins exclusive to Basal conditions included drivers of apoptosis, including Fas cell surface death receptor (FAS) (Table 2.7). Several proteins implicated with mature hematopoietic cell functions (i.e., plasminogen activator; platelet-activating factor receptor; dendritic cell-associated lectin 2; integrin subunit beta 7) were exclusively produced under Basal conditions.

Of the 6,519 proteins common to cells from Basal and DEAB-treated conditions, only 117 proteins demonstrated a >1.2-fold or <1.2-fold difference comparing DEAB-treated to Basal conditions (Fig. 2.6B, C). Common angiogenic factors (ANGPT1; von Willebrand factor, vWF; and transforming growth factor beta 1) were comparable in the proteome of Basal and DEAB-treated cells. Interestingly, DEAB-treatment primarily upregulated intracellular proteins involved in the prevention of apoptosis (i.e., BCL2 family apoptosis regulator, MCL1), in the preservation of progenitor cell function (thrombopoietin receptor, MPL), or with cell motility such as proto-oncogene C-Crk (CRK) and leucine rich repeat containing 16A. Cells harvested from Basal conditions upregulated proteins primarily associated with HPC differentiation; including Fibronectin (FN1), Serpin family B member 8 (SERPINB8), lymphocyte antigen 75 (LY75), and adenosine deaminase 2 (CECR1). Validating our flow cytometry data, CD38 protein levels were decreased 1.68-fold in cells harvested after DEAB-treatment compared with

Basal conditions. Collectively, these analyses suggest that DEAB-treatment increased the production of pro-survival proteins and decreased the production of proteins associated with hematopoietic differentiation.

.
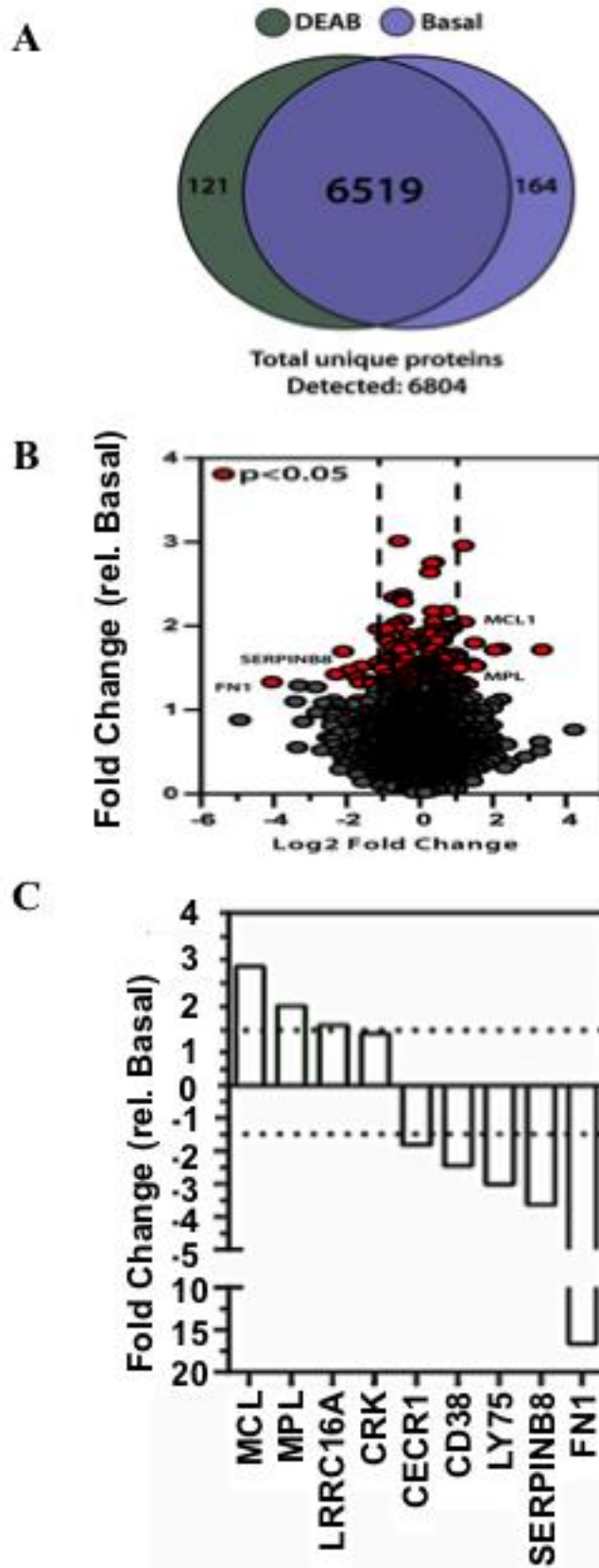
Figure 2.6 Distinct proteomic profiles for DEAB-treated versus Basal cells. (A) Mass spectrometry identified 6804 individual proteins across cell lysates. Out of 6519 proteins were detected in both Basal and DEAB-treated cells (N=3), only 137 proteins were found to be (B) differentially expressed (red circles, *p<0.05). (C) DEAB-treatment increased production of anti-apoptotic proteins, including myeloid cell leukemia-1 (MCL1) and thrombopoietin receptor (MPL). Decreased detection of differentiation factors including CD38, CECR1, SERPINB8, and Fibronectin (FN1) was also observed in DEAB-treated cells. Statistical analyses were performed by students t-test.

Table 2.6 Proteins exclusively found in the cell lysate of DEAB-treated cells

Protein Name	Gene Name	Biological Function
Ring Finger And FYVE Like Domain Containing E3 Ubiquitin Protein Ligase	RFFL	Neg. Regulation of Apoptosis
Proline Rich 5 Like	PRR5L	Cell Survival
Keratin 18	KRT18	Neg. Regulation of Apoptosis
CD47 Molecule	CD47	Cell-Cell Interactions/ Phagocytosis
Transmembrane Protein 208	TMEM208	Neg. Regulator of ER Stress
BAG family molecular chaperone regulator 4	BAG4	Neg. Regulator of Apoptosis
Serpin E2	SERPINE2	Serine protease inhibitor
Caspase recruitment domain-containing protein 6	CARD6	Regulation of Apoptosis
Protein CLN8	CLN8	Cell Proliferation/Survival
NEMO	IKBKG	NF-Kappa-β Signaling

Table 2.7 Proteins exclusively found in the cell lysate of Basal cells

Protein Name	Gene Name	Biological Function
C-Type Lectin Domain Family 12 Member A	CLEC12A	Neg Regulation of Granulocyte and Monocyte Function
Tumor Necrosis Factor Superfamily Member 13	TNFSF13	Granulocyte and Monocyte Function
Fas Cell Surface Death Receptor	FAS	Pos. Regulation of Apoptosis
Lipocalin 2	LCN2	Neutrophil Function
Colony Stimulating Factor 2 Receptor Alpha Subunit	CSF2RA	Hematopoiesis
Plasminogen Activator, Urokinase Receptor	PLAUR	Pos Regulation of Plasmin Formation
Collagen alpha-1(I) chain	COL1A1	Type 1 Collagen Formation
Collagen alpha-2(I) chain	COL1A2	Type 1 Collagen Formation
Cellular Retinoic Acid Binding Protein	CRABP1	Retinoic Acid Signaling
Integrin Subunit Beta 7	ITGB7	Fibronectin Binding
Platelet Activating Factor Receptor	PTAFR	Inflammation/Chemotaxis

2.3.8 Transplantation of DEAB-Treated Cells Accelerated the Recovery of Perfusion

We have previously shown that extended culture of UCB ALDH^{hi} cells resulted in the loss of vascular regenerative functions after transplantation *in vivo*[28]. Therefore, we sought to determine whether DEAB-treatment could generate cells that retained vascular regenerative function following transplantation into mice with hind-limb ischemia. After unilateral FAL surgery, non-obese diabetic/severe combined immunodeficient (NOD/SCID) mice with hind-limb ischemia (Perfusion Ratio, PR; PR < 0.1) received i.m. injection of UCB ALDH^{hi} cells expanded for 9 days under Basal or DEAB-treated culture conditions. Transplantation of 5.0×10^5 cells generated under Basal conditions failed to improve limb perfusion from baseline recovery observed with PBS-injected controls (PR = 0.58 $\pm$ 0.04 vs. 0.49 $\pm$ 0.05 at day 35, respectively; Fig. 2.7A, B). However, i.m.-transplantation with 5.0×105 cells generated under DEAB-treated conditions significantly increased limb perfusion as early as day 21, compared with PBS controls (0.70 $\pm$ 0.04 vs. 0.43 $\pm$ 0.03; **, p < .01), and improved limb perfusion persisted until day 35 post-transplantation (0.76 $\pm$ 0.06; **, p < .01). Limb usage assessed by Catwalk paw print area measurements for all groups were equivalent at day 35. However, at 7 days post-transplantation mice that received DEAB-treated cells showed modestly improved limb usage compared with PBS-controls (p = .17) (Figure 2.7C).
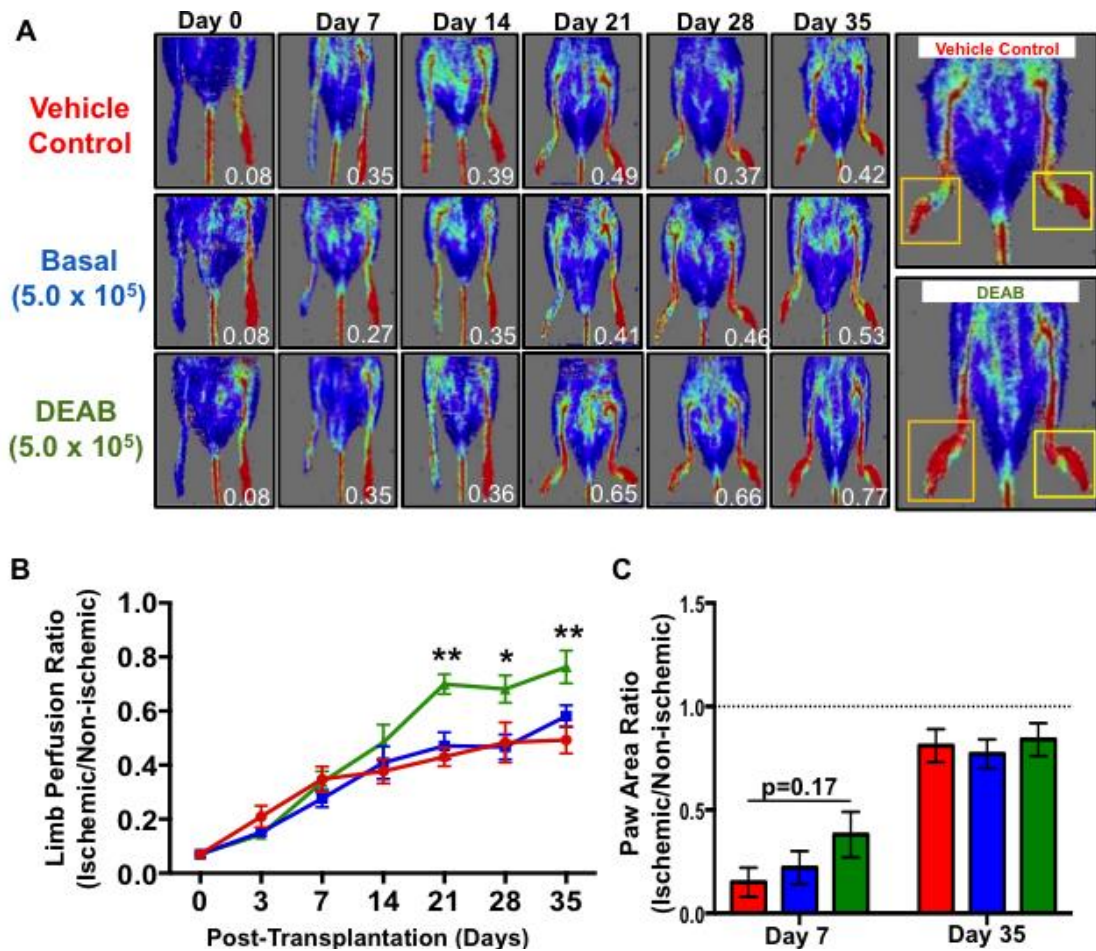
Figure 2.7 DEAB-treated cells accelerated the recovery of limb perfusion after transplantation. (A) Representative LDPI following FAL and intramuscular transplantation of PBS (n=7), $5x10^5$ Basal cells (n=11), or $5x10^5$ DEAB-treated cells (n=11). Perfusion ratio (PR) in the ischemic (orange box) versus non-ischemic (yellow box) limbs are shown in white text. (B) NOD/SCID mice i.m.-injected with Basal cells showed similar recovery of perfusion compared to PBS controls (Day 35 PR=0.58±0.04 vs. 0.49±0.06; respectively). Transplantation of DEAB-treated cells enhanced the recovery of limb perfusion compared to PBS vehicle controls or Basal cells at days 21-35. (C) Paw area ratio of ischemic vs. non-ischemic limb measure at 7- and 35-days post-transplantation (n=5-7). DEAB-treated cells modestly increased limb usage at 7 days post-transplantation, albeit limb usage was equal across transplantation conditions at day 35 post-transplantation. Data represented as Mean ± SEM (*p<0.05, **p<0.01). Statistical analyses were performed by ANOVA with Tukey's multiple comparisons test relative to PBS-injected mice.

2.3.9 Transplantation of DEAB-Treated Cells Stimulated Endothelial Cell Proliferation and Increased Capillary Density within Ischemic Limbs

To investigate potential mechanisms by which DEAB-treated cells accelerated the recovery of limb perfusion, vascular density was assessed alongside human cell engraftment kinetics at day 7 and day 35 post-transplantation in ischemic thigh muscle tissue sections. Human cell engraftment was detected within ischemic thigh muscles at 7-days post-transplantation with either Basal or DEAB-treated cells (Figure 2.8). Compared with Basal cells, DEAB-treated cells demonstrated a trend toward increased engraftment within the ischemia thigh muscle (1.25 ± 0.21 vs. 0.83 ± 0.11 HLA$^+$ cells/mm2, n = 4, p = .13). Moreover, transplanted cells were not detected after 35-days post-transplantation. Mice were injected with EdU 24 hours before euthanasia to allow quantification of proliferating CD31$^+$ endothelial cells. At day 7 post-transplantation, mice transplanted with DEAB-treated cells showed an increased number of EdU$^+$/CD31$^+$ cells/mm^2 within ischemic thigh muscle, compared with mice injected with cells generated under Basal conditions (3.06 ± 1.08 vs. 0.67 ± 0.27, *, p < .05) or PBS (0.11 ± 0.11, **, p < .01; Fig. 2.9A, B). Augmented endothelial cell proliferation corresponded to increased CD31$^+$ capillary density at day 35 with DEAB-treated cells (*, p < .05; Fig. 2.9C). In addition, mice transplanted with DEAB-treated cells increased the number of larger vessels expressing vWF at day 35 (Figure 2.10), compared with PBS-injected controls. Collectively, DEAB-treated cells survived for at least 7 days post-transplantation and stimulated endothelial cell proliferation leading to increased vascular density in the ischemic limb

.
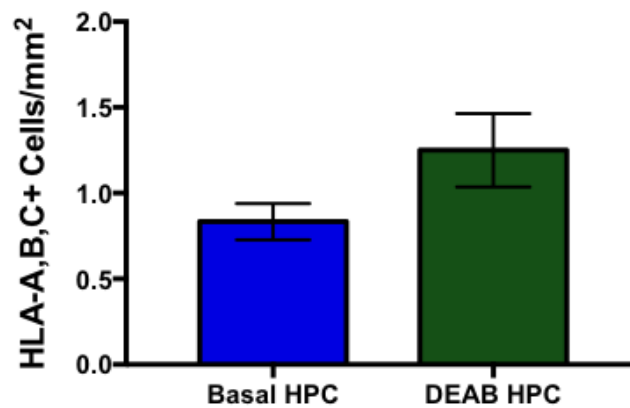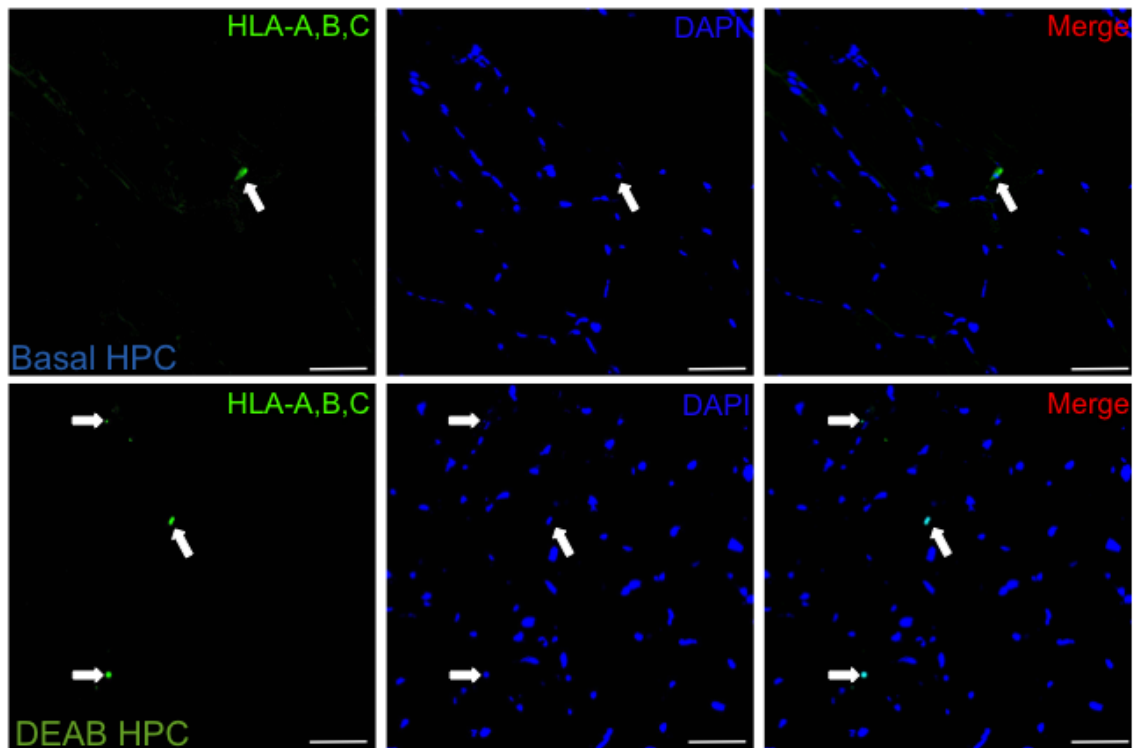
Figure 2.8 Human cell engraftment detected in the ischemic thigh muscle 7 days post-transplantation. Representative confocal photomicrograph (20x) of a thigh muscle cryosections stained for HLA-A, B,C, detecting human cells 7 days after the intramuscular transplantation of (A) Day 9 Basal cells or (B) Day 9 DEAB-treated cells. Arrows indicate location of detected human cells. Scale bar = 50μm
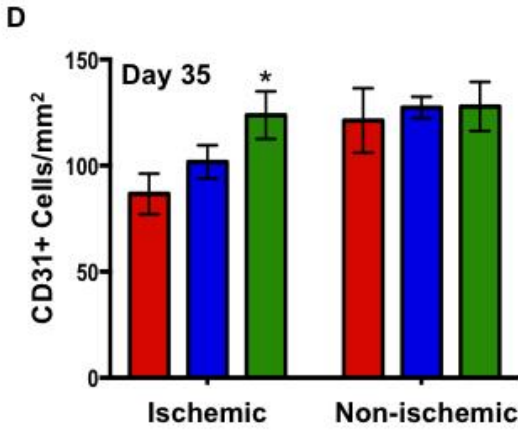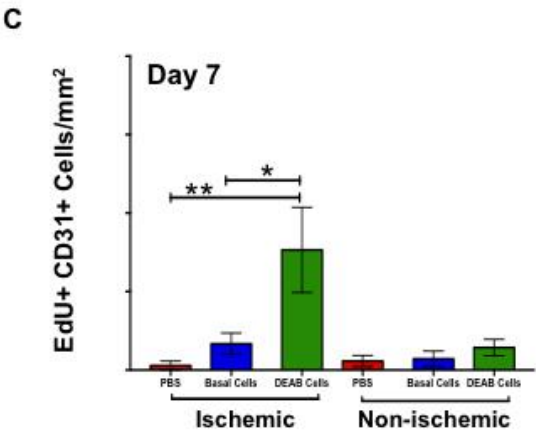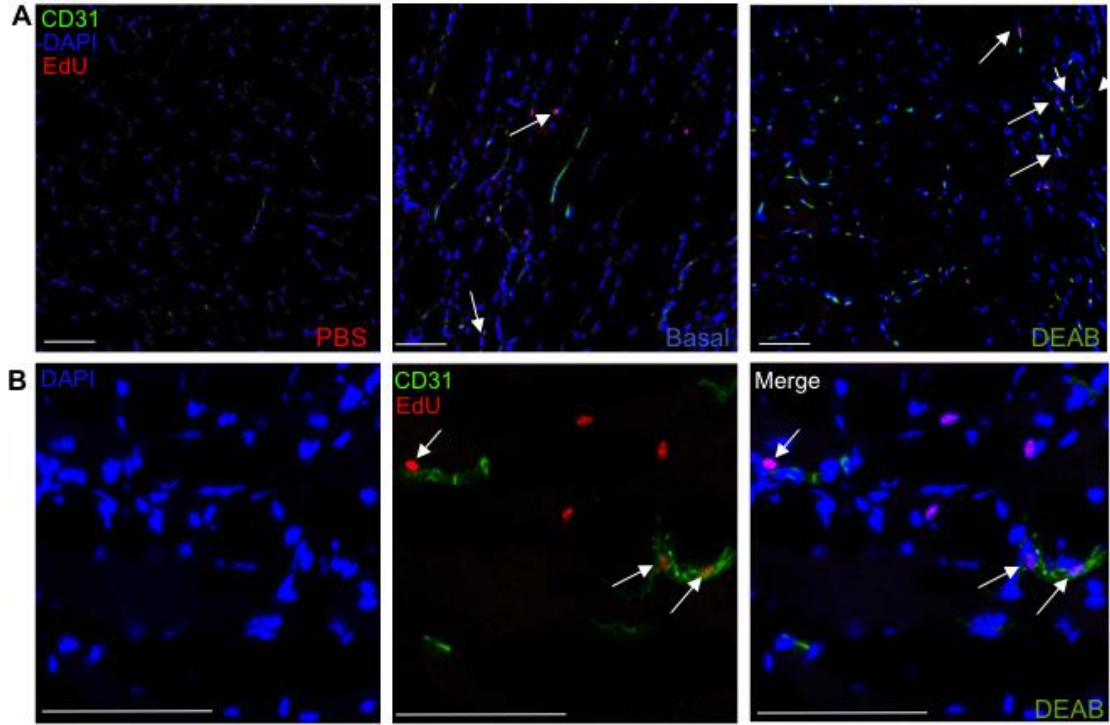
Figure 2.9 Transplantation of DEAB-treated cells increased capillary density via increasing murine endothelial cell proliferation. NOD/SCID mice transplanted with either PBS (n=5), Basal cells (n=6), or DEAB-treated cells (n=6) were injected with EdU 24-hrs prior to euthanasia at 7 days post-transplantation. (A) Representative confocal images (10x) of cryosectioned thigh muscles stained for endothelial cell marker (CD31) and EdU-incorporation (Alexafluor 594). (B) Representative confocal image (40x) of endothelial cell proliferation (EdU+/CD31+) in the ischemic limb of mice transplanted with DEAB-treated cells. (C) Mice transplanted with DEAB-treated cells had a significantly increased number of proliferating endothelial cells within the ischemic limb, compared to PBS-injected or Basal cell transplanted mice. (D) Intramuscular transplantation of DEAB-treated cells increased $CD31^+$ capillary density in ischemic limbs of mice sacrificed at day 35 (n=7-11). Data represented as Mean ± SEM.(*p<0.05, **p<0.01). Statistical analyses were performed by ANOVA with Tukey's multiple comparisons test. Scale bar = 150μm.
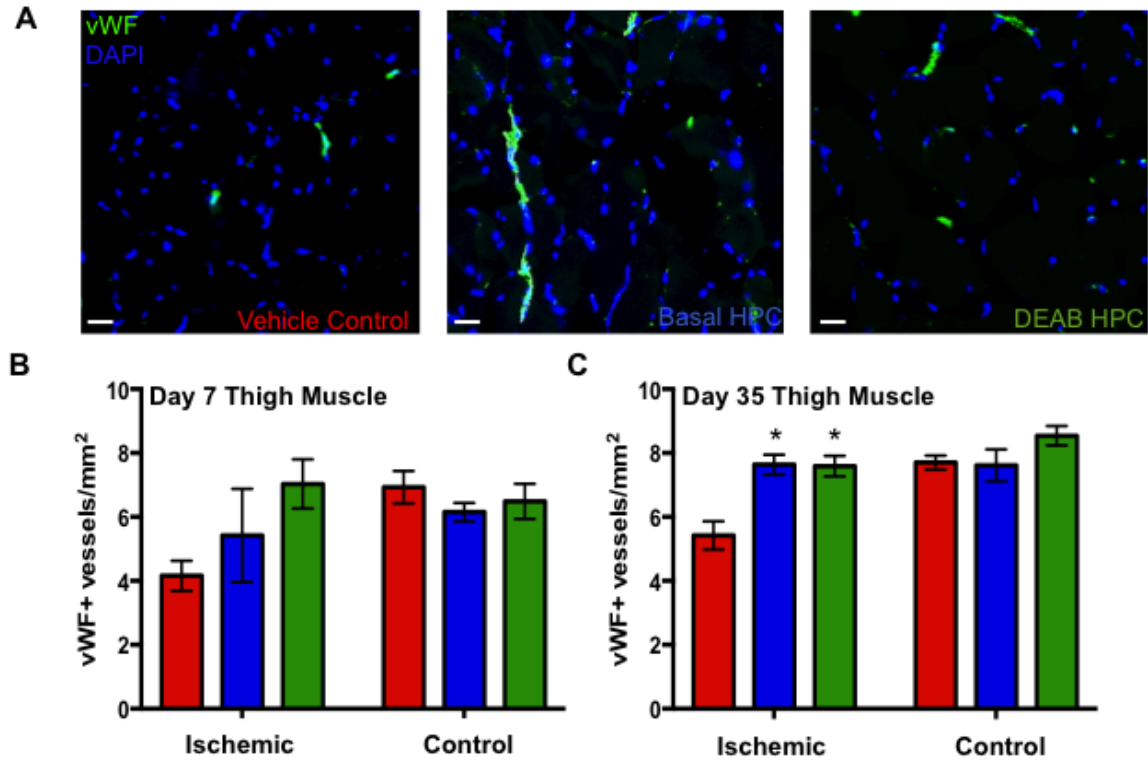
Figure 2.10 Intramuscular transplantation of DEAB-treated cells prevented the loss of von Willebrand factor-positive blood vessel networks after femoral artery ligation-induced CLI. (A) Representative immunofluorescent images (20x) of cyrosectioned thigh muscles harvested 7-days post-transplantation and stained for von Willebrand factor (vWF). (B) DEAB-treated and Basal cells increased the number of vWF$^+$ vessels 35 days post-transplantation, compared to PBS control. Data represented as Mean $\pm$ SEM (*p<0.05; n=5-7). Statistical analyses were determined by ANOVA with Tukey's multiple comparisons relative to PBS-injected mice. Scale bar = 50μm

2.4 Discussion

Blood-derived progenitor cells with ALDH[hi]-activity demonstrate multifaceted regenerative functions in preclinical studies[12, 15]. However, it is becoming well accepted in preclinical studies that harvesting autologous cells from the BM of individuals with diffuse atherosclerosis[19] and associated comorbidities such as obesity and type 2 diabetes[20, 37], results in the accrual of progenitor cells with depleted numbers and dysfunctional vascular regenerative capacity. The use of allogenic UCB cells with limited exposure to damaging metabolic by-products of chronic disease[24] may mitigate progenitor cell exhaustion and facilitate the development of cellular therapies with improved efficacy. UCB represents a readily accessible source of regenerative cells, usually considered discarded material, and is easily harvested with no risk to either the newborn or mother. Recent establishment of national cord blood banking programs generates a renewable multi-donor pool with increased diversity for HLA-matching and subsequent use in allogeneic therapeutic applications. A phase I clinical trial (NCT01019681) was recently initiated to determine the safety and efficacy of UCB-MNC; however, these results have yet to be reported. We have previously demonstrated enhanced vascular regenerative functions of UCB-derived ALDH^{hi} cells compared with unpurified UCB-MNC[12]. However, ALDH^{hi} cells only represent <0.5% of total UCB-MNC and require *ex vivo* expansion to increase the number of progenitor cells needed to support early preclinical studies. Herein, we demonstrate an expansion strategy and early preclinical evidence which indicates expanded allogeneic UCB ALDH^{hi} cells could be used for treating severe ischemic disease[16].

UCB ALDH^{hi} cells are primarily comprised of early myeloid HPC[12] that can be efficiently expanded in short-term culture under serum-free conditions[28]. Unfortunately, when culture time was extended from 6 to 9 days, the vascular regenerative function of expanded progeny was diminished after i.m.-transplantation into NOD/SCID mice with hind-limb ischemia[23]. This led us to speculate that prolonged culture time under serum-free (Basal) conditions reduced pro-angiogenic growth factor production and/or secretion,

such as VEGF-A, from expanded progeny. Despite robust differentiation toward the megakaryocyte lineage between days 6 and 9, we did not observe significant decrease in secreted levels of common pro-angiogenic growth factors (VEGF-A, ANGPT1, CCL5). In contrast, we observed an increased expression of megakaryocyte lineage-specific proteins, including CD41 (ITGA2B) and CD42 (GPIB). Specifically, flow cytometry analyses demonstrated a reduction of primitive surface marker (CD34) expression alongside diminished ALDH-activity, which coincided with the acquisition of a mature megakaryocyte phenotype (CD41$^+$/CD42$^+$/CD38$^+$).

Megakaryocytes represent large hematopoietic cells (50–100 μm) which release platelets into systemic circulation through the fragmentation of proplatelet extensions that protrude into vascular sinuses of the BM niche. The turnover of circulating platelets is frequent (<9 days); therefore, the consistent production of platelets is necessary to ensure vessel hemostasis and injury repair[38,39]. Platelet-derived CD42 binds to vWF on exposed subendothelium collagen during vascular injury, the subsequent activation of platelets will stimulate soluble protein and extracellular vesicle secretion into the local microenvironment and systemic circulation. These stimuli recruit and activate biological processes within endothelial or hematopoietic cells[38, 40,41]. Specifically, platelet-derived stimuli (i.e., VEGF-A) influence both angiogenic and inflammatory pathways during wound healing and vascular regeneration *in vitro* and *in vivo*[39, 40,42]. To our knowledge, this is the first study to characterize and investigate the vascular regenerative potential of a culture-expanded, megakaryocyte-enriched cell population for treating ischemic disease. Indeed, the acquisition of a mature megakaryocyte phenotype (CD41$^+$/CD42$^+$/CD38$^+$) and concomitant loss of ALDH^{hi}-activity under Basal conditions diminished the vascular regenerative capacity of UCB-derived ALDH^{hi} cells.

Chute *et al.* were the first to show that DEAB-treatment enhanced the expansion of UCB-derived CD34$^+$ CD38$^-$ cells with SCID repopulating capacity. Specifically, DEAB-treated cultures were enriched 11.6-fold with cells retaining primitive CD34$^+$/CD38$^-$

phenotype after 7 days. The benefit of DEAB-treatment was reversed after RA-supplementation, suggesting that inhibition of ALDH-activity promoted HSC self-renewal via reduced RA-production. Our study extends these findings to show that inhibition of ALDH-activity and RAR/RXR complex activation could modify the transcription of downstream targets (i.e., CYP26A1)[29]. Despite equal expansion of CD34+ cells compared with Basal conditions, DEAB-treated progeny better retained a primitive phenotype, with a 15-fold expansion in CD34$^+$ CD38$^-$ cells and an 11-fold expansion of the most primitive ALDH^{hi}/CD34$^+$/CD38$^-$ cells. Importantly, DEAB-treatment significantly increased multipotent myeloid colony formation *in vitro*, suggesting that ALDH^{hi} activity can segregate multipotent CD34$^+$ cells from committed, unipotent ALDH^{lo} CD34$^+$ cells[43].

Under Basal conditions, rapid loss of ALDH^{hi}-activity coincided with the acquisition of mature hematopoietic surface marker, CD38. In contrast, DEAB-treatment enhanced retention of ALDH^{hi} phenotype and reduced CD38 expression. CD38 (Cyclic Ribose ADP Hydrolase) is a multifunctional enzyme implicated with intracellular Ca+ signaling, platelet aggregation, and adhesion of leukocytes to CD31+ endothelial cells[44,45]. CD38 is also a direct target of RA-signaling[27], suggesting that DEAB-treatment limited CD38 expression by modifying RA-signaling networks. Furthermore, DEAB-treated cell lysates exhibited increased levels of MCL1 and MPL, cellular proteins implicated with progenitor cell maintenance[46,47]. Conversely, Basal conditions, increased the expression of proteins implicated with hematopoietic differentiation (i.e., CECR1, FN1, SERPINB8, and LY75). Collectively, flow cytometry and proteomic data confirmed DEAB-treatment enhanced the expansion of multipotent HPC by limiting RA-induced differentiation.

We next investigated whether differentiation toward the megakaryocyte lineage was delayed by the inhibition of RA-production. Commitment to the megakaryocyte lineage is marked by the acquisition of CD41 (ITGA2B), whereas CD42 (GP1B) expression occurs later in megakaryopoiesis[48]. However, acquisition of CD41 and CD42 expression

was not altered by DEAB-treatment. This was not a surprise considering treatment with TPO and FLT-3L is known to drive early megakaryopoiesis and increase CD41 expression during *ex vivo* expansion[49]. Several reports have suggested that cells with the immature megakaryoblast phenotype (CD34$^+$/CD38$^-$/CD41$^+$/CD42$^-$) retain multipotency *in vitro* and *in vivo* [36, 50,51].DEAB-treatment increased the accumulation of CD34+/CD38– progenitor cells and delayed the acquisition of CD38 within the megakaryoblast lineage (CD41$^+$/CD42$^-$). DEAB-treatment also limited the production of mature megakaryocytes (CD41$^+$/CD42$^+$/CD38$^+$); suggesting that inhibition of RA-production delayed differentiation at multiple stages of megakaryopoeisis.

Although the secretome and proteome of day 9 Basal cells showed similar expression of pro-angiogenic stimuli (i.e., VEGF-A), day 9 Basal cells did not support the recovery of perfusion after i.m. transplantation into the ischemic limb of NOD/SCID mice. In contrast, DEAB-treated cells accelerated the recovery of blood perfusion by increasing endothelial cell proliferation in ischemic muscle tissue. Both Basal and DEAB-treated cells were detected 7-days post-transplantation but were absent at day 35. DEAB-treated cells demonstrated a trend toward increased engraftment and were found to be closely associated with proliferating endothelial cells, however, did not engraft into murine vasculature. Thus, we predict that survival and/or migration to a regenerative niche is compromised in day 9 Basal cells following i.m.-transplantation. In support of this interpretation, day 9 Basal cells exclusively expressed proteins implicated with the induction of apoptosis, including FAS[52]. In contrast, DEAB-treated cells exclusively expressed several pro-survival molecules (i.e., CARD6, MCL1, KRT18, etc.), in addition to retaining the cytoprotective functions of ALDH^{hi}-activity. Further studies are warranted to determine the role of apoptotic and pro-survival pathways identified in this study. Several studies have demonstrated increased regenerative cell function by pre-treating cells with small molecules to enhance survival following transplantation[53,54]. Our data suggest DEAB-treatment generated heterogeneous myeloid cell progeny with pro-angiogenic secretory capacity that were more likely to survive i.m.-transplantation into a harsh ischemic microenvironment. Furthermore, our data suggest ALDH^{hi} -activity and

reduced CD38 expression may be a characteristic of vascular regenerative hematopoietic cells. Especially considering day 9 DEAB-treated, day 6 Basal, and fresh UCB ALDH^{hi} cells [12] share these characteristics (ALDH^{hi}/CD38^{lo}), in contrast to day 9 Basal cells with diminished vascular regenerative functions (ALDH^{lo}/CD38^{hi}).

Both Basal and DEAB-treated cells were identified by proteomics to equally express integrin complexes including CD41, CD61, CD18, and CD29 after culture on fibronectin. Activation of integrin signaling is expected to increase transplanted cells survival and/or migration. In contrast, detachment induced apoptosis could negatively impact transplanted cell engraftment. In addition, UCB ALDH^{hi} cells cultured under Basal conditions for 9 days increased the production of extracellular matrix (ECM) molecules (fibronectin and collagen), compared with DEAB-treated cells. The increased production of ECM molecules is characteristic of cells within the megakaryocyte lineage that could potentially limit bio-distribution throughout the ischemic muscle. Additional studies are needed to specifically address whether pre-exposure to a matrix influences the engraftment and bio-distribution of transplanted progenitor cells. Interestingly, Whiteley *et al*. demonstrated UCB-derived CD34+/CD45+ cells cultured for 8 days, engrafted ischemic murine muscle tissue at a higher rate than uncultured CD34+ cells or MNC, suggesting that *ex vivo* culture may benefit cellular therapies for PAD[55]. Several early trials have reported modest clinical benefits following the i.m. transplantation of expanded progenitor cells from autologous BM or peripheral blood[56,57]; however, these trials were unable to improve limb amputation rates.

In summary, our previous studies established that UCB ALDH^{hi} cells and day 6 expanded progeny temporally engraft ischemic muscle tissues and induce neovascularization in NOD/SCID mice with hind-limb ischemia[28]. Unfortunately, the low number of transplantable cells would limit or impede a controlled clinical study to effectively investigate currently unestablished parameters of expandable UCB-cells, such as clinical efficacy and cell dose. This study demonstrates limiting RA-induced differentiation

during UCB-cell expansion can expand total cell number by ∼80-fold, and total ALDH^{hi} cells by ∼25-fold, without a significant loss of vascular regenerative function. Therefore, we consider these results early preclinical evidence that reasonable cell numbers can be generated from a single UCB sample to assess currently undetermined parameters leading to improved efficacy, such as cell dose, phenotype (ALDH, CD34, CD38, etc.), or therapeutic cell source (BM vs. UCB). Collectively, (a) advanced understanding of signaling pathways which drive progenitor cell differentiation, (b) identification of vascular regenerative cell subpopulations, and (c) improving culture conditions to facilitate cell type specific expansion is warranted for the development of effective vascular regenerative therapies.

2.5   References

1   Sowers, J. R. & Stump, C. S. Insights into the biology of diabetic vascular disease: what's new? *American journal of hypertension* **17**, 2S-6S (2004).

2   Golomb, B. A., Dang, T. T. & Criqui, M. H. Peripheral arterial disease: morbidity and mortality implications. *Circulation* **114**, 688-699 (2006).

3   Vartanian, S. M. & Conte, M. S. Surgical intervention for peripheral arterial disease. *Circulation research* **116**, 1614-1628 (2015).

4   Thukkani, A. K. & Kinlay, S. Endovascular intervention for peripheral artery disease. *Circulation research* **116**, 1599-1613 (2015).

5   Makowsky, M. *et al.* Prevalence and treatment patterns of lower extremity peripheral arterial disease among patients at risk in ambulatory health settings. *Canadian Journal of Cardiology* **27**, 389. e311-389. e318 (2011).

6   Bonaca, M. P. & Creager, M. A. Pharmacological treatment and current management of peripheral artery disease. *Circulation research* **116**, 1579-1598 (2015).

7   Criqui, M. H. & Aboyans, V. Epidemiology of peripheral artery disease. *Circulation research* **116**, 1509-1526 (2015).

8   Davies, M. G. Criticial limb ischemia: epidemiology. *Methodist DeBakey cardiovascular journal* **8**, 10 (2012).

9   Wahlberg, E. Angiogenesis and arteriogenesis in limb ischemia. *Journal of vascular surgery* **38**, 198-203 (2003).

10   Arpino, J.-M. *et al.* Four-dimensional microvascular analysis reveals that regenerative angiogenesis in ischemic muscle produces a flawed microcirculation. *Circulation research* **120**, 1453-1465 (2017).

11   Lawall, H., Bramlage, P. & Amann, B. Stem cell and progenitor cell therapy in peripheral artery disease. *Thrombosis and haemostasis* **103**, 696-709 (2010).

12   Putman, D. M., Liu, K. Y., Broughton, H. C., Bell, G. I. & Hess, D. A. Umbilical cord blood-derived aldehyde dehydrogenase-expressing progenitor cells promote recovery from acute ischemic injury. *Stem cells* **30**, 2248-2260 (2012).

13   Capoccia, B. J. *et al.* Revascularization of ischemic limbs after transplantation of human bone marrow cells with high aldehyde dehydrogenase activity. *Blood* **113**, 5340-5351 (2009).

14   Bell, G. I. *et al.* Combinatorial human progenitor cell transplantation optimizes islet regeneration through secretion of paracrine factors. *Stem cells and development* **21**, 1863-1876 (2012).

15   Seneviratne, A. K. *et al.* Expanded hematopoietic progenitor cells reselected for high aldehyde dehydrogenase activity demonstrate islet regenerative functions. *Stem Cells* **34**, 873-887 (2016).

16   Perin, E. C. *et al.* A randomized, controlled study of autologous therapy with bone marrow–derived aldehyde dehydrogenase bright cells in patients with critical limb ischemia. *Catheterization and Cardiovascular Interventions* **78**, 1060-1067 (2011).

17   Perin, E. C. *et al.* Rationale and design for PACE: patients with intermittent claudication injected with ALDH bright cells. *American heart journal* **168**, 667-673. e662 (2014).

18   Perin, E. C. *et al.* Evaluation of cell therapy on exercise performance and limb perfusion in peripheral artery disease: the CCTRN PACE trial (patients with intermittent claudication injected with ALDH bright cells). *Circulation* **135**, 1417-1428 (2017).

19   Heeschen, C. *et al.* Profoundly reduced neovascularization capacity of bone marrow mononuclear cells derived from patients with chronic ischemic heart disease. *Circulation* **109**, 1615-1622 (2004).

20   Fadini, G. P. *et al.* Number and function of endothelial progenitor cells as a marker of severity for diabetic vasculopathy. *Arteriosclerosis, thrombosis, and vascular biology* **26**, 2140-2146 (2006).

21   Tan, Q. *et al.* Transplantation of healthy but not diabetic outgrowth endothelial cells could rescue ischemic myocardium in diabetic rabbits. *Scandinavian journal of clinical and laboratory investigation* **70**, 313-321 (2010).

22   Losordo, D. W. *et al.* A randomized, controlled pilot study of autologous CD34+ cell therapy for critical limb ischemia. *Circulation: Cardiovascular Interventions* **5**, 821-830 (2012).

23   Giugliano, D., Ceriello, A. & Paolisso, G. Oxidative stress and diabetic vascular complications. *Diabetes care* **19**, 257-267 (1996).

24   Brownlee, M. Biochemistry and molecular cell biology of diabetic complications. *Nature* **414**, 813 (2001).

25   Rhinn, M. & Dollé, P. Retinoic acid signalling during development. *Development* **139**, 843-858 (2012).

26   Gudas, L. J. in *Seminars in cell & developmental biology.* 701-705 (Elsevier).

27   Drach, J. *et al.* Retinoic acid-induced expression of CD38 antigen in myeloid cells is mediated through retinoic acid receptor-α. *Cancer Research* **54**, 1746-1752 (1994).

28   Putman, D. M. *et al.* Expansion of umbilical cord blood aldehyde dehydrogenase expressing cells generates myeloid progenitor cells that stimulate limb revascularization. *Stem cells translational medicine* **6**, 1607-1619 (2017).

29   Chute, J. P. *et al.* Inhibition of aldehyde dehydrogenase and retinoid signaling induces the expansion of human hematopoietic stem cells. *Proceedings of the National Academy of Sciences* **103**, 11707-11712 (2006).

30   Ghiaur, G. *et al.* Regulation of human hematopoietic stem cell self-renewal by the microenvironment's control of retinoic acid signaling. *Proceedings of the National Academy of Sciences* **110**, 16121-16126 (2013).

31   Wessel, D. m. & Flügge, U. A method for the quantitative recovery of protein in dilute solution in the presence of detergents and lipids. *Analytical biochemistry* **138**, 141-143 (1984).

32   Kulak, N. A., Pichler, G., Paron, I., Nagaraj, N. & Mann, M. Minimal, encapsulated proteomic-sample processing applied to copy-number estimation in eukaryotic cells. *Nature methods* **11**, 319 (2014).

33   Cox, J. & Mann, M. MaxQuant enables high peptide identification rates, individualized ppb-range mass accuracies and proteome-wide protein quantification. *Nature biotechnology* **26**, 1367 (2008).

34   Cox, J. *et al.* Accurate proteome-wide label-free quantification by delayed normalization and maximal peptide ratio extraction, termed MaxLFQ. *Molecular & cellular proteomics* **13**, 2513-2526 (2014).

35   Tyanova, S. *et al.* The Perseus computational platform for comprehensive analysis of (prote) omics data. *Nature methods* **13**, 731 (2016).

36   Debili, N. *et al.* Different expression of CD41 on human lymphoid and myeloid progenitors from adults and neonates. *Blood* **97**, 2023-2030 (2001).

37   Hess, D. A. & Hegele, R. A. Linking diabetes with oxidative stress, adipokines, and impaired endothelial precursor cell function. *Canadian Journal of Cardiology* **28**, 629-630 (2012).

38   Italiano, J. E. *et al.* Angiogenesis is regulated by a novel mechanism: pro-and antiangiogenic proteins are organized into separate platelet α granules and differentially released. *Blood* **111**, 1227-1233 (2008).

39   Brill, A., Dashevsky, O., Rivo, J., Gozal, Y. & Varon, D. Platelet-derived microparticles induce angiogenesis and stimulate post-ischemic revascularization. *Cardiovascular research* **67**, 30-38 (2005).

40   Barry, F. P. & Murphy, J. M. Mesenchymal stem cells: clinical applications and biological characterization. *The international journal of biochemistry & cell biology* **36**, 568-584 (2004).

41   Chatterjee, M. & Gawaz, M. Platelet-derived CXCL12 (SDF-1α): basic mechanisms and clinical implications. *Journal of Thrombosis and Haemostasis* **11**, 1954-1967 (2013).

42   Kim, H. K., Song, K. S., Chung, J. H., Lee, K. R. & Lee, S. N. Platelet microparticles induce angiogenesis *in vitro*. *British journal of haematology* **124**, 376-384 (2004).

43   Storms, R. W. *et al.* Distinct hematopoietic progenitor compartments are delineated by the expression of aldehyde dehydrogenase and CD34. *Blood* **106**, 95-102 (2005).

44   Mushtaq, M., Nam, T.-S. & Kim, U.-H. Critical role for CD38-mediated Ca2+ signaling in thrombin-induced procoagulant activity of mouse platelets and hemostasis. *Journal of Biological Chemistry* **286**, 12952-12958 (2011).

45   Deaglio, S. *et al.* Human CD38 (ADP-ribosyl cyclase) is a counter-receptor of CD31, an Ig superfamily member. *The Journal of Immunology* **160**, 395-402 (1998).

46   Campbell, C. J. *et al.* The human stem cell hierarchy is defined by a functional dependence on Mcl-1 for self-renewal capacity. *Blood* **116**, 1433-1442 (2010).

47   Yoshihara, H. *et al.* Thrombopoietin/MPL signaling regulates hematopoietic stem cell quiescence and interaction with the osteoblastic niche. *Cell stem cell* **1**, 685-697 (2007).

48   Klimchenko, O. *et al.* A common bipotent progenitor generates the erythroid and megakaryocyte lineages in embryonic stem cell–derived primitive hematopoiesis. *Blood* **114**, 1506-1517 (2009).

49   Li, K., Yang, M., Lam, A. C., Yau, F. W. & Yuen, P. M. P. Effects of flt-3 ligand in combination with TPO on the expansion of megakaryocytic progenitors. *Cell transplantation* **9**, 125-131 (2000).

50   Gekas, C. & Graf, T. CD41 expression marks myeloid-biased adult hematopoietic stem cells and increases with age. *Blood* **121**, 4463-4472 (2013).

51   Basch, R. S., Zhang, X. M., Dolzhanskiy, A. & Karpatkin, S. Expression of CD41 and c-mpl does not indicate commitment to the megakaryocyte lineage during haemopoietic development. *British journal of haematology* **105**, 1044-1054 (1999).

52   Hirata, H. *et al.* Caspases are activated in a branched protease cascade and control distinct downstream processes in Fas-induced apoptosis. *Journal of experimental medicine* **187**, 587-600 (1998).

53   Seeger, F. H., Zeiher, A. M. & Dimmeler, S. Cell-enhancement strategies for the treatment of ischemic heart disease. *Nature Reviews Cardiology* **4**, S110 (2007).

54   Chavakis, E., Urbich, C. & Dimmeler, S. Homing and engraftment of progenitor cells: a prerequisite for cell therapy. *Journal of molecular and cellular cardiology* **45**, 514-522 (2008).

55   Whiteley, J. *et al.* An expanded population of CD34+ cells from frozen banked umbilical cord blood demonstrate tissue repair mechanisms of mesenchymal stromal cells and circulating angiogenic cells in an ischemic hind limb model. *Stem Cell Reviews and Reports* **10**, 338-350 (2014).

56   Powell, R. J. *et al.* Cellular therapy with Ixmyelocel-T to treat critical limb ischemia: the randomized, double-blind, placebo-controlled RESTORE-CLI trial. *Molecular Therapy* **20**, 1280-1286 (2012).

57   Szabó, G. V. *et al.* Peripheral blood-derived autologous stem cell therapy for the treatment of patients with late-stage peripheral artery disease—results of the short-and long-term follow-up. *Cytotherapy* **15**, 1245-1252 (2013).

Chapter 3

3   Inhibition of retinoic acid production expands a megakaryocyte-enriched subpopulation with islet regenerative function[ii]

ii A version of this chapter has been published: Cooper, T.T., Bell, G.I. and Hess, D.A., 2018. Inhibition of retinoic acid production expands a megakaryocyte-enriched subpopulation with islet regenerative function. Stem cells and development, 27 (20), pp.1449-1461.

3.1   Introduction

The current ''epidemic'' status of diabetes mellitus (DM) is expected to increase from 425 million individuals in 2017 to >625 million individuals by 2045, amplifying the surging financial burden on the healthcare system[1]. Two classifications of DM exist, each with a distinct etiology and pathology[2,3]. Type 1 DM represents *10% of reported cases and is associated with the autoimmune destruction of insulin-secreting β-cell s. Type II DM accounts for *90% of reported cases and is associated with insulin resistance in peripheral tissues. In both Type I or long-standing Type II DM, exogenous insulin is used for treatment of unregulated glycemic control. Unfortunately, current treatments do not mimic homeostatic insulin secretion, which leads to extreme fluctuations of blood glycemic levels. As a result, >80% of individuals with DM will develop life-threatening cardiovascular complications[3]. There is accumulating evidence that demonstrates human pancreas contains resident stem/progenitor cell populations[4-6] and DM may be effectively treated by the restoration of physiologically functional β-cell mass[6,7]. As a result, cell-based therapies have become a focus of translational research aiming to restore depleted β-cell mass be either replacement or regeneration strategies[8,9]. Recent phase I/II clinical investigations to replace (NCT02239354) or regenerate (NCT00690066) β-cell mass are

currently underway or have reported early results. In 2010, the Joslin Medalist study reported measurable C-peptides levels and actively proliferating β-cell mass in the pancreata of individuals with Type I DM for >50 years[10].

This encouraged the idea that transplantation of appropriate cell types and/or stimuli may boost endogenous β-cell regeneration in the islets of a diabetic individual[5]. We initially demonstrated human bone marrow (BM) and umbilical cord blood (UCB)-derived progenitor cells selected for high aldehyde dehydrogenase (ALDH) activity could stimulate endogenous β-cell regeneration and reduce hyperglycemia in streptozotocin (STZ)-treated NOD/ SCID mice[11,12]. We have recently demonstrated the secretome of blood-derived progenitor cells such as multipotent stromal cells or hematopoietic progenitor cells (HPC) can stimulate human β-cell proliferation in vitro[13,14]. It has also been demonstrated that mature hematopoietic cells, such as platelets, may have β-cell supportive functions during the clinical treatment of Type 1 DM autoimmunity[15]. Collectively, identifying phenotypic characteristics islet-regenerative cell populations and the effectors used to orchestrate robust islet regeneration is crucial to effective treating or reversing DM. UCB represents an accessible source of hematopoietic, endothelial, and mesenchymal progenitor cells and collection imposes no risk to either the newborn or mother. The worldwide establishment of public and private cord blood banking registries has generated a renewable pool with increased diversity for human leukocyte antigen (HLA)-matching for use in therapeutic applications. We view UCB as a favorable source of progenitor cells compared to autologous bone marrow, as accumulating evidence demonstrates loss of progenitor cell number and function when cells are harvested from the microenvironment of chronic diseases[16-19]. Cells harvested from healthy allogenic sources (i.e., UCB) are untouched by damaging metabolites that circulate throughout the body of diabetic individuals[18]. Further research is warranted to determine the full potential of UCB cell progeny for therapeutic strategies to treat DM and common cardiovascular comorbidities. The selection of UCB ALDH^{hi} cells isolates an HPC-enriched cell population with multifaceted regenerative functions[11,20]. Unfortunately, UCB ALDH^{hi} cells represent a rare subpopulation (70-fold after 9 days; >1.0 · 107 viable cells); however, a primitive cell phenotype and regenerative function are rapidly lost[21-23]. We have recently identified that UCB ALDH^{hi} cells preferably differentiate toward the

megakaryocyte lineage as culture time was increased[22]. Specifically, we detected increased expression of megakaryocyte-specific lineage markers, including CD41 (ITGA2) and CD42 (GP1B), by global proteomic analyses and validated by multiparametric flow cytometry. UCB ALDHhi cells became enriched for a megakaryoblast phenotype (CD41$^+$/CD42$^-$) during ex vivo expansion and subsequently acquired a committed megakaryocyte phenotype (CD41$^+$/CD42$^+$); coinciding with loss of high ALDH-activity (UCB hematopoietic progeny capable of robustly stimulating islet regeneration. ALDH is rate limiting enzyme in the production of retinoic acid (RA), a potent driver of HPC differentiation via the activation of the RAR/RXR nuclear receptor complex (RAR/ RXR)[24]. Activation of the RAR/RXR complex will increase the production of downstream products that initiate hematopoietic differentiation and/or cell proliferation[25-27]. This imposes a paradoxical challenge to efficiently expand ALDH^{hi} HPC while limiting the intrinsic propensity for hematopoietic differentiation in vitro. Reversible inhibition of ALDH1A-activity, using diethylaminobenzaldehyde (DEAB) supplementation, limited HPC differentiation during 9-day culture and generated an ALDH^{hi} cell-enriched population (>20% of day 9 progeny; >20-fold increase of ALDH^{hi} cells) that retained vascular regenerative function in vivo[22]. Herein, we investigated the islet regenerative capacity of expanded UCB ALDH^{hi} cells reselected for high versus low ALDH-activity following 9 days culture under previously described DEAB-treated culture conditions. We hypothesized expanded ALDH^{hi} cells reselected from DEAB-treated conditions would demonstrate islet regenerative function following intrapancreatic transplantation into STZ-induced hyperglycemic NOD/SCID mice. Surprisingly, this study identified that only a CD41$^+$ megakaryocyte-lineage enriched ALDH^{lo} cell population harvested from DEAB-treated conditions supported islet regeneration, albeit modestly. Collectively, this study provides evidence that the retention of high ALDH-activity, via DEAB-treated conditions, does not coincide with islet regenerative function.

3.2   Methods

3.2.1   UCB ALDH^{hi} cell isolation and expansion

3.2.2   Human UCB samples were obtained with informed consent by venipuncture of the umbilical vein following Caesarian section at Victoria Hospital Birthing Centre, London, ON, Canada (REB No. 12934). The Human Studies Research Ethics Board (HSREB) at Western University approved all procedures. Within 24 h of collection, UCB samples were initially depleted of mature myeloid, lymphoid and red blood cells using RosetteSep Human Cord Blood Progenitor Cell Enrichment Cocktail (Stem Cell Technologies, Vancouver, BC, Canada). Lineage-depleted (Lin-) mononuclear cells were isolated by Hypaque Ficoll centrifugation and incubated with Aldefluor regent before purification by FACS (FACS Aria III; BD Biosciences, Mississauga, ON, Canada). UCB ALDH^{hi} cells were selected based on low side scatter and high ALDH-activity with >98% purity (n = 5). Purified UCB ALDH^{hi} cells were cultured on fibronectin-coated plates for 9 days under untreated (X-vivo 15 + 10 ng/mL SCF, TPO, FLT-3L) or DEAB-treated (Untreated+10 mM DEAB on days 3–6), as previously described (Figure 3.1A)[22].

3.2.3   Flow cytometry

UCB ALDH^{hi} cells expanded under untreated or DEAB-treated conditions were harvested at day 9 and enumerated by trypan blue exclusion using hemocytometer counts. Cells were labeled with Aldefluor to assess ALDH-activity. and co-stained with 7-amino-actinomycin D to determine viability. Fresh UCB Lin- MNC and expanded UCB ALDH^{hi} cell progeny were co-labeled with anti-human antibodies for CD41 (ITGA2), and CD42 (GP1B; megakaryocyte). Expanded cells were assessed for a primitive HPC phenotype using anti-human CD34 and hematopoietic lineage differentiation was determined using anti-human CD38 (cyclic ADP ribose hydrolase). Cell surface marker expression for fresh cells, and expanded ALDH^{hi} versus ALDHlo subsets was determined using an

LSRII flow cytometer (BD Biosciences) at the London Regional Flow Cytometry Facility. All analyses were performed using FlowJo software v8.2.

3.2.4   Hematopoietic colony formation

Day 9 expanded cells were harvested from untreated or DEAB-treated conditions and reselected for high or low ALDH-activity before being seeded in semi-solid methylcellulose media (H4434; Stem Cell Technologies) at 500 cells/mL in 12-well plates, performed in duplicate (Figure 3.2C). Hematopoietic colonies were enumerated after 12–14 days *in vitro* and scored based on morphological characteristics of burst forming unit erythrocyte (BFU-E), colony forming unit granulocyte (CFU-G), colony forming unit macrophage (CFU-M), colony forming unit granulocyte/macrophage (CFU-GM), or colony forming unit mixed (CFU-Mixed)[20]. CFU/100 cells were calculated by number of colonies formed per 100 cells seeded in the assay. Furthermore, the frequency of lineage-specific colony formation was calculated by dividing the number of a lineage-specific colony (i.e., BFU-E) by the total number of colonies enumerated.

3.2.5   Transplantation of expanded ALDH^{lo} and ALDH^{hi} cells

Pancreatic β-cell ablation was induced in NOD/SCID mice aged 8- to 10-weeks (Jackson Laboratories, Bar Harbor, ME; www.jax.org) by intraperitoneal injection of STZ (35 mg/kg/ day) for 5 consecutive days[11] (Figure 3.3A). All animal procedures were approved by the Animal Care Committee at Western University Canada (AUP 2015-033). On day 10, hyperglycemic (15–25 mM) mice were sublethally irradiated (300 cGy) and transplanted in a blinded fashion by intrapancreatic injection of phosphate-buffered saline (PBS), or 10^5 expanded (bulk) cells, 2.0 x 10^5 ALDH^{lo} cells, or 2.0 x 10^5 ALDH^{hi} cells harvested from untreated or DEAB-treated conditions. Systemic blood glycemic levels were monitored weekly in a blinded fashion for 42 days. Twenty-four hours before sacrifice, mice were i.p.- injected with 200 µg 5-ethynyl-20-deoxyuridine (EdU; Invitrogen) to label proliferating cells in situ. In addition, glucose tolerance tests were performed over 120 min after i.p.-injection of 2 g/kg glucose bolus at day 41, as previously described (Figure 3.4A)[23.]

3.2.6 Immunohistochemistry and immunofluorescent analyses

Pancreata were harvested, embedded in OCT, and cryosectioned (12 µm) to obtain three sections per slide $\pm$ 200 µm apart. Cryosections were fixed in 10% formalin (Sigma) and blocked with 5% serum before immunohistochemical staining for insulin to determine islet number, size, and β-cell area as previously described[23]. Additionally, immunofluorescent co-staining for insulin with EdU, CD31, Nkx6.1, and/or HLA-A,B,C was performed. EdU^{+} proliferating cells were detected using the Click-iT imaging kit (Alexafluor 488; Life Technologies). Intra-islet capillary density was enumerated post-transplantation using rat anti-mouse CD31 (1:100; BD Biosciences) detected with FITC-labeled rabbit anti-rat secondary antibodies (1:200; Vector). Nxk6.1+ cell nuclei were enumerated using anti-rabbit (1:2000; AbCam) and detected using goat anti-rabbit FITC-labeled secondary antibodies (1:200; Vector). Human cell engraftment was enumerated by staining pancreas sections with mouse anti-human HLA A,B,C (1:100; AbCam) detected with horse anti-mouse FITC-labeled secondary antibodies (1:200; Vector). DAPI was used as counterstain to label nuclei. Quantification and analyses were performed using Fiji (Image J v2.0).

3.2.7 Quantification of islet number, size, and β-cell mass

Islet number was quantified across four random images per tissue section (12 images per mouse) by enumerating the presence of insulin+ islet structures containing more than 20 nuclei. Islet size was determined by measuring the circumference of each islet identified in the previous quantification using Fiji (Image J v2.0). Lastly, β-cell mass of each mouse was calculated:

$$Pancreas\ Weight\ (mg)\ x\ \left(\frac{Islet\ Area\ (Insulin\ +)}{Non-islet\ Area}\right) = \beta - cell\ mass$$

3.2.8 Statistical analyses

Statistical analysis for flow cytometry and colony analyses was performed by one-way ANOVA with Tukey's multiple comparisons tests. Analysis of significance was

performed by one-way ANOVA with Tukey's multiple comparisons tests for all *in vivo* experiments and enumeration of histological analyses. Outliers were identified using Grubb's test; P < 0.05.

3.3   Results

3.3.1   High ALDH-activity does not select for the megakaryocyte lineage in fresh UCB cells

We have previously demonstrated that purified UCB Lin− ALDH^{hi} cells represent a heterogeneous progenitor cell population with multifaceted regenerative functions[11,20]. However, the robust expansion of UCB Lin− ALDH^{hi} cells (>70-fold) under serum-free conditions containing SCF, Flt-3L, and TPO generated a megakaryocyte-enriched population with diminished ALDH-activity and progenitor cell surface marker expression[22]. To understand the propensity of UCB Lin− ALDH^{hi} cells to differentiate toward the megakaryocyte lineage, we sought to determine whether the initial selection of primitive cells based on high ALDH-activity also enriched for committed precursors within the megakaryocyte lineage. Therefore, we first compared fresh UCB Lin− MNC, or FACS-purified ALDH[hi] and ALDH^{lo} cells for megakaryoblast (CD41$^+$/CD42$^-$) and megakaryocyte (CD41$^+$/CD42$^+$) cell surface marker expression (Figure 3.11A). The frequency of cells with CD41$^+$/CD42$^-$ megakaryoblast phenotype was equivalent between freshly isolated UCB Lin− MNC (28.8% ± 6.12%), or purified ALDH[hi] (26.9% ± 2.1%) versus ALDHlo cell subpopulations (29.1% ± 6.4%; Figure 3.1B). Moreover, the frequency of committed CD41$^+$/CD42$^+$ megakaryocytes was also equivalent within the fresh UCB Lin− cell subsets (Figure 3.1C). Thus, selection of UCB Lin− cells based on high ALDH-activity did not enrich for cells of the megakaryocyte lineage; although ∼60% of UCB ALDH^{hi} cells expressed early megakaryocyte marker CD41.

A

B Megakaryoblast

C Megkaryocyte

D Megakaryoblast
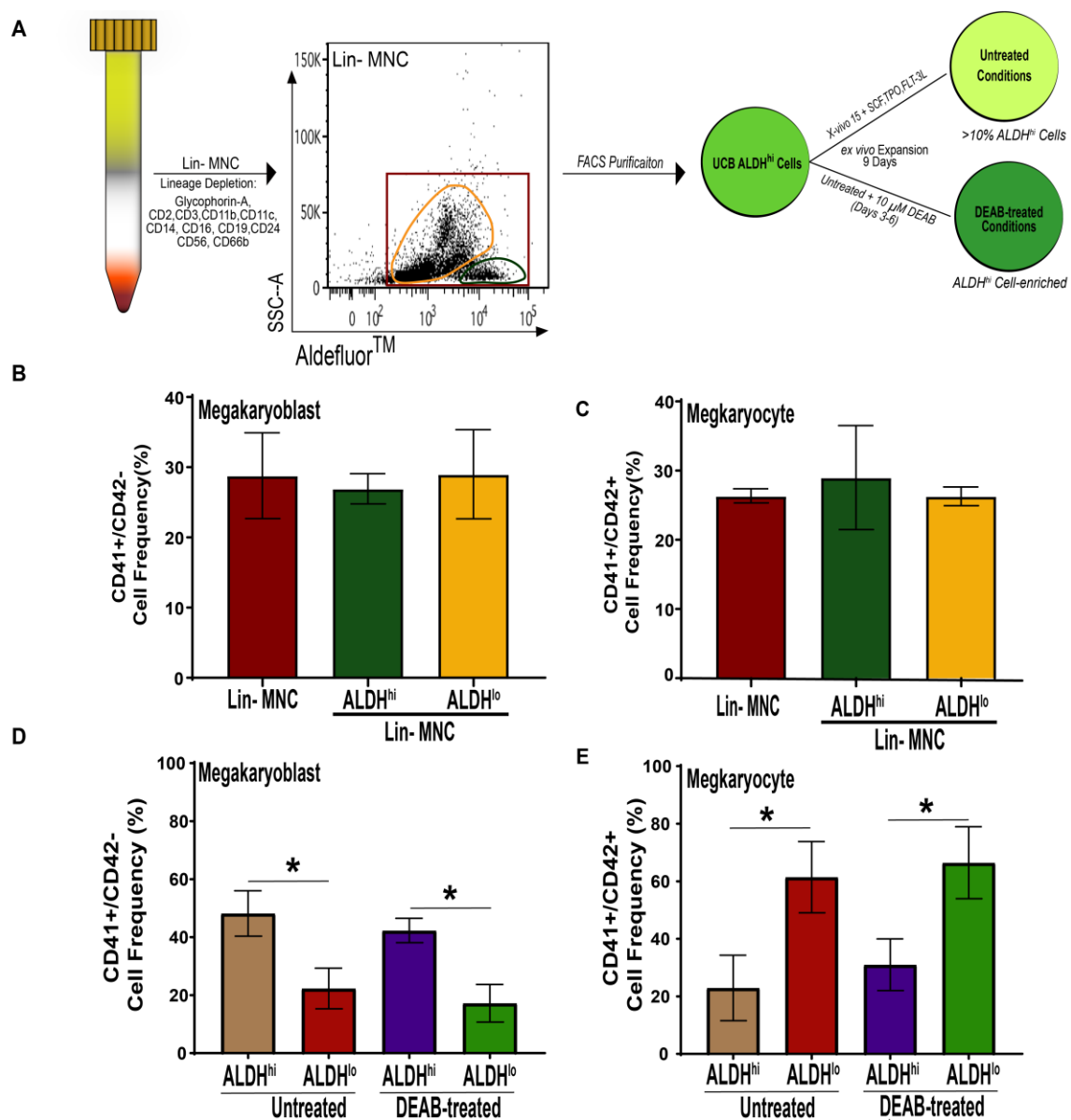
E Megkaryocyte

Figure 3.1 Expansion of UCB ALDH^{hi} cells generated cells of the megakaryocyte lineage *in vitro*. (A) Schematic for the initial FACS-purification of cells with low side-scatter (SSC-A) and high aldehyde dehydrogenase (ALDH) activity from lineage-depleted (Lin-) human umbilical cord blood (UCB) and subsequent expansion under serum-free conditions with or without DEAB-treatment. The frequency of (B) CD41+/CD42- megakaryoblasts, and (C) CD41$^+$/CD42$^+$ megakaryocytes was equivalent within fresh UCB Lin- mononuclear cells, and purified ALDH^{hi} or ALDH^{lo} cell subsets. Following expansion of UCB ALDH^{hi} cells for 9 days with or without DEAB-treatment, (D) expanded cells re-selected for high ALDH-activity were enriched for CD41+/CD42- megakaryoblasts compared to the ALDH^{lo} cell subset. Conversely, (E) expanded cells re-selected for low ALDH-activity were enriched for CD41$^+$/CD42$^+$ megakaryocytes, compared to the ALDH^{hi} cell subset. Data represented as Mean $\pm$ SEM (*p<0.05, N=3-5). Statistical analyses were determined by one-way ANOVA with Tukey's post-hoc test.

3.3.2 The expanded ALDH^{hi} cell subpopulation was enriched for a megakaryoblast phenotype and the ALDH^{lo} cell subpopulation was enriched for a megakaryocyte phenotype

The *ex vivo* expansion of UCB Lin− ALDH^{hi} cells under DEAB-treated culture conditions robustly increased the total number of viable ALDH^{hi} cells for preclinical studies (>20-fold)[22]. Despite the retainment of ALDH^{hi} cells under DEAB-treated conditions, the frequency of CD41$^+$/CD42$^+$ megakaryocytes in the total cell population was comparable to untreated conditions. It is currently unreported whether ALDH^{hi} cells reselected from DEAB-treated conditions are enriched for specific subpopulations of the megakaryocyte lineage, compared to untreated conditions. Following *ex vivo* expansion of UCB Lin− ALDH^{hi} cells under untreated or DEAB-supplemented conditions, cell progeny that retained high ALDH-activity was enriched (*p< 0.05) for early megakaryoblast (CD41$^+$/CD42$^−$) phenotype, compared to the ALDH^{lo} cell subpopulation (Figure 3.1D) from either condition. Conversely, the ALDH^{lo} cell subpopulation generated under untreated and DEAB-treated conditions was significantly enriched (**P < 0.01) for a committed CD41$^+$/CD42$^+$ megakaryocyte phenotype, compared to the ALDH^{hi} cell subpopulation (Figure 3.1E). Collectively, DEAB-treated conditions generated CD41+/CD42− megakaryoblasts that retained ALDH^{hi} progenitor cell characteristics and reduced the commitment of UCB Lin− ALDH^{hi} cells toward an ALDH^{lo} CD41$^+$/CD42$^+$ megakaryocyte phenotype.

3.3.3 Reselection of ALDH^{hi} cells enriched for primitive phenotypes and increased multipotent hematopoietic colony formation *in vitro*

Multipotent HPC with colony formation function *in vitro* and SCID-repopulating capacity *in vivo* can be enriched from fresh UCB samples by the selection of CD34$^+$/CD38$^−$ or ALDH^{hi} cells[28,29]. To determine whether multipotent HPC remained after 9-days culture, we assessed expanded UCB Lin− ALDH^{hi} cells for a primitive progenitor cell phenotype and for clonal colony formation *in vitro*. Following *ex vivo*

expansion of UCB Lin− ALDH^{hi} cells under untreated or DEAB-supplemented conditions, reselected ALDH^{hi} cells were significantly enriched (**$p < 0.01$) for primitive CD34$^+$/CD38$^-$ cell surface marker expression (20.8% ± 7.3% or 15.1% ± 3.9%), compared to the ALDH^{lo} cell subpopulation (1.7% ± 0.7% or 1.7% ± 0.5%; Figure 2A). The frequency of CD34$^+$/CD38$^-$ cells in the ALDH^{hi} subset was comparable between culture conditions (Figure 2A). Regardless, we have previously reported that the enrichment of ALDH^{hi} cells under DEAB-treated conditions induced a more than twofold increase in the number of ALDH^{hi}/CD34$^+$/CD38$^-$ cells, compared to untreated conditions[22]. Importantly, DEAB-treated conditions induced a significant decrease in frequency of ALDH^{hi} or ALDH^{lo} cells with CD38+ expression (Figure 3.2B), a marker of hematopoietic maturation[27]. To determine hematopoietic colony forming capacity *in vitro*, ALDH^{hi} and ALDH^{lo} cells were reselected after expansion under untreated and DEAB-treated conditions and seeded in methylcellulose media. Hematopoietic colony formation was manually enumerated after 14 days (Figure 3.2C). Notably, ALDH^{hi} cells from either untreated or DEAB-treated conditions were significantly enriched for colony forming cells compared to ALDH^{lo} cells (Figure 3.2D). ALDH^{hi} cells from DEAB-treated cultures also demonstrated a higher frequency (*$p < 0.05$) of colony formation (1 CFU in 10.5 cells, *$p < 0.05$) compared to ALDH^{hi} cells expanded under untreated conditions (1 CFU in 30.0 cells). The frequency of myeloid colonies formed was found to be similar to cells expanded under untreated or DEAB-treated conditions (Figure 2E). Within the ALDH^{hi} or ALDH^{lo} subsets only ALDH^{hi} cells demonstrated myeloid multipotency by the formation of CFU-mixed colonies, whereas ALDH^{lo} cells largely contained progenitors restricted to the macrophage (CFU-M) or granulocyte (CFU-G) lineages (Figure 2E). Collectively, these results demonstrate DEAB-treated conditions reduced the acquisition of mature marker CD38 and augmented the expansion of ALDH^{hi} cells that retained multipotent hematopoietic colony forming capacity *in vitro*.

Figure 3.2 Re-selection of expanded cells with high ALDH-activity enriched for cells retaining primitive (CD34+/CD38-) phenotype and multipotent colony forming capacity *in vitro*. (A) Following expansion for 9 days with or without DEAB-treatment, primitive (CD34$^+$/CD38$^-$) cell phenotype was enriched within the expanded ALDH^{hi} cell subset compared to the ALDH^{lo} cell subset. (B) CD38 expression was significantly decreased following DEAB-treatment. Specifically, CD34$^-$/CD38$^+$ cell frequency was reduced in both the ALDH^{hi} and ALDH^{lo} cell subpopulation of cells harvested from DEAB-treated conditions. (C) Following expansion for 9 days with or without DEAB-treatment, expanded cells re-purified for low or high ALDH-activity were seeded in methylcellulose media and colony formation was enumerated after 14 days. (D) Total hematopoietic colony formation was increased within expanded cells re-selected for high ALDH-activity and was also increased for re-selected ALDH^{hi} cells generated under DEAB-treated conditions compared to re-selected ALDH^{hi} cells generated untreated conditions. (E) Only ALDH^{hi} cells from either Untreated or DEAB-treated conditions demonstrated full myeloid-specific multipotency, compared to re-selected ALDH^{lo} cells that did not form mixed colonies. Data represented as Mean $\pm$ SEM (*p<0.05, **p<0.01, ***p<0.001; N=3-5). Statistical analyses were determined by one-way ANOVA with Tukey's post-hoc test.

3.3.4 Intrapancreatic transplantation of ALDH^{lo} cells from DEAB-treated conditions reduced hyperglycemia in STZ-treated NOD/SCID mice

We have shown that *ex vivo* expansion of UCB Lin− ALDH^{hi} cells rapidly diminishes islet regenerative function as culture time was increased[13]. Therefore, we sought to utilize previously reported culture conditions that increase the number (two-fold) of ALDH^{hi} cells following 9-day expansion, compared to untreated conditions[22]. On day 10, STZ-treated, hyperglycemic (>15 mM) NOD/SCID mice received intrapancreatic transplantation (Figure 3.3A) of PBS or 5.0×10^5 bulk cells harvested from either untreated or DEAB-treated conditions. Similar to PBS-injected controls, mice transplanted with untreated bulk cells remained hyperglycemic up to 42 days (Figure 3.3B, C). Compared to PBS-injected controls, transplantation of DEAB-treated bulk cells reduced hyperglycemia on day 17 (*$p < 0.05$); however, a sustained reduction of hyperglycemia was not observed at later time points out to day 42 (*$p = 0.17$; Figure 3.3B, C). In a recent publication, we also demonstrated that sustained reduction in hyperglycemia was only achieved when 6-day expanded cells were reselected for high ALDH-activity before intravenous transplantation[23]. Therefore, we reselected our expanded cell populations for high versus low ALDH-activity before direct intrapancreatic transplantation. Hyperglycemic mice received an intrapancreatic transplantation of 2.0×10^5 ALDH^{hi} or ALDH^{lo} cells harvested from either untreated or DEAB-treated conditions. ALDH^{hi} cells harvested from either untreated or DEAB-treated conditions at 9 days were unable to reduce hyperglycemia, compared to PBS-injected controls (Figure 3D, E). Interestingly, the ALDH^{lo} cell subset from DEAB-treated conditions significantly reduced hyperglycemia at days 14, 17, and 28 (*$p < 0.05$; Figure 3.3D). More importantly, hyperglycemia was significantly reduced by measurement of area under the curve (*$p < 0.05$; Figure 3.3E), compared to PBS-injected controls. After performing glucose tolerance tests 24-h before euthanasia, mice transplanted with bulk, ALDH^{hi}, or ALDH^{lo} cells from either untreated or DEAB-treated conditions did not demonstrate an improved physiological response to i.p. injection of a glucose bolus (Figure 3.4). Thus, DEAB-treated conditions generated ALDH^{lo} cells that modestly

reduced resting glycemia levels in STZ-treated NOD/SCID mice following intrapancreatic transplantation. However, the reduction in hyperglycemia was modest, transient, and mice were unable to respond to glucose bolus in a physiological manner at a later time point.
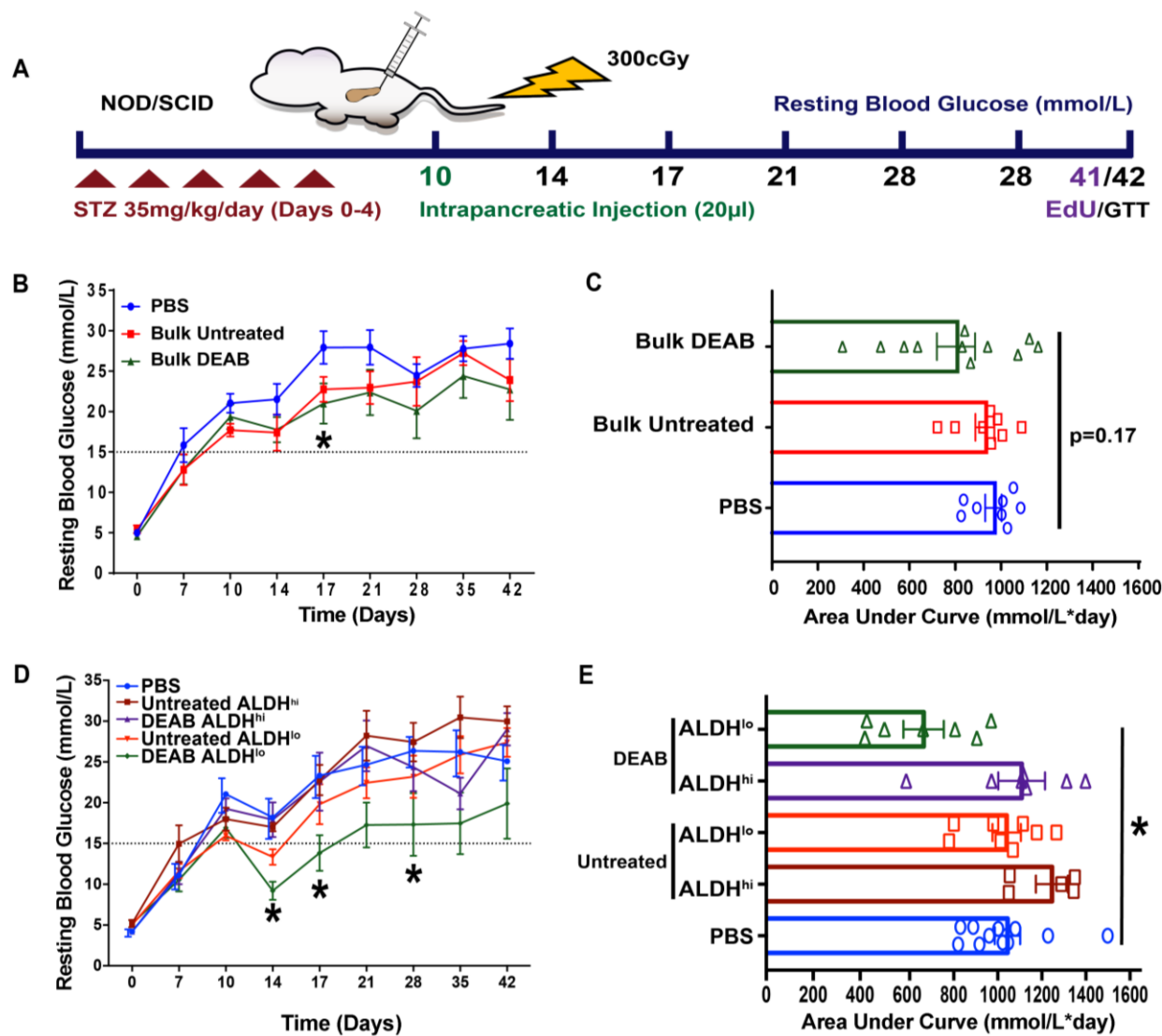
Figure 3.3 Intrapancreatic transplantation of re-selected ALDH^{lo} cells from DEAB-treated conditions reduced hyperglycemia in STZ-treated NOD/SCID mice. (A) Hyperglycemia was induced in NOD/SCID mice by serial injections of STZ (35mg/kg/day) between days 0-4. Hyperglycemic mice (>15.0 mmol/L at day 10) were sublethally irradiated (300 cGy) on Day 10 and received intrapancreatic transplantation of 5.0x10^5 bulk cells, 2.0x10^5 ALDH^{hi} cells or 2.0x10^5 ALDH^{lo} cells harvested after 9 days expansion using either Untreated or DEAB-treated conditions. To serve as a vehicle control (PBS), mice received an intrapancreatic injection of phosphate buffered saline at an equivalent volume (20µl). (B) Resting blood glucose levels of mice transplanted with vehicle control (PBS), or bulk cells expanded under untreated or DEAB-treated conditions. (C) Mice transplanted with untreated (n=10) or DEAB-treated (n=11) expanded cells did not show reduced glycemia area under the curve (AUC), compared to PBS-injected (n=8) controls. (D) Mice transplanted with ALDH^{lo} cells from DEAB-treated conditions (n=7) showed reduced resting blood glucose levels (Day 14, 17 and 28) compared to PBS-injected controls (n=10). (E) Mice transplanted with ALDH^{lo} cells from DEAB-treated conditions (n=7) showed reduced glycemia area under the curve (AUC), compared to PBS-injected (n=8) controls. Data represented as Mean $\pm$ SEM (*p<0.05, n=6-11 mice per group). Statistical analyses were determined by one-way ANOVA with Tukey's post-hoc test compared to PBS control.
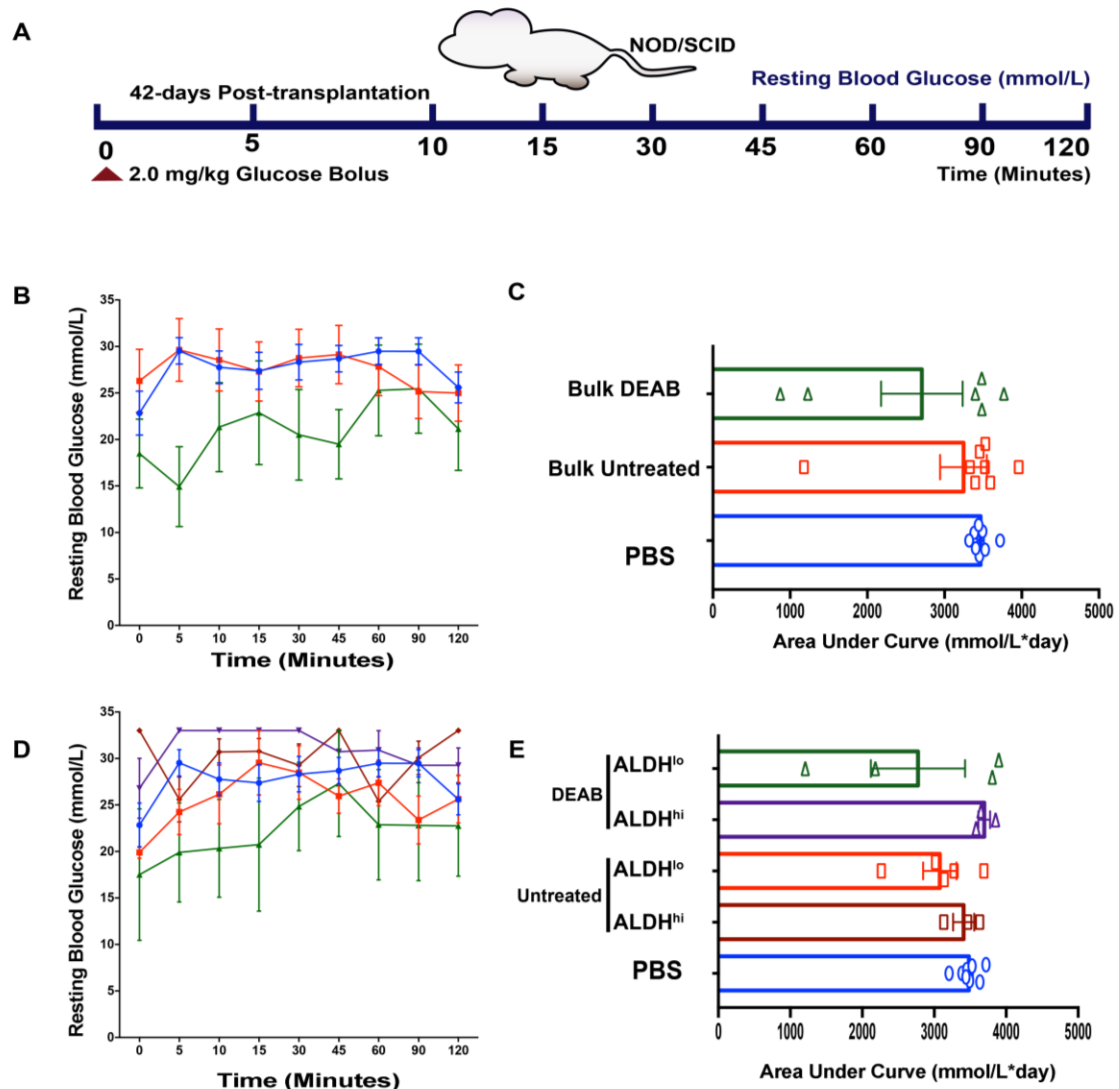
Figure 3.4 Mice transplanted with expanded cells do not respond to intraperitoneal injection of glucose. (A) On Day 41, transplanted mice were fasted (4h) and received intraperitoneal injection of 2.0mg/kg dextrose followed by serial serum glucose measurements up to 120 min. (B, C) Mice transplanted with expanded cells from untreated or DEAB-treated conditions did not demonstrate a physiological response to glucose bolus. (D, E) Similarily, mice transplanted with expanded cells from untreated or DEAB-treated conditions reselected for low or high ALDH-activity did not demonstrate a physiological response to glucose bolus. Data represented as mean + SEM (n= 3-8). Statistical analyses were determined by one-way ANOVA with post-hoc Tukey's t-test.

3.3.5 Intrapancreatic transplantation of expanded ALDH^{lo} cells from DEAB-treated conditions increased islet number

To investigate the mechanisms by which expanded ALDH^{lo} cells generated from DEAB-treated conditions modestly reduced hyperglycemia in NOD/SCID mice, pancreas sections were analyzed for islet size, number, and total β-cell mass (Figure 3.5A–D). Histological analysis revealed a significant increase in the number of insulin+ islets in mice receiving intrapancreatic transplantation of DEAB-treated ALDH^{lo} cells, compared to PBS-injected mice ($*p < 0.05$; Figure 3.5B). In contrast, islet circumference remained comparable between all transplantation conditions (Figure 3.5C). Ultimately, mice transplanted with DEAB-treated ALDH^{lo} cells demonstrated an increased trend in total β cell mass, compared to PBS-injected controls ($p = 0.14$; Figure 3.5D). Thus, expanded DEAB-treated ALDH^{lo} cells did not robustly increase β cell mass and transplanted mice demonstrated a failed physiological response to a glucose challenge, despite modestly improved resting glycemic levels
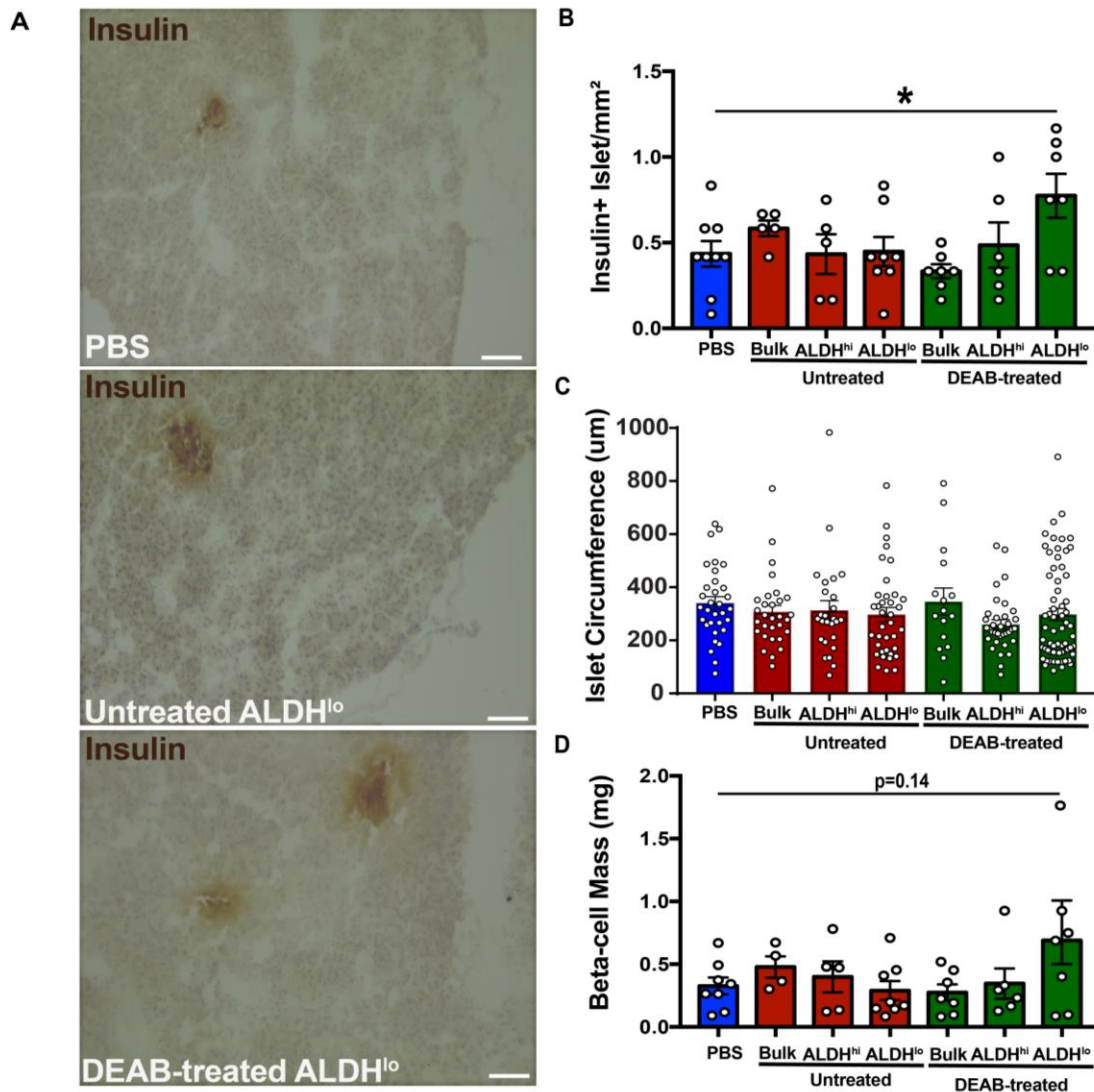
Figure 3.4 Mice transplanted with ALDH^{lo} cells from DEAB-treated conditions showed modestly increased islet number and beta-cell mass. (A) Representative photomicrographs of islets stained for insulin (brown) at day 42 in STZ-treated NOD/SCID mice transplanted with vehicle control or ALDH^{lo} cells harvested from Untreated or DEAB-treated conditions. Compared to vehicle control, mice transplanted with DEAB-treated ALDH^{lo} cells demonstrated (B) increased islet number without (C) measurable changes in islet size. (D) Mice transplanted with ALDH^{lo} cells from DEAB-treated conditions did not show significantly (p=0.14) increased β-cell mass, compared to mice injected with vehicle control. Data represented as Mean $\pm$ SEM (n=6-10). Statistical analyses were determined by one-way ANOVA with Tukey's post-hoc test compared to PBS control. Scale bar = 100µm.

3.3.6 Expanded ALDH^{lo} cells increased intra-islet cell proliferation but did not increase intra-islet vascularity or Nxk6.1+ expression

To better understand regenerative processes induced by intrapancreatic ALDH^{lo} cell xenotransplantation, we assessed intra-islet cell proliferation in mice pulsed with EdU for 24 h before sacrifice at day 42. Pancreata transplanted with ALDH^{lo} cells harvested from DEAB-treated conditions demonstrated an increase in the number of proliferating (EdU$^+$) cells within islets at day 42 (Figure 3.6A). Although increased proliferation was observed, intra-islet vascular density (CD31$^+$ cells/Islet Area; Figure 3.6B) and β cell identity marker expression (Nkx6.1; Figure 3.6C) were equivalent to PBS-injected mice. Thus, indicating proliferating cells were likely not of an endothelial or β cell phenotype. HLA-A,B,C+ human cells were not detected in the pancreas of transplanted mice at day 42, despite detectable engraftment at day 14 (Figure 3.7). Collectively, ALDH^{lo} cells from DEAB-treated conditions transiently engrafted the murine pancreas and modestly increased islet cell proliferation without significantly increasing islet-vascularity or functional β cell mass.

.

A DAPI
Insulin
EdU

Day 42 DEAB-treated ALDH^{lo}

B DAPI
Insulin
CD31

Day 42 DEAB-treated ALDH^{lo}

C DAPI
Insulin
Nkx6.1

Day 42 DEAB-treated ALDH^{lo}
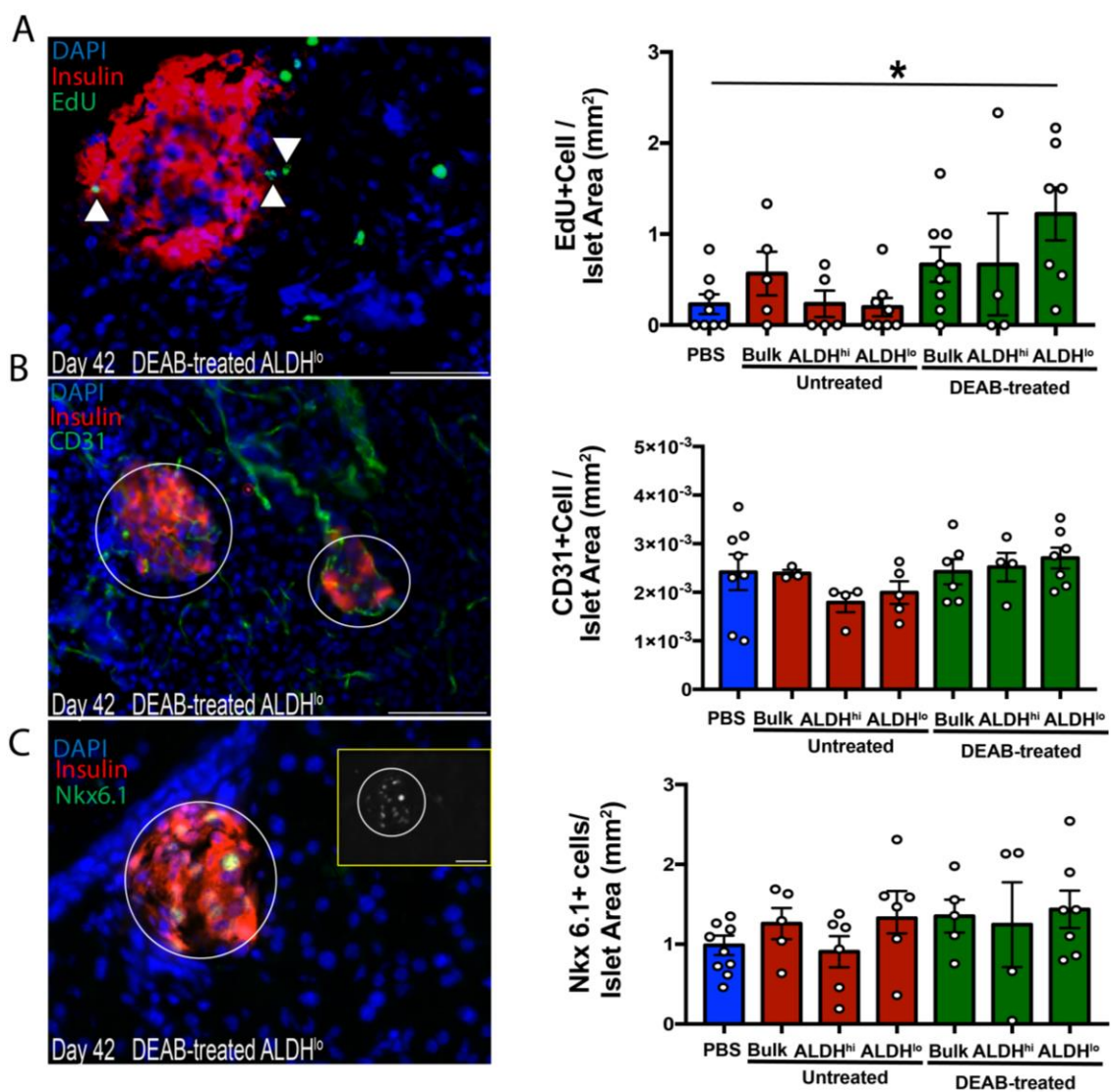
Figure 3.5   Intrapancreatic transplantation of ALDH^{lo} cells from DEAB-treated conditions increased intra-islet cell proliferation. (A) Representative photomicrograph of EdU+ cells within insulin-expressing islets at day 42 in an STZ-treated mouse transplanted with DEAB-treated ALDH^{lo} cells. Compared to PBS-injected control mice (n=9), mice transplanted with DEAB-treated ALDH^{lo} cells (n=7) showed an increased number of proliferating cells (EdU$^+$) within islets. (B) Representative photomicrograph of murine CD31+ cells within insulin-expressing islets at Day 42 in an STZ-treated mouse transplanted with DEAB-treated ALDH^{lo} cells. Intra-islet vascularization (CD31+) was equivalent for all transplanted groups. (C) Representative photomicrograph of murine Nkx6.1+ nuclei with insulin-expressing islets at day 42 in a STZ-treated mouse transplanted with DEAB-treated ALDH^{lo} cells. Intra-islet Nkx6.1$^+$ cells per islet area was equivalent for all transplanted groups. Data represented as Mean $\pm$ SEM (*$p<0.05$; n=6-10). Statistical analyses were determined by one-way ANOVA with post-hoc Tukey's post-hoc test compared to PBS control. Scale bar = 100µm.

A
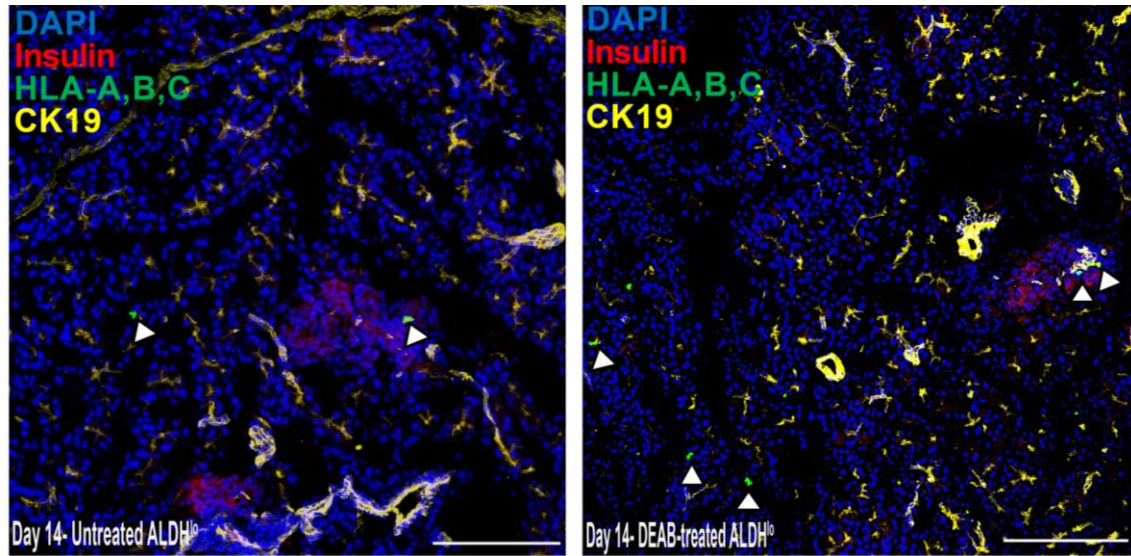
Figure 3.6 Mice transplanted with expanded cells re-selected for low ALDH-activity showed human cell engraftment at 4-days post-transplantation. (A) Representative photomicrographs of human cell engraftment in the pancreas of mice transplanted with expanded cells re-selected for low ALDH-activity at 4 days post-transplantation. HLA-A, B, C-expressing cells were detected in mice transplanted with ALDH^{lo} cells generated under untreated (n=2) and DEAB-treated conditions (n=2). Scale bar = 100µm.

3.4 Discussion

Restoration of β cell mass for the treatment of diabetes has recently become an intense focus of translational research, yet many of the mechanisms facilitating the regeneration of endogenous β cell mass remain elusive. For example, identifying hematopoietic cell subtypes that stimulate islet regenerative mechanisms has largely been unexplored. We have demonstrated selection of UCB Lin− ALDH^{hi} cells enriched for a HPC population capable of reducing hyperglycemia in STZ-injected NOD/SCID mice[11]. Unfortunately, UCB ALDH^{hi} cells are rare and expansion will be required to collect enough cells to potentially treat human subjects. Our recent work and this study demonstrate the challenge in expanding these cells with concurrent retention of islet regenerative capacity[13]. The selection of UCB Lin− ALDH^{hi} cells biases HPC differentiation by active RA-induced differentiation under serum-free conditions that promoted the acquisition of a megakaryocyte phenotype (CD41^{+}/CD42^{+}) and loss of regenerative function (Figure 6). On the other hand, we have recently reported that DEAB-induced inhibition of RA-production enhanced the expansion of HPC that retained vascular regenerative paracrine functions *in vivo*[22]. With these properties in mind, we initially hypothesized that reversible inhibition of ALDH-activity could enhance the expansion of UCB-derived hematopoietic progeny with islet regenerative function by preventing differentiation from an ALDH^{hi} cell phenotype. Herein, we show the robust islet regenerative function of UCB Lin− ALDH^{hi} cells is lost during *ex vivo* culture; however, beneficial functions were partially retained by inhibiting RA-induced differentiation and paradoxically reselecting for CD41^{+} enriched ALDH^{lo} cells.

The islet regenerative function of uncultured UCB Lin− ALDH^{hi} cells was rapidly lost under clinically applicable, hematopoietic selective serum-free culture conditions. With this in mind, we first sought to determine whether the megakaryocyte content of uncultured UCB Lin− ALDH^{hi} cells could provide help elucidate the phenotype of an islet regenerative cell population, as expanded cells are largely committed to the megakaryocyte lineage. CD41^{+}/CD42^{+} cell content was equivalent between uncultured UCB Lin− cells, or Lin− ALDH^{hi} or Lin− ALDH^{lo} cell subsets. These results provided indirect evidence that CD41^{+}/CD42^{+} megakaryocyte content likely played a minimal role

in the islet regenerative function of transplanted uncultured UCB Lin− ALDH^{hi} cells and the enrichment of a megakaryocyte phenotype is a result of subsequent culture conditions. Interestingly, Gentry *et al.* previously reported that the selection of ALDH^{hi} cells enriched for megakaryocyte progenitors by >2000-fold, compared to the ALDH[lo] subpopulation[30]. We attributed our conflicting results observed in this study to our use of a lineage-depletion cocktail, which does not deplete cells of the megakaryocyte lineage from UCB MNC. Furthermore, megakaryoblast and megakaryocyte phenotype in UCB cells was assessed by flow cytometry in our study, as opposed to the use of a clonogenic assay that would assess the megakaryocyte potential of selected subpopulations. Nonetheless, our results corroborate the findings by Gentry *et al.*, such that UCB ALDH^{hi} cells robustly generated cells of the megakaryocyte lineage *in vitro*.

Megakaryocytes are large cells (>50 μm) that primarily reside within the bone marrow[31] or lungs[32] and are derived from a common megakaryocyte/erythroid myeloid progenitor cell[33]. Considering our culture conditions are supplemented with TPO, a known driver of megakaryopoiesis and paradoxically required for effective progenitor cell expansion, it is likely that the expansion of CD41^{+}/CD42^{+} cells from ALDH^{hi} cells can be attributed to active TPO-signaling. Future research would need to determine the role exogenous TPO and/or extracellular matrix molecules have on UCB ALDH^{hi} cell differentiation toward a CD41^{+}/CD42^{+} phenotype, an area that has been extensively studied with other HPC subpopulations[34-36]. Moreover, TPO produced by cells of the megakaryocyte lineage could signal in an autocrine fashion to stimulate the expression of CD41 and CD42[36]. Considering that >60% of freshly isolated UCB Lin− ALDH^{hi} cells express CD41, we propose that UCB Lin− ALDH^{hi} cells are primed to respond to drivers of differentiation, including the RA- and TPO-signaling pathways. Collectively, the expansion of ALDH^{hi} cells and modulation of megakaryopoiesis *in vitro* is complex and future studies would need to consider several parameters including (1) progenitor cell purification, (2) culture conditions, and (3) culture duration.

For nearly 2 decades, high ALDH-activity has served as an enzymatic marker to identify and enrich for hematopoietic progenitor subtypes in fetal and adult tissue[37-39]. Our recent publication demonstrated DEAB supplementation and subsequent inhibition of RA-production enriched for ALDH^{hi} cells progeny (>2-fold) during UCB HPC expansion[24], leading to a >20-fold increase in viable ALDH^{hi} cell number. Supporting our previous studies, we report that CD34^{+}/CD38^{−} cell surface expression was enriched within the ALDH^{hi} cell subset following expansion[23]; moreover, reselected ALDH^{hi} cells demonstrated enhanced multipotent hematopoietic colony formation, compared to ALDHlo cells[23]. Importantly, ALDH^{hi} cells reselected from DEAB-treated conditions showed enhanced hematopoietic colony formation, compared to untreated conditions. Considering CD34^{+}/CD38^{−} enrichment within the ALDH^{hi} subset was comparable between untreated and DEAB-treated conditions, our results support previous reports that high ALDH-activity further enriches for multipotent HPC from the CD34^{+}/CD38^{−} subpopulation[29]. These results indicate that the loss of high ALDH-activity coincides with the loss of multipotent progenitor capacity and hematopoietic colony formation can be retained by temporarily inhibiting RA-production *in vitro*. The loss of ALDH-activity has been associated with HPC differentiation and here we add that the ALDHlo cell subsets were enriched for a CD41^{+}/CD42^{+} megakaryocyte phenotype (>50%) following *ex vivo* expansion. On the other hand, ALDH^{hi} cells were enriched for CD41^{+}/CD42^{−} megakaryoblasts compared to ALDHlo cells. Therefore, we propose a model where high ALDH-activity is gradually diminished during culture as uncommitted multipotent myeloid progenitors lose a primitive CD34+/CD38− phenotype and transition toward a CD41^{+}/CD42^{−} megakaryoblast phenotype, before commitment toward a CD41^{+}/CD42^{+} megakaryocyte phenotype and acquisition of CD38 expression (Figure 6).

In the current study, we observed a modest improvement of glycemia levels in STZ-treated NOD/SCID mice receiving intrapancreatic transplantation of expanded cells harvested from DEAB-treated conditions. However, our histological analysis revealed minimal regeneration of β cell mass had occurred following direct transplantation of bulk expanded cells. These results lead us to predict the reselection of cells based on high

versus low ALDH-activity would be required to purify regenerative cells with enhanced engraftment and/or migration. Intrapancreatic transplantation of expanded cells reselected for high versus low-activity surprisingly revealed that only ALDH^{lo} cells harvested from DEAB-treated conditions (DEAB ALDH^{lo}) reduced hyperglycemia. The capacity of ALDH^{lo} cells harvested from DEAB-treated conditions to reduce hyperglycemia and improve islet function after intrapancreatic transplantation was highly variable, with 3 of 7 mice showing notable recovery. Although we observed increased islet number within the pancreas of mice transplanted with DEAB ALDH^{lo} cells, the size of murine islets and total β cell mass were comparable between all conditions. Our previous reports demonstrated that transplanted fresh UCB ALDH^{hi} cells transiently engrafted the pancreas yet demonstrated sustained regeneration of β cell mass[12]. Similarly, we detected engraftment of transplanted expanded cell progeny at day 14 but not day 42; suggesting that expanded ALDH^{lo} cell engraftment is also transient while islet regenerative function is modest. Nonetheless, DEAB-treated ALDH^{lo} cells modestly reduced hyperglycemia, by increasing islet number through unidentified mechanisms. The results of this study contrast our previous HPC transplantation studies that reported increased β cell mass as a result of increased islet size not islet number[23]. We observed an increased rate of proliferating cells within murine islets at day 42 following direct transplantation of DEAB ALDH^{lo} cells, however, it was concluded that EdU+ cells were not of an endothelial (CD31) or β cell (Nkx6.1) phenotype. Collectively, we provided preliminary evidence that transplanted DEAB ALDH^{lo} cells temporarily engraft the pancreas to support β cell function via unidentified and likely multifactorial mechanisms.

Highly vascularized networks within islets of Langerhans facilitate the release and transport of blood glucose regulating hormones, including insulin and glucagon, through systemic circulation[40]. Seneviratne et al. demonstrated increased intra-islet vascularity islet size and β cell mass after intravenous transplantation of 6-day expanded ALDH^{hi} HPC[23]. Considering DEAB-treated cells robustly stimulate angiogenesis in the ischemic hindlimb, we investigated whether islet vascularity was increased following intrapancreatic transplantation; in return increasing the efficiency of systemic insulin

delivery. Immunofluorescent analysis revealed intra-islet vascularity was equivalent between all transplantation conditions. This was anticipated, considering islet size was not increased following DEAB-treated ALDHlo cell transplantation. These collective results suggest that intra-islet vascularity may increase only when robust recovery β cell mass occurs. Previous studies have demonstrated a "symbiotic" relationship between endothelial cells and pancreatic β-cells[41,42]. Specifically, the proliferation and survival of β-cells was dependent on paracrine signaling from the neighboring vascular network. In this study, DEAB ALDH[lo] cell transplantation increased islet number and not size. Therefore, we suggest the modest reduction of hyperglycemia was likely a result of increasing the number of endogenous islets capable of releasing insulin into systemic circulation. We propose that DEAB ALDH^{lo} cells likely provided unidentified supportive stimuli to surviving islets following STZ-induced β-cell ablation. Nonetheless, identification of these stimuli will require future proteomic studies using cell populations with more robust and consistent islet regenerative function *in vivo*.

In summary, we provide preliminary evidence that expanding ALDH^{hi} cells while retaining islet regenerative function is complex and the loss of islet regenerative function is likely multifactorial. Specifically, we have identified several important findings that may benefit future research aiming to expand HPC *ex vivo* for therapeutic applications. These include results such as the following: (1) FACS purification of UCB Lin− MNC based on ALDH-activity does not enrich for megakaryocytes, (2) inhibition of RA-production generates multipotent ALDH^{hi} cells *in vitro*, and (3) retainment of a primitive ALDH[hi] phenotype does not coincide with islet regenerative function following intrapancreatic transplantation. Collectively, these results indicate that cellular therapies using expanded HPC to accelerate endogenous islet regeneration require further studies to prevent the loss of islet proliferative and vascularizing function.
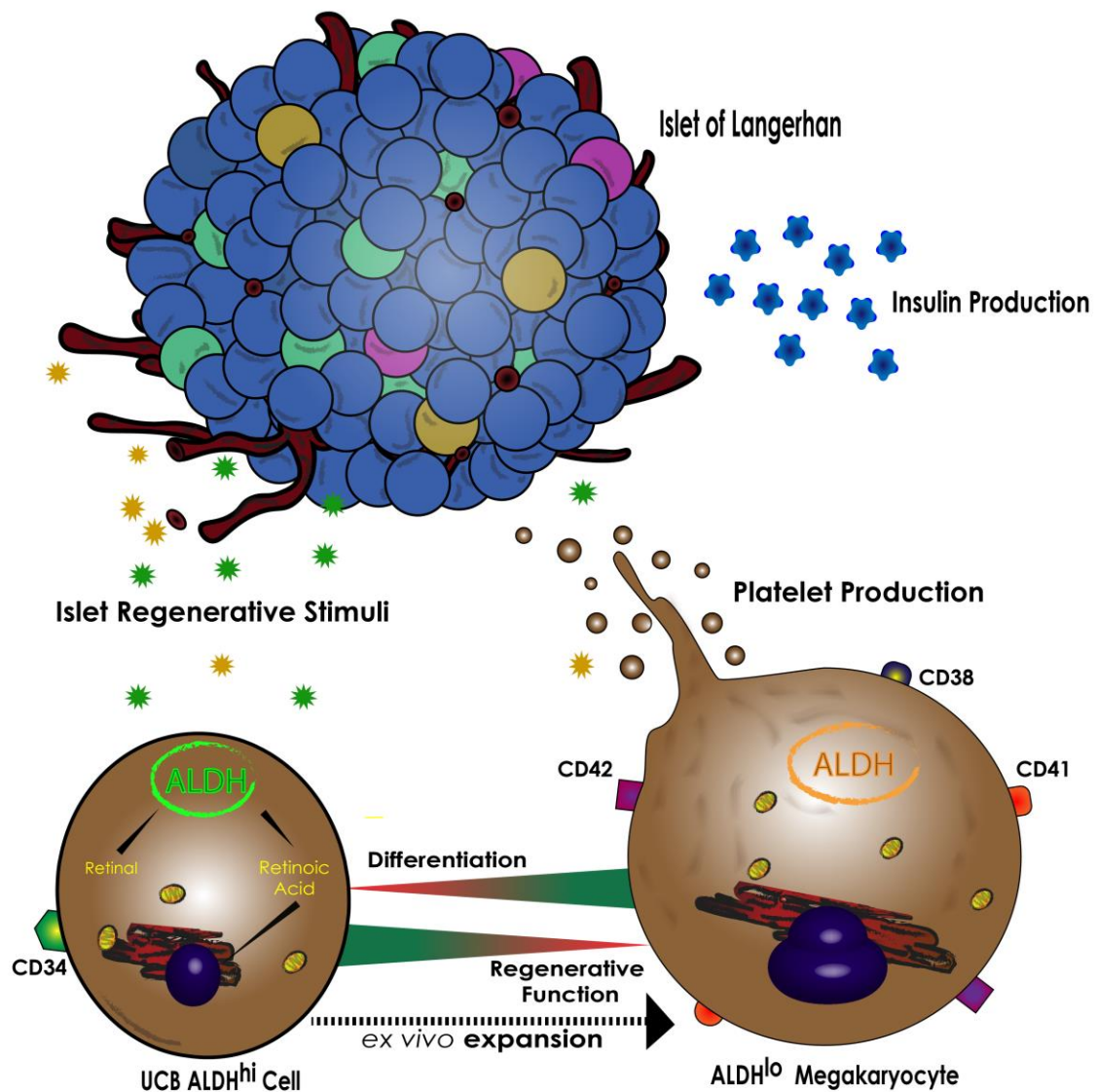
Figure 3.7 UCB Lin- ALDH^{hi} cells acquire megakaryocyte phenotype during expansion that coincide with reduced islet regenerative function. UCB ALDH^{hi} cells efficiently expand under serum-free conditions; however, UCB ALDH^{hi} cells will rapidly lose an ALDH^{hi} phenotype and acquire a committed megakaryocyte phenotype. The differentiation of UCB ALDH^{hi} cells coincides with the loss of islet regenerative function.

3.5 References

1   Atlas, I. D. 1-145 (Brussels, Belgium 2018).

2   Association, A. D. Diagnosis and classification of diabetes mellitus. *Diabetes care* **33**, S62-S69 (2010).

3   Alberti, K. G. M. M. & Zimmet, P. f. Definition, diagnosis and classification of diabetes mellitus and its complications. Part 1: diagnosis and classification of diabetes mellitus. Provisional report of a WHO consultation. *Diabetic medicine* **15**, 539-553 (1998).

4   Razavi, R. *et al.* Diabetes enhances the proliferation of adult pancreatic multipotent progenitor cells and biases their differentiation to more β-cell production. *Diabetes* **64**, 1311-1323 (2015).

5   Meier, J., Bhushan, A., Butler, A., Rizza, R. & Butler, P. Sustained beta cell apoptosis in patients with long-standing type 1 diabetes: indirect evidence for islet regeneration? *Diabetologia* **48**, 2221-2228 (2005).

6   Nir, T., Melton, D. A. & Dor, Y. Recovery from diabetes in mice by β cell regeneration. *The Journal of clinical investigation* **117**, 2553-2561 (2007).

7   Limbert, C., Päth, G., Jakob, F. & Seufert, J. Beta-cell replacement and regeneration: Strategies of cell-based therapy for type 1 diabetes mellitus. *Diabetes research and clinical practice* **79**, 389-399 (2008).

8   Shapiro, A. J. *et al.* Islet transplantation in seven patients with type 1 diabetes mellitus using a glucocorticoid-free immunosuppressive regimen. *New England Journal of Medicine* **343**, 230-238 (2000).

9   D'addio, F. *et al.* Autologous nonmyeloablative hematopoietic stem cell transplantation in new-onset type 1 diabetes: a multicenter analysis. *Diabetes* **63**, 3041-3046 (2014).

10   Keenan, H. A. *et al.* Residual insulin production and pancreatic β-cell turnover after 50 years of diabetes: Joslin Medalist Study. *Diabetes* **59**, 2846-2853 (2010).

11   Bell, G., Putman, D., Hughes-Large, J. & Hess, D. Intrapancreatic delivery of human umbilical cord blood aldehyde dehydrogenase-producing cells promotes islet regeneration. *Diabetologia* **55**, 1755-1760 (2012).

12   Hess, D. *et al.* Bone marrow–derived stem cells initiate pancreatic regeneration. *Nature biotechnology* **21**, 763 (2003).

13   Elgamal, R. M., Bell, G. I., Krause, S. C. & Hess, D. A. BMS 493 Modulates Retinoic Acid-Induced Differentiation During Expansion of Human Hematopoietic Progenitor Cells for Islet Regeneration. *Stem cells and development* **27**, 1062-1075 (2018).

14   Kuljanin, M., Bell, G. I., Sherman, S. E., Lajoie, G. A. & Hess, D. A. Proteomic characterisation reveals active Wnt-signalling by human multipotent stromal cells as a key regulator of beta cell survival and proliferation. *Diabetologia* **60**, 1987-1998 (2017).

15   Zhao, Y. *et al.* Platelet-derived mitochondria display embryonic stem cell markers and improve pancreatic islet β-cell function in humans. *Stem cells translational medicine* **6**, 1684-1697 (2017).

16   Loomans, C. J. *et al.* Endothelial progenitor cell dysfunction: a novel concept in the pathogenesis of vascular complications of type 1 diabetes. *Diabetes* **53**, 195-199 (2004).

17   Hess, D. A. & Hegele, R. A. Linking diabetes with oxidative stress, adipokines, and impaired endothelial precursor cell function. *Canadian Journal of Cardiology* **28**, 629-630 (2012).

18   Giugliano, D., Ceriello, A. & Paolisso, G. Oxidative stress and diabetic vascular complications. *Diabetes care* **19**, 257-267 (1996).

19   Fadini, G. P., Ciciliot, S. & Albiero, M. Concise review: perspectives and clinical implications of bone marrow and circulating stem cell defects in diabetes. *Stem Cells* **35**, 106-116 (2017).

20   Putman, D. M., Liu, K. Y., Broughton, H. C., Bell, G. I. & Hess, D. A. Umbilical cord blood-derived aldehyde dehydrogenase-expressing progenitor cells promote recovery from acute ischemic injury. *Stem cells* **30**, 2248-2260 (2012).

21   Putman, D. M. *et al.* Expansion of umbilical cord blood aldehyde dehydrogenase expressing cells generates myeloid progenitor cells that stimulate limb revascularization. *Stem cells translational medicine* **6**, 1607-1619 (2017).

22   Cooper, T. T. *et al.* Inhibition of Aldehyde Dehydrogenase-Activity Expands Multipotent Myeloid Progenitor Cells with Vascular Regenerative Function. *Stem Cells* **36**, 723-736 (2018).

23   Seneviratne, A. K. *et al.* Expanded hematopoietic progenitor cells reselected for high aldehyde dehydrogenase activity demonstrate islet regenerative functions. *Stem Cells* **34**, 873-887 (2016).

24   Rhinn, M. & Dollé, P. Retinoic acid signalling during development. *Development* **139**, 843-858 (2012).

25   Gudas, L. J. in *Seminars in cell & developmental biology.* 701-705 (Elsevier).

26   Ghiaur, G. *et al.* Regulation of human hematopoietic stem cell self-renewal by the microenvironment's control of retinoic acid signaling. *Proceedings of the National Academy of Sciences* **110**, 16121-16126 (2013).

27   Drach, J. *et al.* Retinoic acid-induced expression of CD38 antigen in myeloid cells is mediated through retinoic acid receptor-α. *Cancer Research* **54**, 1746-1752 (1994).

28   Hess, D. A. *et al.* Functional characterization of highly purified human hematopoietic repopulating cells isolated according to aldehyde dehydrogenase activity. *Blood* **104**, 1648-1655 (2004).

29   Pierre-Louis, O. *et al.* Dual SP/ALDH functionalities refine the human hematopoietic Lin− CD34+ CD38− stem/progenitor cell compartment. *Stem cells* **27**, 2552-2562 (2009).

30   Gentry, T. *et al.* Isolation of early hematopoietic cells, including megakaryocyte progenitors, in the ALDH-bright cell population of cryopreserved, banked UC blood. *Cytotherapy* **9**, 569-576 (2007).

31   Slayton, W. B. *et al.* Developmental differences in megakaryocyte maturation are determined by the microenvironment. *Stem cells* **23**, 1400-1408 (2005).

32   KAUFMAN, R. M., AIRO, R., POLLACK, S. & CROSBY, W. H. Circulating megakaryocytes and platelet release in the lung. *Blood* **26**, 720-731 (1965).

33   Klimchenko, O. *et al.* A common bipotent progenitor generates the erythroid and megakaryocyte lineages in embryonic stem cell–derived primitive hematopoiesis. *Blood* **114**, 1506-1517 (2009).

34   Han, P., Guo, X.-H. & Story, C. Enhanced expansion and maturation of megakaryocytic progenitors by fibronectin. *Cytotherapy* **4**, 277-283 (2002).

35   Hurley, R. W., McCarthy, J. B. & Verfaillie, C. M. Direct adhesion to bone marrow stroma via fibronectin receptors inhibits hematopoietic progenitor proliferation. *The Journal of clinical investigation* **96**, 511-519 (1995).

36   Li, K., Yang, M., Lam, A. C., Yau, F. W. & Yuen, P. M. P. Effects of flt-3 ligand in combination with TPO on the expansion of megakaryocytic progenitors. *Cell transplantation* **9**, 125-131 (2000).

37   Li, J. *et al.* Aldehyde dehydrogenase 1 activity in the developing human pancreas modulates retinoic acid signalling in mediating islet differentiation and survival. *Diabetologia* **57**, 754-764 (2014).

38   Storms, R. W. *et al.* Distinct hematopoietic progenitor compartments are delineated by the expression of aldehyde dehydrogenase and CD34. *Blood* **106**, 95-102 (2005).

39   Storms, R. W. *et al.* Isolation of primitive human hematopoietic progenitors on the basis of aldehyde dehydrogenase activity. *Proceedings of the National Academy of Sciences* **96**, 9118-9123 (1999).

40   Johansson, M., Mattsson, G. r., Andersson, A., Jansson, L. & Carlsson, P.-O. Islet endothelial cells and pancreatic β-cell proliferation: studies in vitro and during pregnancy in adult rats. *Endocrinology* **147**, 2315-2324 (2006).

41   Johansson, Å. *et al.* Endothelial cell signalling supports pancreatic beta cell function in the rat. *Diabetologia* **52**, 2385-2394 (2009).

42   Brissova, M. *et al.* Pancreatic islet production of vascular endothelial growth factor-a is essential for islet vascularization, revascularization, and function. *Diabetes* **55**, 2974-2985 (2006).

Chapter 4

4   The Proteome of Human Pancreas-derived Multipotent
     Stromal Cells Restricts Adipogenesis, Drives Cell Division
     and Defines a Unique Surface Marker Profile

4.1   Introduction

Since initial clinical use for cellular therapy in 1995, human multipotent stromal cells (MSC) has been used in over 400 clinical trials reported by the US National Institutes of Health (http://www.clinicaltrial.gov/), a reflection of the diverse therapeutic potential of MSC [1]. Specifically, MSC have demonstrated beneficial therapeutic characteristics including proangiogenic, immunomodulatory, and tissue-regenerative functions after transplantation in an diverse array of pre-clinical studies and clinical applications. Unfortunately, MSC possess phenotypic and functional characteristics modified by selective culture conditions *in vitro*. The absence of a unique molecular fingerprint has led to establishment of heterogenous MSC populations as a result of different tissue sources, isolation protocols, and culture techniques [2-4].

In a collective effort to unify the field, the International Society of Cellular Therapies (ISCT) established a set of minimal criteria that MSC must demonstrate: 1) growth after plastic adherence, 2) a surface marker profile during culture that distinguishes MSC from related mesodermal cell lineages (i.e. hematopoietic and endothelial), and (3) mesodermal multipotency into bone, cartilage and adipose tissue *in vitro* [5]. Specifically, MSC must express stromal cell markers CD90 (Thy-1), CD73 (Ecto-5'-nucleotidase), and CD105 (Endoglin) during culture; and lack the expression of CD45, CD31, CD14, HLA-DR, CD19, CD79a and CD34. However, several studies have reported conflicting heterogeneity regarding proposed surface markers expression [6].

Cultured MSC are dynamically heterogenous and can be segregated into distinct subsets based on surface marker expression [7,8], enzymatic activity [9] and/or multipotency

in vitro [10]. The use of various adult and fetal sources has amplified the complexity of a standardized MSC-identity generating tissue-specific MSC populations with unique phenotypic, molecular, and functional characteristics *in vitro*. For example, MSC isolated from bone-marrow (BM) express higher levels of CD146 and alkaline phosphatase compared to placental-derived MSC; which reflected inherent transcriptional and epigenetic differences resulting in enhanced osteogenic potential of BM-MSC *in vitro* [10]. Intracellular markers such as vimentin have been utilized to identify MSC populations *in vitro and in vivo* [11], however comparative levels of vimentin and surface marker expression between MSC and progeny prevent culture-independent isolation of pure MSC populations. Considering MSC are the precursors to ECM-modeling fibroblasts and vessel stabilizing pericytes *in vivo*, a hierarchy of MSC identity an function, akin to the hematopoietic system, likely exists *in vitro*.

Bone marrow-derived MSC (BM-MSC) is arguably the most widely utilized MSC populations *in vitro* and *in vivo*, however a limited number of in-depth proteomic and functional comparisons between MSC populations from distinct tissue microenvironments have been reported. This has limited our understanding of molecular and functional diversity across MSC derived from various tissue sources. Therefore, insightful experimentation, such as global proteomic characterization, are warranted to obtain a foundation of knowledge to support the identification of MSC with robust scalability, reduced heterogeneity, and biotherapeutic potential. Herein, we consider BM-MSC the "gold-standard" of therapeutic MSC populations and utilize the phenotypic and molecular fingerprint of BM-MSC to characterize a previously understudied human pancreas-derived MSC population [12-14]. To our knowledge, this is the first in-depth proteomic characterization of human (Pancreas-derived) Panc-MSC combined with multiparametric flow cytometry and functional testing in comparison to BM-MSC. Specifically, we revealed unique phenotypic, molecular, and functional characteristics of Panc-MSC, such as accelerated growth kinetics and restricted adipogenic potential. Overall, this study provides novel insights into MSC population that has been previously understudied for applications of stem cell biology and regenerative medicine.

4.2   Methods

4.2.1   MSC Culture, Expansion and Growth Dynamics

BM-MSC Establishment:

Human BM aspirates were obtained from healthy donors with informed consent from the London Health Sciences Centre (London, ON). BM-MSC were established as previously described [9].

Panc-MSC Establishment:

Ricordi-chamber isolated human islets were obtained through the Integrated Islet Distribution Program (IIDP, USA). 200 islet equivalents were plated in RPMI 1640 + 10% FBS for up to 7 days. Between days 5-7, adherent fibroblast-like cells were separated from non-adherent islets by media aspiration followed by trypzination and filtration using a 40μm cell strainer. Single cell suspensions were subsequently reseeded on tissue culture plastic at 4,000 cells/cm^2 and expanded in Amniomax-C100^{TM} with Amniomax^{TM} E100 Supplement (Life Technologies).

MSC Culture and Growth Dynamics:

Panc-MSC and BM-MSC were utilized for experimentation between passage 2-4. In order to investigate the growth dynamics of Panc-MSC and BM-MSC, manual hemocytometer counts were performed every 24 hours over a 96-hour period.

Microenvironmental Stiffness:

To determine how microenvironmental stiffness (kPa) affects the phenotype or adipogenic potential of MSC, 24-well silicone-based soft substrate plates coated with fibronectin were used to culture MSC under growth or adipogenic conditions (see below).

Specifically, MSC were seeded on substrates at 2, 10, 30, 100 kPA stiffness (ExCellness, Switzerland).

4.2.2   Flow Cytometry

Panc-MSC and BM-MSC were stained with anti-human antibodies for MSC markers (CD73, CD105, CD90; BD Biosciences), hematopoietic markers (CD34, CD14, CD45, CD133; BD Biosciences), endothelial marker CD31 (BD Biosciences), and the pericyte marker CD146 (BD Biosciences). MSC were also co-stained with Aldeflour^{TM} (Stem Cell Technologies) reagent to determine ALDH-activity and cell viability was assessed by co-staining with 7-amino-actinomycin D (7AAD; 5μl; BD Biosciences). Additionally, MSC were stained using antibodies for α-SMA, vimentin, adiponectin, STRO-1, and HLA-DR (BD Biosciences). Adiponectin and α-SMA (AbCam) were detected using anti-mouse or anti-rabbit Cy5 secondary antibody (BD Biosciences), respectively. Neural lineage markers TUBB3, MBP, and GFAP (AbCam) were also measured on cultured MSC and detected using an anti-mouse FITC secondary antibody (Vector). Data was acquired using a LSRII flow cytometer at the London Regional Flow Cytometry Facility. All data was analyzed using FloJo software (v8.2).

4.2.3   Immunohistochemistry and Immunofluorescent Analyses

MSC were cultured on glass coverslips until 60% confluency was achieved. MSC were washed twice with PBS prior to fixation with 10% formalin and permeabilization with 0.1% Triton X-100. Coverslips were stained with hematoxylin and eosin, rinsed with deionized water and embedded in an aqueous mounting media. Additional coverslips were co-stained with PE-conjugated anti-human CD146 (BD Biosciences) and primary rabbit anti-human ALDH1A1 (1:500, AbCam) detected by a goat anti-rabbit FITC secondary antibody (1:200, Vector). Additional coverslips were co-stained with APC-conjugated anti-human STRO-1, PE-conjugated anti-human vimentin (BD-Biosciences) and BV421-conjugated anti-human HLA-DR antibodies. Immunofluorescent images were counterstained with DAPI (1:1000) or DRAQ5. Colorimetric images were acquired

at 40x using an Olympus (BX50) and confocal images were acquired under oil-immersion at 40x and 63x using a Leica TCS SP8.

4.2.4   Determination of Mesodermal Multipotency

Adipogenesis Differentiation Assay:

MSC were seeded at a density of 1 x 10^4 cells/cm^2 in supplemented Amniomax C100 for 24 hours. Media was replaced with Complete Adipogenesis Differentiation Medium with Adipogenesis Supplement (Life Technologies). Complete media changes occurred every 3 days. After 10 days, MSC were stained for lipid accumulation using Oil Red O (Sigma).

Osteogenesis Differentiation Assay:

MSC were seeded at a density of 5 x 10^3 cells/cm^2 in Amniomax C100 + supplement for 24 hours. Media was replaced with Complete Osteogenesis Differentiation Medium with Osteogenesis Supplement (Life Technologies). Media was changed every 3 days. After 21 days, MSC were stained for calcium deposits using Alzarian Red (VWR).

Chondrogenesis Differentiation Assay Protocol:

MSC were seeded as 5μl micro-masses at a density of 2 x 10^4 cells/μl in Amniomax C100 + supplement for 2 hours. Media was replaced with Complete Chondrogenesis Differentiation Medium with Chondrogenesis Supplement (Life Technologies). Media was changed every 3 days. After 21 days, chondrocyte pellets were embedded and OCT and cryosectioned prior to staining glycosaminoglycans using Alcian Blue (Sigma).

4.2.5   Label-free Mass Spectrometry

Lysate protein was subjected to 1D SDS-PAGE fractionation using 12% gels. All MS data was collected using a Q Exactive Plus Orbitrap (ThermoFisher Scientific, Waltham, MA, USA), as previously described[15]. Full MS parameters are outlined in the Supplementary Table 1. Data analysis was performed using PeaksStudio 7.5 and MaxQuant 1.5.2.8.

4.2.6   RT-qPCR Analysis

RNA was collected using RNAeasy purification kit (Qiagen) and quantified using the Nanodrop ND-100 Spectrophotometer at the London Regional Genomics Center at Robarts Research Institute. RNA was converted to 1µg of cDNA per sample using the iScriptTM cDNA Synthesis Kit (Bio-Rad, London, Canada) on the Eppendorf Master Cycler (Thermo Fisher). cDNA was stored at -80ºC. RT-qPCR was performed using the SSofast kit (Bio-rad) along with primers *ALDH1A1* (Cat#HQP005075), *ALDH1A3* (Cat#HQP005252), MCAM (Cat#HQP011099) and housekeeping gene, *GUSB* (Cat#HQP008583) from GeneCopoeia. Information regarding, *PPARG, CEBPA, LPL* primers used for adipogenesis studies are listed in Table 4. 1. The relative quantification of mRNA was acquired using the CFX96 Real-Time PCR Detection System.

Table 4.1 Primer for Adipogenesis RT-qPCR Analyses

Full Name/ Gene Name	Primer Sequences
Peroxisome Proliferator-activated Receptor Gamma/*PPARG*	FWD: TTCAGAAATGCCTTGCAGTG REV: CCAACAGCTTCTCCTTCTCG
CCAAT/enhancer-binding Protein Alpha/*CEBPA*	FWD: CAGAGGGACCGGAGTTATGA REV: TTCACATTGCACAAGGCACT
Lipoprotein Lipase/*LPL*	FWD: GTCCGTGGCTACCTGTCATT REV:TGGCACCCAACTCTCATACA

4.2.7   Statistical Analyses

The majority of statistical analyses were performed by unpaired student's t-test between BM- and Panc-MSC. Phenotypic analyses during culture on soft substrates were analyzed using repeated measures one-way ANOVA with post-hoc Tukey's t-test. Outliers were identified using Grubb's test; $p<0.05$.

4.3   Results

4.3.1   Panc-MSC robustly expand *ex vivo* and express a classical MSC-like phenotype.

We have recently reported that the secretome of human BM-MSC stimulated human β-cell proliferation *in vitro* [15]. During these studies we observed emergence of fibroblast-like cells that formed colonies adherent to plastic from islets cultured with media supplemented with FBS or MSC-generated CM. Fibroblast-like cells were subcultured into supplemented AmnioMax C-100 media and compared to BM-MSC for phenotypic, functional, and molecular characteristics. Herein, we refer to this cell population as pancreatic-MSC (Panc-MSC).

After colony establishment, Panc-MSC were adherent to tissue culture plastic (TCP) and demonstrated spindle-like morphology (Supplemental Figure 1A), albeit the size (forward-scatter area) of Panc-MSC was smaller than BM-MSC (Supplemental Figure 1B). Panc-MSC underwent robust expansion across several passages under typical BM-MSC growth conditions in AmnioMax C-100. Notably, when each MSC subtype were seeded at an equal density between passages 2-4, Panc-MSC demonstrated a 2-fold increase (*$p<0.05$) in cell growth kinetics over 4 days compared to BM-MSC, (Figure 1A). Panc-MSC also expressed classical MSC surface markers, including CD73, CD105, and CD90 (Figure 1B-C). Importantly, Panc-MSC did not express surface markers of the endothelial (CD31, or PECAM-1) or hematopoietic (CD45, pan-leukocyte) lineages (Figure 1D-E). Overall, Panc-MSC demonstrated a classical MSC phenotype and robust growth kinetics in plastic adherent culture.

4.3.2   The multipotency of Panc-MSC is skewed away from adipogenesis.

BM-MSC harbor tri-lineage differentiation potential under pro-differentiation culture conditions *in vitro* [5]. Panc-MSC were found to efficiently undergo chondrogenesis and osteogenesis marked by the positive identification of glycoprotein (Alcian Blue) and

calcium deposition (Alazarian Red), respectively (Figure 1F). Compared to BM-MSC, the capacity of Panc-MSC to make adipocytes was restricted, albeit lipid droplet formation was consistently detected across all Panc-MSC cell lines. We performed transcriptional analysis of adipogenesis-associated mRNA transcripts Peroxisome Proliferator-activated Receptor Gamma (PPARγ; PPARG), CCAAT/enhancer-binding protein α (CEBPα; *CEBPA*), and Lipoprotein Lipase (*LPL)* 10 days after induction in differentiative adipogenic media (Figure 1G) and compared to mRNA expression levels to MSC harvested before induction. Interestingly, BM-MSC robustly increased transcription of PPARγ, CEBP∝, and LPL mRNA (15.8±6.52, 172.6±142.1, 4549.0±3072.0 fold-increase, respectively); whereas transcriptional adipogenic induction was significantly lower in Panc-MSC (1.27±0.29, 0.71±0.33, 2.30±1.44 fold-increase, respectively; *p<0.05). Furthermore, the frequency of adiponectin+ cells, detected by flow cytometry, generated from Panc-MSC was significantly reduced compared to BM-MSC (4.40±1.43 versus 22.47±5.02 % of MSC, *p<0.05; Figure 1H). Thus, Panc-MSC demonstrated mesodermal multipotency with robust osteogenic and chondrogenic potential; however, adipogenesis was transcriptionally and functionally restricted in response to pro-adipogenic stimuli.
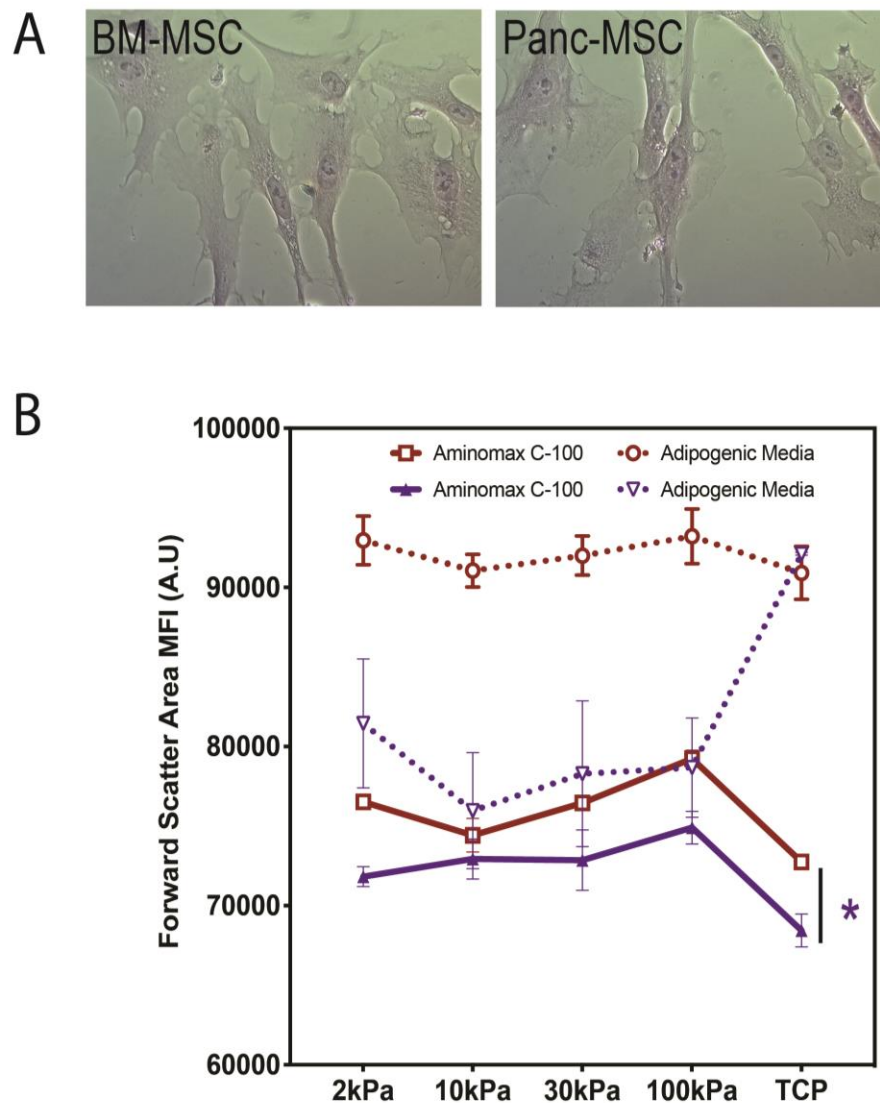
Figure 4.1 Panc-MSC demonstrate spindle-like morphology and decreased forward scatter area compared to BM-MSC. (A) Representative photomicrographs of BM-MSC and Panc-MSC stained with hematoxylin and eosin. (B) Panc-MSC are significantly smaller than BM-MSC under MSC-growth conditions or under adipogenic conditions as microenvironmental stiffness is decreased, measured by forward scatter area. Data represented as Mean $\pm$ SEM (*$p<0.05$; N=3). Statistical analyses were determined by Student's t-test.
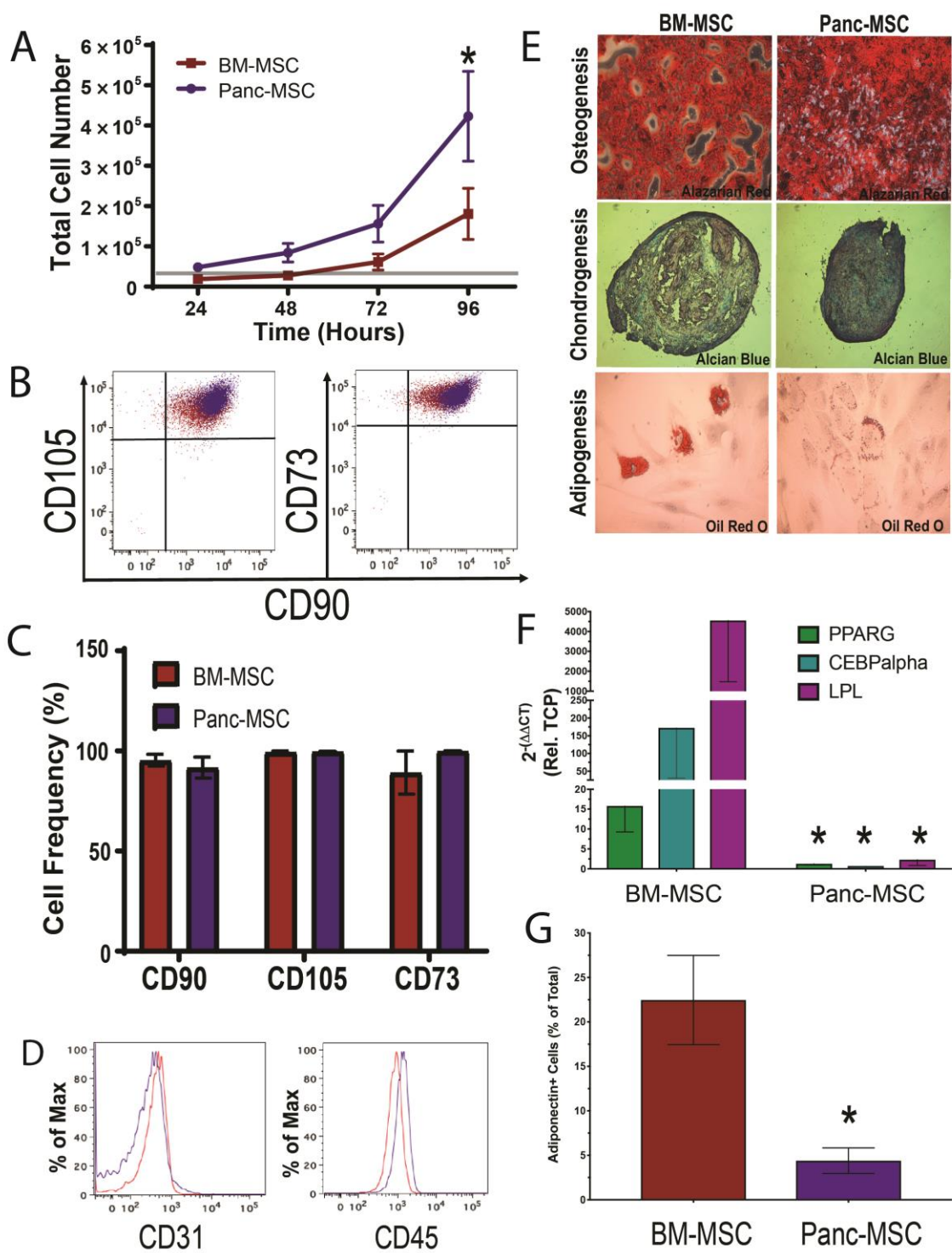
Figure 4.2 Panc-MSC demonstrated robust growth kinetics, classical MSC surface marker expression and restricted adipogenic potential. (A). Panc-MSC demonstrated robust cell expansion kinetics *in vitro* and generated increased cell number after 96 hours *in vitro*, compared to BM-MSC. (B-C) Representative flow cytometry plots showing comparable expression (>95%) of CD73, CD90, and CD105 in BM-MSC and Panc-MSC. (D) Panc-MSC did not express endothelial or endothelial (CD31) or hematopoietic (CD45) lineage markers, respectively. (E) Panc-MSC demonstrated osteogenic and chondrogenic differentiation *in vitro*; however, adipogenic differentiation was qualitatively less pronounced than observed in BM-MSC. (F) BM-MSC robustly increased transcription of *PPARG*, *CEBPA*, and *LPL* following adipogenic induction for 14 days. In contrast, Panc-MSC demonstrated a minimal increase of adipogenesis-related transcriptional targets after adipogenic induction. β-glucuronidase (GUSB) was used as a housekeeping gene. (G) The frequency of Panc-MSC acquiring adiponectin expression after adipogenic induction was ~5-fold less than BM-MSC. Data represented as Mean ± SEM (*p<0.05; n=3-5). Statistical analyses were determined by unpaired Student's t-test**.**
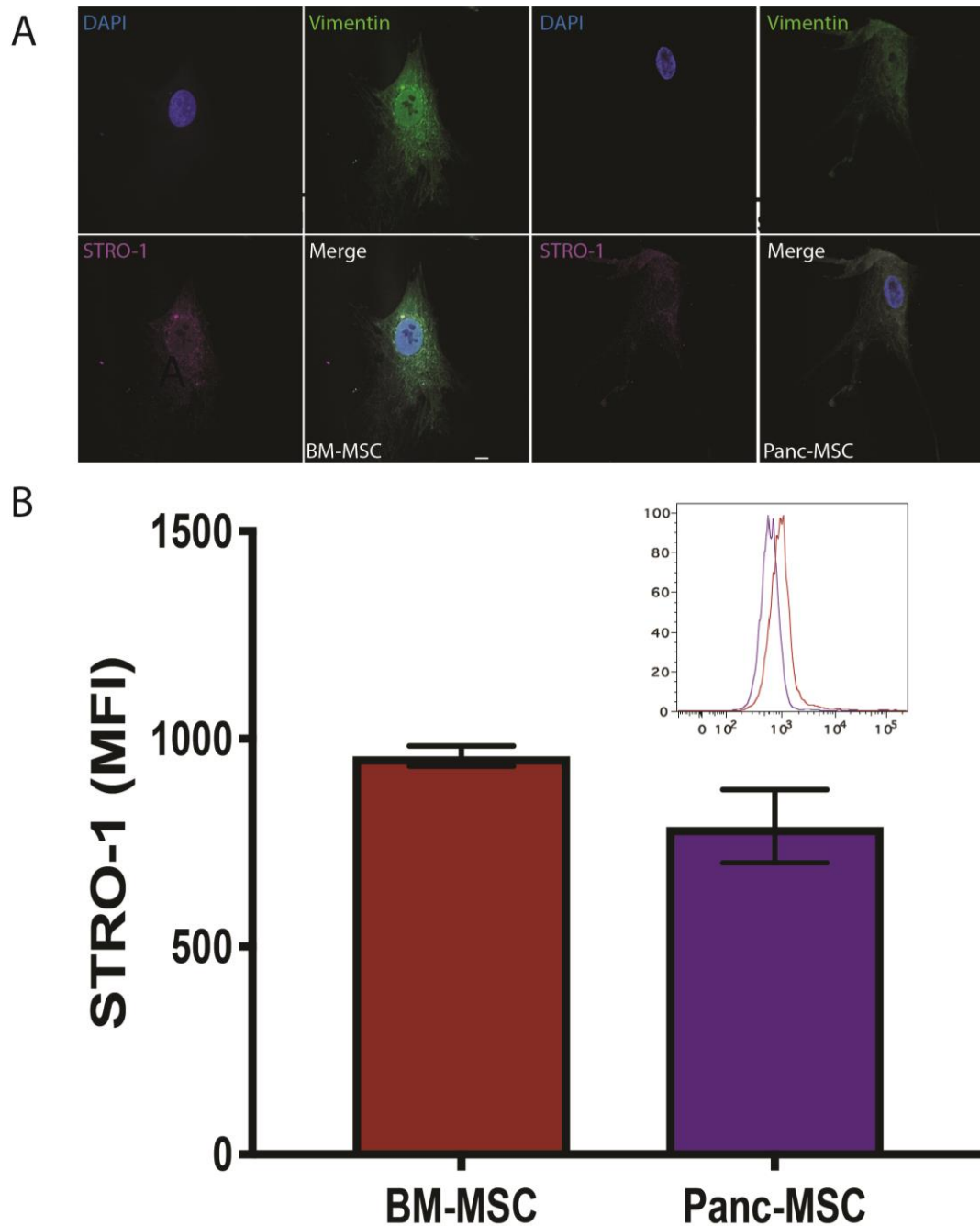
Figure 4.3 Panc-MSC exhibit comparable STRO-1 membrane-surface expression compared to BM-MSC. (A) Representative confocal images of vimentin and STRO-1 expression by BM-MSC and Panc-MSC. (B) Representative flow cytometry plots (insert) demonstrated comparable expression of STRO-1 between Panc-MSC and BM-MSC, measured by MFI. Data represented as Mean ± SEM (*p<0.05; N=3). Statistical analyses were determined by Student's t-test.

4.3.3   Selection of 500 highest expressed proteins generates a unique fingerprint for Panc-MSC.

Proteomic technologies provide a unique opportunity to characterize global protein content between related cell types. Using label-free mass spectrometry, we identified >7500 unique proteins in the proteome of both BM-MSC or Panc-MSC (Figure 2A). Principle component analyses of the entire dataset generated a unique signature that tightly clustered BM-MSC samples distinct from Panc-MSC samples (Figure 2B). We focused our initial analyses on the top 500 (T-500) identified proteins based on expression intensity (LFQ). Vimentin was the most abundant protein detected in both MSC subtypes and was expressed at comparable levels (BM/Panc; Log_{10} p=1.14, Figure 2C). We additionally detected STRO-1 expression on both BM-MSC and Panc-MSC at comparable expression levels (Supplemental Figure 2A-B). Furthermore, Panther pathway enrichment analysis of the T-500 proteome identified that both MSC-types robustly expressed components of integrin signaling (P00034), including ITGB1 and ITGA1 (Figure 2D-E). Moreover, both MSC-types produced several secreted ECM molecules at comparable levels, although fibronectin-1 (FN1) expression was significantly increased in BM-MSC (**p>0.01; Figure 2F). Human Gene Atlas enrichment analysis suggested the T-500 proteome of both MSC sub-type was statistically comparable to smooth muscle cells, reflected by high expression of α-SMA (Figure 2G). On the other hand, BM-MSC were determined to harbor a T-500 proteome that was statistically more comparable to adipocytes (*p<0.05), suggesting a distinct propensity of BM-MSC to generate cells of the adipocyte lineage compared to Panc-MSC.

Next, we identified differential expressed proteins in the T-500 proteome comparing BM and Panc-MSC (Figure 2H). As previously mentioned, expression proteins associated with lipid metabolism such as Acetyl-CoA Acyltransferase 2 (ACAA2), Aldo-Keto Reductase Family 1 Member C2 (ARK1C1), or Hydroxysteroid 17-B Dehydrogenase 4 (HSD17B4) were significantly increased in BM-MSC compared to Panc-MSC. Conversely, Panc-MSC showed increased expression of the proliferation marker Ki67 (MKI67), progenitor cell marker nestin (NES) and intermediate filament

keratin 18 (KRT18). Collectively, these proteomic fingerprints established a unique protein expression signature distinguishing each MSC sub-types that correlated with key functional distinctions including growth kinetics and adipogenic potential.
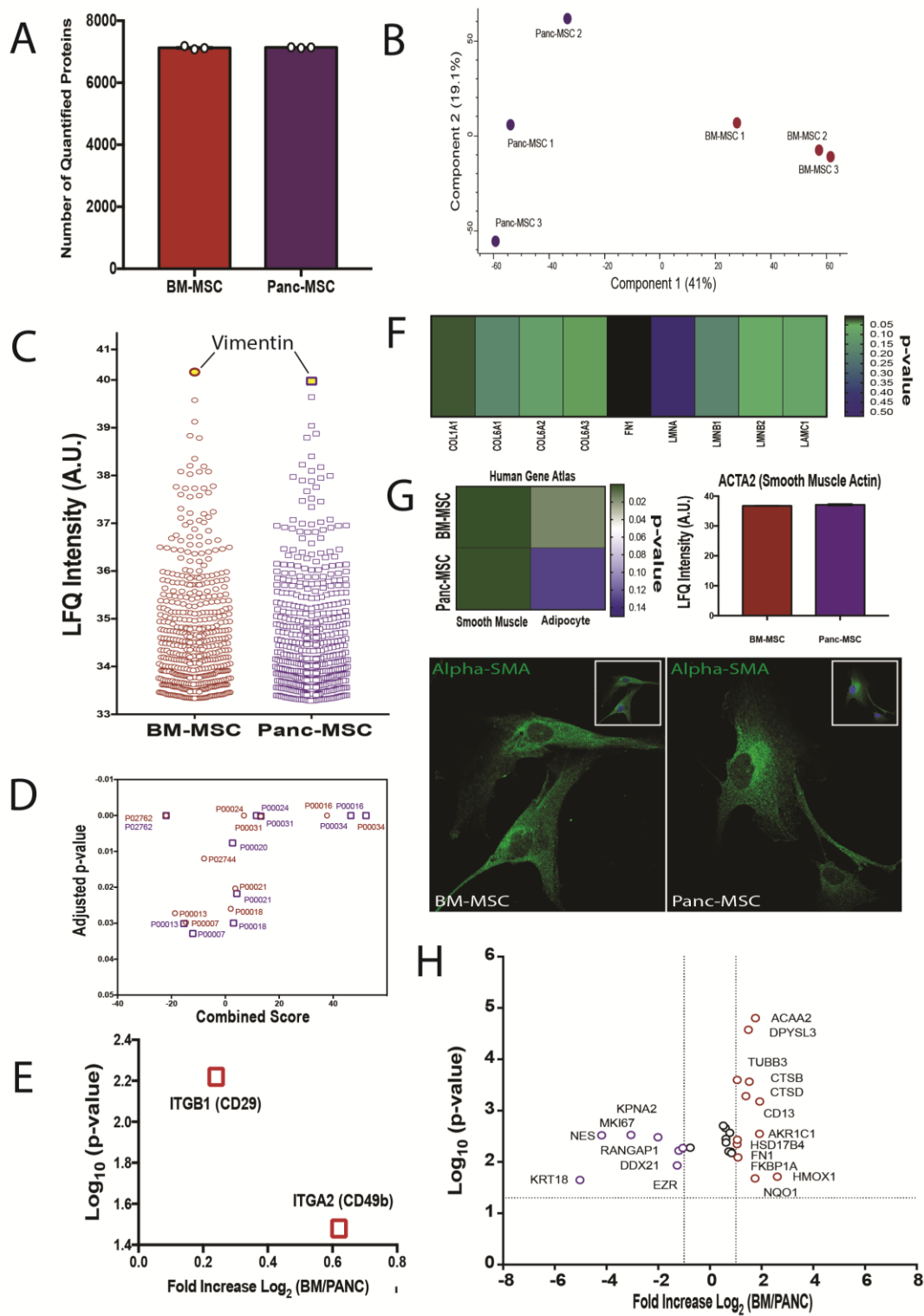
Figure 4.4 Label-free mass spectrometry reveals unique proteomic signatures comparing Panc-MSC and BM-MSC. (A) >7500 unique proteins were identified in the proteome of MSC subtypes. (B) PCA analysis demonstrated the unique proteomes of BM-MSC and Panc-MSC. (C) Top 500 proteins based on LFQ intensities identified vimentin as the most highly expressed protein in both MSC populations. (D) Top 500 proteins were matched to Panther Pathway enrichment annotations and revealed a significant enrichment of integrin signaling components (P00034), (E) including the expression of ITGB1 and ITGA2 in both MSC sub-types. (F) Extracellular matrix proteins were comparably expressed between MSC subtypes, with the exception of FN1 with increased expression in BM-MSC. (G) Human Gene Atlas enrichment analyses determined the BM-MSC proteome was comparable to adipocytes, whereas both MSC populations showed similarities to smooth muscle cells with comparable expression of alpha-SMA. Representative confocal photomicrographs of alpha-SMA expression in BM- and Panc-MSC. (H) Out of the top 500 proteins, 8 proteins were upregulated in Panc-MSC, including Nestin (NES), Ki67 (MKI67) and cytokeratin 18 (CK18). Selected enrichment annotations contained >3 protein hits with p-value cutoff of $p < 0.01$ and minimal overlap of 1.5-fold. Data represented as Mean ± SEM (N=3).

4.3.4 Panc-MSC demonstrate accelerated competency to pro-neurogenic stimuli.

To further investigate the relevance of elevated Nestin expression in Panc-MSC, we determined whether additional neural-lineage markers were detected by mass spectrometry that fell below our initial T-500 cut-off. Surprisingly, we identified 15 additional proteins, expressed in Panc-MSC, associated with the neural lineage (Figure 3A). This included markers of neurons (Tubulin 3, TUBB3), oligodendrocytes (Myelin Binding Protein, MBP) and astrocytes (Glial Fibrillary Acidic Protein, GFAP). GFAP and MBP were detected at comparable levels within both MSC-types, however detection of TUBB3 was increased 2-fold in BM-MSC. Flow cytometry validated the expression of TUBB3, MBP, and GFAP in both MSC subtypes cultured under MSC-expansion conditions (Figure 3B).

To assess the competency of Panc-MSC to respond to pro-neurogenic stimuli *in vitro*, MSC were cultured in Neurocult media for up to 10 days. Compared to maintenance in AmnioMax C-100 media, both MSC populations significantly increased expression of TUBB3, MBP, and GFAP after 10 days of culture in Neurocult media, measured by flow cytometry. Interestingly, Panc-MSC showed significantly elevated TUBB3 and GFAP expression within 4-days culture in Neurocult (Figure 3C-E). However, the frequency of cells expressing TUBB3 or GFAP remained high when BM or Panc-MSC were cultured in either MSC-growth media (AmnioMax C-100) or Neurocult (Figure 3F). In contrast, the frequency of MBP$^+$ MSC was significantly increased when ether MSC subtype was cultured in pro-neurogenic media (**$p<0.01$). Collectively, these results confirmed both MSC populations expressed neural-lineage markers; albeit, Panc-MSC were initially more competent to pro-neural stimuli compared to BM-MSC.
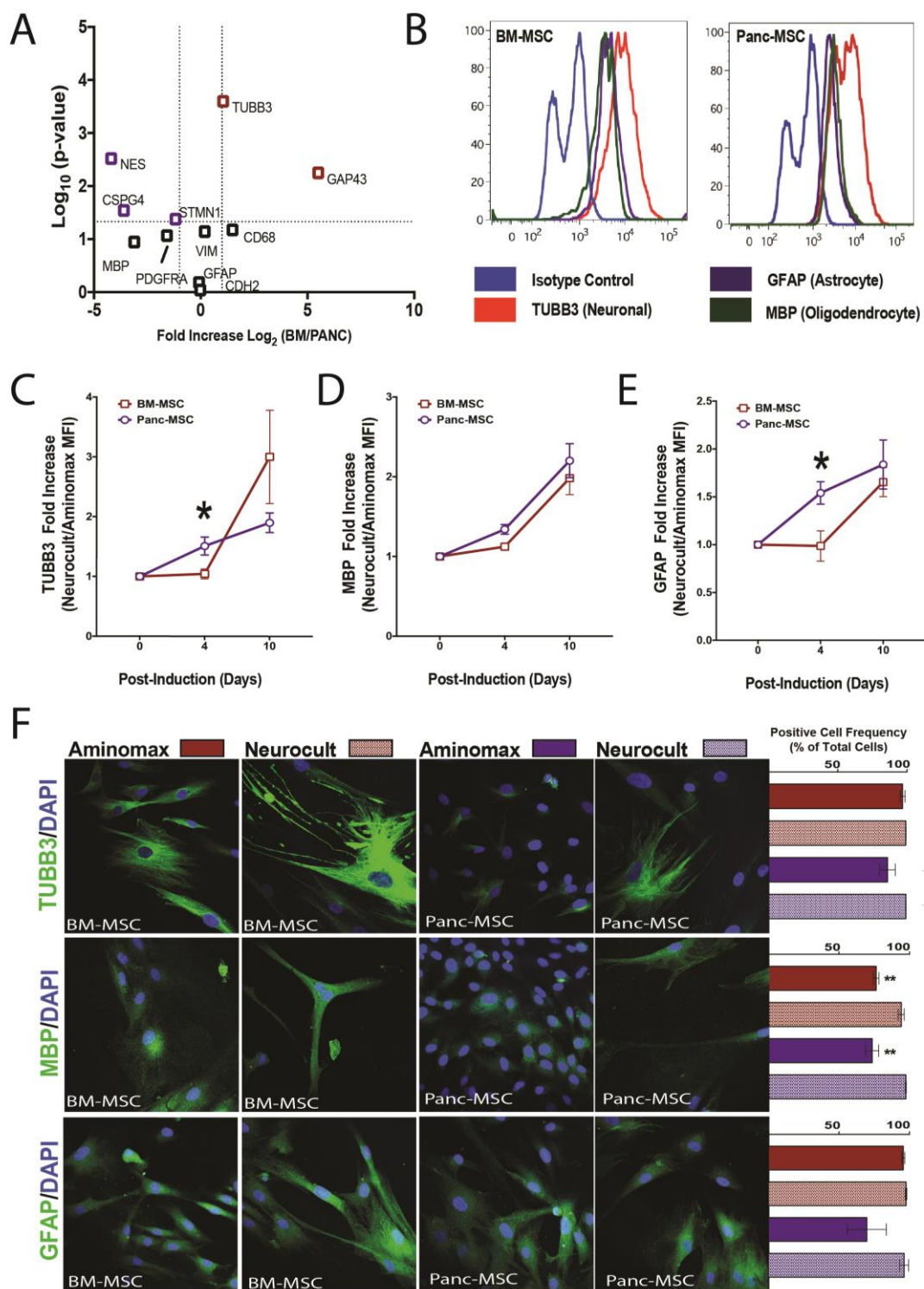
Figure 4.5 Panc-MSC express neural-lineage markers and respond to neurogenic stimuli. (A) Volcano plot of neural lineage-associated proteins expressed within Panc- and BM-MSC. (B) Representative flow cytometry plots validate the expression of neural-lineage markers Tubulin-3/TUBB3 (neuron), Myelin Binding Protein/MBP (oligodendrocyte) and Glial Fibrillary Acidic Protein/ GFAP (astrocyte) during culture in Aminomax C-100. After culture in Neurocult, Panc-MSC increased expression of (C) TUBB3, (D) MBP and (E) GFAP between 4 – 10 days post-induction. (F) Representative confocal photomicrographs of TUBB3, MBP, and GFAP expression in BM- and Panc-MSC cultured in Aminomax or Neurocult at 10 days. Bar graphs demonstrate the frequency of cells positive for TUBB3, MBP, or GFAP under each condition. Expression was measured by geometrical mean fluorescence intensity (MFI) and normalized to expression levels of MSC cultured in Aminomax C-100. Data represented as Mean ± SEM (n=3). Statistical analyses were determined by unpaired Student's t-test.

4.3.5   Panc-MSC upregulate cell-cycle proteins driving cellular division while BM-MSC upregulated proteins associated with lipid metabolism.

Differential protein expression between MSC populations may translate to functional characteristics [10]. Accordingly, Panc-MSC demonstrated unique functional characteristics compared to BM-MSC, including increased growth kinetics and restricted adipogenic competency. Our mass spectrometry analyses identified 483 and 383 significantly upregulated in BM-MSC and Panc-MSC, respectively (Figure 4A). Pathway enrichment analysis on differentially expressed proteins was performed using Gene Ontology (GO) pathway, and Reactome (R-HSA) annotations, uncovered distinguishable molecular signatures when comparing the BM- and Panc-MSC populations (Figure 4B). Notably, BM-MSC upregulated proteins involved in the metabolism of lipids (R-HSA-556833, Figure 4C), whereas Panc-MSC upregulated proteins involved in the control of cell cycle and mitosis (R-HSA-1640170, Figure 4D). More specifically, BM-MSC also upregulated proteins with small molecule biosynthetic functions, including members of retinoic-acid signaling pathways such as ALDH1A3, ALDH2, and STRA6 (Figure 4E). On the other hand, Panc-MSC upregulated proteins associated with cell cycle complexes; including origin of replication components such as ORC2/6, MCM2/5, GMNN, CCNB1 (Figure 4F). Collectively, Panc-MSC and BM-MSC demonstrated protein expression signatures that drive distinctive cellular functions such as cell division and lipid metabolism, respectively.
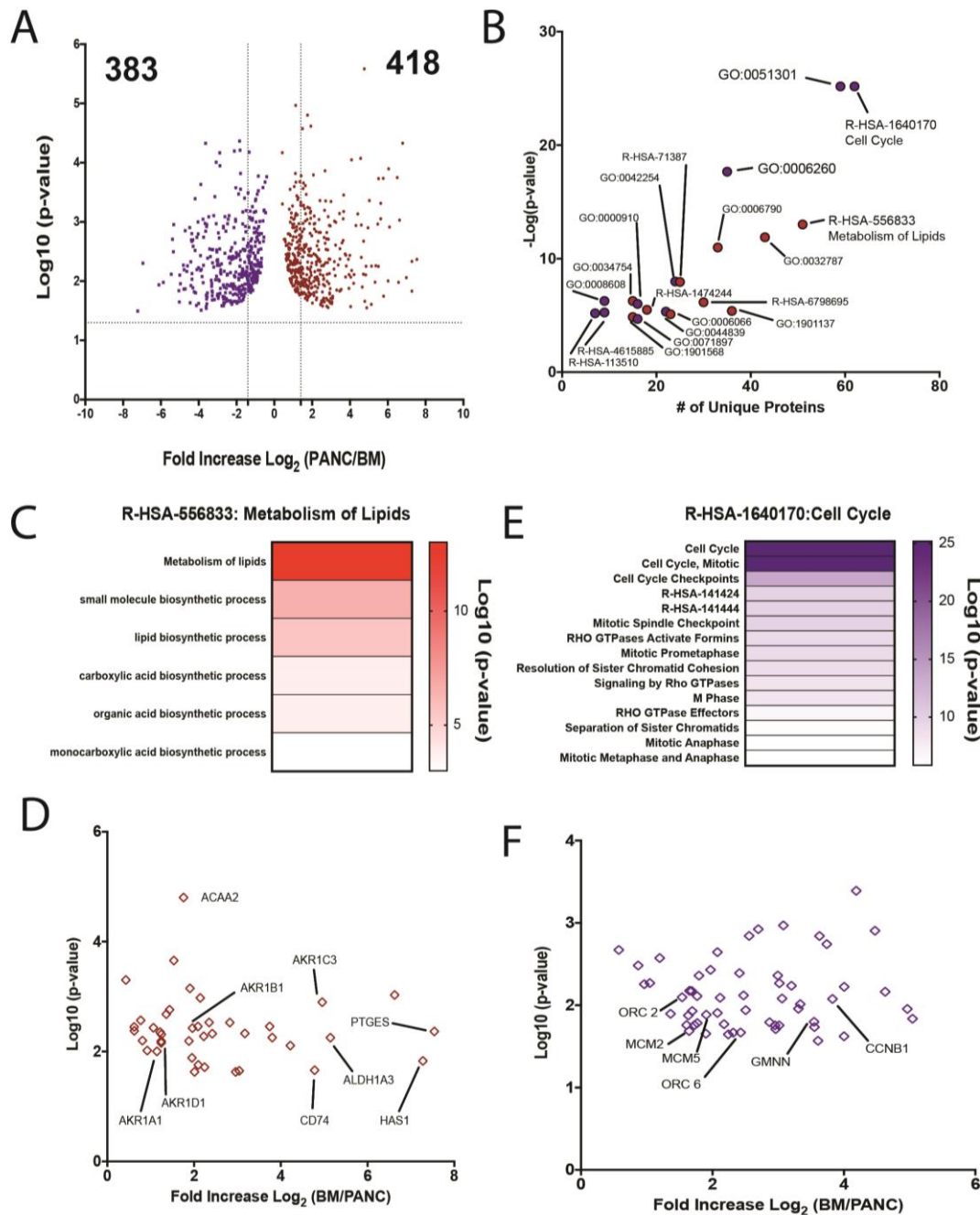
Figure 4.6 Panc-MSC proteome was enriched for cell cycle proteins and BM-MSC proteome was enriched for proteins involved with lipid metabolism. (A) Volcano plot of 418 and 383 proteins significantly increased in the proteome of Panc-MSC (purple dots) and BM-MSC (red dots), respectively. Upregulated proteins from BM-MSC and Panc-MSC were matched to GO- pathway, Reactome, and BioCarta enrichment annotations. (B) 10 annotations with smallest adjusted p-values from each cell-type were plotted against the number of unique proteins identified within each annotation. (C) Proteins upregulated in BM-MSC were strongly associated with the metabolism of lipids annotation (R-HSA-556833), which included small molecule biosynthetic pathways (i.e. retinoic acid production, ALDH1A3). In contrast, (D) Panc-MSC upregulated proteins associated with cell cycle annotation (R-HSA-1640170), specifically with (F) mitotic function. Selected enrichment annotations contained >3 protein hits with p-value cutoff of 0.01 and minimal overlap of 1.5-fold. N=3, p<0.05.

4.3.6 Panc-MSC and BM-MSC share common phenotypic proteins, however each harbour distinct expression levels and unique surface protein expression.

It is well established that cultured human MSC classically express surface markers including CD73, CD105, CD90, however, cell surface marker expression selective for tissue specific MSC subtypes is much less well established. We directly compared surface marker expression of both Panc-MSC and BM-MSC using mass spectrometry. In addition to classical MSC surface marker expression, we identified an additional 64 CD surface markers with similar expression levels in both MSC populations, validated by flow cytometry (i.e. CD109) using both MSC subtypes (Figure 5A). 15 CD-markers were differentially expressed (Figure 5B). Specifically, Panc-MSC showed upregulated expression of 7 surface markers, including CD142, CD9, CD168, CD55, CD166, CD97, and CD49d (Figure 5B). In contrast, BM-MSC showed upregulated expression of 8 surface markers including CD63, CD74, CD146, CD318, CD297, CD230, CD304, and CD276 (Figure 5B). Interestingly, our mass spectrometry and flow cytometry analyses identified the expression of CD14 and HLA-DR (Figure 5C), previously reported to be absent from plasma membrane of MSC. Specifically, 6 isoforms of HLA-DR were upregulated in the proteome of BM-MSC (Figure 5D-E), albeit only HLA-DRA was significantly elevated compared to Panc-MSC. Collectively, these results validated that Panc-MSC possessed a unique surface marker profile compared to BM-MSC.

A

CD14	CD51	CD82	CD107a/b	CD155	CD249	CD325	CD340
CD18	CD54	CD87	CD108	CD156b/c	CD262	CD339	CD362
CD29	CD56	CD88	CD109	CD157	CD264		
CD36	CD58	CD90	CD120a	CD172a	CD266		
CD44	CD59	CD91	CD130	CD200	CD273		
CD47	CD63	CD92	CD138	CD201	CD274		
CD49a	CD68	CD95	CD140a/b	CD217	CD280		
CD49b	CD71	CD98	CD147	CD222	CD298		
CD49e	CD73	CD99	CD148	CD239	CD315		
CD49f	CD81	CD105	CD151	CD248	CD317		

CD109

B

Fold Increase Log$_2$ (PANC/BM)

C

CD14

HLA-DR

D

Fold Increase Log$_2$ (BM/PANC)

E

Figure 4.7 Panc-MSC demonstrate a unique CD marker expression profile compared to BM-MSC. (A) 67 CD markers were detected by label-free mass spectrometry that showed comparable expression levels on both Panc- and BM-MSC. Validated detected of CD109 using flow cytometry. (B) Volcano plot of CD markers significantly upregulated in Panc-MSC (i.e. CD9) and BM-MSC (i.e. CD146). (C) Expression of CD14 and HLA-DR surface expression was validated by flow cytometry compared to isotype control (green line). (D-E) Several isoforms of HLA-DR were upregulated by BM-MSC, compared to Panc-MSC. Horizontal dashed line is representative of $p<0.05$. N=3

4.3.7 Panc-MSC exhibit dampened CD146 expression and retinoic acid-signaling.

We sought to further investigate the phenotypic profile of Panc-MSC compared to BM-MSC generated using label-free mass spectrometry. We determined pericyte marker (CD146) expression was reduced at the level of protein translation (25.60 ± 11.19 versus 76.25 ± 4.02 % of MSC, $*p<0.05$; Figure 5A-B) and mRNA transcription (0.53 ± 0.05 fold-increase, $*p<0.05$; Figure 5C) in Panc-MSC compared to BM-MSC, respectively. Furthermore, Panc-MSC expressed dampened levels of ALDH-activity (7.58 ± 2.54 versus 54.2 ± 9.51 % of MSC, $*p<0.05$; Figure 6A,6D), measured by cytoplasmic Aldefluor accumulation. Aldefluor is reduced to a cell-impermeable product primarily by several ALDH family members, which was confirmed at both the level of ALDH1A3 mRNA transcription (0.34 ± 0.15 fold-increase, $*p<0.05$; Figure 6C) and ALDH1A3 protein expression (Figure 4E) in Panc-MSC. Interestingly, Panc-MSC had elevated ALDH1A1 mRNA transcription (59.54 ± 37.13 fold-increase, $*p<0.05$; Figure 5C) that was detected in the proteome (Figure 6E). Furthermore, mass spectrometry detected differential expression of several components and/or targets of the retinoic acid signaling pathway (Figure 6F-G). In addition to increased ALDH-activity, we identified an increased detection of increased detection of retinol transporter (STRA6), alcohol dehydrogenase (RDH11), and regulators of retinoic signaling (i.e. DGAT1, DHRS3) in BM-MSC. Collectively, a mosaic of phenotype differences, such as dampened CD146 expression and retinoic acid-signaling pathways, can distinguish Panc-MSC from BM-MSC *in vitro*.
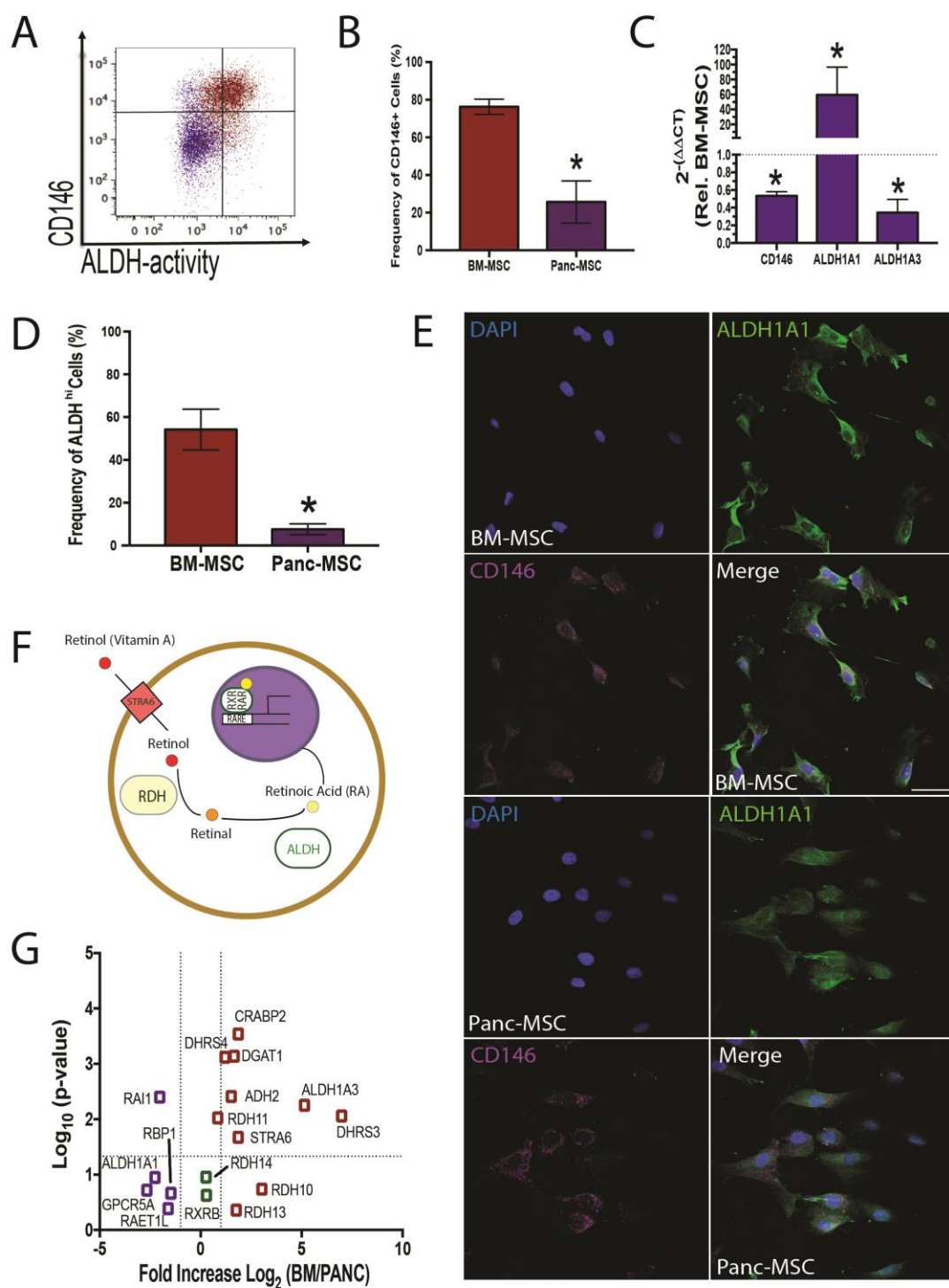
Figure 4.8 Panc-MSC exhibit reduced expression of pericyte marker CD146 and reduced aldehyde dehydrogenase-activity. (A) Representative flow cytometry plots for BM-MSC (red) or Panc-MSC (purple) co-stained for pericyte marker CD146 and cytosolic ALDH-activity. (B) Compared to BM-MSC, Panc-MSC demonstrated reduced expression of pericyte marker CD146, and (C) reduced *MSAM* (CD146) mRNA expression. Panc-MSC also demonstrated increased expression of ALDH1A1 mRNA, however ALDH1A3 mRNA expression was reduced compared to BM-MSC. β-glucuronidase (GUSB) was used as a housekeeping gene. (D) Panc-MSC demonstrated (D) reduced ALDH-activity by flow cytometry. (E) CD146 and ALDH1A protein expression was confirmed in BM- and Panc-MSC by confocal microscopy. Immunofluorescent images were acquired under 40x oil-immersion, scale bar = 20μm. (F) Schematic highlighting retinoic acid signaling pathway components with (G) differential expression in BM-MSC. Data represented as Mean ± SEM (*p<0.05; N=3-5). Statistical analyses were determined by Student's t-test.

4.3.8 Adipogenic potential of Panc- and BM-MSC is independent of microenvironment stiffness.

We sought to further investigate functionally relevant phenotypic differences between Panc-MSC compared to BM-MSC generated using label-free mass spectrometry. Pericyte marker (CD146) expression was reduced at the level of protein translation (25.60 ± 11.1 versus 76.25 ± 4.02 % in Panc- versus BM-MSC, $*p<0.05$; Figure 6A-B) and mRNA expression (0.53 ± 0.05 fold difference in Panc- versus BM-MSC, $*p<0.05$; Figure 6C). Panc-MSC also demonstrated a reduced frequency of cells with high ALDH-activity (7.58 ± 2.54 versus 54.2 ± 9.51 % of cells, $*p<0.05$; Figure 6A,6D), measured by flow cytometric assessment of Aldefluor^{TM} accumulation. Aldefluor^{TM} reagent is reduced to a cell-impermeable product primarily by several cytosolic ALDH isoforms, primarily ALDH1A family members. ALDH1A3 mRNA expression (0.34 ± 0.15 fold difference in Panc- versus BM-MSC, $*p<0.05$; Figure 6C) and ALDH1A protein expression (Figure 6E) was decreased in Panc-MSC. Interestingly, Panc-MSC demonstrated elevated ALDH1A1 mRNA expression (59.54 ± 37.13 fold-increase, $*p<0.05$; Figure 6C). Indeed, our mass spectrometry data confirmed differential expression of several components of the retinoic acid signaling pathway (Figure 6F-G). In addition to increased ALDH1A3 expression in BM-MSC, we identified an increased expression of retinol transporter (STRA6), retinol dehydrogenase 11 (RDH11), alcohol dehydrogenase 2 (ADH2), cellular retinoic acid binding protein 2 (CRABP2), and other regulators of retinoic signaling (i.e. DGAT1, DHRS3) in BM-MSC. Collectively, a mosaic of phenotype differences, such as reduced pericyte marker CD146 expression and retinoic acid-signaling, can distinguish Panc-MSC from BM-MSC *in vitro*.
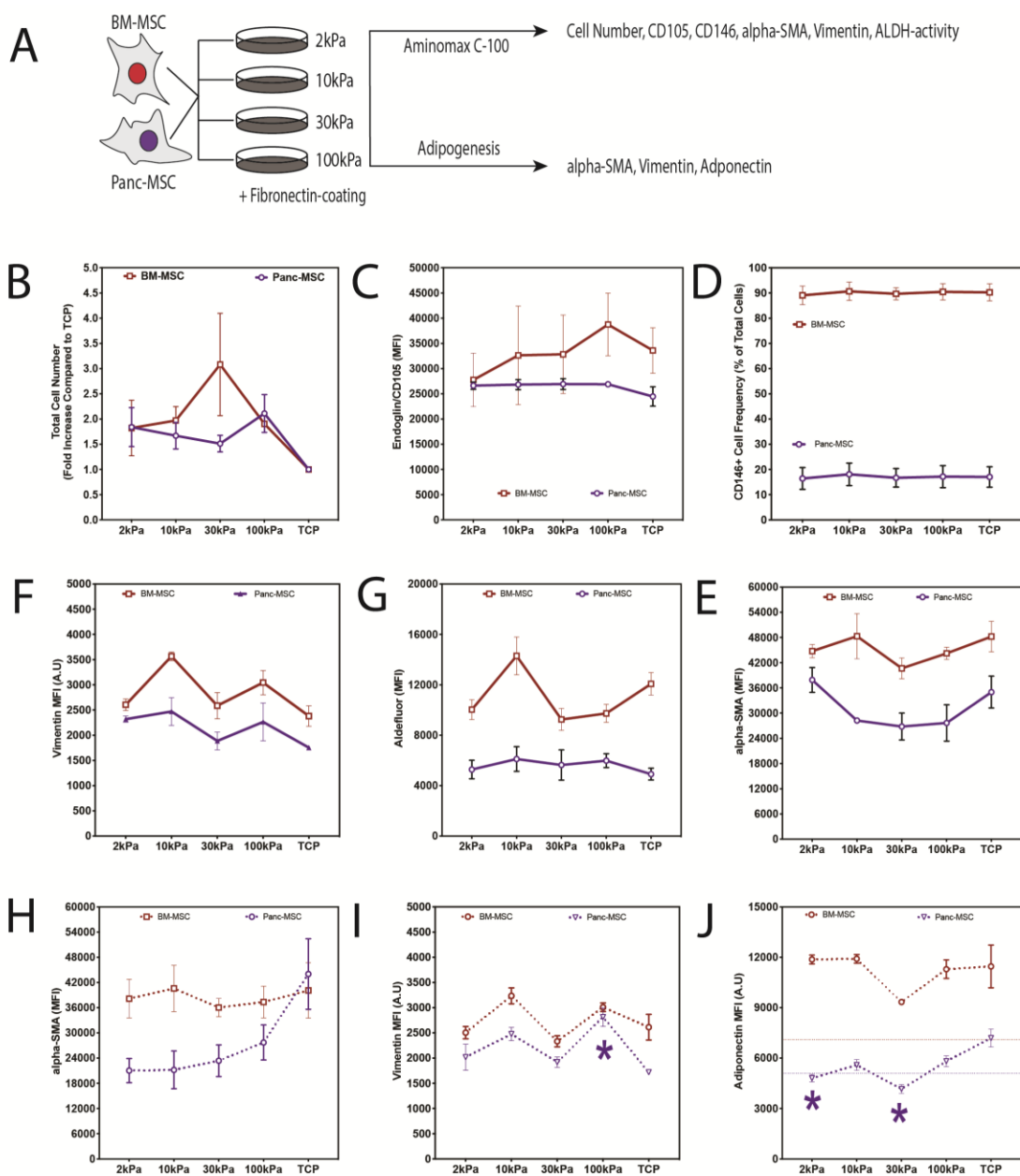
Figure 4.9 Soft culture stiffness increased growth kinetics but did not enhance adipogenic differentiation in BM- or Panc-MSC. (A) A schematic briefly describing MSC culture on substrates with a range of Young's Modulus (2-100kpa) in MSC-growth (solid line) or pro-adipogenic media (dashed line). (B) Both MSC subtypes generated greater cell numbers after 5 days expansion culture on soft substrate compared to TCP. (C) CD105 or (D) CD146 or (E) vimentin expression was not altered when MSC were cultured on softer substrates compared to TCP. Similarly, (F) the frequency of cells with high ALDH-activity was not changed when MSC were cultured on softer substrates, compared to TCP. (G) ∝-SMA expression was not altered by expansion of either MSC subtype on soft substrates. (H-J) In response to adipogenic stimuli, Panc-MSC cultured on softer substrates reduced (H) ∝-SMA expression compared to TCP, whereas (I) vimentin expression was increased in Panc-MSC cultured on 10kPa or 100kPa. Although BM-MSC were capable of robust adipocyte formation quantified by adiponectin expression (MFI), Panc-MSC cultured on soft substrates remained resistant to adipogenic differentiation *in vitro*. Horizontal dashed lines represent MFI of adiponectin in BM-MSC or Panc-MSC cultured under expansion conditions in Amniomax™ media. Data represented as Mean ± SEM (*p<0.05; N=3-5). Statistical analyses were determined by repeated measures one-way Anova with post-Hoc Tukey's t-test, comparing MSC subtypes across varying substrate stiffness.

4.4 Discussion

This study employed label-free mass spectrometry and multiparametric flow cytometry to determine the proteomic and phenotypic profile of human Panc-MSC, a MSC subtype that can be readily isolated from cultured human pancreatic tissue. Using BM-derived MSC as the 'gold standard' for therapeutic MSC, this study provides novel evidence that distinguished Panc-MSC as a tissue-specific MSC population with unique phenotypic, molecular, and functional characteristics *in vitro*. Specifically, Panc-MSC harbour a proteome that drives robust expansion kinetics, defines a surface marker profile with reduced CD146 and ALDH1A3 expression, and increases competency towards pro-neurogenic stimuli. Additionally, Panc-MSC were resistant to adipogenic differentiation, a feature independent of vimentin expression, or decreased ∝-SMA expression in response to decreased microenvironmental stiffness. Collectively, we provide foundational proteomic, phenotypic and functional characterizations *in vitro*, towards a tissue-specific MSC whose therapeutic potential has yet to be determined.

The prospective purification of MSC from human tissues has been complicated by the lack of a selective cell surface marker expression [4] that permits efficient purification of MSC. As a result, MSC cultures are highly heterogeneous due to dependence on clonogenic expansion using selective media(s) and autonomous adherence to TCP dependent on adhesion protein expression and ECM deposition [17]. Accordingly, Panc-MSC readily adhered to TCP and our proteomic analyses demonstrated diverse integrin expression accompanied by robust ECM production. Integrins detected on Panc-MSC were expressed at comparable levels to BM-MSC, albeit integrin α-4 (CD49d) was upregulated in Panc-MSC. Integrins heterodimers play a vital role in cell migration, survival, and proliferation through the prorogation of intracellular signaling networks [17-19]. We did not directly assess the functional relevance of integrin expression in this study. Regardless, Panc-MSC exhibited accelerated growth kinetics *in vitro* compared to BM-MSC. Further studies are warranted to elucidate the functional roles of integrin expression and ECM molecule deposition in the coordination of pro-mitotic signaling in Panc-MSC.

To elucidate phenotypic characteristics that distinguish MSC subtypes from different tissue sources, we investigated differential CD-marker expression between Panc-MSC and BM-MSC. Both MSC subtypes highly expressed cell surface markers CD73, CD90, and CD105; and were devoid of CD45 and CD31 expression. These characteristics satisfy the minimal criteria to identify MSC colony formation adherent to plastic, however our proteomic detection of cell surface marker expression conflicted with the current ISCT guidelines [5], which suggest that MSC should be devoid of CD14 and HLA-DR expression. Here, we validated expression of CD14 on both MSC subtypes and elevated HLA-DR expression on BM-MSC. These results and previous reports [6,20,21], demonstrate highly sensitive proteomic approaches are required to establish surface marker expression within heterogeneous MSC populations. Nonetheless, Panc-MSC and BM-MSC demonstrated mesodermal multipotency, vimentin and α-SMA expression, and STRO-1 surface marker expression [22,23]. Additionally, 64 CD-markers were detected at comparable levels between Panc-MSC and BM-MSC, suggesting that a uniform phenotype between tissue-specific MSC likely exists. Conversely, we demonstrated differential expression of 15 CD-markers, whose functional roles on MSC remain undetermined. For example, CD9 is a multifunctional tetraspanin family member that is upregulated in Panc-MSC. Halfon *et al*. previously reported CD9 was enriched on the surface of fibroblasts compared to BM-MSC and was upregulated on BM-MSC with extended culture [24]. On the other hand, we observed increased expression of the pericyte marker CD146 on BM-MSC. Nestin+/CD146+ MSC have been shown to maintain hematopoietic stem cell pools in the perivascular niche of bone marrow [25] and purification of CD146+ cells from several human tissue sources can enrich for MSC colony forming cells [26]. However, the functional relevance of CD146 expression on MSC *in vitro* remains undetermined. Collectively, we have reported a unique surface "fingerprint" for Panc-MSC that reflects a different tissue source of origin. Thus, future studies are warranted to elucidate the functional roles of CD-markers identified in this study.

Directed differentiation of MSC *in vitro* is currently the standard assay for assessing progenitor cell multipotency, yet these assays remain primarily reliant on qualitative histology. Accordingly, Panc-MSC demonstrated robust osteogenic and

chondrogenic potential *in vitro*, however adipogenic potential was notably restricted with Panc-MSC showing small lipid-droplet formation and infrequent Oil Red O staining. We build upon these qualitative observations to demonstrate adipogenesis was quantitatively restricted in Panc-MSC at the transcriptional and translational level. Proteomic analysis revealed BM-MSC demonstrated protein expression patterns similar to adipocytes with functions involved in lipid metabolism. Notably, we also detected expression of progenitor cell marker Nestin, in Panc-MSC alongside accelerated response to pro-neurogenic stimuli compared to BM-MSC. It has been proposed that some MSC may arise from non-mesodermal tissues, such as the neural crest [27]. In addition, it has been previously suggested that pancreas-derived MSC may be generated from a ductal epithelial-to-mesenchymal transition initiated by culture *in vitro* [12]. Our proteomic findings support both these hypotheses, as Panc-MSC also highly expressed epithelial cell markers such at KRT18. Conversely, Kubo *et al*. found that KRT18 was transcribed >30-fold higher in BM-MSC [28] compared to fibroblasts, osteoblasts or adipocytes, suggesting a better understanding of the functional relevance in Panc-MSC is warranted. These observations amongst other studies suggest the multipotency of MSC may be tissue-specific and likely entails epigenetic, transcriptional, and translation regulation tightly controlled alongside extrinsic microenvironmental cues. Ultimately, the development of *in vivo* functional testing will be required to further understand the true multipotent potential of MSC.

Pathways activated by lipid metabolites drive cellular functions including tissue patterning, cell division, cell survival, and differentiation [29]. We identified that BM-MSC up-regulated several members of the RA-signaling pathway, including ALDH1A3, ALDH2, STRA6 and RDH10. ALDH-activity has been reported to be differentially expressed by cells with high proliferative capacity, engraftment, and/or multipotency in tissues such as blood, pancreas, or cancer [30,31]. We have previously demonstrated selection of high ALDH-activity can isolate hematopoietic progenitors with multifaceted regenerative functions *in vivo* [30,32]; in addition to enhanced multipotency and growth kinetics *in vitro*. Conversely, BM-MSC with high ALDH-activity did not demonstrate enhanced multipotency but instead generated a pro-angiogenic secretome with pro-vascular functions *in vivo* [9]. Here we report Panc-MSC, with dampened ALDH-activity,

demonstrated accelerated growth kinetics in addition to reduced adipogenic potential. Thus, the functional role of ALDH-activity in Panc-MSC *in vitro* remains elusive and the pro-angiogenic potential of Panc-MSC *in vivo* is currently undetermined.

It is well established that microenvironmental properties *in vitro* can affect MSC functional characteristics; including, lineage-differentiation and surface marker expression [4,16]. Talele *et al*. demonstrated ∝-SMA expression could be linked to microenvironmental stiffness and was upregulated in BM-MSC with reduced adipogenic capacity. In our studies, we observed comparable ∝-SMA expression between BM- and Panc-MSC subtypes with restricted adipogenesis and reduced cell size in Panc-MSC. Similar to Talele we observed reducing ∝-SMA expression when Panc-MSC were cultured on a softer substrate, however adipogenesis was not recovered by Panc-MSC cultured on a microenvironmental stiffness <100kPa. Notably, microenvironmental stiffness appeared to have a minimal impact on CD105, CD146, vimentin expression or ALDH-activity in both BM or Panc-MSC, suggesting alternate control mechanisms may govern the multipotent capacity of MSC *in vitro*.

In summary, we employed label-free mass spectrometry and multiparametric flow cytometry to characterize the proliferative and multipotent functions of Panc-MSC *in vitro*. The foundational knowledge acquired in this study will support our future investigations comparing the regenerative potential of distinct MSC subtypes *in vivo*, a characteristic considered exclusive to MSC populations [33,34]. Moreover, proteomic and functional differences observed in this study would benefit from complementary epigenetic and transcriptional profiling, with specific-focus on RA-signaling pathways, adipogenesis, and the functional role(s) of surface marker expression.

4.5 References

1   Squillaro, T., Peluso, G. & Galderisi, U. Clinical trials with mesenchymal stem cells: an update. *Cell transplantation* **25**, 829-848 (2016).
2   Hass, R., Kasper, C., Böhm, S. & Jacobs, R. Different populations and sources of human mesenchymal stem cells (MSC): a comparison of adult and neonatal tissue-derived MSC. *Cell Communication and Signaling* **9**, 12 (2011).
3   Araújo, A. B. *et al.* Comparison of human mesenchymal stromal cells from four neonatal tissues: amniotic membrane, chorionic membrane, placental decidua and umbilical cord. *Cytotherapy* **19**, 577-585 (2017).
4   Adamzyk, C. *et al.* Different culture media affect proliferation, surface epitope expression, and differentiation of ovine MSC. *Stem cells international* **2013** (2013).
5   Dominici, M. *et al.* Minimal criteria for defining multipotent mesenchymal stromal cells. The International Society for Cellular Therapy position statement. *Cytotherapy* **8**, 315-317 (2006).
6   Pilz, G. A. *et al.* Human mesenchymal stromal cells express CD14 cross-reactive epitopes. *Cytometry Part A* **79**, 635-645 (2011).
7   Battula, V. L. *et al.* Isolation of functionally distinct mesenchymal stem cell subsets using antibodies against CD56, CD271, and mesenchymal stem cell antigen-1. *Haematologica* **94**, 173-184 (2009).
8   Barilani, M. *et al.* Low-affinity Nerve Growth Factor Receptor (CD271) Heterogeneous Expression in Adult and Fetal Mesenchymal Stromal Cells. *Scientific reports* **8**, 9321 (2018).
9   Sherman, S. E. *et al.* High aldehyde dehydrogenase activity identifies a subset of human mesenchymal stromal cells with vascular regenerative potential. *Stem Cells* **35**, 1542-1553 (2017).
10   Pilz, G. A. *et al.* Human term placenta-derived mesenchymal stromal cells are less prone to osteogenic differentiation than bone marrow-derived mesenchymal stromal cells. *Stem cells and development* **20**, 635-646 (2010).
11   Takashima, Y. *et al.* Neuroepithelial cells supply an initial transient wave of MSC differentiation. *Cell* **129**, 1377-1388 (2007).
12   Seeberger, K. L., Eshpeter, A., Rajotte, R. V. & Korbutt, G. S. Epithelial cells within the human pancreas do not coexpress mesenchymal antigens: epithelial–mesenchymal transition is an artifact of cell culture. *Laboratory Investigation* **89**, 110 (2009).
13   Hu, Y. *et al.* Isolation and identification of mesenchymal stem cells from human fetal pancreas. *Journal of Laboratory and Clinical Medicine* **141**, 342-349 (2003).
14   Baertschiger, R. M. *et al.* Mesenchymal stem cells derived from human exocrine pancreas express transcription factors implicated in β-cell development. *Pancreas* **37**, 75-84 (2008).
15   Kuljanin, M., Bell, G. I., Sherman, S. E., Lajoie, G. A. & Hess, D. A. Proteomic characterisation reveals active Wnt-signalling by human multipotent stromal cells as a key regulator of β cell survival and proliferation. *Diabetologia* **60**, 1987-1998 (2017).
16   Talele, N. P., Fradette, J., Davies, J. E., Kapus, A. & Hinz, B. Expression of α-smooth muscle actin determines the fate of mesenchymal stromal cells. *Stem cell reports* **4**, 1016-1030 (2015).
17   Semon, J. A. *et al.* Integrin expression and integrin-mediated adhesion *in vitro* of human multipotent stromal cells (MSCs) to endothelial cells from various blood vessels. *Cell and tissue research* **341**, 147-158 (2010).
18   Kumar, S. & Ponnazhagan, S. Bone homing of mesenchymal stem cells by ectopic α4 integrin expression. *The FASEB Journal* **21**, 3917-3927 (2007).

19 Martino, M. M. *et al.* Controlling integrin specificity and stem cell differentiation in 2D and 3D environments through regulation of fibronectin domain stability. *Biomaterials* **30**, 1089-1097 (2009).

20 Niehage, C. *et al.* The cell surface proteome of human mesenchymal stromal cells. *PloS one* **6**, e20399 (2011).

21 Grau-Vorster, M. *et al.* Levels of IL-17F and IL-33 correlate with HLA-DR activation in clinical-grade human bone marrow–derived multipotent mesenchymal stromal cell expansion cultures. *Cytotherapy* **21**, 32-40 (2019).

22 Carnevale, G. *et al.* Human dental pulp stem cells expressing STRO-1, c-kit and CD34 markers in peripheral nerve regeneration. *Journal of tissue engineering and regenerative medicine* **12**, e774-e785 (2018).

23 Ning, H., Lin, G., Lue, T. F. & Lin, C.-S. Mesenchymal stem cell marker Stro-1 is a 75kd endothelial antigen. *Biochemical and biophysical research communications* **413**, 353-357 (2011).

24 Halfon, S., Abramov, N., Grinblat, B. & Ginis, I. Markers distinguishing mesenchymal stem cells from fibroblasts are downregulated with passaging. *Stem cells and development* **20**, 53-66 (2010).

25 Tormin, A. *et al.* CD146 expression on primary nonhematopoietic bone marrow stem cells is correlated with in situ localization. *Blood* **117**, 5067-5077 (2011).

26 Crisan, M. *et al.* A perivascular origin for mesenchymal stem cells in multiple human organs. *Cell stem cell* **3**, 301-313 (2008).

27 Isern, J. *et al.* The neural crest is a source of mesenchymal stem cells with specialized hematopoietic stem cell niche function. *Elife* **3**, e03696 (2014).

28 Kubo, H. *et al.* Identification of mesenchymal stem cell (MSC)-transcription factors by microarray and knockdown analyses, and signature molecule-marked MSC in bone marrow by immunohistochemistry. *Genes to cells* **14**, 407-424 (2009).

29 de Carvalho Schweich, L. *et al.* All-trans retinoic acid induces mitochondria-mediated apoptosis of human adipose-derived stem cells and affects the balance of the adipogenic differentiation. *Biomedicine & Pharmacotherapy* **96**, 1267-1274 (2017).

30 Cooper, T. T. *et al.* Inhibition of Aldehyde Dehydrogenase-Activity Expands Multipotent Myeloid Progenitor Cells with Vascular Regenerative Function. *Stem Cells* **36**, 723-736 (2018).

31 Rhinn, M. & Dollé, P. Retinoic acid signalling during development. *Development* **139**, 843-858 (2012).

32 Seneviratne, A. K. *et al.* Expanded hematopoietic progenitor cells reselected for high aldehyde dehydrogenase activity demonstrate islet regenerative functions. *Stem Cells* **34**, 873-887 (2016).

33 Caplan, A. I. & Correa, D. The MSC: an injury drugstore. *Cell stem cell* **9**, 11-15 (2011).

34 Caplan, A. I. MSCs: the sentinel and safe-guards of injury. *Journal of cellular physiology* **231**, 1413-1416 (2016).

Chapter 5

5   Human Pancreas-derived Multipotent Stromal Cells Secrete Extracellular Vesicles that Stimulate Microvessel Formation

5.1   Introduction

Human multipotent stromal cells (MSC) have been described as regenerative 'biofactories' or 'sentinals' of the regenerative response [1,2]. However, clinical translation of promising preclinical studies utilizing MSC has not fulfilled expectations [3], due to the transfer of heterogeneous cells showing transient engraftment [4], poor survival and biodistribution [5-7], and/or the loss of pro-regenerative functions after exposure to a diseased or inflamed microenvironment [8-11]. We recently demonstrated bone marrow (BM) MSC may be employed as 'biofactories' *in vitro* to generate a serum-free and cell-free mixture of effectors that stimulate islet regeneration in hyperglycemic mice following intrapancreatic delivery [12,13]. Moreover, pharmaceutical manipulation of BM-MSC *in vitro* successfully tailored a secretome enriched for pro-regenerative stimuli that improved islet regenerative capacity *in vivo*. Collectively, development of cell-free biotherapeutic approaches for regenerative medicine mitigates many of the translational barriers associated with allogeneic MSC transplantation, yet in-depth investigation of the biotherapeutic products secreted by various MSC subtypes are required to better understand and stimulate the regenerative response.

We recently conducted an in-depth proteomic and phenotypic characterization of MSC derived from human pancreatic islet preparations (Panc-MSC) that shared classical MSC characteristics with BM-MSC. Panc-MSC demonstrated reduced aldehyde dehydrogenase (ALDH)-activity and CD146 pericyte marker expression, compared to BM-MSC, suggesting functional differences may exist between tissue specific human MSC subtypes that can be exploited for therapeutic gain. Although identification of a selective cell surface or functional phenotype to distinguish MSC from differentiated progeny has been met with limited success [14]; the capacity for MSC isolated from

different tissues to coordinate complex regenerative processes, such as angiogenesis, may arguably segregate therapeutic MSC from non-therapeutic sources [15]. Because Panc-MSC are derived from healthy islets containing an intricate microvascular network [16], we hypothesized Panc-MSC would possess a vascular supportive or pro-angiogenic secretome.

The secretome generated by MSC contains a complex mixture of regenerative stimuli, in the form of protein, bioactive lipids and nucleic acids that contribute to tissue regeneration *in vivo* [17,18]. Notably, extracellular vesicles (EVs) secreted into the peripheral microenvironment or circulation facilitate the transportation of regenerative stimuli from tissue-specific MSC subtypes to target cells [19-21]. EVs can be subclassified based on their size and cellular-origin; moreover, MSC-derived EVs are phenotypically distinct from apoptotic bodies [22]. Small extracellular vesicles or exosomes (30nm-100nm) are generated through the endosomal pathway and are actively released through exocytosis. In contrast, larger EVs referred to as microparticles (100nm-1µm) are generated by blebbing of the cytoplasm and localized 'pinching' of the plasma membrane, leading to the direct release of microparticles to the surrounding microenvironment or systemic circulation. Despite containing the parent cell cytoplasmic components, EVs are packaged with a unique set of cargo (bioactive proteins, lipids and RNA moieties) within an intact a bilayer membrane. Although generation of both exosomes and microparticles represents a highly regulated cellular process, understanding of the mechanisms by which MSC organize the generation and delivery of EVs to areas of tissue damage is warranted for regenerative medicine applications. We have recently demonstrated EVs-derived from Panc-MSC contain a diversity of cargo including proteins, lipids, and nucleic acids using surface-enhanced Ramen spectroscopy [18], although the functional significance of this cargo remains to be determined.

Collectively, the contribution of EVs to the regenerative functions of MSC requires further investigation to: 1) better understand cellular communication mechanisms driving tissue regeneration 2) to identify vascular regenerative stimuli that may improve therapeutic applications in regenerative medicine. Herein, we demonstrate

that Panc-MSC generate a unique pro-angiogenic secretome that promoted endothelial cell recruitment, proliferation and microvessel formation *in vitro* and *in vivo*. Notably, these functions were transmitted primarily within Panc-MSC EV-enriched subfraction which accelerated the recovery of blood perfusion in mice with femoral artery ligation-induced unilateral hindlimb ischemia.

5.2 Methods

5.2.1 BM-MSC and Panc-MSC Isolation and Culture

BM-MSC:

Human BM aspirates were obtained from healthy donors with informed consent from the London Health Sciences Centre (London, ON). BM-MSC were established and cultured in Amniomax-C100™ media + AmnioMax C100 (Life Technologies) supplement as previously described [23].

Panc-MSC:

Ricordi-chamber isolated human islets were obtained through the Integrated Islet Distribution Program (IIDP) funded by the National Institute of Diabetes and Digestive and Kidney Diseases (NIDDK). Panc-MSC were established by plastic adherence during islet suspension cultures and expanded as previously described[37].

5.2.2 Enrichment of EVs from MSC Conditioned Media

Conditioned media (CM) was generated by culturing BM-MSC and Panc-MSC to ~80% confluency, rinsed twice with pre-warmed PBS, switched to basal Aminomax C100 media without supplement and media was collected after 24-hours culture. CM was subsequently processed in one of three ways (Supplemental Figure 2). 1) Cell-free CM was concentrated (~20-fold by volume) by centrifugation in 3kDa centrifuge filter unit for 45 minutes at 2800g. This fraction contained both EVs and soluble proteins >3kDa

and is referred to as bulk CM. 2) Cell-free CM was concentrated in 100kDa centrifuge filter units for 20 minutes at 2800g. This fraction (EV+) was enriched with EVs and proteins complexes larger than 100kDa This fraction was referred to as EV+ CM or EV-enriched CM. 3) CM which passed through the 100kDA filter was centrifuged in 3kDA centrifuge filter units for 40 minutes at 2800g to concentrate soluble proteins between >3kDa and <100kDA size. This fraction was referred to as EV- CM or EV-depleted CM.

Figure 5.1 Concentration of MSC CM and segregation of EV+ versus EV- CM subfractions.

5.2.3   Pierce 660nm protein quantification

CM fractions BM- and Panc-MSC subtypes were analyzed for total protein content using the detergent compatible reagent to measure 660nm absorbance using a micro-plate reader. The membranes of EVs were dissociated using a urea-based lysis buffer containing ammonium bicarbonate, DTT, and 20% SDS. Lysed CM was then diluted 200-fold with an ionic detergent compatibility reagent (Thermo Fisher) incubated for 5 minutes at room temperature.

5.2.4   Mass Spectrometry

Methodological details of protein precipitation, digestion, SFX peptide fractionation, liquid chromatography-tandem mass spectrometry, and proteomic data base analysis are described thoroughly in Supplemental Methods and previous studies [13,38].

5.2.5   Directed *in vivo* Angiogenesis Assay (DIVAA)

The directed *in vivo* angiogenesis assay (DIVAA) was performed as per manufacturer's instructions (Trevigen, Gaithersburg, MD, www.trevigen.com). DIVAA angioreactors were loaded with $2.0x10^5$ Panc-MSC, $2.0x10^5$ BM-MSC, or with 10μg of BM-MSC or Panc-MSC bulk CM suspended in 20μl basement membrane extract. Angioreactors were incubated at 37^oC *ex vivo* for 10 days prior to subcutaneous implantation into the upper dorsal flank of 10-12-week-old nonobese diabetic/severe combined immunodeficiency (NOD/SCID) mice. After 10 days, the recruitment of murine endothelial cells into implanted angioreactors was quantified by lectin-uptake, detected with a SpectraMax plate reader (MolecularDevices, Sunnyvale, CA, www.moleculardevices.com).

5.2.6   Assessment of HMVEC Survival and Proliferation

Human Microvascular Endothelial Cells (HMVEC) were seeded at 10^4 cells/cm^2 in complete endothelial growth media, EGM-2 (EBM-2 + 5%FBS, IGF, bFGF, EGF, and VEGF) for 24 hours. HMVEC were washed twice with pre-warmed PBS and switched to serum/growth factor-deprived EBM-2 for up to 48 hours. 40µg total protein of BM-MSC

or Panc-MSC CM was supplemented into EBM-2 without serum or growth factors (<5% of total culture volume), and 750nM of EdU was added 24 prior to harvest to label proliferating cells. HMVEC were harvested at 48-hours and enumerated using automated hematocytometer counts (Life Technologies). Harvested HMVEC were divided in half prior for detecting EdU incorporation in fixed (10% Formalin) and permeabilized (1x Saponin Buffer) cells using the Click-It system with Alexfluor 594 (Life Technologies), according to manufacturer's instructions. Nonpermeabilized HMVEC were co-stained with BV421- Annexin V and 7-AAD to assess early apoptosis or cell death, respectively.

man Microvascular Endothelial Cells (HMVEC) were seeded at 104 cells/cm2 in complete endothelial growth media, EGM-2 (EBM-2 + 5%FBS, IGF, bFGF, EGF, and VEGF) for 24 hours. HMVEC were washed twice with pre-warmed PBS and switched to serum/growth factor-deprived EBM-2 for up to 48 hours. 40µg total protein of BM-MSC or Panc-MSC CM was supplemented into EBM-2 without serum or growth factors (<5% of total culture volume), and 750nM of EdU was added 24 prior to harvest to label proliferating cells. HMVEC were harvested at 48-hours and enumerated using automated hematocytometer counts (Life Technologies). Harvested HMVEC were divided in half prior for detecting EdU incorporation in fixed (10% Formalin) and permeabilized (1x Saponin Buffer) cells using the Click-It system with Alexfluor 594 (Life Technologies), according to manufacturer's instructions. Nonpermeabilized HMVEC were co-stained with BV421- Annexin V and 7-AAD to assess early apoptosis or cell death, respectively.

5.2.7 Nanoscale Flow Cytometry

Bulk, EV+, and EV- CM from Panc- or BM-MSC were analyzed for the number of microparticles/μl. 20μl of each concentrate was diluted to 300μl with 0.22um-filtered PBS at room temperature. Microparticles secretion were detected using the A-50 nanoscale flow cytometer (Apogee), capable of multi-parametric analyses on microparticles between 150nm-1000nm diameter [24]. 150μl of diluted CM was injected and analyzed at 10.5μl/min for 1 minute. The size of secreted microparticles was estimated using silca beads ranging 110nm-1300nm using properties of large-angle light scatter (LALS) and small-angle light scatter (SALS). Silica beads provide a refractive

index (λ=1.42) that is similar to cells (λ=1.35-1.39). The resolution of exosomes (<100nm) or large protein complexes compared to background noise was not reliably attained based on the limitations of the A-50 nanoscale flow cytometer.

5.2.8   Atomic Force Microscopy

EV+ and EV- CM fractions were washed with 0.22um filtered PBS twice, diluted 1:20, and CM fractions were pipetted as 10uL microdroplets onto sterile glass coverslips and allowed to dry at room temperature in a sterile biological safety cabinet in preparation for atomic force microscopy (AFM) imaging. AFM measurements were performed using a BioScope Catalyst AFM (Bruker) equipped with NCL tips (NanoWorld) and Nanoscope software. Images were recorded in noncontact mode at a line rate of 0.5 Hz and processed using post-acquisition software Gwyddion.

5.2.9   Visualization of EVs derived from Panc-MSC

CM generated by BM-MSC or Panc-MSC was incubated for 40 minutes at room temperature with 1uM of Cell Tracker CTMPX, a fluorescent dye that becomes a membrane intercalated product. CTMPX-labelled CM was used to visualize EVs and semi-quantify uptake by HMVEC using flow cytometry and confocal imaging. Specifically, CTMPX-labelled CM was processed to generate EV+ and EV- CM. EV-CM was used as a negative control, as this fraction is devoid of membrane structures that retain CTMPX fluorescence. CMPTX+ EVs were visualized using oil immersion confocal imaging at 63X with 4x digital zoom (Leica TSP8).

5.2.10   EV Uptake by Human Endothelial Cells

To confirm EV- CM was devoid of EVs, HMVEC were cultured in EBM-2 with equal volumes of CMTPX labelled CM separated into EV+ and EV- fractions. Geometric mean fluorescent intensity (MFI) was measured at 0.5, 1, and 12 hours using a LSRII flow

cytometer. Furthermore, CTMPX-labelled EV+ CM uptake was spiked at increasing doses into single-cell suspensions of 1.0 x 10^6 HMVEC and immediately measured using MFI via flow cytometry.

Additionally, CTMPX+ EV uptake was visualized by adding CTMPX+ EV+ or EV- CM to serum-free HMVEC cultures for up to 12 hours. Confocal images were acquired at 1 or 12 hours after CFMPM-labelled HMVEC were fixed using 10% formalin and counterstained with DAPI. EV and CMPTX internalization were visualized through the Z-plane at 0.1μm increments under 63x oil immersion and 2x digital zoom (Leica TSP8).

5.2.11   HMVEC Tubule Formation

To assay for tubule forming function *in vitro*, 1.2x10^5 HMVEC were cultured on growth factor-reduced Geltrex matrices (LifeTechnologies) in EGM-2, EBM-2 or EBM-2 supplemented with 30ug of bulk, EV+ or EV- CM generated by BM-MSC or Panc-MSC. After 24 hours, four photo-micrographs were taken per well, and complete tube formation was quantified by manual counting in a blinded fashion using open-source Fiji Image Analysis Software.

5.2.12   Femoral Artery Ligation and Transplantation

Unilateral hind limb ischemia was induced in anesthetised (100mg/kg ketamine/xylazine, maintain with 2% isoflurane, 0.8L/min) NOD/SCID mice via surgical ligation and cauterization of the femoral artery and vein (FAL), as previously described [39]. Mice with unilateral hind-limb ischemia (perfusion ratio <0.1), were transplanted 24-hours after surgery (Day 0) with 40μg total protein intramuscularly (i.m) injected (20μL) at 3 sites in the thigh muscle and one site in the calf muscle. As a vehicle control, mice received i.m.-injections of 80μl of basal Aminomax[TM] C100 media.

5.2.13   Laser Doppler Perfusion Imaging

Anesthetised mice were warmed to 37ºC for 5 minutes and hindlimb blood perfusion was measured using Laser Doppler perfusion imaging (LDPI) as previously described [39].

Recovery of blood flow was quantified on 3-, 7-, 14- and 21-days post-transplantation by quantifying the perfusion ratio (ischemic/non-ischemic limb) of transplanted mice.

5.2.14   Endothelial Cell Density

Adductor muscle from ischemic and non-ischemic thighs were harvested at Day 28, embedded in OCT, and cryosectioned (14μm) to obtain three sections per slide $\geq 100\mu$m apart. Cryosections were fixed in 10% formalin (Sigma) and blocked with 5% serum. CD31$^+$ area was quantified at 21-days post-transplantation using rat anti-mouse CD31 (BD Biosciences; 1:100) detected with alkaline phosphatase-labelled rabbit anti-rat secondary antibodies (Vector; 1:200) stained with Vector Blue (Vector). CD31$^+$ cell area was enumerated using 3 randomly selected fields of view per section, totaling 9 images per limb. Images were converted to RBG stack and threshold of was set between 180-210 using Fiji Image Analysis Software.

5.2.15   Statistical Analyses

Analysis of significance was performed by one-way ANOVA with Tukey's multiple comparisons tests for all *in vitro* or *in vivo* experiments and enumeration of histological analyses. Outliers were identified using Grubb's test; $*p < 0.05$.

5.3   Results

5.3.1   The secretome of Panc-MSC was enriched for proteins that contribute to vascular development, wound response, and chemotaxis

We recently demonstrated Panc-MSC express tissue-specific MSC characteristics, however, the therapeutic potential of Panc-MSC is currently undetermined. We considered BM-MSC as the gold-standard of therapeutic MSC and utilized the secretome of BM-MSC as a comparator for the secretome of Panc-MSC. Using label-free mass

spectrometry we detected >1700 proteins in bulk CM generated by both MSC-types (Figure 1A), and 540 proteins were considered secreted effectors based on GO-terminologies. 343 of the 540 secreted proteins were detected at equivalent levels in both MSC subtypes (Figure 1B), referred to herein as the shared MSC secretome. GO-pathway enrichment analyses determined the majority of shared MSC secretome (182/343) were associated with wound response, vascular development, and/or inflammation (Supplemental Figure 1A-B). Specifically, 54 of these 182 proteins were associated with overlapping (>1) GO-pathway annotation (Figure 1B), and 12 proteins were associated with all 3 GO-pathway terminology and included pleiotropic signals including WNT5A, TIMP1, HGF, TGFB1, IL-6 and CCL2. Alternatively, Panther pathway enrichment analysis determined the shared MSC secretome was enriched with proteins associated with integrin signaling and angiogenesis (Supplemental Table 1-2).

Of the 540 shared secreted proteins, 115 and 82 were significantly upregulated (total=197 differentially expressed) in the secretome of Pan-MSC or BM-MSC, respectively (Figure 1C; Supplemental Figure 1C). GO-pathways enrichment analyses suggested there was a significant representation (95/197=48%) of differentially expressed proteins that have functional contributions towards wound response (GO:0009611), chemotaxis (GO:0006935), and/or blood vessel development (GO:0001568). 54 of these proteins were exclusively associated with a single GO-pathway annotation term (Figure 1D), 27 of which were significantly upregulated in Panc-MSC. Moreover, 41 differential proteins were associated with 2 or more GO-pathway annotations (Figure 1E), 27 which were significantly enriched in the secretome of Panc-MSC. Specifically, the secretome of Panc-MSC was significantly enriched with proteins that contribute to chemotaxis and blood vessel development (i.e. Platelet-derived Growth Factor D/PDGFD).

We previously demonstrated the secretome of BM-MSC with high ALDH-activity can stimulate robust endothelial cell recruitment in a murine model of endothelial cell chemotaxis [23]. Accordingly, we used the directed *in vivo* angiogenesis assay (DIVAA) methodology to assess the capacity of BM-MSC or Panc-MSC to recruit endothelial cells *in vivo* (Figure 1F). Interestingly, BM-MSC or Panc-MSC seeded in angioreactors did not stimulate endothelial cell recruitment, compared to vehicle controls.

In contrast, concentrated CM generated by Panc-MSC significantly stimulated the recruitment of murine endothelial cells, compared to vehicle controls (Figure 1G). Collectively, these results suggest the secretome of Panc-MSC is enriched for proteins involved in chemotaxis, wound response and vascular development compared to BM-MSC; however, there exists a comparable functional capacity to stimulate endothelial cell chemotaxis *in vivo*.

A Total Unique Proteins Quantified

GOCC: 540 Secreted Proteins

Panc-MSC   BM-MSC

115 343 82

p<0.05

B

GOCC:Inflammatory Response 68

15

GOCC: Response to Wounding 24

12

11 16

GOCC:Blood Vessel Development 24

53% of Non-Sig. Proteins (182/343)

Wound Response Vascular Development

FAP	SERPINF1	SEMA3F	MET
VEGFA	SERPINE1	SEMA3C	MCAM
FGF7	CTGF	SEMA3A	MAP2K1
COL5A1	PDGFA	AIMP1	NDNF

Inflammation Wound Response

F10	C1QTNF3	TFPI	ACTG1	WNT5A	TIMP1
FBLN1	S100A8	S100A9	F13A1	CCL2	ANXA1
GSN	HTRA1	PROS1	ARG1	APOE	IL6
SERPINC1	SERPING1		LTF	THBS1	TGFB1
				FN1	HGF
				HMOX1	C1QBP

Inflammation Vascular Development

ANGPT1	APOB	B4GALT1
JAG1	JAM3	CALR
PRSS3	SCG2	MMP2	C3/6

Wound — Vascular

C

BM-MSC 82   Panc-MSC 115

-log10(P)

0 2 3 4 6   10   20

GO:0002576: platelet degranulation
GO:0005925: focal adhesion
GO:0031983: vesicle lumen
GO:0009611: response to wounding
GO:0050839: cell adhesion molecule binding
GO:0031012: extracellular matrix
GO:0000904: cell morphogenesis involved in differentiation
GO:1901681: sulfur compound binding
GO:0019838: growth factor binding
GO:0006935: chemotaxis
GO:0005788: endoplasmic reticulum lumen
GO:0005201: extracellular matrix structural constituent
GO:0031589: cell-substrate adhesion
GO:0001568: blood vessel development
GO:0050840: extracellular matrix binding
GO:0001501: skeletal system development
GO:0005509: calcium ion binding
GO:0071363: cellular response to growth factor stimulus
GO:0098644: complex of collagen trimers
GO:0030199: collagen fibril organization

D

Wound Response

HIST2H3A, CST3, PROCR, CD59, PLAT, YWHAZ, LGALS1, SOD1, VCL, ACTN1, TLN1, CAPZA1, DPYSL3, AKR1B1, PKM, SERPINE2

Blood Vessel Development

LAMA5, COL18A1, SERPINB7, CCBE1, COL4A1, COL4A2, HSPG2, THBS2, COL8A1, LOXL2, ANPEP, LAMB1, ESM1, ANGPTL4, CHI3L1

Chemotaxis

SPON2, TNFRSF11B, LAMA2, LRP8, DKK3, FUCA2, GPC1, FBN1, PXDN, EZR, SSC5D, METRNL, HPX, MSN, MANF, C8B, TWF2, LAMB2, CTHRC1, CXCL1, ADAMTS5, CXCL6, CFI

Fold   5 0 -5

E

Panc-MSC   BM-MSC

Log (p-value)

COL1A1, COL3A1, APP, STC1, DCN, EGFR, GAS6, POSTN, PF4V1, POSTN, ECM1, SLIT2, EMILIN1, CXCL8, COL1A2, AXL, SDCBP, EPHB2, CDH13, PDGFD, GREM1, COPA, GPI, TGFB2, NOV, ERAP1, HSPB1, TMSB4X, PTN, FN1, DAG1, SPARC, ADAM9, FLNA, HMGB1, MATN2, NRP1, SPP1, MMP14, CYR61, LOXLY

Fold Increase (Log2)

■ Chemotaxis/Blood Vessel
● Wound Response/Blood Vessel
♦ Wound Response/Blood Vessel
★ Wound/ Chemotaxis/Vessel

F

2.5 x 10⁵ BM-MSC or Panc-MSC
or Cell-free Conditioned Media

NOD/SCID

Lectin-FITC Uptake (519nm Spectometry)

10-Days

Endothelial Cell Recruitment

G

Lectin-FITC (A.U.)

** *** ***

VEGF-A + FGF2   Vehicle   BM-MSC   Panc-MSC   BM-MSC   Panc-MSC

Cell   CM

Figure 5.2 The secretome of Panc-MSC was enriched for pro-vascular proteins that stimulate endothelial cell recruitment *in vivo*. Conditioned Media (CM) generated by BM-MSC or Pan-MSC was analyzed by label-free mass spectrometry. (A) Mass spectrometry identified 1912 and 1872 unique proteins in the secretome of BM-MSC and Panc-MSC, respectively. Identified proteins filtered using GOCC analysis identified 540 secreted proteins were shared in the secretome of BM-MSC and Panc-MSC. Of the secreted proteins identified, 343 secreted proteins were equally expressed, 115 secreted proteins were upregulated in the secretome of Panc-MSC, whereas 82 secreted proteins were upregulated in the secretome of BM-MSC (*p<0.05). (B) Of the 343 shared proteins, 182 were associated with Inflammation, Response to Wounding, or Blood Vessel Development. Specifically, 8 of the 182 shared proteins were associated with all 3 GO-terms. (C) Differentially expressed proteins cross referenced to GO-pathway database revealed a significance enrichment of pro-vascular proteins in the secretome of Panc-MSC. Specifically, (D) differentially expressed proteins associated with one GO-pathway annotation or (E) multiple annotations were enriched in Panc MSC CM. (F) Schematic of 2.5 x10^5 MSC or 20µg MSC CM-loaded DIVAA angioreactor implantation into NOD/SCID mice. (G) Panc-MSC CM significantly increased endothelial cell recruitment compared to vehicle or cellular controls. Data represented as Mean ± SEM (*p<0.05; N=3, n=3). Statistical analyses were determined by one-way ANOVA with Tukey's post-hoc test.

A

B

-log10(P)
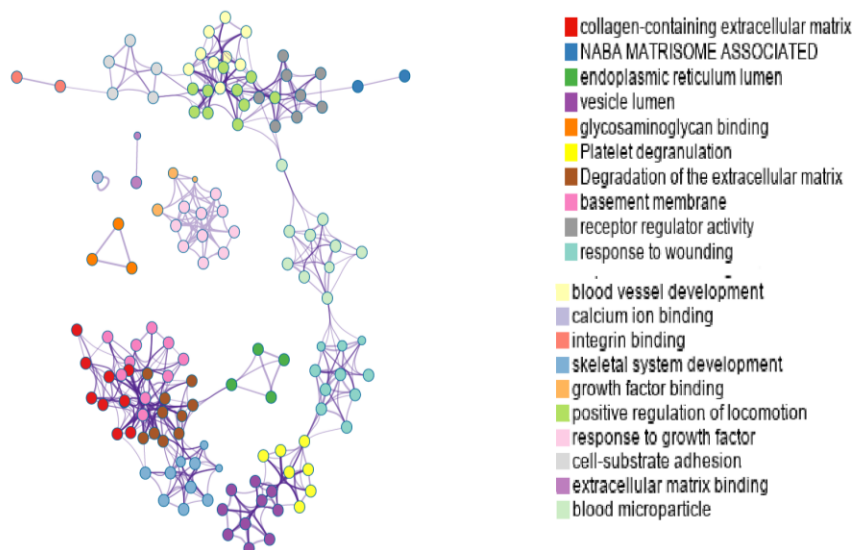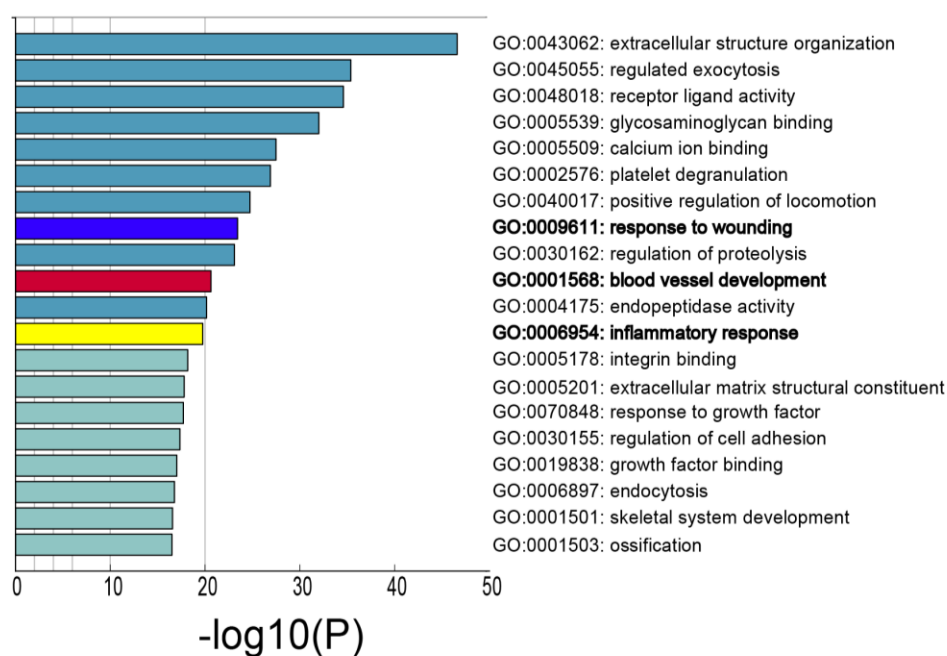
C
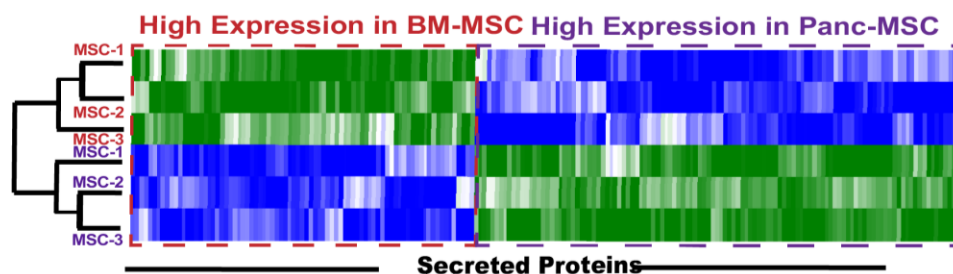
Figure 5.3 GO-Pathways Analysis of Panc-MSC and BM-MSC Conditioned Media.
Label-free mass spectrometry was performed on concentrated conditioned media
generated by human BM-MSC or Panc-MSC. (A) Pathways networks and (B) pathway
enrichment analyses demonstrate the secretome of both MSC-types are enriched with
proteins that have functional roles in wound response, blood vessel development and
chemotaxis.

Table 5.1 Protein enrichment analysis on the secretome of of Panc-MSC cross-referenced to the Panther 2016 Database.

Function	Adjusted p-value	Z-score	Combined Score
Integrin Signaling	2.58×10^{-24}	-1.78	103.88
Blood Coagultion	8.55×10^{-11}	-1.39	36.89
Angiogenesis	4.50×10^{-4}	-1.18	11.73
Plasminogen-activating cascade	3.84×10^{-7}	-0.30	5.13
Inflammation	4.01×10^{-2}	-1.02	5.09

Table 5.2 Protein enrichment analysis on the secretome of BM-MSC cross-referenced to the Panther 2016 Database.

Function	Adjusted p-value	Z-score	Combined Score
Integrin Signaling	7.74×10^{-26}	-1.78	110.15
Blood Coagultion	6.38×10^{-11}	-1.39	37.33
Plasminogen-activating cascade	4.40×10^{-7}	-0.69	12.14
Angiogenesis	3.50×10^{-5}	-1.18	12.03
Inflammation	4.49×10^{-3}	-1.22	9.03

5.3.2   Panc-MSC CM increased HMVEC proliferation and survival.

Blood vessel regeneration requires fine-tuned orchestration of endothelial cell recruitment, proliferation, and tube formation. We have previously demonstrated the secretome of BM-MSC can support HMVEC survival, proliferation, and tube formation *in vitro* [23]. Accordingly, we sought to investigate whether CM generated by Panc-MSC similarly supported HMVEC survival and/or proliferation under serum and growth factor-starved conditions *in vitro*. After 48 hours culture under starvation conditions in EBM-2 without serum or growth factors, HMVEC supplemented with 40μg of CM generated by BM-MSC or Panc-MSC demonstrated increased cell survival (**$p<0.05$, Figure 2A) and proliferation (**$p<0.01$; Figure 2B). The frequency of HMVEC undergoing apoptosis (Annexin V$^+$/7-AAD$^-$) was reduced when EBM-2 was supplemented with BM-MSC or Panc-MSC CM (**$p<0.01$; Figure 2C). Moreover, the frequency of dead cells (Annexin V$^+$/7-AAD$^+$) was also reduced when HMVEC were supplemented with BM- or Panc-MSC generated CM (Figure 2D). As a result, the total number of viable HMVEC was significantly increased after 48 hours, when HMVEC cultures were supplemented with BM- or Panc-MSC CM under starvation conditions (**$p<0.01$; Figure 2E). Collectively, these results demonstrated the capacity of Panc-MSC CM to support HMVEC survival and proliferation *in vitro* was comparable to BM-MSC CM.
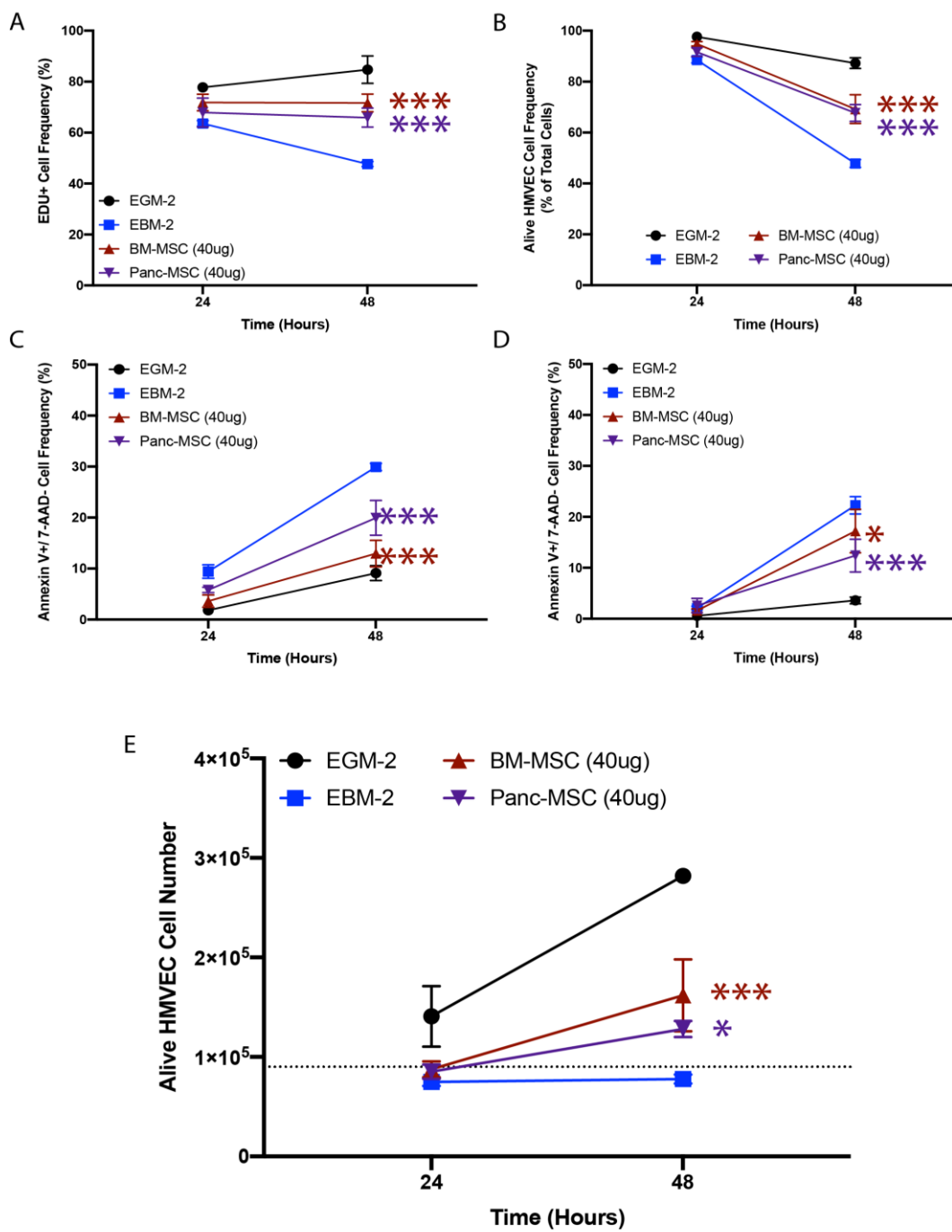
Figure 5.4 Panc-MSC CM promoted endothelial cell survival and proliferation under growth-factor and serum-starved conditions *in vitro*. HMVEC were cultured up to 48 hours in EBM-2 without serum or growth factors with or without 40µg of BM-MSC CM or Panc-MSC CM. As a control for optimal HMVEC growth, HMVEC were also cultured under EGM-2 conditions. (A) Panc-MSC increased the frequency of EdU+ HMVEC after 48 hours. Panc-MSC CM increased (B) viable HMVEC frequency by decreasing the frequency of (C) apoptotic and (D) dead HMVEC after 48 hours. (E) Total viable HMVEC cell number was increased after 48 hours. Data represented as Mean ± SEM (*$p < 0.05$; n=3). Statistical analyses were determined by one-way ANOVA with Tukey's post-hoc test

### 5.3.3   Panc-MSC CM contains extracellular vesicles

We have recently demonstrated using custom fabricated nano-hole trapping and surface enhanced Ramen-spectrometry that the secretome of Panc-MSC contains vesicle-like structures with packaged cargo including proteins, lipids, and nucleic acids [18]. Because this technique does not assess vesicle size or distinguish the identity of common markers in the EV membrane (i.e. CD9, CD63, or CD81), we identified an enrichment of proteins associated with exosomes within bulk Panc-MSC generated CM, according to the ExoCarta database (exocarta.org) and FunRich (funrich.org) functional enrichment analyses (Figure 3A). Accordingly, we detected a high abundance of the EV membrane markers CD9, CD63, and CD81 in the secretome of Panc-MSC (Figure 3B). EV-associated proteins such as Pyruvate Kinase M1/2 (PKM) or Tumor susceptibility gene 101 (TSG101) were also detected. The detection of EVs by conventional flow cytometry is limited by resolution of particle size and obscuration from sample debris, underestimating EV concentrations in analyzed samples [24]. To address this, we employed nanoscale flow cytometry to measure microparticle content in EV-enriched (EV$^+$) and EV-depleted (EV$^-$) CM (Figure 3C). The number of detectable microparticles (170nm-1μm) was increased above media control only in EV$^+$ CM, whereas the number of events in EV- CM did not exceed background measurements (Figure 3D). Interestingly, the majority of total protein by mass for both BM-MSC and Panc-MSC was contained within the EV- CM fraction (Figure 3E). The majority of microparticles detected were relatively small (170-250nm) and aligned with the size range of microparticles (Figure 3F). Atomic force microscopy (AFM) was used to visualize the enrichment of EVs after ultrafiltration (Figure 3G). EV$^+$ CM contained many vesicle-like structures demonstrating appropriate microparticle dimensions and morphology, whereas vesicle-like structures were not observed in EV$^-$ CM. Collectively, these results demonstrate Panc-MSC secrete EVs and ultrafiltration is sufficient to segregate EVs from vesicle-free proteins.
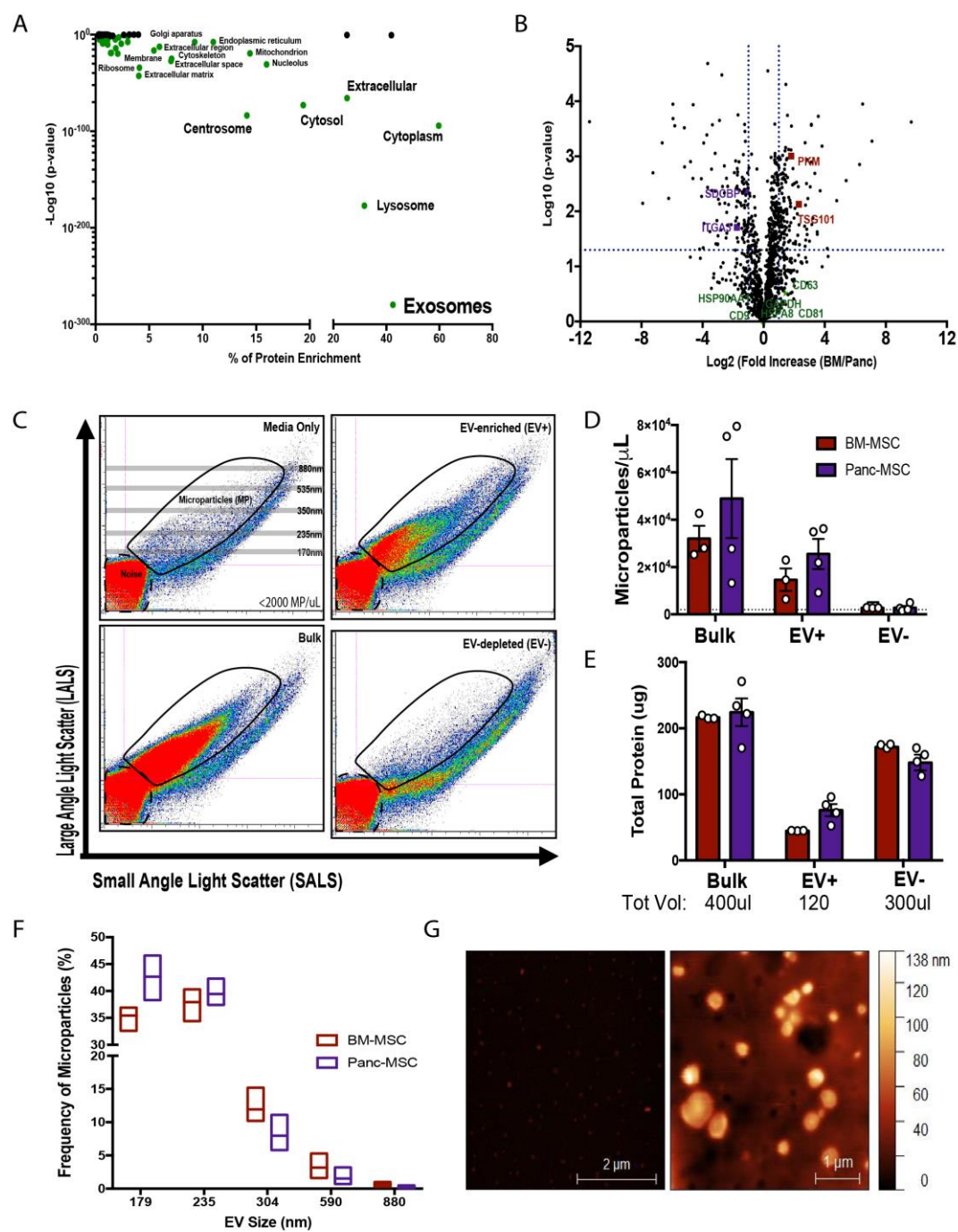
Figure 5.5 Panc-MSC secrete extracellular vesicles that can be detected by nano-scale flow cytometry. (A) Mass spectrometry analysis identified 1298 unique proteins in the secretome of Panc-MSC and BM-MSC that were associated with exosomes using FunRich enrichment analysis. (B) Mass spectrometry detected proteins associated with extracellular vesicles, including CD63, CD81, CD9, PKM or TSG101 in the secretome of both BM-MSC and Panc-MSC. (C) Representative nanoscale flow cytometry plots, acquired using Apogee A-50 and calibrated using silca beads ranging from 178 to 1300nm, demonstrated only bulk and EV^+ CM fractions exhibited detectable microparticle detection. (D) On the other hand, levels of microparticles in EV^- CM was not detectable above background levels observed with media (horizontal dashed line). (E) Total protein measured by 660nm spectrophotometry revealed the majority of bulk mass was contained within EV-CM. Tot. Vol = Volume of CM after typical ultrafiltration when 10mL of CM was concentrated. (F) Size distribution of EVs detected by nanoscale flow cytometry. (G) Representative atomic force microscopy image demonstrating enrichment of EVs within EV^+ CM. Data represented as Mean ± SEM (*p<0.05; n=3-4).

5.3.4 HMVEC demonstrate uptake of EVs generated by Panc-MSC

EVs contain bioactive cargo enclosed by a plasma membrane that can up taken by target cells either through endocytosis or fusion with the plasma membrane [25]. To assess whether endothelial cells were competent to EVs generated by Panc-MSC, we incubated cell-free CM with a fluorescent label (CMTPX red) that is metabolized to a membrane impermeable by-product (Figure 4A). This approach ensures that only vesicles with enzymatic activity would retain CTMPX and free CTMPX(<3kDa) would be removed during CM concentration and purification into EV^+ and EV^- subfractions. $CTMPX^+$ vesicle-like structures were observed using oil-immersion confocal microscopy and diameters validated EV sizes detected by nanoscale flowcytometry and AFM (Figure 4B). HMVEC cultured with CMTPX-labelled EV^+ CM demonstrated distinct accumulation of CMTPX after 12 hours whereas, HMVEC supplemented with EV^- CM did not accumulate CTMPX fluorescence above non-supplemented HMVEC controls (Figure 4C). Furthermore, rapid accumulation of CMTPX+ fluorescence was observed within 400ms of exposure to labelled EV^+ CM, and accumulation of CMTPX fluorescence occurred in a dose-dependent manner (Figure 4D). Next, we wanted to determine whether $CTMPX^+$ accumulation in HMVEC was a result of vesicle internalization or vesicle fusion to the plasma membrane. Accordingly, HMVEC were first labelled with CMFPR (green) to define cytoplasmic contents and incubated with either CMTPX-labelled EV^+ or EV- CM. Robust CMTPX internalization was observed after HMVEC were cultured with EV^+ CM for 1 hour, suggesting active EV uptake in HMVEC via an endocytotic mechanism. In contrast, CMTPX internalization was not observed in HMVEC cultured with EV^- CM for up to 12 hours (Figure 4E). High resolution oil-immersion confocal microscopy detected the presence of $CMTPX^+$ vesicle-like structures in both the plasma membrane and cytoplasm of HMVEC (Figure 4F). Thus, HMVEC EV uptake demonstrated characteristics consistent with EV internalization to the cytoplasm and fusion at the plasma membrane.
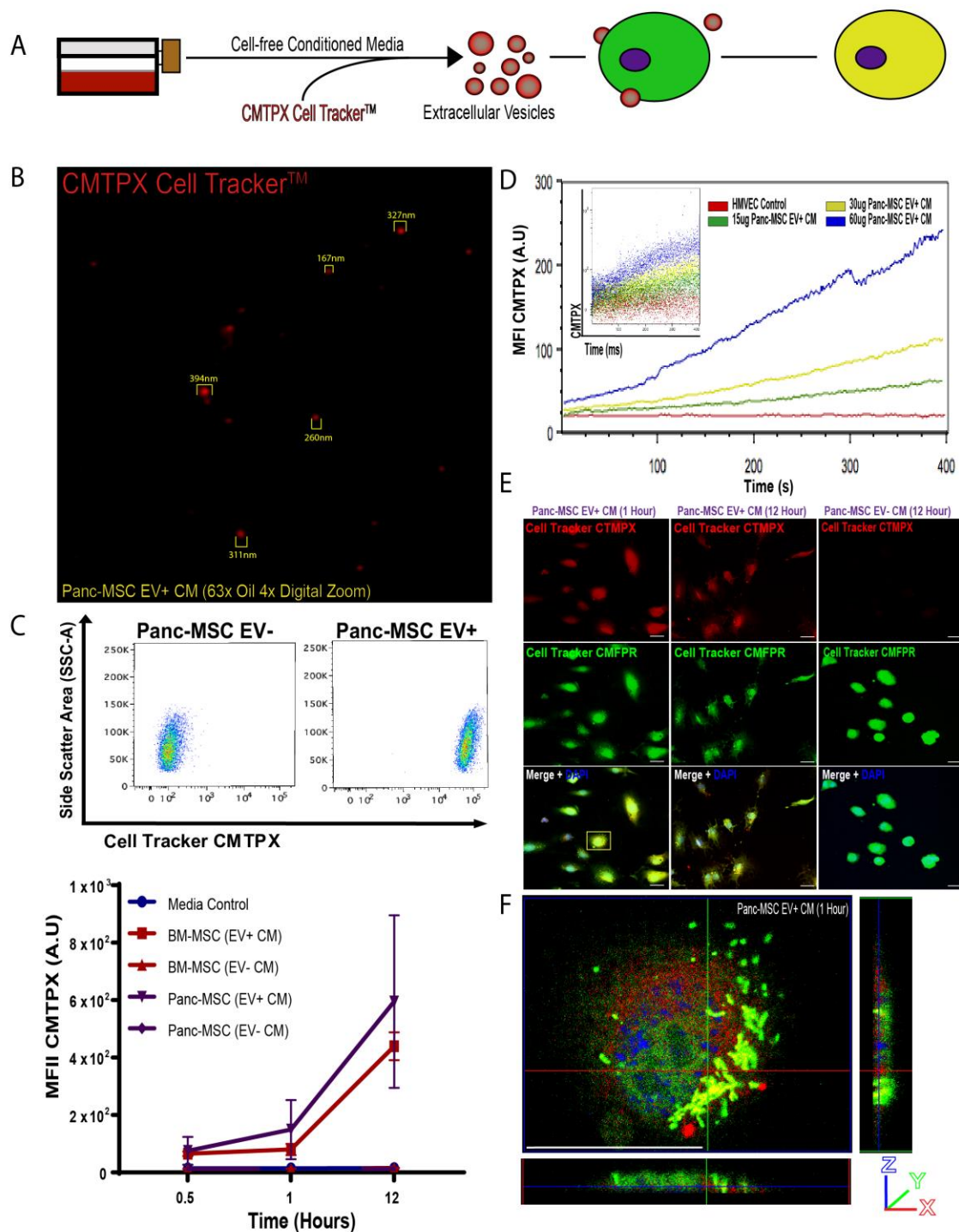
Figure 5.6 HMVEC uptake EVs generated by Panc-MSC. (A) Panc-MSC and BM-MSC CM was stained with Cell Tracker CTMPX, allowing for the labelling of EVs. (B) Representative oil immersion confocal photomicrograph of Panc-MSC EV+ CM labelled with Cell Tracker CTMPX. (C) Representative flow cytometry plots demonstrate that only the EV+ CM fraction was able to increase the Cell Tracker CTMPX fluorescence in HMVEC, as measured by geometric mean fluorescence intensity (MFI).   (D) HMVEC in single cell suspension were exposed to increasing amounts of CTMPX-labelled EVs and immediately analyzed for CMTPX accumulation up to 400s by MFI. (E) CMTPX-labeled EVs were detected within HMVEC at 1 hour and (F) visualized in the Z-plane using oil immersion confocal imaging at 63x oil and 2x digital zoom. Data represented as Mean ± SEM (*$p<0.05$; n=3).

5.3.5   Classical EV-markers were exclusively detected in EV+ CM

It is well established that EVs contain specific cargo distinct from the parent cytoplasm. However, currently undetermined is the identities of proteins exclusively released within EVs versus conventional vesicle-free exocytosis from the parent cell. We employed an additional label-free mass spectrometry screen on EV+ versus EV- CM generated by Panc-MSC to investigate proteomic make-up of each compartment. Although we have previously demonstrated EV- CM contained the majority of bulk protein content based on 660nm spectrophotometry, we determined the EV+ CM fraction contained a significantly more protein diversity compared to EV- CM. Specifically, we detected 1458±63.02 versus 877.30±78.19 proteins in EV+ CM versus EV- CM, respectively (Figure 5A). PCA analysis demonstrated a clear distinction between the proteomic profile of EV+

A

B

C

EV+   EV-

637   1047   74

D

E

3 OF 3 EV- CM

F

3 OF 3 EV- CM
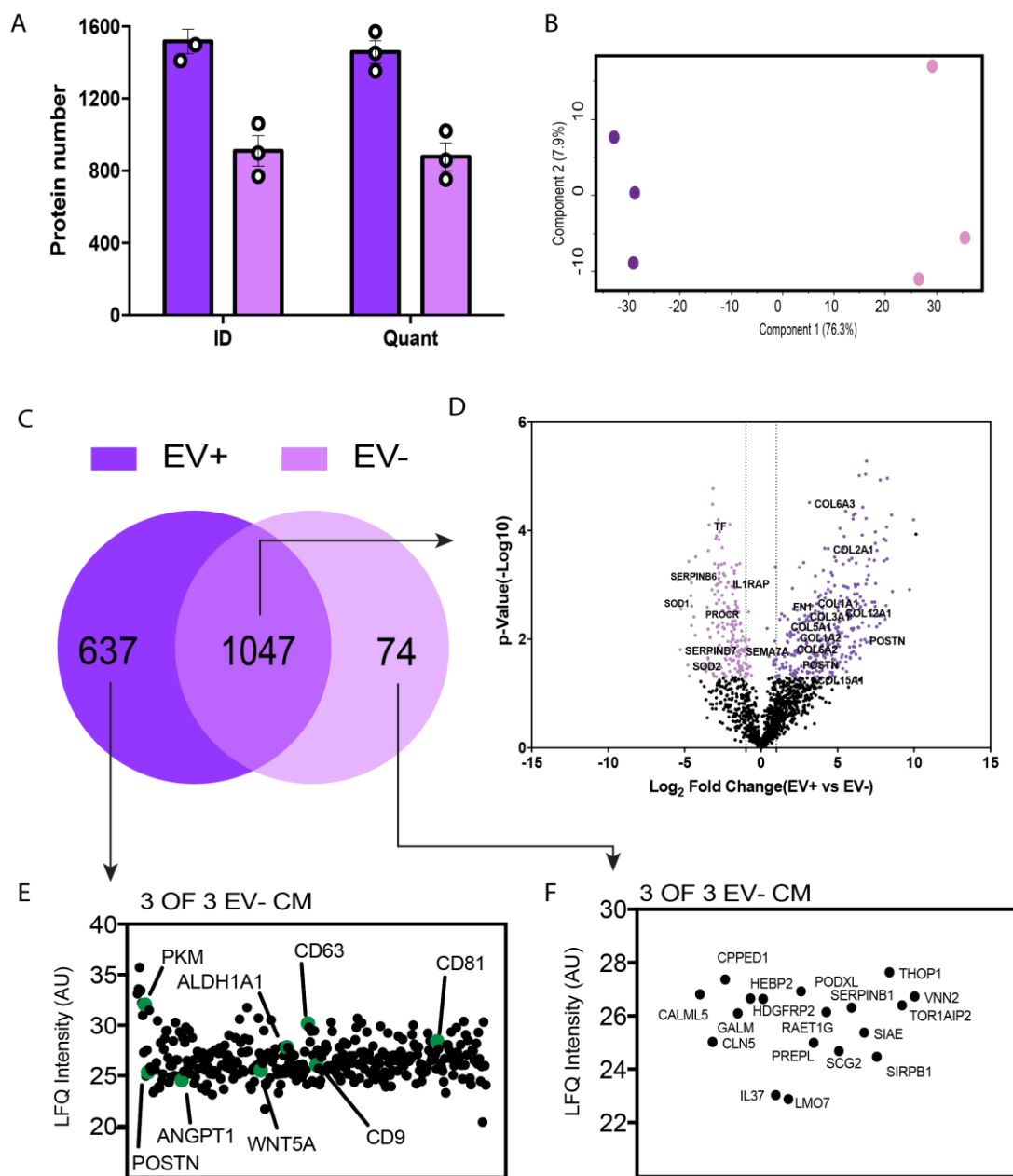
Figure 5.7 Panc-MSC EV+ CM demonstrates a diverse proteomic profile with exclusive enrichment of EV-associated proteins. Panc-MSC CM was processed into EV+ CM and EV- CM and analyze by mass spectrometry. (A) ~1450 and 870 proteins were quantified in EV+ or EV- CM, respectively. (B) PCA analysis demonstrates distinct composition between EV+ and EV- CM. (C) Specifically, expression levels of 1047 proteins were equally detected, whereas 637 proteins were exclusively detected in at least 1 EV+ CM. On the other hand, 74 proteins were exclusively detected in at least 1 EV- CM. (D) Volcano plot of comparably detected proteins. EV+ CM was significantly enriched for ECM molecules, such as FN1, and POSTN. (F) Of the 637 proteins exclusive to 1 of 3 EV+ CM, 142 were detected in 3 of 3 EV+ CM samples. (G) Of the 74 proteins exclusive to EV- CM, 18 were detected in 3 out of 3 EV- CM. Data represented as Mean ± SEM (*p<0.05; n=3).

versus EV$^-$ CM (Figure 5B). Although 1047 common proteins were detected in both EV$^+$ or EV$^-$ CM (Figure 5C), 322 of these proteins were significantly enriched in the EV$^+$ CM fraction, whereas 180 proteins were significantly enriched in the EV$^-$ CM fraction (Figure 5D). Proteins with increased abundance in EV$^+$ CM included several ECM

molecules (i.e. COL1A2, COL6A2, COL5A, FN1) and two isoforms of Periostin (POSTN). On the other hand, EV$^-$ CM was significantly enriched for proteins including SERPINB6/7, CD201/PROCR, and Tissue Factor/TF.

Next, we investigated which proteins were robustly and exclusively detected in each CM fraction. 637 proteins were detected in at least 1 of 3 EV$^+$ CM sample and exclusively absent from 3 out of 3 EV$^-$ CM samples. We filtered these 637 unique proteins to include only those which were detected in 3 out of 3 EV$^+$ CM samples. These subsequent analyses identified 142 proteins that are robustly expressed and exclusively detected in the Panc-MSC EV$^+$ CM fraction (Figure 5E). Proteins exclusive to EV$^+$ CM included classical EV markers such as CD9, CD81, CD63 and PKM; and regenerative/pro-angiogenic proteins ALDH1A1, ANGPT1, and WNT5A. In contrast, 74 proteins detected in at least one EV- CM sample and excluded from EV$^+$ CM were identified. We filtered these 74 unique proteins to only those detected in 3 of out 3 EV$^-$ CM samples, in return identifying 18 proteins with robust expression that exclusively detected in EV$^-$ CM (Figure 5F). Collectively, these results confirmed the segregation of EVs using ultrafiltration and provide novel insight into proteins which may be exclusively secreted within EVs by Panc-MSC.

5.3.6 HMVEC tubule formation was enhanced by CM fractions generated by Panc-MSC

CM generated by Panc-MSC supported endothelial cell proliferation and survival (Figure 2). To determine whether Panc-MSC CM could support HMVEC tubule formation, HMVEC in seeded on Geltrex media and treated with Panc-MSC CM subfractions *in vitro*. After 24 hours, we observed a significant increase in the number of tubules formed by HMVEC supplemented with Panc-MSC bulk CM (Figure 6A), compared to EBM-2 without supplements (*$p<0.05$). Furthermore, when Panc-MSC CM was segregated into EV$^+$ CM and EV$^-$ CM, both subfractions enhanced tubule formation compared to EBM-2 conditions (*$p<0.05$; Figure 6A). Collectively, the soluble and EV secretome compartments from Panc-MSC equally supported endothelial tubule formation under serum-deprived culture conditions *in vitro*.

5.3.7 Intramuscular-injection of Panc-MSC EV+ CM enhanced recovery of blood perfusion in mice with hindlimb ischemia

Although MSC demonstrate diverse pro-regenerative functions *in vitro*, transplantation of MSC has produced modest and often inconsistent results due to culture-induced functional heterogeneity, poor cell engraftment and transient cell survival. We recently demonstrated direct injection of MSC-generated CM can facilitate tissue regeneration in a model of β-cell regeneration, eliminating the requirement for cell transfer to stimulate a regenerative cascade [12]. Therefore, we investigated the vascular regenerative potential of Panc-MSC CM following direct intramuscular injection and determined if vascular regenerative stimuli were contained in EV$^+$ and/or EV$^-$ CM compartments. Mice with unilateral hind-limb ischemia received 4 x 20μg injections of bulk, EV$^+$ or EV$^-$ CM (Figure 6B) 24 hours following femoral artery/vein ligation and excision. Specifically, two injections were proximal to site the site of ligation, one immediately distal to ligation, and one into the calf muscle. Unconditioned media of equal volume was injected as a vehicle control. Interestingly, only EV$^+$ CM significantly increased blood perfusion

(days 14 and 21), compared to vehicle control (*p<0.05; Figure 6C). Recovery of blood perfusion (Figure 6C, insert), measured by area under the curve (AUC), was significantly improved in mice that received bulk (*p<0.05) or EV$^+$ CM (**p<0.01). Accelerated recovery of perfusion was not observed in mice that received i.m. injections of EV$^-$ CM and was statistically comparable to the injection of vehicle control. Collectively, these results provide foundational evidence that the secretome of Panc-MSC contains vascular regenerative stimuli contained primarily within extracellular vesicles.
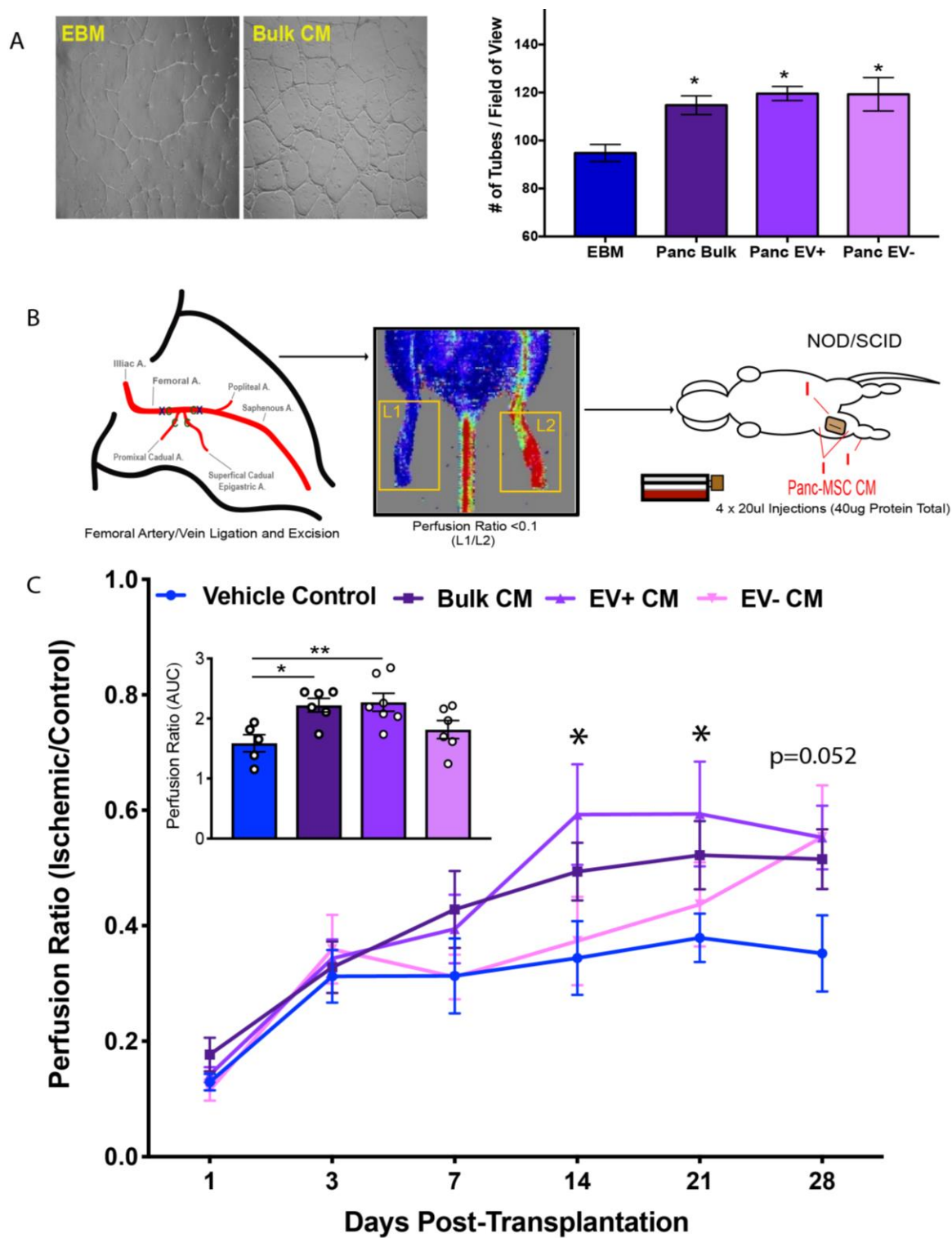
Figure 5.8 Panc-MSC CM supports HMVEC tubule formation *in vitro* and supports the recovery of hindlimb blood perfusion *in vivo*. (A) Representative photomicrographs at 24-hours of HMVEC tubule formation following culture with (30µg) of bulk, EV+, or EV- CM generated by either Panc-MSC or BM-MSC. Panc-MSC bulk, EV- and EV+ CM significantly increased HMVEC tubule formation under EBM-2 conditions. (B) Schematic of femoral artery ligation (x) and cauderization (c) sites and laser doppler perfusion imaging following intramuscular transplantation of Panc-MSC CM fractions into NOD/SCID mice. (C) Intramuscular injection of bulk or EV+ CM significantly improved hindlimb perfusion over 28 days (insert). Specifically, EV+ increased hind limb blood perfusion at days 14 and 21 post-transplantation. Data represented as Mean ± SEM (*p<0.05; n=3-6). Statistical analyses were determined by one-way ANOVA with post-hoc tukey's t-test.

5.3.8 Injection of Panc-MSC CM increased vessel density in ischemic thigh muscle.

Microvascular density was assessed in the thigh muscles of mice 28 days after Panc-MSC CM injection (Figure 7A). Consistent with improved perfusion induced by Panc-MSC subfractions, mice I.M.-injected with bulk or EV$^+$ CM showed significantly increased CD31$^+$ cell area (3.13±0.46 or 3.53±0.40 CD31+ % of area, respectively), compared to mice injected with unconditioned media control (1.83 ± 0.35 CD31+ % of area; Figure 7B). In contrast, mice injected with EV- CM fraction did not demonstrate significant recovery of blood vessel area (2.39 ± 0.28 CD31$^+$ % of area). Collectively, bulk and EV$^+$ CM generated by Panc-MSC stimulated the recovery of hind-limb blood perfusion which coincided with increased vessel density in the ischemic thigh muscles of NOD/SCID mice with femoral artery ligation-induced unilateral hindlimb ischemia.

A

CD31 Vector Blue

Vehicle
Bulk
EV+
EV-

B

CD31+ Area (%)

Vehicle Bulk EV+ EV-

* **

Ischemic   Control
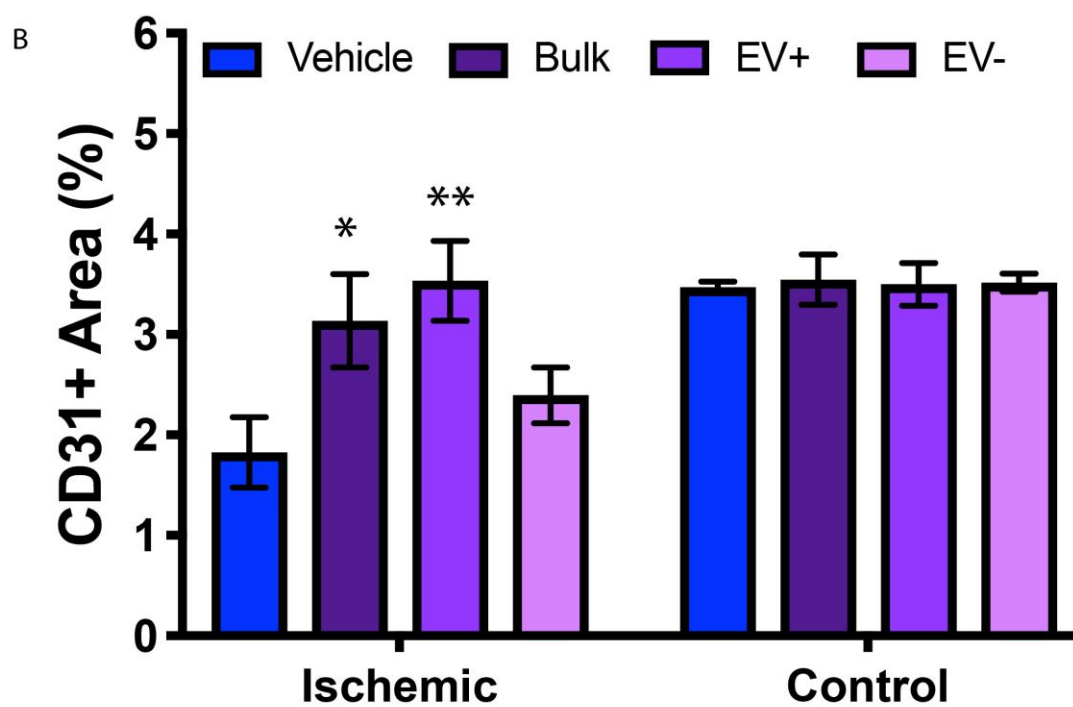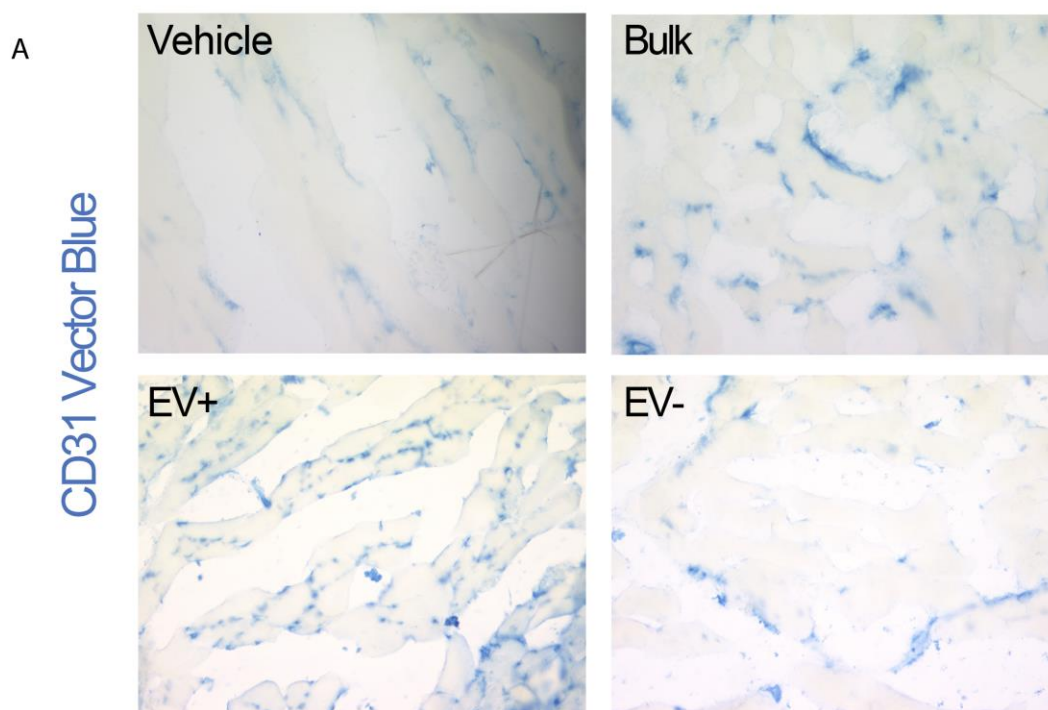
Figure 5.9 Revascularization of thigh muscle tissue is stimulated after i.m. injection of Panc-MSC CM. Thigh muscles were harvested at Day 28 from NOD/SCID mice with hindlimb ischemia that received intramuscular injections of Panc-MSC CM. (A) Representative photomicrographs demonstrate Panc-MSC bulk and EV+ CM significantly increased CD31+ area in ischemic thigh muscles, compared to vehicle control. Conversely, i.m. injection of EV- CM did not significantly increase CD31+ area, compared to vehicle control. Data represented as Mean ± SEM (*$p<0.05$; N=5). Statistical analyses were determined by one-way ANOVA with post-hoc tukey's t-test.

5.4   Discussion

MSC hold notable therapeutic potential and can be isolated from a diverse selection of tissue sources. However, it is currently undetermined whether a pro-vascular secretome is uniform across MSC isolated from different tissue types. We provide novel evidence that human Panc-MSC possess a unique secretome containing vascular regenerative stimuli, primarily packaged into EVs, that demonstrates proangiogenic function when injected into ischemic muscle. These characteristics combined with ease of MSC expansion after cadaveric islet harvest suggests that Panc-MSC CM may serve as a biotherapeutic agent to support vascular regenerative therapy. We demonstrated: 1) Panc-MSC generate a secretome composition distinct to BM-MSC, albeit CM generated by BM MSC also demonstrated pro-vascular functions *in vitro* and *in vivo*; 2) EVs generated by Panc-MSC contained a diverse portfolio of protein cargo that supported the recovery of blood perfusion and stimulated revascularization after im-injection into ischemic murine hindlimbs. Collectively, this study has provided foundational knowledge to further understand proteomic and functional characteristics which may be uniform across MSC from different tissue-types. In addition, we provide proof-of-concept and continuing evidence that the cell-free delivery of MSC biotherapeutics (i.e. MSC CM) may represent a useful tool for applications of regenerative medicine.

We recently characterized the total proteome of human Panc-MSC and conducted a parallel molecular and functional comparison with BM-MSC *in vitro,* demonstrating Panc-MSC were enriched for cell division protein machinery and depleted for proteins involved in lipid metabolism compared to BM-MSC. Panc-MSC also demonstrated phenotypic differences such as reduced ALDH1A3 and CD146 expression and adipogenic competency compared to BM-MSC. Considering, the secretome of both Panc- and BM-MSC harbour pro-vascular stimuli and demonstrated comparable functions *in vitro* and *in vivo*, the phenotypic differences previously reported (i.e. CD146 or ALDH-activity) may not correlate with a pro-vascular secretome [23]. Other MSC subtypes, including adipose-derived MSC, have also demonstrated the secretion of pro-vascular stimuli alongside differential cell surface phenotypes [26]. Whether the production of pro-angiogenic stimuli is a uniform characteristic across tissue specific MSC subtypes

remains to be established. However, fibroblasts from several tissues did not demonstrate pro-vascular effects in a comparable *in vitro* or *in vivo* model [15,27], therefore future studies are warranted.

Extracellular vesicles contain a diverse range of cargo that 'communicate' with a target cells at levels of transcriptional, translational, or directly as ligands to activate target receptors [20]. Panc-MSC generated extracellular vesicles with diverse protein content compared to EV- CM, despite representing <50% of the bulk protein mass secreted. Nonetheless, cargo within Panc-MSC EVs was readily incorporated by HMVEC and stimulated endothelial tubule-formation *in vitro*. Importantly, EV+ CM generated by Panc-MSC accelerated the recovery of hindlimb blood perfusion after femoral artery ligation *in vivo*. We cannot conclude that proteomic stimuli were exclusively responsible for the pro-vascular effects observed in this study. Losordo and colleagues recently demonstrated that human CD34+ hematopoietic progenitors generated exosomes that transfer miR-126-3p to reduce SPRED1 mRNA and increase revascularization in a murine model of hind-limb ischemia [28]. The potential role of miRNA content within Panc-MSC EVs was not assessed in this study. Moreover, several studies have demonstrated secreted MSC signals alter the infiltration hematopoietic cell populations, such as promoting a pro-regenerative M2 macrophage recruitment opposed to pro-inflammatory M1 macrophages [29]. Thus, future studies are needed to investigate the functional role of nucleic acid content within EVs and to elucidate the roles of infiltrating hematopoietic cell populations in angiogenesis. Nonetheless, we demonstrate a relatively uncostly method to concentrate and enrich EVs from MSC in an injectable volume (<100ul). Future work designed to investigate the functional role of protein stimuli that exert pro-vascular benefits in a pre-clinical models of critical limb ischemia are needed.

Utilizing the secretome of vascular regenerative MSC subtypes, we envision the creation of a cell-free biotherapeutic 'tailored' to combat a pathological condition. For instance, stimuli with known pro-regenerative functions were detected in MSC CM and/or exclusively in the EV+ CM fraction. Wnt5a signals through both the canonical and non-canonical signaling pathways to activate pro-angiogenic pathways *in vivo* through

endothelial cells or through M2-polarization of infiltrating monocytes [30,31]. Likewise, VEGF-A, ANGPT1 and POSTN have also demonstrated pro-angiogenic and regenerative function in previous studies [32-34]. Although we did not assess the contribution of individual proteins, or defined protein mixtures detected in EV+ CM to the recovery of hind-limb blood perfusion, this study provides a foundation to explore targetable pathways during MSC expansion to 'tailor' the secretome towards a specific regenerative response. For example, we have recently demonstrated activation of canonical Wnt-signaling during BM-MSC expansion (via GSK3-inhibition) can enhance islet regenerative secretory function *in vivo* [12]. Other studies have demonstrated genetic modification [35] or hypoxic priming [36] may improve the regenerative or proangiogenic functions of MSC respectively. Therefore, our future studies will address whether pharmaceutical or genetic manipulation of specific MSC subtypes can enhance the pro-vascular secretome of MSC to generate therapeutics for vascular regenerative therapies.

In conclusion, this study provides foundational insight to elucidate vascular regenerative potential of MSC-generated CM. Moreover, we further defined the central role of EVs generated by Panc-MSC and conducted two proteomic screens that identified future biological targets. Collectively, vascular regenerative medicine has demonstrated pre-clinical potential to treat macro- and micro-vascular pathologies, however direct cell transplantation has endured several setbacks during translation to clinical studies. Our recent studies suggest regenerative MSC populations may be used as 'biofactories' to generate a cell-free biotherapeutics, although future research is crucial to determine the 'therapeutic ceiling' of these approaches.

5.5 References

1   Caplan, A. I. & Correa, D. The MSC: an injury drugstore. *Cell stem cell* **9**, 11-15 (2011).
2   Caplan, A. I. MSCs: the sentinel and safe-guards of injury. *Journal of cellular physiology* **231**, 1413-1416 (2016).
3   Squillaro, T., Peluso, G. & Galderisi, U. Clinical trials with mesenchymal stem cells: an update. *Cell transplantation* **25**, 829-848 (2016).
4   Bell, G. I. *et al.* Transplanted human bone marrow progenitor subtypes stimulate endogenous islet regeneration and revascularization. *Stem cells and development* **21**, 97-109 (2011).
5   Leibacher, J. & Henschler, R. Biodistribution, migration and homing of systemically applied mesenchymal stem/stromal cells. *Stem Cell Research & Therapy* **7**, 7 (2016).
6   Kumar, S. & Ponnazhagan, S. Bone homing of mesenchymal stem cells by ectopic α4 integrin expression. *The FASEB Journal* **21**, 3917-3927 (2007).
7   Nitzsche, F. *et al.* Concise review: MSC adhesion cascade—insights into homing and transendothelial migration. *Stem Cells* **35**, 1446-1460 (2017).
8   Rombouts, W. & Ploemacher, R. Primary murine MSC show highly efficient homing to the bone marrow but lose homing ability following culture. *Leukemia* **17**, 160 (2003).
9   Martino, M. M. *et al.* Inhibition of IL-1R1/MyD88 signalling promotes mesenchymal stem cell-driven tissue regeneration. *Nature communications* **7**, 11051 (2016).
10   Fiore, D. *et al.* Pharmacological blockage of fibro/adipogenic progenitor expansion and suppression of regenerative fibrogenesis is associated with impaired skeletal muscle regeneration. *Stem cell research* **17**, 161-169 (2016).
11   Hoffmann, J. *et al.* Angiogenic effects despite limited cell survival of bone marrow-derived mesenchymal stem cells under ischemia. *The Thoracic and cardiovascular surgeon* **58**, 136-142 (2010).
12   Kuljanin, M. *et al.* Human multipotent stromal cell secreted effectors accelerate islet regeneration. *Stem Cells* (2019).
13   Kuljanin, M. *et al.* Quantitative Proteomics Evaluation of Human Multipotent Stromal Cell for β Cell Regeneration. *Cell reports* **25**, 2524-2536. e2524 (2018).
14   Soundararajan, M. & Kannan, S. Fibroblasts and mesenchymal stem cells: Two sides of the same coin? *Journal of Cellular Physiology* (2018).
15   Shumakov, V., Onishchenko, N., Rasulov, M., Krasheninnikov, M. & Zaidenov, V. Mesenchymal bone marrow stem cells more effectively stimulate regeneration of deep burn wounds than embryonic fibroblasts. *Bulletin of experimental biology and medicine* **136**, 192-195 (2003).
16   Ballian, N. & Brunicardi, F. C. Islet vasculature as a regulator of endocrine pancreas function. *World journal of surgery* **31**, 705-714 (2007).
17   Konala, V. B. R. *et al.* The current landscape of the mesenchymal stromal cell secretome: a new paradigm for cell-free regeneration. *Cytotherapy* **18**, 13-24 (2016).
18   Kaufman, L. *et al.* in *Plasmonics in Biology and Medicine XVI.* 108940B (International Society for Optics and Photonics).
19   Bian, S. *et al.* Extracellular vesicles derived from human bone marrow mesenchymal stem cells promote angiogenesis in a rat myocardial infarction model. *Journal of molecular medicine* **92**, 387-397 (2014).
20   Andaloussi, S. E., Mäger, I., Breakefield, X. O. & Wood, M. J. Extracellular vesicles: biology and emerging therapeutic opportunities. *Nature reviews Drug discovery* **12**, 347 (2013).
21   Phinney, D. G. *et al.* Mesenchymal stem cells use extracellular vesicles to outsource mitophagy and shuttle microRNAs. *Nature communications* **6**, 8472 (2015).

22   Raposo, G. & Stoorvogel, W. Extracellular vesicles: exosomes, microvesicles, and friends. *J Cell Biol* **200**, 373-383 (2013).

23   Sherman, S. E. *et al.* High aldehyde dehydrogenase activity identifies a subset of human mesenchymal stromal cells with vascular regenerative potential. *Stem Cells* **35**, 1542-1553 (2017).

24   Gomes, J. *et al.* Analytical considerations in nanoscale flow cytometry of extracellular vesicles to achieve data linearity. *Thrombosis and haemostasis* **118**, 1612-1624 (2018).

25   Mulcahy, L. A., Pink, R. C. & Carter, D. R. F. Routes and mechanisms of extracellular vesicle uptake. *Journal of extracellular vesicles* **3**, 24641 (2014).

26   Moon, M. H. *et al.* Human adipose tissue-derived mesenchymal stem cells improve postnatal neovascularization in a mouse model of hindlimb ischemia. *Cellular Physiology and Biochemistry* **17**, 279-290 (2006).

27   Blasi, A. *et al.* Dermal fibroblasts display similar phenotypic and differentiation capacity to fat-derived mesenchymal stem cells, but differ in anti-inflammatory and angiogenic potential. *Vascular cell* **3**, 5 (2011).

28   Mathiyalagan, P. *et al.* Angiogenic mechanisms of human CD34+ stem cell exosomes in the repair of ischemic hindlimb. *Circulation research* **120**, 1466-1476 (2017).

29   Cao, X., Han, Z.-B., Zhao, H. & Liu, Q. Transplantation of mesenchymal stem cells recruits trophic macrophages to induce pancreatic β cell regeneration in diabetic mice. *The international journal of biochemistry & cell biology* **53**, 372-379 (2014).

30   S^{hi}, Y.-N. *et al.* Wnt5a and its signaling pathway in angiogenesis. *Clinica Chimica Acta* **471**, 263-269 (2017).

31   Ekström, E. J. *et al.* WNT5A induces release of exosomes containing pro-angiogenic and immunosuppressive factors from malignant melanoma cells. *Molecular cancer* **13**, 1 (2014).

32   Gerhardt, H. *et al.* VEGF guides angiogenic sprouting utilizing endothelial tip cell filopodia. *The Journal of cell biology* **161**, 1163-1177 (2003).

33   Fiedler, U. & Augustin, H. G. Angiopoietins: a link between angiogenesis and inflammation. *Trends in immunology* **27**, 552-558 (2006).

34   Siriwardena, B. *et al.* Periostin is frequently overexpressed and enhances invasion and angiogenesis in oral cancer. *British journal of cancer* **95**, 1396 (2006).

35   Zhang, J., Zheng, G., Wu, L., Ou Yang, L. & Li, W. Bone marrow mesenchymal stem cells overexpressing human basic fibroblast growth factor increase vasculogenesis in ischemic rats. *Brazilian Journal of Medical and Biological Research* **47**, 886-894 (2014).

36   Liu, J. *et al.* Hypoxia pretreatment of bone marrow mesenchymal stem cells facilitates angiogenesis by improving the function of endothelial cells in diabetic rats with lower ischemia. *PLoS One* **10**, e0126715 (2015).

37   Cooper, T. T. J., MA; Jose, Shauna E; Lajoie, Giles A; Hess, David A. Proteome of Human Multipotent Stromal Cells Derived from Pancreatic Islets. *Under Review* **TBD** (2019).

38   Kuljanin, M., Bell, G. I., Sherman, S. E., Lajoie, G. A. & Hess, D. A. Proteomic characterisation reveals active Wnt-signalling by human multipotent stromal cells as a key regulator of β cell survival and proliferation. *Diabetologia* **60**, 1987-1998 (2017).

39   Cooper, T. T. *et al.* Inhibition of Aldehyde Dehydrogenase-Activity Expands Multipotent Myeloid Progenitor Cells with Vascular Regenerative Function. *Stem Cells* **36**, 723-736 (2018).

Chapter 6

6   Pancreatic MSC secrete islet regenerative stimuli*

*This chapter was primarily incorporated to supplement Chapters 4 and 5 as foundational evidence to 1) establish a common multifaceted secretome across MSC populations 2) demonstrate the therapeutic potential of cell-free biotherapeutics for complex tissue regeneration. Additionally, this chapter provides preliminary experimental evidence to establish discussion points in Chapter 7.

6.1   Introduction

We have recently demonstrated that the secretome of BM-MSC harbours bioactive stimuli capable of supporting beta-cell proliferation and survival *in vitro*[1]. Notably, intrapancreatic (iPan) injection of concentrated BM-MSC CM stimulated complex islet regenerative programs, including characteristic consistent with the induction of islet neogenesis, increased β-cell proliferation, and accelerated *β*-cell maturation in STZ-induced hyperglycemic NOD/SCID mice[2]. Currently, we are utilizing this reproduceable injection platform combined with thorough secretome analyses to identify stimuli that mediate islet regenerative processes in pre-clinical models which may be translated to human application for diabetes treatment[2,3]. To this end, mass spectrometry-based analyses of BM-MSC revealed active canonical Wnt-signaling was a conserved characteristic of islet-regenerative BM-MSC that significantly lowered hyperglycemia following intravenous cell transplantation[3]. Inhibition of GSK3 activity (CHIR99021), resulting in the stabilization of β-catenin during *ex vivo* cell expansion led to enrichment of islet regenerative effectors in the secretome of BM-MSC that could be injected as a cell-free biotherapeutic to reverse hyperglycemia in NOD/SCID mice. Taken together, these studies suggested that 1) the secretome of MSC may determine islet regenerative functions *in vivo* and 2) cell-biotherapeutics can be 'tailored' to enhance the induction of islet regenerative programs.

Considering Panc-MSC are derived from the islet microenvironment, I hypothesized that Panc-MSC will generate a secretome that demonstrates islet regenerative function after

direct iPan-delivery. In chapter 6, I present functional evidence that the Panc-MSC secretome of also capable of inducing islet recovery and reducing STZ-treated hyperglycemic mice, similar to BM-MSC. The knowledge acquired within this chapter will serve as preliminary proof-of-concept for future studies aiming to utilize the secteome of Panc-MSC as a cell-free biotherapeutic for the treatment of diabetes.

6.2   Methods

6.2.1   BM-MSC and Panc-MSC Isolation and Culture

BM-MSC:

Human BM aspirates were obtained from healthy donors with informed consent from the London Health Sciences Centre (London, ON). BM-MSC were established and cultured in Amniomax-C100 media + C100 supplement (Life Technologies) as previously described in Chapter 4.

Panc-MSC:

Ricordi-chamber isolated human islets were obtained through the Integrated Islet Distribution Program (IIDP) funded by the National Institute of Diabetes and Digestive and Kidney Diseases (NIDDK). Panc-MSC were established by plastic adherence during islet suspension cultures and expanded in Amniomax-C100 media + supplement as previously described in Chapter 4.

6.2.2   Enrichment of EVs from Panc-MSC CM

Conditioned media (CM) was generated by culturing BM-MSC and Panc-MSC to ~80% confluency, rinsed twice with pre-warmed PBS, switched to basal Aminomax C100 media without supplement and media was collected after 24-hours culture. CM was subsequently processed in one of three ways (Supplemental Figure 2). 1) Cell-free CM was concentrated (~20-fold by volume) by centrifugation in 3kDa centrifuge filter unit for 45 minutes at 2800g. This fraction contained both EVs and soluble proteins >3kDa and is referred to as bulk CM. 2) Cell-free CM was concentrated in 100kDa centrifuge filter units for 20 minutes at 2800g. This fraction (EV+) was enriched with EVs and

proteins complexes larger than 100kDa This fraction was referred to as EV$^+$ CM or EV$^-$ enriched CM. 3) CM which passed through the 100kDA filter was centrifuged in 3kDA centrifuge filter units for 40 minutes at 2800g to concentrate soluble proteins between >3kDa and <100kDA size. This fraction was referred to as EV$^-$ CM or EV-depleted CM (also see Chapter 5 Methods).

6.2.3 Intrapancreatic or Intravenous Transplantation of Panc-MSC in hyperglycemic NOD/SCID mice

Pancreatic β-cell ablation was induced in NOD/SCID mice aged 8- to 10-weeks by intraperitoneal injection of STZ (35 mg/kg/ day) for 5 consecutive days. All animal procedures were approved by the Animal Care Committee at Western University Canada (AUP 2015-033). On day 10, hyperglycemic (15–25 mM) mice were sublethally irradiated (300 cGy) prior to intrapancreatic transplantation of 5.0x10^5 Panc-MSC (20μl). Alternatively, 5.0x10^5 Panc-MSC were intravenously infused within 500ul of Basal Aminomax C-100 via tail vein injection. Equal volumes of Basal Aminomax C-100 were used as vehicle control for both injection modalities. Systemic blood glycemic levels were monitored in a blinded fashion weekly for 42 days.

6.2.4 Intrapancreatic or Intravenous Injection of MSC-derived CM in hyperglycemic NOD/SCID mice

Hyperglycemic NOD/SCID mice, generated as described above were transplanted on day 10 by intrapancreatic or intravenous injection of MSC-derived CM fractions. Specifically, hyperglycemic mice received a single intrapancreatic injection of bulk, EV$^+$, EV$^-$ CM (6μg total protein in 20ul) derived from Panc-MSC or bulk CM (6μg total protein 20µl) derived from BM-MSC. In addition, STZ-treated NOD/SCID mice received i.v. injection of 100μg total protein of Panc-MSC CM via the tail vein, as described above. Equal volumes of Basal Aminomax C-100 were used as vehicle control for both routes of CM injection. Systemic blood glycemic levels were monitored in a blinded fashion weekly for 42 days.

6.3 Results

6.3.1 Intravenous or intrapancreatic transplantation of Panc-MSC did not reduce hyperglycemia in STZ-treated mice

We have previously demonstrated that BM-MSC can lower hyperglycemia and stimulate islet regeneration when infused into the systemic circulation[4-6]. However, regenerative functions were variable and donor specific. Furthermore, direct intrapancreatic - transplantation of islet-regenerative UCB ALDH^{hi} cells augmented the reduction in hyperglycemia[7], compared to intravenous transplantation. Therefore, I sought to investigate if Panc-MSC could stimulate islet regeneration following intravenous infusion or after intrapancreatic transplantation. Accordingly, we demonstrated that neither intravenous or intrapancreatic transplantation of Panc-MSC reduced hyperglycemia in STZ-treated NOD/SCID mice (Figure 6.1), compared to mice injected with vehicle control.
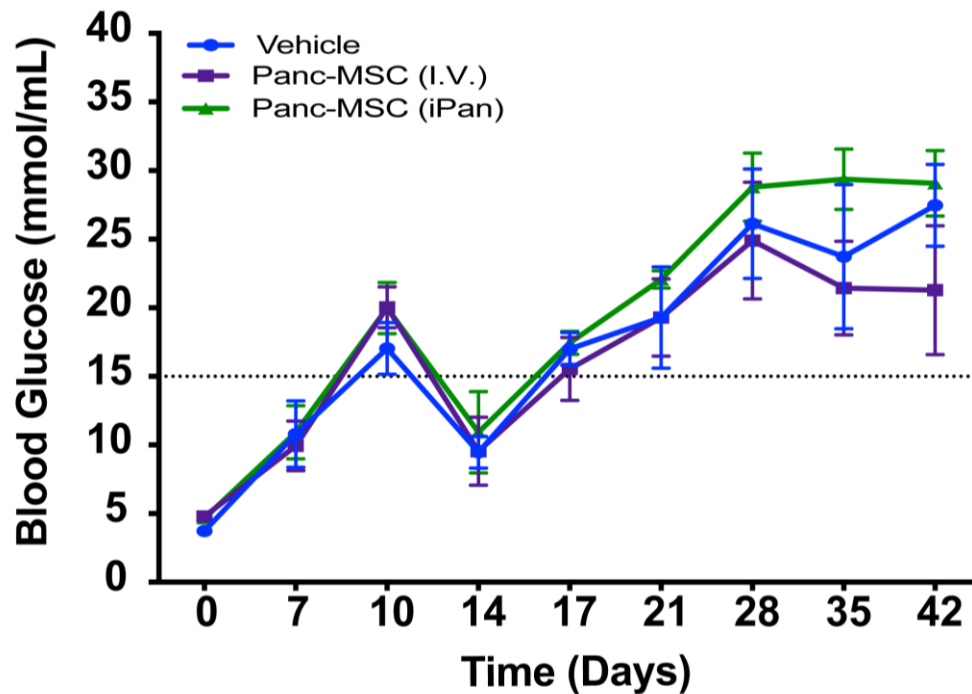
Figure 6.1 Intravenous or Intrapancreatic-injection does not reduce hyperglycemia in STZ-treated NOD/SCID mice. 8-10-week-old NOD/SCID mice were injected with STZ days 0-5 to induce β-cell ablation. On day 10, hyperglycemic mice (>15mmol/mL) received 5.0×10^5 Panc-MSC by either intravenous (i.v.) infusion or intrapancreatic (iPan) transplantation. Basal Aminomax C-100 was injected as vehicle control. (A) i.v. or iPan transplantation of Panc-MSC did not significantly reduce blood glucose levels in NOD/SCID mice, compared to vehicle injected control mice. Data represented as Mean + SEM (n=3-4 mice per group). Statistical analyses were performed by two-way ANOVA with Tukey's post-hoc test.

6.3.2 Panc-MSC CM reduced hyperglycemia in STZ-treated NOD/SCID mice after intrapancreatic-injection but not after intravenous injection

STZ-treated mice injected with concentrated CM generated by BM-MSC demonstrated reduced hyperglycemia via the stimulation of potent islet regenerative and islet neogenic programs following direct injection into the pancreas[2]. However, it has yet to be determined if the intravenous infusion of CM generated by MSC could similarly stimulate islet regeneration. Accordingly, I sought to determine if 1) intrapancreatic injection of Panc-MSC CM could stimulate islet regeneration similar to BM-MSC and 2) if intravenous infusion of Panc-MSC CM via tail-vein injection could stimulate islet regeneration in hyperglycemic NOD/SCID mice.

First, I injected hyperglycemic mice with CM (3 or 6μg total protein) generated by BM-MSC or Panc-MSC. To serve as a vehicle control, non-conditioned media was iPan injection. Compared to vehicle control, $6\mu g$ CM generated by both BM-MSC and Panc-MSC significantly reduced (*p<0.05) hyperglycemia in STZ-treated NOD/SCID mice (Figure 6.2). In contrast, 3μg of BM-MSC or Panc-MSC CM did not reduce hyperglycemia *in vivo*, compared to vehicle control. To assess whether secreted stimuli could induce murine islet from distant sites, I tested whether tail vein-injection of 100μg total protein of Panc-MSC CM could reduce hyperglycemic in STZ-treated mice. Compared to vehicle control, intravenous-infusion of Panc-MSC CM did not significantly decrease hyperglycemia *in vivo* (Figure 6.3). Collectively, I demonstrated CM generated by Panc-MSC reduced hyperglycemia in NOD/SCID mice, albeit direct injection into the pancreas was required.

A
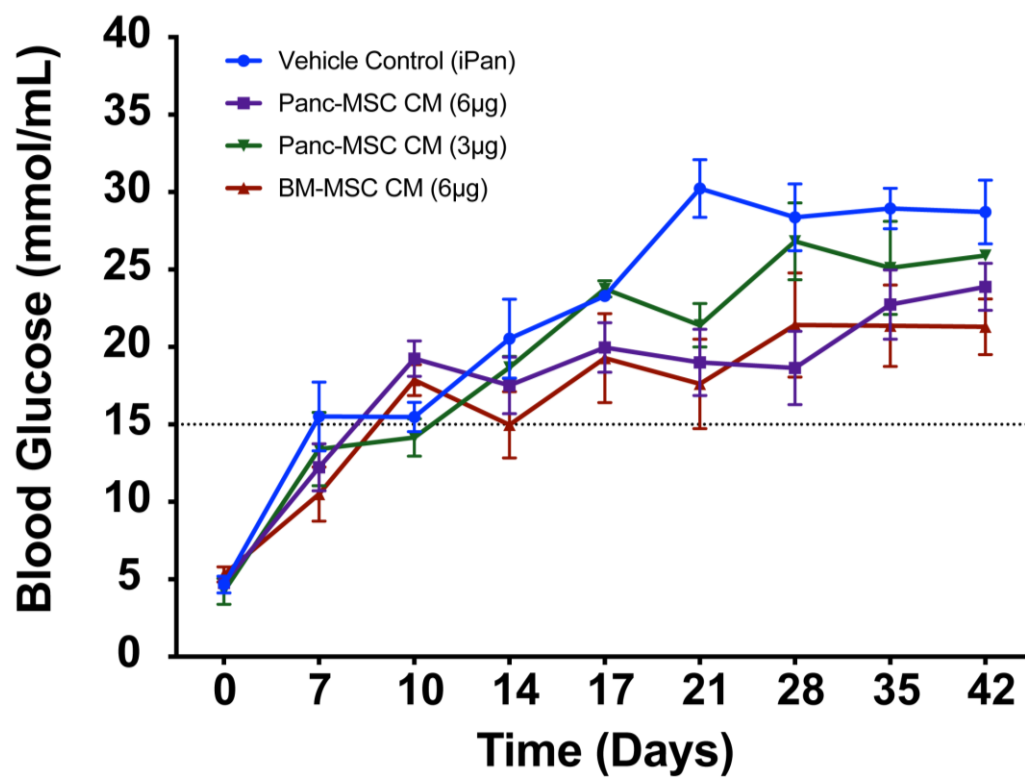
B
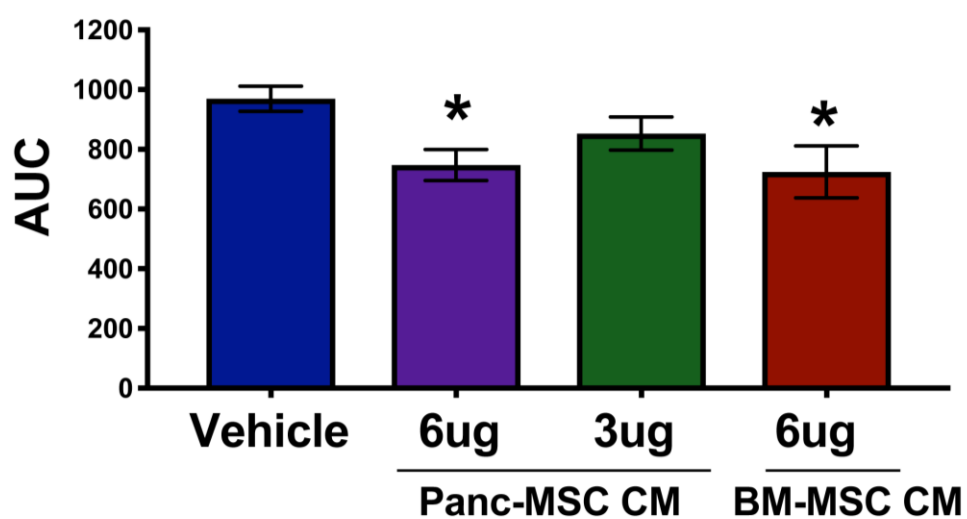
Figure 6.2 Intrapancreatic injection of MSC-derived CM reduced resting blood glucose levels in STZ-treated NOD/SCID mice. 8-10-week-old NOD/SCID mice were rendered hyperglycemic by STZ-induced β-cell ablation between days 0-5. On day 10, hyperglycemic mice (>15mmol/mL blood glucose) received 3 or 6**μ**g of Panc-MSC or BM-MSC derived CM. Basal Aminomax C-100 served as vehicle control. (A) Collectively, iPan transplantation of 6ug CM derived from Panc-MSC or BM-MSC significantly reduced resting blood glucose levels, (B) as measured by area under the curve (AUC). Conversely, 3μg of Panc-MSC CM did not demonstrate hyperglycemic reduction. Data represented as Mean +/- SEM (n=5-8). Statistical analyses performed by one-way ANOVA with post-hoc Tukey's t test (*p<0.05).
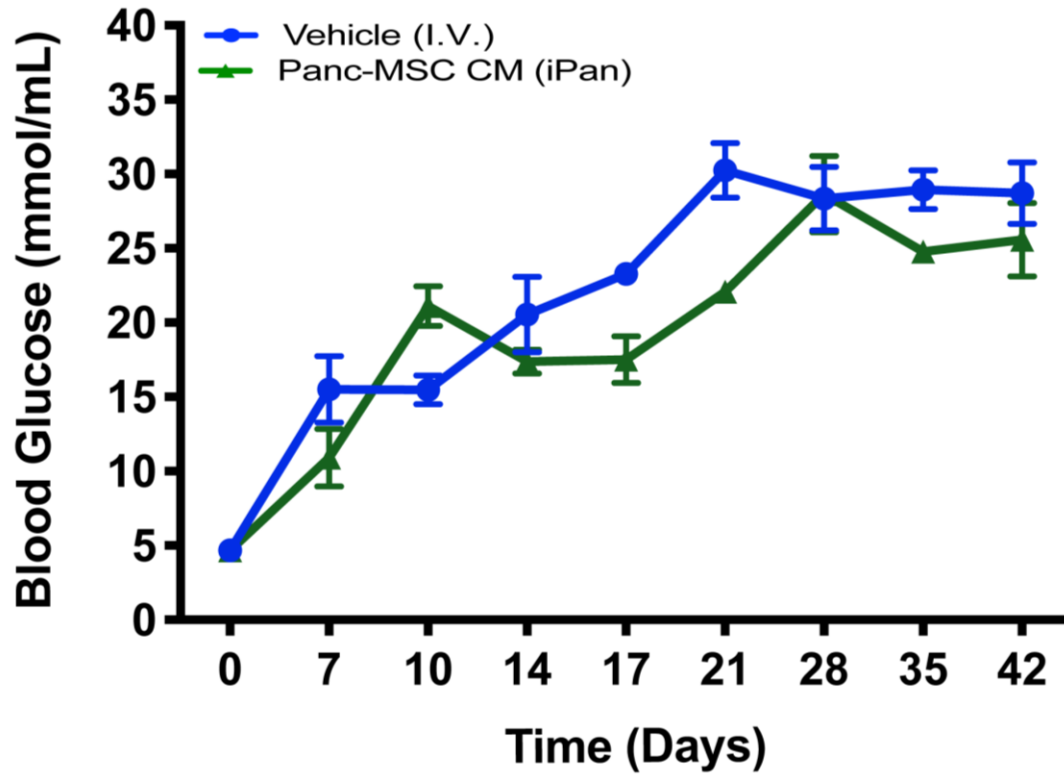
Figure 6.3 Intravenous infusion of Panc-MSC CM did not reduce hyperglycemia in STZ-treated NOD/SCID mice. 8-10-week-old NOD/SCID mice were treated with STZ for 5 consecutive days to induce β-cell ablation between days 0-5. On day 10, hyperglycemic mice (>15mmol/mL blood glucose) received 100ug total protein of Panc-MSC by either intravenous (i.v.) infusion. 500μl of basal Aminomax C-100 served as vehicle control. (A) i.v. infusion of Panc-MSC CM did not significantly reduce resting blood glucose levels in NOD/SCID mice, compared to vehicle control. Data represented as Mean + SEM (n=3-4 mice / group). Statistical analyses were performed by one-way ANOVA with Tukey's post-hoc test.

6.3.3　Islet regenerative stimuli are haboured throughout the secretome of Panc-MSC

In Chapter 5, I demonstrated that EVs generated by Panc-MSC contained pro-angiogenic stimuli able to stimulate the recovery of hindlimb blood perfusion in mice with femoral artery ligation induced hindlimb ischemia. To investigate the role of Panc-MSC secreted EVs in islet regeneration, EV^+ and EV^- CM was generated in a similar fashion as described in Chapter 5. Interestingly, intrapancreatic injection of both the EV^+ and EV^- CM fractions reduced hyperglycemia in NOD/SCID mice compared to vehicle control and the extent of hyperglycemia reduction was comparable after EV^+ and EV^- CM injection, suggesting islet regenerative stimuli were found in the soluble fraction of the Panc-MSC secretome and in EV-bound vesicles secreted by Panc-MSC.
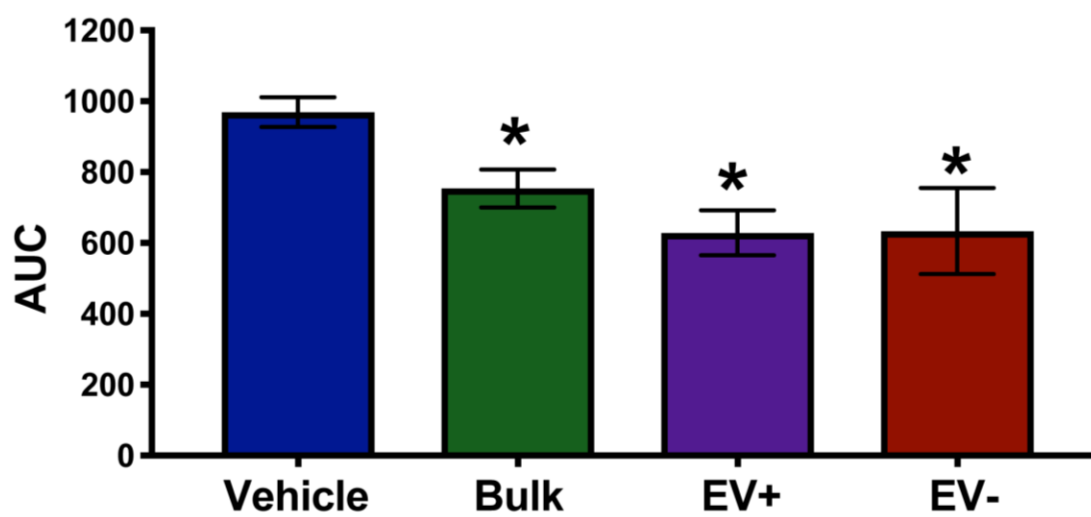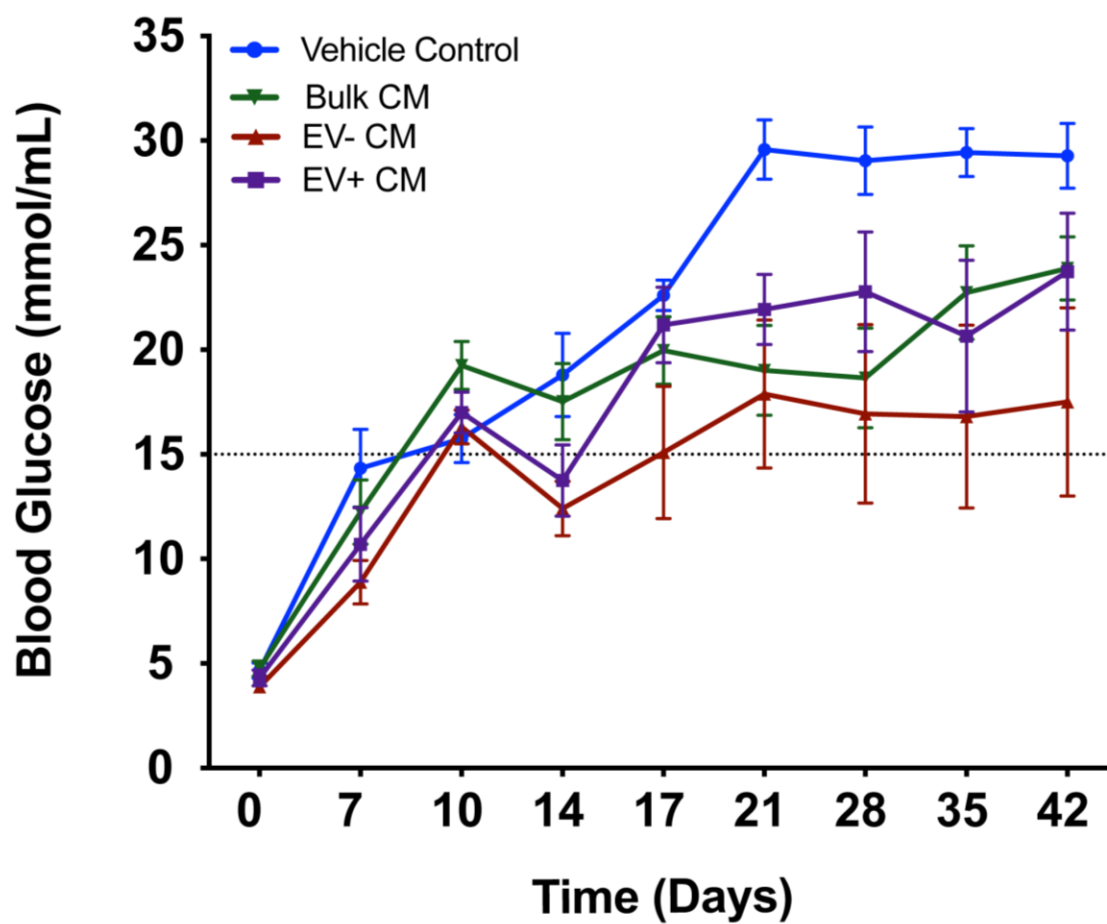
Figure 6.4 Islet regenerative stimuli contained in the soluble and EV+ fractions generated by Panc-MSC. 8-10-week-old NOD/SCID mice were rendered hyperglycemic by STZ-induced β-cell ablation between days 0-5. On day 10, hyperglycemic mice (>15mmol/mL blood glucose) received iPan-injection of 6ug EV⁻ CM or EV⁺ CM generated by Panc-MSC. Basal Aminomax C-100 served as vehicle control. (A) Collectively, iPan transplantation of both EV- and EV+ CM was able to significantly reduce resting blood glucose levels, (B) as measured by area under the curve (AUC). Conversely, iPan-injection of 3ug of Panc-MSC CM did not induce hyperglycemia reduction. Data represented as Mean +/- SEM (n=4-8 mice per group). Statistical analyses were performed by one-way ANOVA with post-hoc Tukey's t test. (*p<0.05).

6.4 Discussion

Endogenous regeneration of β-cells may hold the promise of providing sustained glucose control without exogenous insulin in patients with diabetes[8-10]. We have previously shown to islet regeneration could occur in response to the direct injection of BM-MSC CM[2]. Using an alternative source, we predicted Panc-MSC may provide a 'fine-tuned' secretome for islet regeneration, albeit islet regenerative stimuli could also be a conserved characteristic 'common' to the secretome MSC populations from different tissue sources. Herein, I provide preliminary evidence that islet regenerative stimuli are contained within both BM-MSC and Panc-MSC CM with comparable capacity to reduce hyperglycemia in STZ-treated NOD/SCID mice. Thus, these data suggest that secretion of pro-regenerative stimuli may be a shared characteristic across different MSC from different tissue sources.

Furthermore, I demonstrated islet regenerative stimuli were contained within both EV+ and EV- CM fractions of the Panc-MSC secretome. Further studies are needed to elucidate specific stimuli contained within either fraction, or whether similar regenerative proteins were present in both EV^+ and EV^- CM. Conversely, it remains possible that EV^- and EV^+ CM contain unique stimuli which activate a common regenerative mechanism. In addition to proteins, EVs may also contain nucleic acid or lipid effectors that can influence recipient cell populations (Figure 1.11). Losordo and colleagues demonstrated that EVs isolated from $CD34^+$ HPC could activate VEGF pathways in recipient endothelial cells through the transfer of miRNA that repressed translation of VEGF-pathway inhibitors[11]. Collectively, future studies will need to characterize a vast array of stimuli collectively responsible for the activation of biological pathways in recipient cells.

Nonetheless, islet regeneration only occurred when stimuli generated by Panc-MSC were delivered directly to the site of injury (intravenous versus intrapancreatic) at a high therapeutic dose (3μg versus 6μg). The results highlight the generation of a "therapeutic islet microenvironment" that may tip the balance in favour of regeneration versus inflammation and destruction[12-14]. In continuation with Chapter 4 and 5, Chapter 6

supports the thesis that Panc-MSC generate a multifaceted secretome with potential as a cell-free biotherapeutic. This work will lead us to better unravel the mechanisms of islet regeneration using transgenic model systems to identify activated cell populations resident within the pancreas, discussed below.

6.5   References

1   Kuljanin, M., Bell, G. I., Sherman, S. E., Lajoie, G. A. & Hess, D. A. Proteomic characterisation reveals active Wnt-signalling by human multipotent stromal cells as a key regulator of β cell survival and proliferation. *Diabetologia* **60**, 1987-1998 (2017).

2   Kuljanin, M. *et al.* Human multipotent stromal cell secreted effectors accelerate islet regeneration. *Stem Cells* (2019).

3   Kuljanin, M. *et al.* Quantitative Proteomics Evaluation of Human Multipotent Stromal Cell for β Cell Regeneration. *Cell reports* **25**, 2524-2536. e2524 (2018).

4   Hess, D. *et al.* Bone marrow–derived stem cells initiate pancreatic regeneration. *Nature biotechnology* **21**, 763 (2003).

5   Bell, G. I. *et al.* Combinatorial human progenitor cell transplantation optimizes islet regeneration through secretion of paracrine factors. *Stem cells and development* **21**, 1863-1876 (2012).

6   Bell, G. I. *et al.* Transplanted human bone marrow progenitor subtypes stimulate endogenous islet regeneration and revascularization. *Stem cells and development* **21**, 97-109 (2011).

7   Bell, G., Putman, D., Hughes-Large, J. & Hess, D. Intrapancreatic delivery of human umbilical cord blood aldehyde dehydrogenase-producing cells promotes islet regeneration. *Diabetologia* **55**, 1755-1760 (2012).

8   Zhou, Q. & Melton, D. A. Pancreas regeneration. *Nature* **557**, 351 (2018).

9   Murtaugh, L. C. & Keefe, M. D. Regeneration and repair of the exocrine pancreas. *Annual review of physiology* **77**, 229-249 (2015).

10   Aguayo-Mazzucato, C. & Bonner-Weir, S. Pancreatic β cell regeneration as a possible therapy for diabetes. *Cell metabolism* **27**, 57-67 (2018).

11   Mathiyalagan, P. *et al.* Angiogenic mechanisms of human CD34+ stem cell exosomes in the repair of ischemic hindlimb. *Circulation research* **120**, 1466-1476 (2017).

12   DeCarolis, N. A., Kirby, E. D., Wyss-Coray, T. & Palmer, T. D. The role of the microenvironmental niche in declining stem-cell functions associated with biological aging. *Cold Spring Harbor perspectives in medicine* **5**, a025874 (2015).

13   Brissova, M. *et al.* Islet microenvironment, modulated by vascular endothelial growth factor-A signaling, promotes β cell regeneration. *Cell metabolism* **19**, 498-511 (2014).

14   Huang, Y.-C., Leung, V. Y., Lu, W. W. & Luk, K. D. The effects of microenvironment in mesenchymal stem cell–based regeneration of intervertebral disc. *The Spine Journal* **13**, 352-362 (2013).

Chapter 7

7   Summary of Objectives

The global objective of this thesis was to investigate scalable biotherapeutic approaches of regenerative medicine utilizing post-natal progenitor cells to stimulate endogenous islet regeneration and/or revascularization of ischemic tissue. In Chapters 2 and 3, I focused on enhancing the *ex vivo* expansion of human UCB ALDH[hi] hematopoietic cell progeny that retain vascular and islet regenerative functions after transplantation. Furthermore, I provide the first comprehensive proteomic and regenerative function analyses of human Panc-MSC (Chapter 4) demonstrating extracellular vesicles generated by Panc-MSC harbor vascular (Chapter 5) and islet regenerative protein cargo (Chapter 6). Below, I briefly summarize the significant findings of each chapter to highlight the contributions of this work to the field of regenerative medicine and to outline intellectual and technical limitations encountered throughout these studies. Subsequently, I propose future experimentation required to further refine the breadth of knowledge obtained within this thesis. Finally, I will discuss the implications of these findings, with specific focus on regenerative medicine strategies to treat diabetes and related cardiovascular pathologies.

7.1   Summary of Findings

In chapter 2, I determined that expanded hematopoietic progeny from UCB ALDH^{hi} cells retained a characteristic of pro-angiogenic secretome, despite reduced capacity to stimulate angiogenesis *in vivo*. Moreover, I discovered that UCB ALDH^{hi} cells will primarily differentiate towards the megakaryocyte lineage during expansion as primitive progenitor cell phenotype is diminished *in vitro*. Accordingly, I demonstrated that preventing HPC differentiation by temporally inhibition of RA-production (via DEAB-treatment) enhanced the expansion of hematopoietic progeny retaining primitive phenotype *in vitro* and vascular regenerative function *in vivo* (**Figure 7.1**). Mass spectrometry analyses suggested the inhibition of ALDH-activity enriched the proteome of expanded HPC with a pro-survival signature which coincided with improved cell engraftment. In chapter 3, I sought to determine if expanded hematopoietic progeny reselected for high ALDH-activity (ALDH^{hi}) after DEAB-treatment culture conditions retained islet regenerative function, analogous to freshly-isolated UCB ALDH^{hi} cells. Surprisingly, only ALDH^{lo} cells reselected after culture demonstrated islet regenerative stimuli, despite ALDH^{hi} cells retaining progenitor cell characteristics. DEAB-treated ALDH^{lo} cells were significantly enriched for cells of the megakaryocyte-lineage, albeit the mature hematopoietic cell marker CD38 was significantly reduced.

UCB ALDH^hi cells
- <5% of total UCB Lin- cells
- Enriched with CD34+/CD38- hematopoietic progenitors
- >25% Lin- ALDH^hi cells expressed CD41 (megkaryocyte-lineage)
- Vascular regenerative function *in vivo*
- Islet regenerative function *in vivo*

X-vivo15 (TPO, FLT-3L, SCF)

10µM DEAB + X-vivo15 (TPO, FLT-3L, SCF)

9-day UCB ALDH^hi cell Expansion (DEAB-treated Conditions)
- >70-fold increase total cell number *ex vivo*
- ~5-fold enrichment of ALDH^hi cells
- ~10-fold increase in ALDH^hi/CD34+/CD38- Progenitor Cells
- ~80% of bulk cells expressed CD41 (megkaryocyte-lineage)
- Expanded cells retained islet and vascular regenerative functions *in vivo*
- Islet regenerative function is mediated by ALDH^lo cells (~60% CD41+/ CD42+ megkaryocytes)

9-day UCB ALDH^hi cell Expansion (Basal Conditions)
- >70-fold increase total cell number *ex vivo*
- <10% of expanded cells that retained high ALDH-activity
- ~5-fold increase in ALDH^hi/CD34+/CD38- Progenitor Cells
- >60% of Bulk cells express CD41 (megkaryocyte-lineage)
- Expanded cells fail to stimulate vascular or islet regeneration *in vivo*

Figure 7.1 Inhibition of Retinoic Acid Production Enhances the Expansion of Hematopoietic Progeny with Multifaceted Regenerative Functions.

In chapter 4, I characterized the proteome on an understudied MSC population from human pancreatic tissue, Panc-MSC (**Figure 7.2**). In this study, I conducted a direct comparison of Panc-MSC versus BM-MSC using mass spectrometry, flow cytometry, and functional differentiation assays *in vitro*. The proteome of Panc-MSC was enriched with increased pro-mitotic protein expression, coinciding with accelerated growth kinetics *in vitro*. Adipogenic pathways were restricted within Panc-MSC, whereas the proteome of BM-MSC was 'primed' for adipogenic differentiation, lipid metabolism, and RA-induced differentiation. Nonetheless, I detected 15 differentially expressed CD markers between Panc- and BM-MSC as candidates for future investigation to reduce the heterogeneity of potentially therapeutic MSC subpopulations based on surface marker expression (i.e. $CD146^+$ versus $CD146^-$ Panc-MSC). In Chapter 5 and 6, I demonstrated the secretome of Panc-MSC was enriched for pro-regenerative stimuli capable of promoting vascular or islet regeneration *in vivo*. Furthermore, extracellular vesicle protein content of Panc-MSC proved pro-regenerative and provided a foundation for the development of cell-free biotherapeutics employing Panc-MSC as mini 'bio-factories' for regenerative medicine applications.

Vascular Regeneration by Panc-MSC CM
- The recovery of vascular networks and blood perfusion in murine models of hindlimb ischemia stimulated by the intramuscular injection of Panc-MSC CM

β-cell Regeneration by Panc-MSC CM
- The recovery of islet cell mass and reduced hypeglycemia in NOD/SCID mice can be stimulated by the intrapancreatic injection of Panc-MSC CM

Pancreatic-MSC
- Express a classic MSC profile (i.e CD90+/CD73+/CD105+/CD45-/CD31-)
- Demonstrate robust growth kinetics driven by a pro-mitotic proteome
- Restricted capacity to differentiate in response to pro-adipogenic stimuli
- Competency to pro-neural stimuli
- Robust Vimentin and Nestin expression
- Diminished ALDH-activity and CD146 expression

Figure 7.2 Human Pancreas-derived Multipotent Stromal Cells Secrete Multifaceted Pro-Regenerative Stimuli.

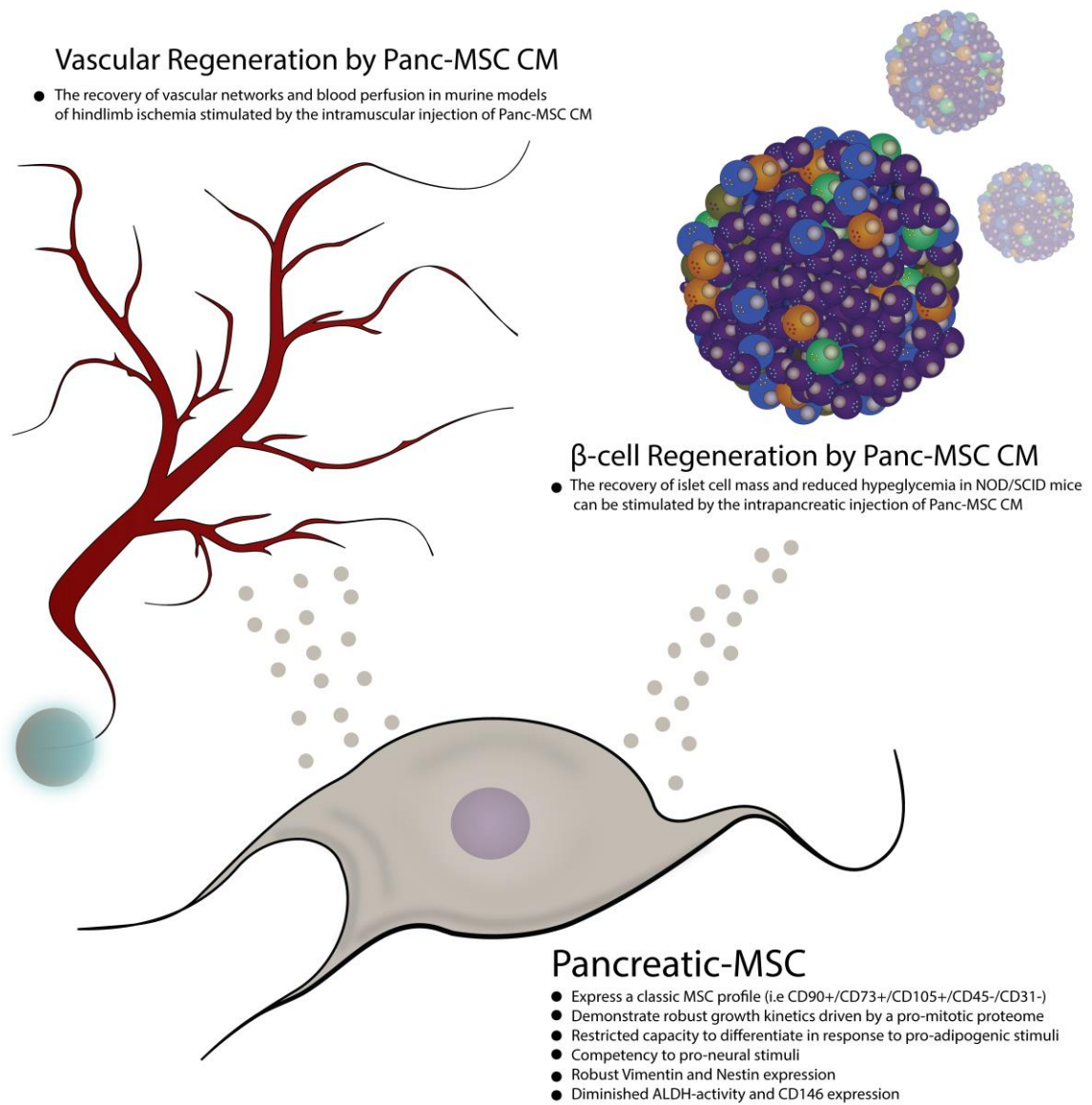In summary, I have demonstrated human HPC and MSC possess multifaceted therapeutic functions in murine models of vascular or islet regeneration. Unfortunately, previous clinical use of autologous therapeutic cell populations has led to modest efficacy in patients with critical limb ischemia presumably limited by poor cell engraftment in the ischemic limb post-transplantation and/or a diminished pro-regenerative secretome following extensive expansion *ex vivo*. Thus, allogenic cell sources such as healthy BM or UCB combined with cell-free biotherapeutic approaches may help circumvent many of the limitations of autologous cell transplantation. Further understanding of central regenerative pathways and functional synergies through future research is warranted. Towards this end, improving the capacity to expand therapeutic cell populations while retaining regenerative secretory function is essential to refining our current regenerative medicine approaches for treating diabetes and cardiovascular comorbidities.

7.1.1   Limitations of Progenitor Cell Isolation and Hematopoietic Cell Expansion

In chapter 2 and 3, I isolated and expanded ALDH^{hi} cells from UCB mononuclear cell samples in serum-free conditions supplemented with TPO, FLT-3L, SCF. Leading up to transplantation, several notable limitations were encountered with UCB ALDH^{hi} cell expansion. Firstly, lineage-depletion of UCB samples was achieved with a tetrameric antibody system that binds multiple mature hematopoietic cell surface markers and allows for depletion of mature cell populations during mononuclear cell isolation. After I discovered that expanded ALDH^{hi} cells preferentially differentiate towards the megakaryocyte lineage, it was established this methodology did not deplete cells of the megakaryocyte lineage using an antibody for CD41 or CD42. At the time of this study, the initial enrichment of Lin- cells may have biased UCB ALDH^{hi} cells towards megakaryopoiesis by indirectly enriching for cells expressing these megakaryocyte-lineage markers. This limitation can easily be addressed in future studies by performing a secondary depletion of CD41+ cells during FACS or simply using current lineage-depletion kits that include depletion of CD41+ cells.

Paradoxically, TPO is a known driver of megakaryopoiesis[1,2] and through pleiotropic functions is also required for maintenance for human HSC pool[3,4]. Furthermore, HPC express the thrombopoietin receptor Mpl, and can be directed to a megkaryocyte fate when cultured with TPO *in vitro*4. I demonstrate in chapters 2 and 3 that exogenous TPO drives UCB ALDH[hi] cell expansion, albeit at the cost of progenitor cell differentiation (Figure 7.3). Developing megakaryocytes also secrete additional factors that further promote progenitor cell differentiation *in vitro*. Given that UCB ALDH^{hi} cells are enriched with megakaryocyte-precursors and culture under conditions supplemented with known drivers of megakaryopoiesis, the outcome of HPC expansion observed in this study were likely predisposed by the aforementioned factors. Future studies will need to individually address the influence of Lin- selection and culture conditions utilized for the expansion of therapeutic ALDH^{hi} cells.

Throughout this thesis, *ex vivo* expansion of UCB ALDH[hi] cell was performed in static suspension culture and bulk media changes were performed every 3 days. Integration of additional technologies, such as real-time bioreactor expansion chambers developed by Zandstra and colleagues[5-8], is expected to further enhance the expansion therapeutic HPC by permitting a dynamic and control of culture conditions. Nevertheless, knowledge acquired within this study provides insight towards targetable pathways that further enhance the expansion of therapeutic HPC for applications of regenerative medicine.
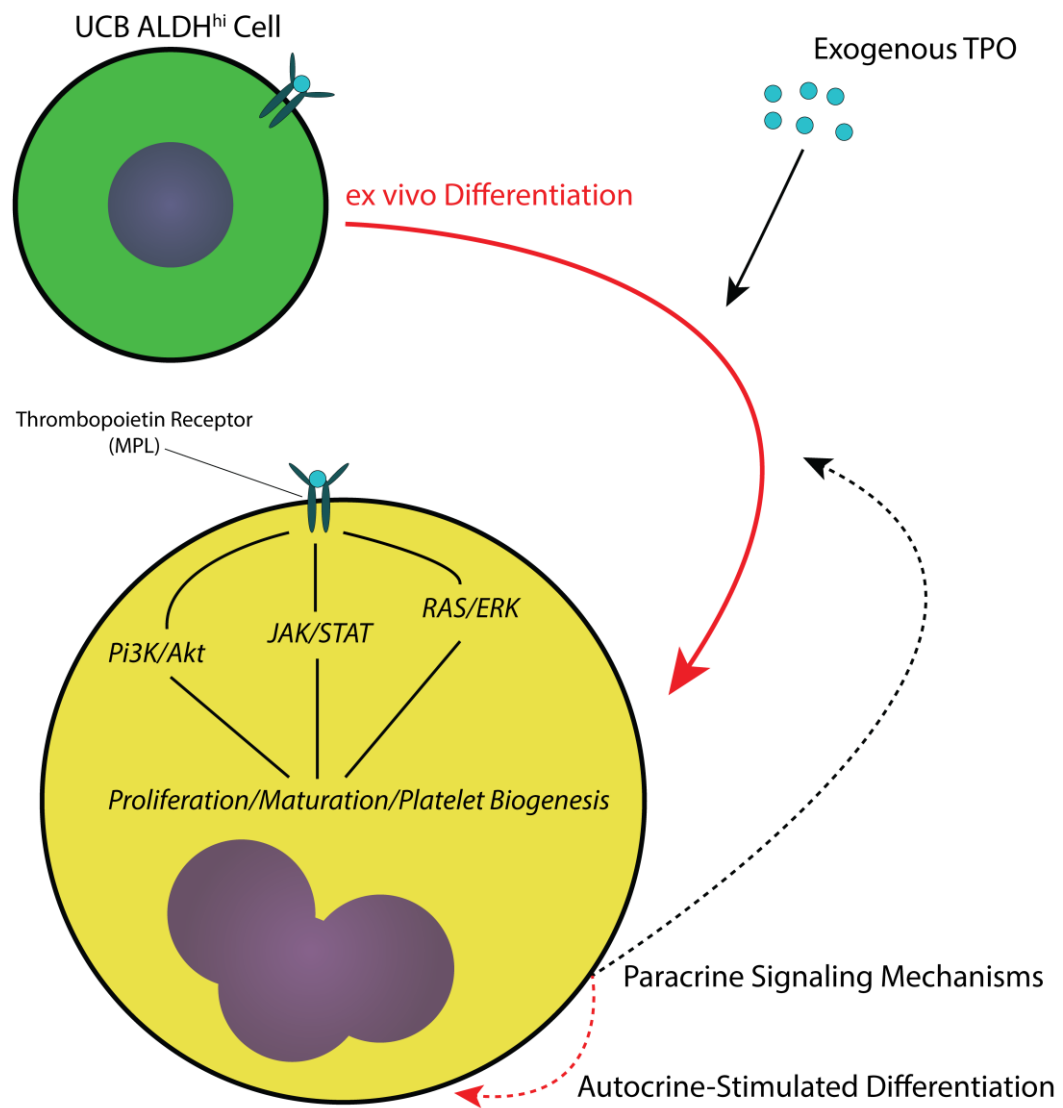
Figure 7.3 UCB ALDH^{hi} cell Expansion and Differentiation is Paradoxically driven by TPO.

7.1.2 Elucidating the Complexity of ALDH-activity and Retinoic Acid Signaling Pathways

Retinoic acid signaling exerts regulatory functions through the complex network of upstream cytosolic effectors and nuclear receptors[9-12], each containing distinct and redundant isoforms. For example, genetic deletion of ALDH1A1 within transgenic mice is rescued by increased ALDH1A3 expression and leads to normal fetal and adult hematopoiesis[13]. An intellectual limitation encountered in chapter 2 was we did not directly quantify the abundance of individual ALDH isoforms which contribute to cannonical RA-signaling. Instead, we measured ALDH-activity using Aldefluor[TM] substrate which acts as a substrate for multiple ALDH isoforms. ALDH-activity is also regulated through post-translation modifications, such as acetylation or deacetylation. Thus, further quantification of specific ALDH isoforms will be needed to support future studies utilizing Aldefluor[TM]. Furthermore, ALDH-activity also measures a regulatory function independent of RA-production, including the reduction of ROS production and detoxification of reactive aldehydes[14]. DEAB-inhibition in chapters 2 and 3 inhibits several isoforms of ALDH[15,16], thus future studies using selective inhibitors or siRNA interference would be better suited to address individual roles of ALDH isoforms and subsequent ROS production during UCB ALDH[hi] cell expansion.

RA can be produced in cis- or trans- isoforms and is capable of activating receptors aside from canonical RAR/RXR heterodimers, such as the PPAR[17,18] or RAR-related orphan receptors isoforms[11,12,19]. Likewise, the canonical RAR/RXR heterodimer complex can be activated by additional ligands that selectively bind sites on either RAR or RXR subunits bound to RA response elements[11,20]. RAREs are genetic loci of canonical RAR/RXR regulatory complexes and exists at 100s of genes throughout the human genome, thus active RA-signaling networks can provide a considerable amount of transcriptional and epigenetic regulation within expanding ALDH^{hi} cells[21]. Collectively, these properties highlight the complexity of the RA-signaling network, that was largely understudied in Chapters 2 and 3 as a result of technical limitations. Specifically, the future use of global transcriptional (microarray or RNAseq) and proteomic analyses would provide more fruitful insight into the ability of DEAB-supplementation to modify the complete RA-

signaling network. To this end, concurrent manipulation of additional effectors and/or receptors of may provide further regulation of complex RA-signaling networks *in vitro*.

7.1.3 Current Limitations of Murine Model of CLI

In Chapter 2 and 5, I utilized a murine model of hindlimb ischemia to assess distinct biotherapeutic approaches to stimulate revascularization. Hindlimb ischemia in this model is induced by surgical removal of the femoral artery and vein to induce acute localized ischemia[22,23]. Unfortunately, acute ischemia induced in healthy NOD/SCID mice does not fully reflect the pathogenesis observed in human patients with severe atherosclerosis developed over a prolonged cardiometabolic imbalance[24-26]. Specifically, the surgical model employed in this study does not reflect the gradual atherosclerotic occlusion of peripheral arterioles that leads to distal tissue ischemia, inflammation and necrosis in human patients. Therefore, inducing cardiometabolic imbalances within preclinical models will improve translation of novel regenerative medicine approaches towards reproduceable clinical efficacy in human patients.

Mice are highly resistant to atherosclerosis when fed a high-fat 'Western' diet, thus modeling PAD/CLI in a standard rodent model is nearly impossible without genetic perturbation. Single or dual transgenic knockouts of Apolipoprotein E/APOE or Lipoprotein Lipase/LPL in mice provide models for the pathogenesis of atherosclerosis[27-30], albeit even these genetic models do not entirely reflect the pathophysiology or secondary complications of human CVD. Additional exogenous insults would be necessary to model concurrent cardiometabolic syndromes such as diabetes. Ultimately, the physiology of murine models limit our capacity to accurately model human PAD/CLI with or without concurrent cardiometabolic syndromes. The physiology of large animals, such as porcine or non-human primates, more accurately reflect human physiology, although financial and logistical limitations must be considered with these models[31-34]. Furthermore, the necessity of using immunodeficient models to study human cell transplantation limits the relevance of an intact immune system that would likely require larger animal models combined with immunosuppressive therapies. Later in this chapter,

I will briefly discuss the theoretical use of human organoids as a complimentary model to study human PAD/CLI.

7.1.4   Limitations of Using Mouse and Human Tissues to Elucidate Islet Regenerative Mechanisms

In chapters 3 and 6, we employed a murine model of hyperglycemia induction through STZ-induced β-cell ablation in immune deficient NOD/SCID mice that permit the survival of transferred human cells[35-37]. Pathogenesis in this model was induced by the administration of STZ, a glucose analog which specifically targets and damages β-cells with high Glut2 expression. Therefore, autoimmune pathogenesis of human Type 1 DM is not accurately reflected in the murine model employed[38]. Furthermore, NOD/SCID mice provide a functional platform for human cell transplantation studies[39], however the lack of functional lymphocytes responsible for autoimmune destruction of β-cell in human subjects. The initiation of autoimmunity is proceeded by a chronic infiltration of inflammatory cells (insulitis) that will change the inflammatory microenvironment within islets[38]. Future studies will need to employ more immunocompetent mice to better model T1D and to assess the critical question whether β-cell regeneration can occur in the face of ongoing autoimmunity? NOD mice spontaneously develop diabetes through a pathogenic insulitis similar to human subjects[40-42], however β-cell regeneration may not be feasible without immunosuppression or reversal or autoimmunity. Our future studies aim to explore whether human-derived cell-free biotherapeutics can be injected into autoimmune NOD mice as described in chapter 6. If proof-of-concept can be established, cell-free biotherapeutic delivery would be required to address whether islet regeneration can occur in the face of autoimmunity and whether biotherapeutics generated by Panc-MSC can also dampen local autoimmunity in pre-clinical models of Type 1 DM.

The molecular and morphogenic mechanisms underlying endogenous islet regeneration observed in Chapter 3 and 6 remain elusive. Specifically, putative signal-receiving cells within the NOD/SCID pancreas can only be inferred through antibody-based histological analyses following euthanasia, thus lacking fate-mapping capabilities captured using current transgenic reporter systems (i.e. lineage-tracing). Several mechanisms for

endogenous islet regeneration have been proposed and each require inducible lineage-specific transgenic systems to fully determine the origin of regenerating islet cells. For example, the Melton laboratory used a tamoxifen-inducible transgenic human placental alkaline peroxidase-reporter system driven by the insulin-promoter to suggest that mature β-cell duplication was the primary source of regenerated β-cell mass following partial pancreatomy[43]. In contrast, several cell alternative populations within rodent and human pancreata have been suggested to possess a facultative capacity to transdifferentiate to β-cells (α cells, exocrine cells, ductal epithelial cells) following specific pancreatic injury (partial pancreatectomy, ductal ligation, STZ-treatment) to generate new β-cell mass during pregnancy or early stages of Type 2 DM[44-51]. The ductal epithelium has been repletely suggested to dedifferentiate into a bipotent progenitor cell that transiently expresses NEUROG3 prior to endocrine cell neogenesis[52,53]. For example, the Collombat lab used inducible expression of PAX4 to expand β-cell mass through the transdifferentiation of Glucagon$^+$ or Somatostatin$^+$ cells cells[54-57]. Accordingly, replacement of depleted glucagon cell populations was also suggested by this group to occur through ductal epithelial cell transdifferentiation through a peusdo-mesenchymal state. These novel findings demonstrate endocrine plasticity within the adult mouse pancreas is possible, however further studies are required to determine the functional relevance of this phenomea in humans without genetic manipulation. Liu et al recently demonstrated inducible dual-lineage fate-mapping system, utilizing Dre- and Cre-recombinase, to identity a multipotent stem cell population within the lungs activated after injury[58]. With this system in mind, future fate-mapping studies investigating islet regeneration can be designed using MSC-derived biotherapeutic approach in sophisticated lineage-tracing models that selectively label cells with 'transitional' phenotype (i.e. Insulin/Glucagon; see **Figure 7.4**).
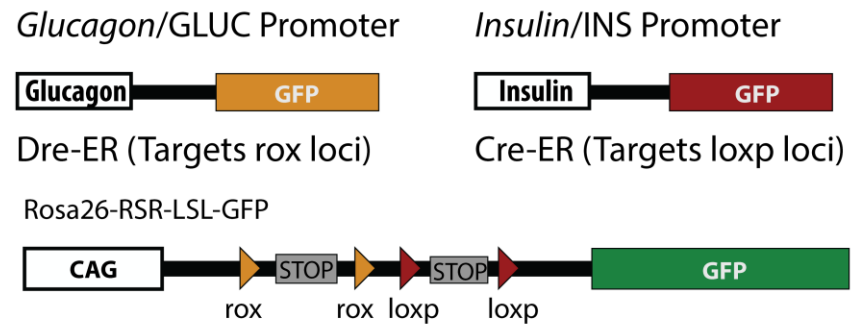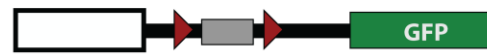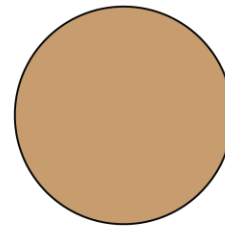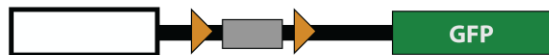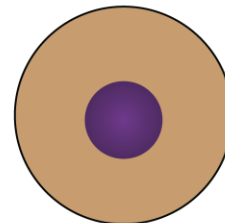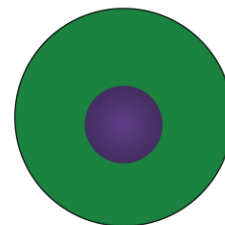
Figure 7.4 Working model of Dual-lineage transgenic system utilizing Cre- and Dre-recombinase to labelled potential cells with polyhormonal expression.

7.1.5 EV isolation and transplantation to identify pro-regenerative subfractions

Several approaches are currently used to effectively purify EVs[60-62], however I employed a simple ultrafiltration fractionation in chapters 5 and 6 to enrich for EVs from CM generated by Panc-MSC. I demonstrated ultrafiltration was sufficient to separate EVs from soluble proteins of 3-100kDa using biological validation by mass spectrometry and physical validation using nanoscale flow cytometry and atomic force microscopy. As such, the purity of EVs within EV^+ CM was limited by co-enrichment with large ECM molecules (i.e. fibronectin) or large protein complexes. Generally, ECM components are typically integrated as large heteromeric complexes selectively bound to additional proteins[63,64]. Therefore, ECM molecules and large proteins complexes would be concentrated with EVs using the ultrafiltration employed in chapters 5 and 6. Potential contamination with large protein/complexes within the EV^+ CM subfraction limited the ability to demonstrate regenerative pathway stimulation *in vivo* was exclusive to EVs secreted by Panc-MSC. Proteomic analysis of Panc-MSC CM encountered similar limitations, such that effectors detected within the EV-enriched fraction were 'most likely' contained within the lumen or membrane of EVs. Future studies would benefit by using ultrafiltration to obtain pure EV preparations prior to transplantation[64,65]. Alternatively, the implementation of siRNA interference or CRISPR-mediated genetic modifications to Panc-MSC would provide insight towards the effectors secreted by Panc-MSC that may provide multifaceted regenerative functions *in vivo*.

7.2 Clinical Applications

Throughout my thesis, I have demonstrated that both HPC and MSC demonstrate multifaceted therapeutic potential using two pre-clinical models. Likewise, HPC and MSC have been used previously in clinical trials for vascular or islet regenerative applications[66-68]. Unfortunately, current clinical efficacy using these progenitor cell population in the autologous has been modest at best. Several primary explanations for

the lack of translational efficacy have been postulated including: (1) autologous progenitor cells exposed to a harsh microenvironment shaped by chronic disease have shown diminished therapeutic function and decreased engraftment following transplantation[69], and (2) extensive expansion *ex vivo* is often required to generate sufficient cell numbers for transplantation yet expansion paradoxically drives the loss of progenitor cell identify and therapeutic functions *in vivo*[70], Thus, refinement of expansion protocols to generate high cell number with therapeutic functions provide the greatest clinical benefit. Results obtained in chapters 2 and 3, provide insight towards targetable pathways (i.e. RA-signaling) to enhance expansion of regenerative progeny retaining multifaceted therapeutic functions; potentially through the enrichment of pro-survival signaling pathways which improves engraftment after transplantation.

Transplantation of biotherapeutic stimuli holds potential to activate specific regenerative signaling pathways without many of the regulatory limitations encountered by direct cell transplantation[71,72]. MSC demonstrate multifaceted regenerative functions primarily mediated by a paracrine secretion of regenerative stimuli. Thus, MSC have been previously used in numerous clinical trials[68,73] for their secretory profile, however clinical efficacy utilizing direct MSC transplantation into tissues has been limited by low engraftment in an unfamiliar or harsh microenvironment. In chapters 4-6, I provide the first in-depth and functional characterization of human Panc-MSC. Within the context of clinical applications, I demonstrated Panc-MSC are an accessible cell population with robust expansion kinetics and a pro-regenerative secretome. Future studies are now warranted to determine whether cell-free biotherapeutics generated by Panc-MSC can be used to directly stimulate endogenous regeneration or to better support regenerative cell types after transplantation into relevant pre-clinical models.

7.3 Future Studies and Proposed Experimentation

7.3.1   Enhancing the Engraftment of Therapeutic HPC

UCB provides a readily accessible source of allogenic progenitor cells used for regenerative medicine applications[74,75]. Although efficacy following transplantation is often limited by transient engraftment, in chapter 2, I identified that DEAB-treatment during culture expansion enriched for HPC that generated proteins associated with pro-survival functions. To further elucidate the functional roles of these proteins, I would implement siRNA interference prior to intramuscular transplantation to knockdown identified proteins effectors in UCB ALDH^{hi} cells expanded under DEAB-treated conditions. Histological analyses performed shortly after transplantation would provide insight into pathways that influence the engraftment of transplanted cell populations. Alternatively, proteins of interest could also be upregulated through ectopic vector expression or pharmaceutical activation of up/downstream effectors.

7.3.2   Do cells of the megakaryocyte-lineage possess multifaceted therapeutic potential?

It was discovered in chapters 2 and 3 that UCB ALDH[hi] cell expansion was biased towards generation of progeny from the megakaryocyte lineage. Interestingly, expanded cells with low ALDH-activity were enriched for committed megakaryocytes with previously unrecognized islet regeneration *in vivo*. Unfortunately, I was not able to determine potential contribution of megakaryocytes to islet regeneration, although FACS purification based on CD41 and/or CD42 could be employed to enrich for cells at different stages of megakaryopoiesis. Direct FACS purification of megakaryocyte-related cell populations could be transplanted into murine models of Type 1 diabetes or severe CLI utilized throughout this thesis. Furthermore, platelet-rich plasma (PRP) has recently emerged as a source of pro-angiogenic or anti-inflammatory stimuli with therapeutic benefit for treating articular cartilage osteoarthritis in early clinical trials[76-80]. Platelets are anucleated fragments generated by megakaryocyte burst is essential for wound healing and vascular homeostasis[81-83]. Notably, it has been recently demonstrated that platelets

can transfer potent vascular and tissue regenerative stimuli to exposed cell populations[77,84]. Thus, future research would benefit from investigation of the therapeutic potential culture-generated platelets transplanted into pre-clinical models of Type 1 DM or PAD/CLI.

7.3.3 Identification of Panc-MSC during human pathology and regeneration

The true phenotype of MSC in human tissues remains controversial and represents a persistent limitation to the advancement of regenerative medicine approaches using MSC[85]. Further fate-mapping studies are necessary to elucidate MSC hierarchies within human tissues, however clinical use of native human Panc-MSC will ultimately rely on elucidating unique functional benefits not demonstrated by BM-derived MSC. Here, I demonstrated Panc-MSC demonstrated a unique proteome and enriched expression progenitor cell markers, such as vimentin and nestin. Furthermore, I provided a surface marker profile of Panc-MSC, including over 70 CD markers which may potentially serve as candidate markers for further subset purification and functional analyses (**Figure 7.5**). As observed in this study, heterogenicity is a current limitation of MSC culture. Until this heterogeneity is minimized, functional variation between tissue-specific MSC will limit consistent therapeutic benefit. Fibrosis following wounding is mediated by MSC-like progeny, such that fibroblasts or myofibroblasts, robustly deposit ECM components that comprise scar tissue and formation of an inflammatory microenvironment that generally inhibits regeneration of functional cell populations[86-88]. Other groups have demonstrated that tissue-specific MSC exist using fate-mapping in mice, however their multipotency was facultative to injury and potency was restricted to fibroblast or adipocyte-lineages when exposed to a pro-inflammatory microenvironment[88]. In the context of diabetes, the BM niche becomes populated with MSC-derived adipocytes due to local metabolic imbalances[89,90]. Although mesoderm-derived BM-MSC effectively differentiates into adipocytes within this thesis, I demonstrated human Panc-MSC were restricted from adipogenic differentiation *in vitro*. Adipocyte formation can occur within the pancreas; however, the origin of these adipocytes remains elusive and requires further

investigation. Lastly, several groups have proposed that select MSC populations may not be derived from a mesodermal origin during embryogenesis[91-96], but are developmentally-derived from the neural crest. Collectively, future studies will need to investigate the pathogenesis of human Panc-MSC during established Type 1 and Type 2 diabetes. Moreover, fate-mapping studies using pluripotent ESCs or iPSCs may be required to elucidate the developmental origins of human Panc-MSC and their contributions to endogenous islet regeneration.

(A_i)

(A_ii)

(B_i)

(B_ii)

Islet of Langerhans

(C)

(E)

(F)

(G)

"Panc-MSC"-labelled Models

Single-cell Colony Formation
MSC-like Cells
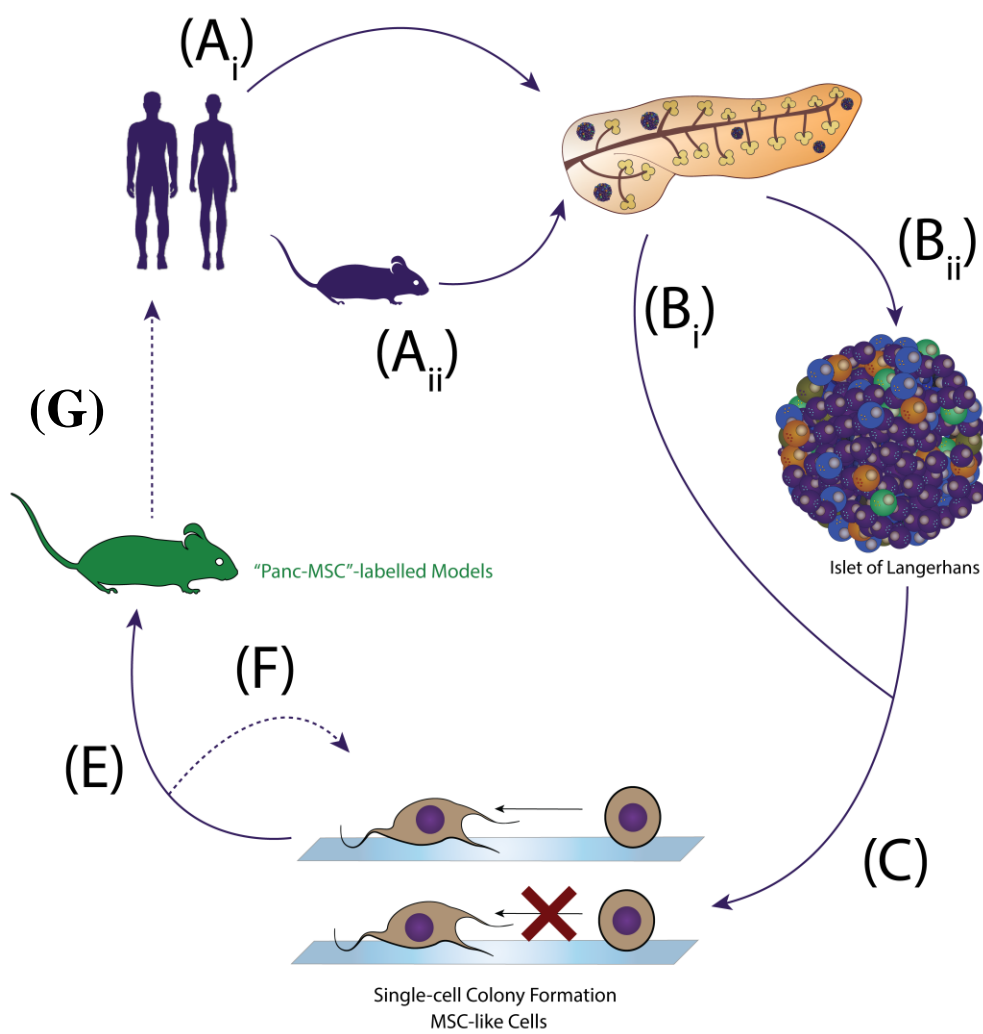
Figure 7.5 Working model to elucidate the phenotype and function of Panc-MSC in situ in humans and mice. Pancreas concurrently harvested from (Ai) human or (Aii) murine donors would be used to isolate single cells from (Bi) whole pancreas digests or (Bii) dissociated islet preps. (C) Single cells would be FACS purified based on CD candidates identified in Chapter 4 and (D) tested for single- cell colony formation and MSC characteristics *in vitro*. MSC-like cells would be subjected to further molecular and functional experimentation. (E) Transgenic mouse models could be created based on relevant MSC-phenotypes, albeit (F) refinement of purification strategies may be required. (G) Ultimately, the pathological role and therapeutic function of Panc-MSC could be tested in stitu and used to develop of Panc-MSC could be tested in clinical trials for regenerative medicine applications.

7.3.4 Elucidating the pro-regenerative microenvironment generated by cell-free biotherapeutics

The recent advancement in human organoid generation and culture may provide an sustainable high-throughput platform to accurately model human disease *in vitro* and after organoid implantation *in vivo*[97,98]. Furthermore, iPSC technologies offer the opportunity to assess genetic and epigenetic differences encountered between human patients with a given pathology. As eluded to in Chapter 1, designer cells would allow for patient-specific organoids that reflect complex and concurrent pathogenesis, such as Type 2 DM or atherosclerosis. Although these technologies hold undoubtable potential, standardized generation of human organoids is in its infancy and further development is necessary before organoids are routinely used as translational models of disease. The Penniger lab recently demonstrated the generation of human vascular organoids which effectively modelled diabetes-induced vasculopathy in a multi-well culture system[97]. In theory, we could use a cell-free biotherapeutics generated from 'designer' MSC and test regenerative functions on similar organoid systems to elucidate targetable pathways that reverse pathogenesis[99]. For example, periostin and Wnt5a was significantly enriched within EV+ CM generated by Panc-MSC. Results for previous studies suggest Wnt5a[100-103] and periostin[104-106] has proangiogenic and islet proliferative functions, respectively[100-103]. Additionally, global proteomic analyses and biotherapeutic agent transfer into immunocompetent or inducible lineage-specific lineage tracing models suggested in this thesis could provide additional insight towards understanding how ECM and microenvironmental architecture influences both vascular and islet regenerative mechanisms. It is essential to consider the signaling contribution of the 3D microenvironment, as many studies have demonstrated the role of the extracellular matrix on progenitor cell survival and differentiation[8,107-109]. Ultimately, the success of biotherapeutic approaches, aiming to stimulate endogenous regeneration, will rely on the ability to generate and sustain a 'development-like' microenvironment in the face of chronic disease.

References

1 Hitchcock, I. S. & Kaushansky, K. Thrombopoietin from beginning to end. *British journal of haematology* **165**, 259-268 (2014).

2 Majka, M. *et al.* Stromal-derived factor 1 and thrombopoietin regulate distinct aspects of human megakaryopoiesis. *Blood* **96**, 4142-4151 (2000).

3 Fox, N., Priestley, G., Papayannopoulou, T. & Kaushansky, K. Thrombopoietin expands hematopoietic stem cells after transplantation. *The Journal of clinical investigation* **110**, 389-394 (2002).

4 Yoshihara, H. *et al.* Thrombopoietin/MPL signaling regulates hematopoietic stem cell quiescence and interaction with the osteoblastic niche. *Cell stem cell* **1**, 685-697 (2007).

5 Csaszar, E., Chen, K., Caldwell, J., Chan, W. & Zandstra, P. W. Real-time monitoring and control of soluble signaling factors enables enhanced progenitor cell outputs from human cord blood stem cell cultures. *Biotechnology and bioengineering* **111**, 1258-1264 (2014).

6 Csaszar, E. *et al.* Rapid expansion of human hematopoietic stem cells by automated control of inhibitory feedback signaling. *Cell stem cell* **10**, 218-229 (2012).

7 Kirouac, D. C. & Zandstra, P. W. Understanding cellular networks to improve hematopoietic stem cell expansion cultures. *Current Opinion in Biotechnology* **17**, 538-547 (2006).

8 Madlambayan, G. J. *et al.* Dynamic changes in cellular and microenvironmental composition can be controlled to elicit *in vitro* human hematopoietic stem cell expansion. *Experimental hematology* **33**, 1229-1239 (2005).

9 Chanda, B., Ditadi, A., Iscove, N. N. & Keller, G. Retinoic acid signaling is essential for embryonic hematopoietic stem cell development. *Cell* **155**, 215-227 (2013).

10 Chen, Y. *et al.* Retinoic acid signaling is essential for pancreas development and promotes endocrine at the expense of exocrine cell differentiation in Xenopus. *Developmental biology* **271**, 144-160 (2004).

11 Mark, M., Ghyselinck, N. B. & Chambon, P. Function of retinoid nuclear receptors: lessons from genetic and pharmacological dissections of the retinoic acid signaling pathway during mouse embryogenesis. *Annu. Rev. Pharmacol. Toxicol.* **46**, 451-480 (2006).

12 Rhinn, M. & Dollé, P. Retinoic acid signalling during development. *Development* **139**, 843-858 (2012).

13 Levi, B. P., Yilmaz, Ö. H., Duester, G. & Morrison, S. J. Aldehyde dehydrogenase 1a1 is dispensable for stem cell function in the mouse hematopoietic and nervous systems. *Blood* **113**, 1670-1680 (2009).

14 Ma, I. & Allan, A. L. The role of human aldehyde dehydrogenase in normal and cancer stem cells. *Stem cell reviews and reports* **7**, 292-306 (2011).

15 Moreb, J. S. *et al.* The enzymatic activity of human aldehyde dehydrogenases 1A2 and 2 (ALDH1A2 and ALDH2) is detected by Aldefluor, inhibited by diethylaminobenzaldehyde and has significant effects on cell proliferation and drug resistance. *Chemico-biological interactions* **195**, 52-60 (2012).

16 Luo, M., Gates, K. S., Henzl, M. T. & Tanner, J. J. Diethylaminobenzaldehyde is a covalent, irreversible inactivator of ALDH7A1. *ACS chemical biology* **10**, 693-697 (2015).

17 Kliewer, S. A., Umesono, K., Noonan, D. J., Heyman, R. A. & Evans, R. M. Convergence of 9-cis retinoic acid and peroxisome proliferator signalling pathways through heterodimer formation of their receptors. *Nature* **358**, 771 (1992).

18 Noy, N. in *The Biochemistry of Retinoid Signaling II* 179-199 (Springer, 2016).

19   Cook, D. N., Kang, H. S. & Jetten, A. M. Retinoic acid-related orphan receptors (RORs): regulatory functions in immunity, development, circadian rhythm, and metabolism. *Nuclear receptor research* **2** (2015).

20   Bastien, J. & Rochette-Egly, C. Nuclear retinoid receptors and the transcription of retinoid-target genes. *Gene* **328**, 1-16 (2004).

21   Gudas, L. J. & Wagner, J. A. Retinoids regulate stem cell differentiation. *Journal of cellular physiology* **226**, 322-330 (2011).

22   Niiyama, H., Huang, N. F., Rollins, M. D. & Cooke, J. P. Murine model of hindlimb ischemia. *JoVE (Journal of Visualized Experiments)*, e1035 (2009).

23   Limbourg, A. *et al.* Evaluation of postnatal arteriogenesis and angiogenesis in a mouse model of hind-limb ischemia. *Nature protocols* **4**, 1737 (2009).

24   Zaragoza, C. *et al.* Animal models of cardiovascular diseases. *BioMed Research International* **2011** (2011).

25   von Scheidt, M. *et al.* Applications and limitations of mouse models for understanding human atherosclerosis. *Cell metabolism* **25**, 248-261 (2017).

26   McNeill, E., Channon, K. & Greaves, D. Inflammatory cell recruitment in cardiovascular disease: murine models and potential clinical applications. *Clinical science* **118**, 641-655 (2010).

27   Olszanecki, R. *et al.* Effect of curcumin on atherosclerosis in apoE/LDLR-double knockout mice. *Journal of physiology and pharmacology: an official journal of the Polish Physiological Society* **56**, 627-635 (2005).

28   Nakashima, Y., Plump, A. S., Raines, E. W., Breslow, J. L. & Ross, R. ApoE-deficient mice develop lesions of all phases of atherosclerosis throughout the arterial tree. *Arteriosclerosis and thrombosis: a journal of vascular biology* **14**, 133-140 (1994).

29   Ko, K. W., Paul, A., Ma, K., Li, L. & Chan, L. Endothelial lipase modulates HDL but has no effect on atherosclerosis development in apoE−/− and LDLR−/− mice. *Journal of lipid research* **46**, 2586-2594 (2005).

30   Carmeliet, P. & Collen, D. Transgenic mouse models in angiogenesis and cardiovascular disease. *The Journal of pathology* **190**, 387-405 (2000).

31   Worthley, S. G. *et al.* High-resolution *ex vivo* magnetic resonance imaging of in situ coronary and aortic atherosclerotic plaque in a porcine model. *Atherosclerosis* **150**, 321-329 (2000).

32   Veseli, B. E. *et al.* Animal models of atherosclerosis. *European journal of pharmacology* **816**, 3-13 (2017).

33   McDonald, T. O. *et al.* Diabetes and arterial extracellular matrix changes in a porcine model of atherosclerosis. *Journal of Histochemistry & Cytochemistry* **55**, 1149-1157 (2007).

34   Getz, G. S. & Reardon, C. A. in *Animal Models for the Study of Human Disease*   205-217 (Elsevier, 2017).

35   Herr, R. R., Jahnke, H. K. & Argoudelis, A. D. Structure of streptozotocin. *Journal of the American Chemical Society* **89**, 4808-4809 (1967).

36   Lenzen, S. The mechanisms of alloxan-and streptozotocin-induced diabetes. *Diabetologia* **51**, 216-226 (2008).

37   Hess, D. *et al.* Bone marrow–derived stem cells initiate pancreatic regeneration. *Nature biotechnology* **21**, 763 (2003).

38   Van Belle, T. L., Coppieters, K. T. & Von Herrath, M. G. Type 1 diabetes: etiology, immunology, and therapeutic strategies. *Physiological reviews* **91**, 79-118 (2011).

39   Seneviratne, A. K. *et al.* Expanded hematopoietic progenitor cells reselected for high aldehyde dehydrogenase activity demonstrate islet regenerative functions. *Stem Cells* **34**, 873-887 (2016).

40   Nakayama, M. *et al.* Prime role for an insulin epitope in the development of type 1 diabetes in NOD mice. *Nature* **435**, 220 (2005).

41   Kodama, S., Kühtreiber, W., Fujimura, S., Dale, E. A. & Faustman, D. L. Islet regeneration during the reversal of autoimmune diabetes in NOD mice. *Science* **302**, 1223-1227 (2003).

42   Rees, D. & Alcolado, J. Animal models of diabetes mellitus. *Diabetic medicine* **22**, 359-370 (2005).

43   Dor, Y., Brown, J., Martinez, O. I. & Melton, D. A. Adult pancreatic β-cells are formed by self-duplication rather than stem-cell differentiation. *Nature* **429**, 41 (2004).

44   Ye, L., Robertson, M. A., Hesselson, D., Stainier, D. Y. & Anderson, R. M. Glucagon is essential for α cell transdifferentiation and beta cell neogenesis. *Development* **142**, 1407-1417 (2015).

45   Bergemann, D. *et al.* Pancreatic Beta Cell Regeneration: Duct Cells Act as Progenitors in Adult Zebrafish. (2016).

46   Ben-Othman, N. *et al.* Long-term GABA administration induces α cell-mediated beta-like cell neogenesis. *Cell* **168**, 73-85. e11 (2017).

47   Rieck, S. & Kaestner, K. H. Expansion of β-cell mass in response to pregnancy. *Trends in Endocrinology & Metabolism* **21**, 151-158 (2010).

48   Liu, Y. *et al.* Proliferating pancreatic beta-cells upregulate ALDH. *Histochemistry and cell biology* **142**, 685-691 (2014).

49   Kim, H. *et al.* Serotonin regulates pancreatic beta cell mass during pregnancy. *Nature medicine* **16**, 804 (2010).

50   Butler, A. *et al.* Adaptive changes in pancreatic beta cell fractional area and beta cell turnover in human pregnancy. *Diabetologia* **53**, 2167-2176 (2010).

51   Jacovetti, C. *et al.* MicroRNAs contribute to compensatory β cell expansion during pregnancy and obesity. *The Journal of clinical investigation* **122**, 3541-3551 (2012).

52   Lee, J. *et al.* Expansion and conversion of human pancreatic ductal cells into insulin-secreting endocrine cells. *Elife* **2**, e00940 (2013).

53   Bonner-Weir, S. *et al.* β-cell growth and regeneration: replication is only part of the story. *Diabetes* **59**, 2340-2348 (2010).

54   Collombat, P. *et al.* The ectopic expression of Pax4 in the mouse pancreas converts progenitor cells into α and subsequently β cells. *Cell* **138**, 449-462 (2009).

55   Collombat, P. *et al.* Opposing actions of Arx and Pax4 in endocrine pancreas development. *Genes & development* **17**, 2591-2603 (2003).

56   Druelle, N. *et al.* Ectopic expression of Pax4 in pancreatic δ cells results in β-like cell neogenesis. *J Cell Biol* **216**, 4299-4311 (2017).

57   Blyszczuk, P. *et al.* Expression of Pax4 in embryonic stem cells promotes differentiation of nestin-positive progenitor and insulin-producing cells. *Proceedings of the National Academy of Sciences* **100**, 998-1003 (2003).

58   Liu, Q. *et al.* Lung regeneration by multipotent stem cells residing at the bronchioalveolar-duct junction. *Nature genetics*, 1 (2019).

59   Yoneda, S. *et al.* Predominance of β-cell neogenesis rather than replication in humans with an impaired glucose tolerance and newly diagnosed diabetes. *The Journal of Clinical Endocrinology & Metabolism* **98**, 2053-2061 (2013).

60   van Niel, G., D'Angelo, G. & Raposo, G. Shedding light on the cell biology of extracellular vesicles. *Nature reviews Molecular cell biology* **19**, 213 (2018).

61   Shao, H. *et al.* New technologies for analysis of extracellular vesicles. *Chemical reviews* **118**, 1917-1950 (2018).

62   Raposo, G. & Stoorvogel, W. Extracellular vesicles: exosomes, microvesicles, and friends. *J Cell Biol* **200**, 373-383 (2013).

63   Hay, E. D. *Cell biology of extracellular matrix*. (Springer Science & Business Media, 2013).

64   Yuana, Y., Levels, J., Grootemaat, A., Sturk, A. & Nieuwland, R. Co-isolation of extracellular vesicles and high-density lipoproteins using density gradient ultracentrifugation. *Journal of extracellular vesicles* **3**, 23262 (2014).

65   Nordin, J. Z. *et al.* Ultrafiltration with size-exclusion liquid chromatography for high yield isolation of extracellular vesicles preserving intact biophysical and functional properties. *Nanomedicine: Nanotechnology, Biology and Medicine* **11**, 879-883 (2015).

66   Perin, E. C. *et al.* Evaluation of cell therapy on exercise performance and limb perfusion in peripheral artery disease: the CCTRN PACE trial (patients with intermittent claudication injected with ALDH bright cells). *Circulation* **135**, 1417-1428 (2017).

67   Perin, E. C. *et al.* Rationale and design for PACE: patients with intermittent claudication injected with ALDH bright cells. *American heart journal* **168**, 667-673. e662 (2014).

68   Squillaro, T., Peluso, G. & Galderisi, U. Clinical trials with mesenchymal stem cells: an update. *Cell transplantation* **25**, 829-848 (2016).

69   Kornicka, K., Houston, J. & Marycz, K. Dysfunction of mesenchymal stem cells isolated from metabolic syndrome and type 2 diabetic patients as result of oxidative stress and autophagy may limit their potential therapeutic use. *Stem Cell Reviews and Reports* **14**, 337-345 (2018).

70   Putman, D. M. *et al.* Expansion of umbilical cord blood aldehyde dehydrogenase expressing cells generates myeloid progenitor cells that stimulate limb revascularization. *Stem cells translational medicine* **6**, 1607-1619 (2017).

71   Konala, V. B. R. *et al.* The current landscape of the mesenchymal stromal cell secretome: a new paradigm for cell-free regeneration. *Cytotherapy* **18**, 13-24 (2016).

72   Kim, H. O., Choi, S.-M. & Kim, H.-S. Mesenchymal stem cell-derived secretome and microvesicles as cell-free therapeutics for neurodegenerative disorders. *Tissue Engineering and Regenerative Medicine* **10**, 93-101 (2013).

73   Barry, F. P. & Murphy, J. M. Mesenchymal stem cells: clinical applications and biological characterization. *The international journal of biochemistry & cell biology* **36**, 568-584 (2004).

74   Putman, D. M., Liu, K. Y., Broughton, H. C., Bell, G. I. & Hess, D. A. Umbilical cord blood-derived aldehyde dehydrogenase-expressing progenitor cells promote recovery from acute ischemic injury. *Stem cells* **30**, 2248-2260 (2012).

75   Bell, G., Putman, D., Hughes-Large, J. & Hess, D. Intrapancreatic delivery of human umbilical cord blood aldehyde dehydrogenase-producing cells promotes islet regeneration. *Diabetologia* **55**, 1755-1760 (2012).

76   Thurston, G. *et al.* Angiopoietin-1 protects the adult vasculature against plasma leakage. *Nature medicine* **6**, 460 (2000).

77   Marx, R. E. Platelet-rich plasma: evidence to support its use. *Journal of oral and maxillofacial surgery* **62**, 489-496 (2004).

78   Kon, E. *et al.* Platelet-rich plasma intra-articular injection versus hyaluronic acid viscosupplementation as treatments for cartilage pathology: from early degeneration to osteoarthritis. *Arthroscopy: The Journal of Arthroscopic & Related Surgery* **27**, 1490-1501 (2011).

79   Foster, T. E., Puskas, B. L., Mandelbaum, B. R., Gerhardt, M. B. & Rodeo, S. A. Platelet-rich plasma: from basic science to clinical applications. *The American journal of sports medicine* **37**, 2259-2272 (2009).

80   De Vos, R. J. *et al.* Platelet-rich plasma injection for chronic Achilles tendinopathy: a randomized controlled trial. *Jama* **303**, 144-149 (2010).

81   Davì, G. & Patrono, C. Platelet activation and atherothrombosis. *New England Journal of Medicine* **357**, 2482-2494 (2007).

82   Verheul, H. *et al.* Platelet: transporter of vascular endothelial growth factor. *Clinical cancer research* **3**, 2187-2190 (1997).

83   Ruggeri, Z. Von Willebrand factor, platelets and endothelial cell interactions. *Journal of Thrombosis and Haemostasis* **1**, 1335-1342 (2003).

84   Zhao, Y. *et al.* Platelet-derived mitochondria display embryonic stem cell markers and improve pancreatic islet β-cell function in humans. *Stem cells translational medicine* **6**, 1684-1697 (2017).

85   Caplan, A. I. Mesenchymal stem cells: time to change the name! *Stem cells translational medicine* **6**, 1445-1451 (2017).

86   Yates, C. C. *et al.* Multipotent stromal cells/mesenchymal stem cells and fibroblasts combine to minimize skin hypertrophic scarring. *Stem cell research & therapy* **8**, 193 (2017).

87   Carlson, S., Trial, J., Soeller, C. & Entman, M. L. Cardiac mesenchymal stem cells contribute to scar formation after myocardial infarction. *Cardiovascular research* **91**, 99-107 (2011).

88   Joe, A. W. *et al.* Muscle injury activates resident fibro/adipogenic progenitors that facilitate myogenesis. *Nature cell biology* **12**, 153 (2010).

89   Piccinin, M. A. & Khan, Z. A. Pathophysiological role of enhanced bone marrow adipogenesis in diabetic complications. *Adipocyte* **3**, 263-272 (2014).

90   Keats, E. C., Dominguez, J. M., Grant, M. B. & Khan, Z. A. Switch from canonical to noncanonical Wnt signaling mediates high glucose-induced adipogenesis. *Stem Cells* **32**, 1649-1660 (2014).

91   Xu, X. *et al.* Gingivae contain neural-crest-and mesoderm-derived mesenchymal stem cells. *Journal of dental research* **92**, 825-832 (2013).

92   Morikawa, S. *et al.* Development of mesenchymal stem cells partially originate from the neural crest. *Biochemical and biophysical research communications* **379**, 1114-1119 (2009).

93   Miller, F. D. Riding the waves: neural and nonneural origins for mesenchymal stem cells. *Cell Stem Cell* **1**, 129-130 (2007).

94   Jinno, H. *et al.* Convergent genesis of an adult neural crest-like dermal stem cell from distinct developmental origins. *Stem cells* **28**, 2027-2040 (2010).

95   Isern, J. *et al.* The neural crest is a source of mesenchymal stem cells with specialized hematopoietic stem cell niche function. *Elife* **3**, e03696 (2014).

96   George, E. L., Georges-Labouesse, E. N., Patel-King, R. S., Rayburn, H. & Hynes, R. O. Defects in mesoderm, neural tube and vascular development in mouse embryos lacking fibronectin. *Development* **119**, 1079-1091 (1993).

97   Wimmer, R. A. *et al.* Human blood vessel organoids as a model of diabetic vasculopathy. *Nature* (2019).

98   Fatehullah, A., Tan, S. H. & Barker, N. Organoids as an *in vitro* model of human development and disease. *Nature cell biology* **18**, 246 (2016).

99   Cooper, T. T., Hess, D. A. & Verma, S. Vascular Organoids: Are We Entering a New Area of Cardiometabolic Research? *Cell metabolism* **29**, 792-794 (2019).

100   Rauner, M. *et al.* WNT5A is induced by inflammatory mediators in bone marrow stromal cells and regulates cytokine and chemokine production. *Journal of bone and mineral research* **27**, 575-585 (2012).

101   Miyoshi, H., Ajima, R., Luo, C. T., Yamaguchi, T. P. & Stappenbeck, T. S. Wnt5a potentiates TGF-β signaling to promote colonic crypt regeneration after tissue injury. *Science* **338**, 108-113 (2012).

102   Ekström, E. J. *et al.* WNT5A induces release of exosomes containing pro-angiogenic and immunosuppressive factors from malignant melanoma cells. *Molecular cancer* **13**, 88 (2014).

103   Arderiu, G., Espinosa, S., Peña, E., Aledo, R. & Badimon, L. Monocyte-secreted Wnt5a interacts with FZD5 in microvascular endothelial cells and induces angiogenesis through tissue factor signaling. *Journal of molecular cell biology* **6**, 380-393 (2014).

104   Smid, J. K., Faulkes, S. & Rudnicki, M. A. Periostin induces pancreatic regeneration. *Endocrinology* **156**, 824-836 (2015).

105   Kudo, A. Periostin in fibrillogenesis for tissue regeneration: periostin actions inside and outside the cell. *Cellular and molecular life sciences* **68**, 3201 (2011).

106   Dorn, G. W. Periostin and myocardial repair, regeneration, and recovery. *New England Journal of Medicine* **357**, 1552 (2007).

107   DeCarolis, N. A., Kirby, E. D., Wyss-Coray, T. & Palmer, T. D. The role of the microenvironmental niche in declining stem-cell functions associated with biological aging. *Cold Spring Harbor perspectives in medicine* **5**, a025874 (2015).

108   Huang, Y.-C., Leung, V. Y., Lu, W. W. & Luk, K. D. The effects of microenvironment in mesenchymal stem cell–based regeneration of intervertebral disc. *The Spine Journal* **13**, 352-362 (2013).

109   Brissova, M. *et al.* Islet microenvironment, modulated by vascular endothelial growth factor-A signaling, promotes β cell regeneration. *Cell metabolism* **19**, 498-511 (2014).

Appendices

Appendix 1 Permission to reproduce Cooper et al. Stem Cells

JOHN WILEY AND SONS LICENSE
TERMS AND CONDITIONS

May 10, 2019

This Agreement between Tyler T. Cooper ("You") and John Wiley and Sons ("John Wiley and Sons") consists of your license details and the terms and conditions provided by John Wiley and Sons and Copyright Clearance Center.

License Number	4585521336528
License date	May 10, 2019
Licensed Content Publisher	John Wiley and Sons
Licensed Content Publication	Stem Cells
Licensed Content Title	Inhibition of Aldehyde Dehydrogenase-Activity Expands Multipotent Myeloid Progenitor Cells with Vascular Regenerative Function
Licensed Content Author	Tyler T. Cooper, Stephen E. Sherman, Miljan Kuljanin, et al
Licensed Content Date	Feb 12, 2018
Licensed Content Volume	36
Licensed Content Issue	5
Licensed Content Pages	14
Type of use	Dissertation/Thesis
Requestor type	Author of this Wiley article
Format	Electronic
Portion	Full article
Will you be translating?	No
Title of your thesis / dissertation	Expansion of Adult Progenitor Cells with Multifaceted Regenerative Functions
Expected completion date	Jun 2019
Expected size (number of pages)	300
Requestor Location	Western University 1151 Richmond St.
	London, ON N6A 3K7 Canada Attn: Tyler T. Cooper
Publisher Tax ID	EU826007151
Total	0.00 CAD
Terms and Conditions	

TERMS AND CONDITIONS

This copyrighted material is owned by or exclusively licensed to John Wiley & Sons, Inc. or one of its group companies (each a"Wiley Company") or handled on behalf of a society with which a Wiley Company has exclusive publishing rights in relation to a particular work (collectively "WILEY"). By clicking "accept" in connection with completing this licensing transaction, you agree that the following terms and conditions apply to this transaction (along with the billing and payment terms and conditions established by the Copyright

Appendix 2 Animal Use Protocol Ethics Approval: β-cell Regeneration

AUP Number: 2015-033

AUP Title: Transplantation of Novel Stem Cells for the Regeneration of B-Cell Function

Yearly Renewal Date: 07/01/2019

The YEARLY RENEWAL to Animal Use Protocol (AUP) 2015-033 has been approved by the Animal Care Committee (ACC), and will be approved through to the above review date.

Please at this time review your AUP with your research team to ensure full understanding by everyone listed within this AUP.

As per your declaration within this approved AUP, you are obligated to ensure that:

1) Animals used in this research project will be cared for in alignment with:

a)   Western's   Senate   MAPPs   7.12,   7.10,   and   7.15
http://www.uwo.ca/univsec/policies_procedures/research.html

b) University Council on Animal Care Policies and related Animal Care   Committee   procedures http://uwo.ca/research/services/animalethics/animal_care_and_use_policies.html

2) As per UCAC's Animal Use Protocols Policy

a) this AUP accurately represents intended animal use;

b) external approvals associated with this AUP, including permits and scientific/departmental peer approvals, are complete and accurate;

c) any divergence from this AUP will not be undertaken until the related Protocol Modification is approved by the ACC; and

d) AUP form submissions - Annual Protocol Renewals and Full AUP Renewals - will be submitted   and attended to within timeframes   outlined   by   the   ACC. http://uwo.ca/research/services/animalethics/animal_use_protocols.html

3) As per MAPP 7.10 all individuals listed within this AUP as having any hands-on animal contact will

a) be made familiar with and have direct access to this AUP;

b) complete all required CCAC mandatory training (training@uwo.ca); and

c) be overseen by me to ensure appropriate care and use of animals.

4) As per MAPP 7.15,

a) Practice will align with approved AUP elements;

b) Unrestricted access to all animal areas will be given to ACVS Veterinarians and ACC Leaders;

c) UCAC policies and related ACC procedures will be followed, including but not limited to:

i) Research Animal Procurement

ii) Animal Care and Use Records

iii) Sick Animal Response

iv) Continuing Care Visits

5) As per institutional OH&S policies, all individuals listed within this AUP who will be using or potentially   exposed to hazardous materials will have completed in advance the appropriate institutional OH&S training, facility-level training, and reviewed related (M)SDS Sheets, http://www.uwo.ca/hr/learning/required/index.html

Submitted by: Copeman, Laura on behalf of the Animal Care Committee
University Council on Animal Care

The University of Western Ontario

Animal Care Committee / University Council on Animal Care

London, Ontario Canada N6A 5C1

519-661-2111 x 88792 Fax 519-661-2028

auspc@uwo.ca�

http://www.uwo.ca/research/services/animalethics/index.html

Appendix 3 Animal Use Protocol Ethics Approval: Hindlimb Ischemia

AUP Number: 2015-012

AUP Title: Characterization of the Angiogenic Potential of Aldehyde Dehydrogenase Expressing Stem cells from Human Bone Marrow and Umbilical Cord Blood

Yearly Renewal Date: 07/01/2019

The YEARLY RENEWAL to Animal Use Protocol (AUP) 2015-012 has been approved by the Animal Care Committee (ACC), and will be approved through to the above review date.

Please at this time review your AUP with your research team to ensure full understanding by everyone listed within this AUP. As per your declaration within this approved AUP, you are obligated to ensure that:

1) Animals used in this research project will be cared for in alignment with:
　　a) Western's Senate MAPPs 7.12, 7.10, and 7.15
　　b) University Council on Animal Care Policies and related Animal Care Committee procedures
http://uwo.ca/research/services/animalethics/animal_care_and_use_policies.html

2) As per UCAC's Animal Use Protocols Policy,

　　a) this AUP accurately represents intended animal use;
　　b) external approvals associated with this AUP, including permits and scientific/departmental peer approvals, are complete and accurate;
　　c) any divergence from this AUP will not be undertaken until the related Protocol Modification is approved by the ACC; and
　　d) AUP form submissions - Annual Protocol Renewals and Full AUP Renewals - will be submitted and attended to within timeframes outlined by the ACC.
http://uwo.ca/research/services/animalethics/animal_use_protocols.html

3) As per MAPP 7.10 all individuals listed within this AUP as having any hands-on animal contact will
　　a) be made familiar with and have direct access to this AUP;
　　b) complete all required CCAC mandatory training (training@uwo.ca); and

c) be overseen by me to ensure appropriate care and use of animals.

4) As per MAPP 7.15,

a) Practice will align with approved AUP elements;

b) Unrestricted access to all animal areas will be given to ACVS Veterinarians and ACC Leaders;

c) UCAC policies and related ACC procedures will be followed, including but not limited to:

i) Research Animal Procurement
ii) Animal Care and Use Records
iii) Sick Animal Response iv) Continuing Care Visits

5) As per institutional OH&S policies, all individuals listed within this AUP who will be using or potentially exposed to hazardous materials will have completed in advance the appropriate institutional OH&S training, facility-level training, and reviewed related (M)SDS Sheets, http://www.uwo.ca/hr/learning/required/index.html

Submitted by: Copeman, Laura on behalf of the Animal Care Committee University Council on Animal Care

The University of Western Ontario
Animal Care Committee / University Council on Animal Care
London, Ontario Canada N6A 5C1
519-661-2111 x 88792 Fax 519-661-2028
auspc@uwo.ca◆
http://www.uwo.ca/research/services/animalethics/index.html

Curriculum Vitae

Name: Tyler T. Cooper

Post-secondary   Western University
Education and   London, Ontario, Canada
Degrees: 2009-2014 Hon. BSc Biology.

                  Western University
                  London, Ontario, Canada
                  2009-2014 BSc. Physiology

                  Western University
                  London, Ontario, Canada
                  2014-2019 PhD. Physiology and Pharmacology
                  Collaborative Graduate Program in Developmental Biology

Honours and Awards:

Western Graduate Research Scholarship, University of Western Ontario, September 2014 – Present, $4500/year

Ontario Graduate Studentship (OGS), University of Western Ontario, May 2015- April 2016, $15,000/year

Ontario Graduate Studentship (OGS), University of Western Ontario, May 2016- April 2017, $15,000/year

Ontario Graduate Studentship (OGS), University of Western Ontario, May 2017- April 2018, $15,000/year

Stem Cell Network Travel Award, Till & McCulloch Meeting, October 2015

Stem Cell Network Travel Award, Till & McCulloch Meeting, October 2016

Stem Cell Network Travel Award, Till & McCulloch Meeting, November 2017

Ontario Institute of Regenerative Medicine Travel Award, Till & McCulloch
Meeting, November 2018

Best Poster, Category of Cardiovascular Physiology, Department of Physiology
and Pharmacology Stevenson Research Day, Western University, 2016.

Related Work Experience:

1.   Graduate Teaching Assistant, 3130z Human Physiology Laboratory, Western
University, September 2014-April 2015

2.   Graduate Teaching Assistant, 3130z Human Physiology Laboratory, Western
University, September 2015-April 2016

3.   Graduate Teaching Assistant, 2130 Human Physiology, Western University,
September 2016-April 2017

4.   Graduate Teaching Assistant, 2130 Human Physiology, Western University,
September 2017-April 2018

5.   Graduate Teaching Assistant, 3140a Cellular Physiology, Western University,
September 2018-December 2018

6.   Graduate Teaching Assistant, 4520b Stem Cells & Regenerative Medicine,
Western University, January 2019-April 2019

Publications:

1.   **Cooper TT,** Elgamal RM, Hess DA. Chapter 10: Induction of β-Cell
Regeneration by Human Postnatal Stem Cells. Frontiers in Physiology: Control
of Pancreatic β-cell Function and Plasticity in Health and Diabetes. Bentham
Science; 2016

2.   **Cooper TT** and Hess DA. The IsletCore Program: Improving the Supply of
Human Islets to Satisfy the Demand for Research. *ENDOCINOLOGY*. 2016

3.   Seneviratne A, Bell GI, **Cooper TT**, Sherman SE, Putman DM, Hess DA. A Sub-
Population of Expanded Hematopoietic Progenitor Cells that Retain High
Aldehyde Dehydrogenase Demonstrates Islet Regenerative Functions. *STEM
CELLS*. 2016

4.   Sherman SE, Kuljanin M, **Cooper TT**, Putman DM, Lajoie GA, Hess DA. High

Aldehyde Dehydrogenase Activity Identifies Human Mesenchymal Stromal Cells with Vascular Regenerative Potential. *STEM CELLS*. 2017.

5.   Putman DM, **Cooper TT**, Hewit M, Seneviratne AK, Sherman SE, Bell GI, Hess DA. *Ex vivo* Expansion of Aldehyde Dehydrogenase-Expressing Cells Identifies Early Myeloid Progenitor Cell Progeny as Potent Stimulators of Ischemic Limb Revascularization. *Stem Cells & Translational Medicine*. 2017.

6.   Young SA, Sherman SE, **Cooper TT**, Brown C, Anjum F, Hess DA, Flynn LE, Amsden BG. Mechanically Robust Injectable Scaffolds for Intramuscular Stem Cell Delivery and Cytokine Release. *Biomaterials*. 2018

7.   **Cooper TT**, Sherman SE, Kuljanin M, Bell GI, Lajoie GA, Hess DA. Inhibition of Aldehyde Dehydrogenase-activity Expands Multipotent Myeloid Progenitor Cellswith Vascular Regenerative Function. *STEM CELLS*. 2018

8.   Gomes J, Lucien Fabrice, **Cooper TT**, Kim Y, Williams KC, Liao X, Kaufman L, Lagugne-Labarthet F, Flesh N, McIntyre CW, Leong HS. Linearized Detection of Platelet Microparticles by Nanoscale Flow Cytometry. *Thrombosis and Hematostasis*. 2018

9.   Ali SN, Dayatathna T, Ali AN, Osumah T, Ahmed M, **Cooper TT**, Power NE, Zhan D, Kim D, Kim R, St. Amant A, Hou J, Tailly T, Yang J, Luyt L, Spagnuolo P, Burton J, Razvi H, and Leong HS. Drosophilla Melanogaster as a Function based High-throughput Screening Model for Anti-Nephrolithiasis Agents in Kidney Stone Patients. *Disease Models & Mechanisms*. 2018

10.   **Cooper TT**, Bell GI, Hess DA. Inhibition of Retinoic Acid Production Expands a Megakaryocyte-enriched Subpopulation with Islet Regenerative Function. *Stem Cells & Development.* 2018

11.   Kaufman LH, **Cooper TT**, Wallace GQ, Poon AC, Dayarathna TL, Hawke DC, Betts D, Leong HS, Hess DA, Lagugne-Labarthet F. Trapping and SERS Identification of Extracellular Vesicles. *Plasmonics in Biology XVI*, 2019

12.   **Cooper TT**, Hess DA, Subdoh V. Vascular Organoids: Are we entering a new era of cardiometabolic research? Cell Metabolism. 2019

13.   **Cooper TT** and Hess DA. Bronchioalveolar Stem Cells: At the Crossroads of Lung Regeneration. Biotarget. 2019